VNiVERSiDAD D SALAMANCA

DEPARTAMENTO DE MATEMÁTICA APLICADA

INSTITUTO DE FÍSICA FUNDAMENTAL Y MATEMÁTICAS

Topological defects on manifolds with curvature

Alberto José Balseyro Sebastián

Supervisors

Dr. Miguel Ángel González León

Dr. Alberto Alonso Izquierdo

DOCTORAL THESIS

Salamanca, 2023

VNiVERSiDAD D SALAMANCA

DEPARTAMENTO DE MATEMÁTICA APLICADA
INSTITUTO DE FÍSICA FUNDAMENTAL Y MATEMÁTICAS

Dr. Miguel Ángel González León
Profesor Titular del área de Matemática Aplicada de la Universidad de Salamanca

y

Dr. Alberto Alonso Izquierdo
Profesor Titular del área de Matemática Aplicada de la Universidad de Salamanca

CERTIFICAN:

Que el trabajo de investigación que se recoge en la presente memoria de tesis doctoral titulada *TOPOLOGICAL DEFECTS ON MANIFOLDS WITH CURVATURE*, presentada por **D. Alberto José Balseyro Sebastián** para optar al Título de Doctor por la Universidad de Salamanca con la Mención de Doctorado Internacional, ha sido realizada en su totalidad bajo su dirección y autorizan su presentación.

En Salamanca, a 7 de Noviembre de 2023

Miguel Ángel González León

GONZALEZ LEON, MIGUEL ANGEL (FIRMA)
Firmado digitalmente por GONZALEZ LEON, MIGUEL ANGEL (FIRMA)
Fecha: 2023.11.07 14:26:21 +01'00'

Alberto Alonso Izquierdo

ALONSO IZQUIERDO ALBERTO - 04181918N
Firmado digitalmente por ALONSO IZQUIERDO ALBERTO - 04181918N
Fecha: 2023.11.07 16:22:01 +01'00'

In loving memory of
María Cristina

Abstract

In this thesis different aspects of kinks in non-linear Sigma models are studied. Sigma models where families of kinks can be analytically identified will be successfully constructed on different Riemannian manifolds. The stability of these kinks will also be analysed. Moreover, kinks of field theories in Euclidean spaces will be geometrically constricted in a continuous manner by extending its target manifold and choosing interesting families of geometries on it.

On the other hand, Sigma models with analytical solutions will be sought for non-simply connected target manifolds. The different homotopy classes of curves that arise will give rise to the existence of brochosons under certain conditions. This is, these homotopy classes will allow the existence of non-topological kinks that cannot decay into vacuum. This will be accomplished by introducing singularities in the potential in simply connected spaces and by directly considering a non-simply connected manifold like the torus.

Furthermore, the methods of deformation of Bazeia et al. will be generalised to the context of Sigma models, also allowing seed-dependent deformations in the process. Lastly, new methods for identifying kinks in new Sigma models are developed. On one hand, procedures for cutting and gluing kinks will allow us to design kink orbits for other Sigma models. In addition to this, Sigma models will be combined to intertwine their dynamics while retaining the original solutions.

Acknowledgments

La culminación de una tesis suele esconder, entre público y bambalinas, un apoyo prolongado a lo largo de los años. El fin de esta tesis no es diferente en este sentido. Este espacio está dedicado a todos aquellos que aportaron significativamente a mi desarrollo y compartieron mi camino, tanto a nivel académico como personal.

En primer lugar, no podría agradecer suficiente a mis directores Miguel Ángel y Alberto por acogerme años atrás. Este fue con certeza un gesto de inmensas repercusiones al que debo el norte. Gracias también por vuestra paciencia, inestimable ayuda y consejos durante estos años. Pese a que el desarrollo haya sido lo más no lineal de esta tesis, aquí está gracias a vosotros. Agradezco también a todo el grupo de investigación del que he aprendido y sigo aprendiendo tanto.

Gracias a María Cristina por el apoyo infinito e incondicional, principal motor de esta tesis. Gracias a Sergio por enseñarme tanto con y sin palabras. Si bien el origen del carácter que me ha permitido llegar hasta aquí puede ser difuso, la raíz es sin duda vosotros. Gracias también a todo el entorno santapolero por todos esos años que guardo con cariño. También a César, que estuvo allí para avivar la llama que me llevaría a esta misma tesis.

Gracias a Alicante y a las amistades que generosamente me brindó. Éstas han sido un pilar imprescindible durante estos años. Cómo empezar si no es agradeciendo a Carlos, no compañero de pocas facetas de la vida. Gracias también a sus padres, Ana y Paco, cuya amabilidad excede cualquier medida. Gracias a Pedro y a Juan Carlos, porque tampoco a ellos podría pagarles por todo lo que han hecho estos años. Agradezco a Gascón, Jorge, Camps, Borja y Pascual por estar ahí desde siempre. También a Valencia y a todos sus entornos donde comencé mi aventura. Particularmente a Gomis, porque es una figura irremplazable.

Gracias a Salamanca también, a sus gentes y a sus idiomas. Difícil me es imaginar un doctorado sin intercambios y las especiales almas que los frecuentan. Gracias Pedro, Lena, Chinatsu, Fran, María, Adri, Tsuguka, Yuka, Luis, Camili, Dani y demás por acompañarme y ser un robusto apoyo estos años. Tampoco olvidaré el respaldo que me proporcionaron Carlos, Roberto y Judit cuando el reloj más apremiaba. Gracias a Rubén, por ser un gran amigo y profesor. También a Sergio, quien me ha demostrado que su maestría para los pliegues espacio-temporales no es su mejor virtud. Agradezco también a los valientes que estudian esas almas, Guille, Elena y Gema. Tampoco sería posible imaginar estos cinco años sin la familia Astete. A Carlos, que fue, es y será siempre mi eterno compañero de piso. A Jose, Javi, Jesús, Jorge y Alberto, con los que tantas noches y aficiones compartí. Quiero agradecer también a los allegados de Astete, Cris, Carlota, Aitana y Bea entre otros. Gracias también a los compañeros de despacho, Dani, Carlos, Isa y Domenico. Sin ellos hubiese perdido práctica en el arte de la tortura. También a los compañeros de doctorado de Salamanca y Valladolid que también compartieron su viaje conmigo.

Gracias Paz por tu ayuda, he podido ir siguiendo tu estela hasta el final.

Gracias a João Pessoa y a la experiencia que me regaló Brasil y la gente que allí conocí. Quisiera expresar mi más profundo agradecimiento a Dionisio Bazeia y a Matheus Araújo Marques por su más que cálida bienvenida y guía durante mi estancia en Brasil. También por todo lo que allí aprendí, a todos los niveles. Mil gracias también a Miriam, Carl, Judith, Joyce, Dani y Agustín por hacer de esos meses una etapa inolvidable.

Agradezco la financiación recibida por el Proyecto Q-CAYLE, Plan Complementario en Comunicación Cuántica (Ref: PRTRC17.I1) dentro del Plan de Recuperación, Transformación y Resiliencia - Next Generation UE, cofinanciado por el Ministerio de Ciencia e Innovación y la Junta de Castilla y León.

Por último, querría recordar también a todos los profesores que han tenido un impacto profundo en mi educación. Gracias a Aitor, cuya paciencia y optimismo tuvieron un impacto crucial en los años que siguieron. También a Elena y a Mónica, cuyo apoyo aprecié y aprecio años después. Gracias al Prof. Azcárraga por dar impulso al estudiante. Y a todos mis profesores, que en mayor o en menor medida, siempre han contribuido.

Contents

Introduction

This thesis will be focusing on the study of topological defects. In particular, in those arising in $1+1-$dimensional scalar field theories, known as kinks. These are localised structures that travel at constant velocity and without losing their form, for which several applications in physics can be found. Indeed, their topological properties allow us to model a wide range of physical phenomena. Nowadays a great variety of topological defects can be found in the literature. However, the key notion behind was originated almost two centuries ago with the appearance of the solitary wave and subsequently with the notion of soliton. In 1844, the Scottish engineer John Scott Russell reported to the British Association the events [119] he had witnessed some years before

> "I was observing the motion of a boat which was rapidly drawn along a narrow channel by a pair of horses, when the boat suddenly stopped - not so the mass of water in the channel which it had put in motion; it accumulated round the prow of the vessel in a state of violent agitation, then suddenly leaving it behind, rolled forward with great velocity, assuming the form of a large solitary elevation, a rounded, smooth and well-defined heap of water, which continued its course along the channel apparently without change of form or diminution of speed. I followed it on horseback, and overtook it still rolling on at a rate of some eight or nine miles an hour, preserving its original figure some thirty feet long and a foot to a foot and a half in height. Its height gradually diminished, and after a chase of one or two miles I lost it in the windings of the channel. Such, in the month of August 1834, was my first chance interview with that singular and beautiful phenomenon which I have called the Wave of Translation."

This phenomenon that he called "Wave of Translation" was the seed of what many years later would become an incredibly active field of research. The description of this phenomenon was ignored by the scientific community at that time, as it seemed to violate the laws of hydrodynamics. In fact, Airy and Stokes stated that they had mathematically proven the impossibility of this type of phenomenon. For many years the veracity of this story was being called into question until Korteweg and de Vries published their paper [93] in 1895. In that work, the existence of waves of unchanging profile and constant velocity in the context that Russell was describing was theoretically proven. This gave the starting signal for the discovery of new phenomena in the subsequent years. This equation, where these travelling waves were predicted, has been known as the KdV equation ever since.

Years later, in 1953, Fermi, Pasta, Ulam and Tsingou conducted an experiment that led to significant advancements in this field, known by the name of FPUT

experiment. In this experiment, an elastic vibrating string with fixed ends was computationally simulated with non-linear terms. As result of this experiment, the thermalisation of all vibrational modes of the strings was expected, that is, the energy was expected to be equally distributed in all modes. Instead, a quasi-periodic behaviour in this string was found, where the energy was passing through different modes of vibration. These results were published two years later [65, 110], but they were not properly understood until the contribution of Kruskal and Zabusky [139] in 1965. In this paper [139], numerical solutions of the KdV equation were identified, in which multiple "Waves of Translation" were colliding. They observed that collisions were taking place in such a manner that form and velocity of these solutions were recovered after the impact. The identity of these solutions was therefore being preserved. This surprising fact made them baptise these single solutions as "solitons", from the latin term *solus*, meaning "alone".

This behaviour that solitons exhibit has been identified in the emerging dynamics of other non-linear differential equations throughout history, such as the sine-Gordon equation or the non-linear Schrödinger equation. In fact, the recovery of the original forms after collisions is connected to the integrability of these systems, which in infinite-dimensional systems as are those in field theory, implies the existence of an infinite number of conserved quantities. In other words, only an infinite number of constrictions can force solutions to behave in this manner at each and every one of the infinite number of points. Of course, delving into details is far beyond the scope of this historical introduction, but the description above provides a good intuition of the phenomenon of collision.

Another landmark in history is also related to this mentioned infinite number of conserved quantities. This turning point is the inverse scattering method, originally introduced by Gardner, Greene, Kruskal and Miura [66] for solving the KdV equation. This formalism expands the collection of methods for solving non-linear partial differential equations by transforming the problem into an initial value problem. In that paper, a Schrödinger equation is constructed using as potential the initial value data for the KdV equation. This enables us to evolve the scattering data solution of this equation and subsequently reconstruct the potential for the original problem but at future time points [1, 109]. The implementation of this method is highly challenging, but it constitutes a breakthrough due to its direct implications in the field of solitons. On the other hand, it is worth mentioning that several notions of soliton coexist in the literature. In the context of partial differential equations, one of the standard definitions is that of Drazin and Johnson [61], which is encouraged by this type of behaviour after collision. This can be stated as follows:

Definition 0.0.1 (Drazin and Johnson) *A soliton is any solution of a non-linear partial differential equation (or system) such that:*

1. *It represents a wave of permanent form.*

2. *It is localised and does not diverge at infinities.*

3. *It can interact with other solitons without losing its identity.*

This definition will be adapted to consider the type of solutions that we shall encounter in our field theories, but it forms the core of the concept of kink. More

specifically, the localised permanent form will correspond to the energy density, preserving the identity of a possible extended particle. Additionally, the third condition will be dropped, allowing non-integrable models to be considered.

Korteweg-de Vries equation

Given the impact that the KdV equation and its solutions had in the history of solitons, let us obtain explicitly these mentioned travelling solutions. This will also shed some light into the form of solutions that shall be sought in field theories. The KdV equation was derived to study the propagation of water waves in the surface of a canal similar to the one Russel was studying. This is, a shallow canal with high viscosity water. Imposing these conditions in the hydrodynamic equations, that is, motion and continuity equations, these can be reduced to the following differential equation in partial derivatives

$$u_t + \alpha\, u u_x + \beta\, u_{xxx} = 0\,,$$

where $u(x,t)$ denotes the height over the reference surface at a point x and at time t and parameters $\alpha, \beta \in \mathbb{R}$ capture the properties of the viscous water, see Figure 1. Notice that the reference surface from which the height is measured corresponds to the equilibrium state of the canal.

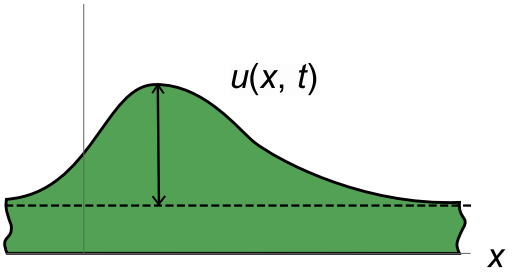

Figure 1: Pictorial representation of the profile of the surface of the water during the propagation of viscous water waves along the shallow canal.

While the presence of the two real parameters α and β suggests that this may be a family of unrelated differential equations, the transformation $x \to \beta^{1/3}x$ and $u \to \alpha\beta^{-1/3}u$ reveals that all these correspond to the same differential equation

$$u_t + u u_x + u_{xxx} = 0\,.$$

For historical reasons, let us choose as representative the following member to study

$$u_t - 6 u u_x + u_{xxx} = 0\,,$$

whose solutions will define solutions for other values of the parameters α and β. In order to identify Russell's waves of translations, let us search for travelling solutions with constant velocity $u(x,t) = u(x - vt)$. Moreover, let us restrict to functions for which height at infinities lies at the equilibrium level and first and second derivatives tend to zero at infinities. From a physical perspective this is a natural imposition. Indeed, the energy of a physical configuration must be finite. These conditions allow

us to find once the KdV equation is integrated the following travelling localised solution

$$u(x,t) = -\frac{c}{2}\,\mathrm{sech}^2\left(\frac{x-ct-x_0}{\sqrt{2}}\right).$$

The minus sign present in this solution appears as a consequence of the choice of α and β. Physically acceptable values of these parameters would lead to a solitary wave profile with positive amplitude as would be expected. Notice that the maximum height of the wave of translation is proportional to its velocity c. This counter-intuitive fact is due to the non-linearity of this equation. It is also important to hightlight that other types of solitons can emerge, each characterised by a distinct number of independent "heaps" that move at different velocities. For instance, the solution of the sine-Gordon equation known as breather describes different heaps that travel oscillating around each other. Lastly, one can prove that the KdV equation can correspond to different Hamiltonian systems, in which an infinite number of conserved quantities can be identified. This is, integrable systems associated to the KdV equation can be found. It should be emphasised that the differential equations that shall arise in field theory will differ significantly from the KdV equation. Nevertheless, these will also be non-linear differential equations, and a similar approach will be applied to identify localised solutions.

Kinks in field theories

The context where this type of solutions will be sought in this thesis is classical field theory. As it will be described in detail later on, kinks are localised finite-energy solutions of field theories on the $(1+1)-$Minkowski space for which the energy density travels at constant velocity and without losing its form. This is, in field theory the energy density profile inherits the notion behind the "moving heap". The requirement of finite energy forces this type of solution to tend to vacua of the field theory at both ends of the spatial line. As a consequence, kinks will be classified according to whether the vacua at both ends coincide. Topological kinks will asymptotically link different vacua, while non-topological kinks will asymptotically join a vacuum point with itself.

The underlying framework of this thesis is built upon the progress made during the latter part of the 20th century in three distinct directions. On one hand, a technique developed by Bogomol'nyi, which shall be summarised later on, allows us to simplify the analytical identification of kinks in scalar field theories. This will be one of the cornerstones of the present work. In particular, this procedure can be applied in the context of non-linear Sigma models, which are field theories where the target space is a general Riemannian manifold. In this scenario, Bogomol'nyi's method will be associated to the integrability of a classical mechanical system on a Riemannian manifold.

Secondly, making use of the mentioned Bogomol'nyi's technique, non-topological kinks that cannot decay into vacuum have been found for field theories in the plane in [16, 25]. This property, typically found for topological kinks, can therefore also be displayed by non-topological kinks. These solutions will be referred to as brochosons in this thesis. Lastly, it is of special interest the techniques of deformations of kinks developed by Bazeia et al., see [3–5, 7, 21, 32, 34–39, 50, 53, 55]. These allow us to

construct an infinite number of new field theories for which analytical kinks can be identified by deforming other field theories.

Applications in physics

Topological defects play an important role when modelling phenomena in several fields of physics. For example, in optics several applications can be found in optical communication [2, 6, 103, 122]. Solitons can propagate in optical fibers over long distances without dissipating and the dispersion of different wavelengths can be controlled. In molecular systems topological defects provide mechanisms for charge and energy transport [31, 52, 54, 72, 137]. For instance, employing a continuum approximation, a sine-Gordon equation can model the angular displacements of DNA bases from their equilibrium positions. Other applications can be found in conducting polymers [75], electron displacement in polyacetylene [43, 127] or in graphene deformations [100, 138]. For instance, a modified sine-Gordon equation can be employed to model the propagation of solitary electromagnetic waves in a graphene superlattice. Solitons are also sought in the propagation of action potentials along neurons [82], given the non-linearity of the differential equations of the Hodgkin-Huxley model.

Solitons are prevalent in both cosmology and in high-energy physics [88, 91, 131, 133–135]. For instance, these can appear as cosmic strings, which are hypothetical one-dimensional topological defects that may have been formed during phase transitions in the early universe. These may contain information on the large-scale structure of the universe. Domain walls are also found in String Theory [90, 118]. More examples of Topological defects can be listed in several other fields like supersymmetric systems [124], gold dislocations [62] or Rydberg atoms [120]. However, let us highlight a field that has been specially enriched by topological defects, which is condensed matter physics [44, 48, 63, 83, 97, 115, 126, 132]. Magnetic domains and the domain walls between them generate a great interest due to the important role that they play in determining the electrical properties of ferromagnetic materials [42, 76, 86, 114]. The emergence of an electric current between superconductors in proximity in Josephson junctions can also be modelled by a sine-Gordon equation [130]. Furthermore, domain walls allow the manipulation of electron spins in spintronic devices, such as magnetic sensors, magnetic random-access memory (MRAM) and spin transistors [49, 77, 78, 89, 96, 123].

Simple models that describe topological defects, like the ϕ^4-model, are broadly employed in physics [87, 99, 125, 131]. However, more sophisticated models can be used to further understand several phenomena. For example, Sigma models on the sphere $\mathbb{S}^2$ have important applications in solid state physics, particularly in spintronics. The presence of multiple non-collinear ground state configurations can be originated by phenomena like exchange, anisotropy and dipole-dipole interactions in magnetic materials. This scenario can give rise to the presence of topological defects describing spin chains in magnetic materials. For instance, in [74] Haldane constructs a $O(3)$ non-linear Sigma model in order to describe the low-energy dynamics of large-spin one-dimensional Heisenberg antiferromagnets, performing a semiclassically quantisation in the soliton type solution of the model. Exact expressions for spin solitary waves in similar scenarios are obtained in [18, 20]. Moreover, the one-loop mass shifts to the classical masses of these solutions is succesfully

computed in [19]. Another relevant contribution in this line of research is the identification of chiral magnetic soliton lattices present on chiral helimagnets $Cr_{\frac{1}{3}}NbS_2$, see [129]. In [92], the study delves into topologically protected magnetic solitons and their relevance to logical operations and/or information storage. Moreover, extensive research on topological defects in massive non-linear Sigma models in several supersymmetric models can be found in the literature, see [28, 60, 64, 107]. In this context, a worth highlighting result is that composite solitons in $d = 3 + 1$ of Q-strings and domain walls are exact BPS solutions that preserve a quarter of the supersymmetries [67, 79].

In conclusion, the ubiquity of topological defects makes them a versatile tool to describe several phenomena in nature, where non-linearity is present. The examples shown above represent just a fraction of the numerous applications in physics. However, they will serve as a testament to the existence of the bridge between this type of models and physics.

Objectives of this thesis

This thesis aims to further develop several aspects of kinks in non-linear Sigma models. The main objectives can be summarised in two points, each of which will be in turn divided into two subobjectives:

- **Objective** $O1$: Kinks in non-linear Sigma models will be studied:
  - **Subobjective** $O1.1$: Kinks will be sought in manifolds with curvature. Particular emphasis will be put on finding kinks in the two-dimensional sphere and the two-dimensional torus.
  - **Subobjective** $O1.2$: The existence of brochosons in non-linear Sigma models will be investigated by exploring non-simply connected target manifolds.
- **Objective** $O2$: Methods of deformations of kinks between non-linear Sigma models will be studied:
  - **Subobjective** $O2.1$: A generalisation of the methods of deformation of kinks developed by Bazeia et al. will be sought.
  - **Subobjective** $O2.2$: New techniques of deformations of kinks will be pursued, further expanding our tools to identify kinks in new non-linear Sigma models.

Structure of the thesis

The fulfillment of the previously described two objectives will be divided into six chapters. The first objective $O1$ will be achieved in the first four chapters, simultaneously accomplishing both subobjectives $O1.1$ and $O1.2$. Chapters 5 and 6 will be devoted to objective $O2$. Subobjective $O2.1$ will be addressed in Chapter 5, while Objective $O2.2$ will be discussed in Chapter 6. A brief summary of the particular focus of each chapter will be presented to establish the structure of this thesis.

In the first chapter a review of field theories with Euclidean target space is presented. The conserved quantities that arise in the type of field theories that shall be considered and Nöether's theorem in field theory are summarised. In this context, the notion of topological defect is introduced. In particular, we shall focus on kinks, defined on $1+1-$dimensional Minkowski spaces. Unlike in field theories on higher-dimensional Minkowski spaces, Derrick theorem will allow us to search for finite-energy static kinks in general. The problem of identifying this type of solutions in the field equations will be equivalent to solving the equations of a mechanical system with vanishing mechanical energy. This will lead us to delve into the notion of integrability in classical mechanics. In particular, Arnold-Liouville's definition of integrability will be considered. The Hamilton-Jacobi formalism will be employed, obtaining a system of first order differential equations, generally significantly simpler to solve than Newton's equations. This will restrict the type of models that shall be considered. As we shall see, the Bogomol'nyi arrangement will impose an identical condition on the potential of the field theory.

On the other hand, given the importance of identifying stable solutions, the linear stability under small perturbations will be discussed for kink-like solutions of these field theories. This will be accomplished by analysing the spectral equation that describe the modes of vibration of linear perturbations. Subsequently, three emblematic models in field theory with one and two fields will be discussed. This is, the ϕ^4-model, the sine-Gordon model and the MSTB model. While the first two models will illustrate the general features of kinks, the MSTB model will serve as an example of field theory with two fields with integrable analogue mechanical system. Moreover, considering multiple fields will also allow the existence of families of kinks. Lastly, a collection of field theories in the plane that support brochosons will be constructed. In this case, the property of simply-connectedness will be lost due to the presence of a singularity in the potential. Specifically, the use of elliptic coordinates in the plane will introduce the required singularity.

In Chapter 2 the Euclidean target space is replaced by a general Riemannian manifold, leading to the context of non-linear Sigma models. Following a formalism similar to the one employed for mechanics in [71], the free-coordinate field equations of a Sigma model will be derived. Derrick theorem will also hold for Sigma models, allowing static solutions to exist for $1+1-$dimensional Minkowski spaces. As it is well-known, the Bogomol'nyi arrangement can also be performed for Sigma models, leading once more to first order differential equations. The notion of linear stability discussed in Chapter 1 can also be adapted to Riemannian target manifolds, even though this makes the stability analysis of solutions more complicated. Lastly, a generalisation of the mechanism for geometrical constriction of kinks [40] is presented. This new method, published in [30], extends the target space proposing a continuous family of new geometries on it, so that once the new solutions are obtained and projected to the original target space, continuously geometrically constricted solutions are constructed. This mechanism is applied to a field theory with one field and another with two fields.

In Chapter 3, Hamilton-Jacobi separable Sigma models on the two-dimensional sphere will be constructed. On one hand, results published in [22] will be summarised, where a model with a family of homogeneous quartic potentials is considered. This model with six vacua will exhibit a rich kink variety, which can be analytically calculated. This includes singular topological kinks between adjacent

vacua and two families of topological kinks. The stability of these solutions is analysed. On the other hand, a model on the sphere where brochosons can be found is constructed by introducing singularities in the poles.

In Chapter 4, results published in [26] and [27] are summarised, where a non-simply connected manifold is considered as target manifold. In particular, Sigma models on the two-dimensional torus will be explored. This will allow us to find brochosons as a consequence of the topological properties of this manifold, as the emergence of different homotopy classes will prevent an infinite number of types of loops from contracting to a point. Two families of Sigma models with a variable number of vacua on the torus will be thoroughly discussed. Among these models, a particularly interesting one with only one vacuum point on the torus is found. This forces every kink to be non-topological, as only one vacuum point is present in the torus. Moreover, the stability of these kinks will be analysed.

In Chapter 5, the techniques of deformations of Bazeia et al. are generalised to the context of Sigma models. Furthermore, the new formalism will also allow seed-dependent deformations. This is, the deformed Sigma models will be allowed to depend on the employed kink for the deformation. This procedure will assign a parametrised curve on the target manifold to the kink used as seed, which is transferred to another Riemannian manifold with another parametrisation. On this new manifold, a Sigma model for which the deformed curve is a kink will be constructed. This allows us to construct new Sigma models, for which the new solutions can be derived from those of the original models. Compatibility conditions between the superpotentials of the original and deformed Sigma models will appear. Examples of different types of deformations for field theories with one scalar field will be shown to show the connection between this formalism and that of Bazeia et al. Then, deformations between the plane and the sphere will be performed via the stereographic projection. These coordinates will allow us to include a reparametrisation of curves to correct the change of curvature of both manifolds and to solve the compatibility equation. Other possibilities will immediately follow from this particular procedure. For instance, the deformation between any two conformally flat target Riemannian manifolds. Lastly, examples of deformations between Sigma models with target manifolds of different dimension will be presented.

In Chapter 6 new techniques to construct Sigma models for which analytical expressions of kinks can be automatically obtained are developed. In particular, three methods will be discussed in this chapter. First, the procedure of deformation described in Chapter 5 will be employed to cut kink orbits on a Riemannian manifold and construct Sigma models for which the trimmed curve is indeed a kink. This will be by construction a seed-dependent deformation. This procedure will be applied for Euclidean target spaces, but also for the two-dimensional sphere and for the two-dimensional torus. The second method consists in gluing different kinks to form a piecewise hybrid kink. Since in general more than one field will be considered, a procedure to interpolate the potential functions outside the junctions of the gluings of curves will be necessary. Examples in field theories with one and two fields will be shown. In particular, this method will be applied to construct piecewise non-topological kinks on the plane or other Riemannian manifolds like the two-dimensional torus. Lastly, as third method of deformation, the dynamics of two different Sigma models will be intertwined in a more general Sigma model. Even though new general solutions will emerge, the superpotentials will be defined so that

the original solutions will be maintained. In order to achieve this, these composite Sigma models will employ as target manifold the Cartesian product of the original target manifolds. By construction, the potentials of these composite Sigma models will present higher-order terms modulated by a parameter that allows us to control the strength of the coupling of fields. This formalism will be applied to create a composite double ϕ^4-model, a composite triple ϕ^4-model, a combination of the ϕ^4-model and a sine-Gordon model, and a composite triple sine-Gordon model, generalising the uncoupled analogue models. Lastly, the form of this extended superpotential will also be employed in a Sigma model on the sphere, where similar solutions can be derived.

Finally, in the concluding chapter of this thesis, the most significant findings and insights derived from the preceding six chapters will be summarised.

Chapter 1

Classical scalar field theory and kinks

1.1 Scalar field theories

Solitons arise in several fields of physics such as hydrodynamics, cosmology, biophysics, physics of materials or particle physics among others. These frequently find their bases in field theory and it is precisely in this scenario where solitons will be sought in this thesis. Therefore, in order to identify these objects it will be of utmost importance to describe in detail the inner workings of these theories. First, the fundamental aspects of classical field theory will be summarised and the notion of topological defect presented. Methods for obtaining such solutions and for analysing their stability will be discussed with some representative examples. Finally, the notion of a new type of topological defect, baptised as brochoson, is introduced and models where this type of solution arises are studied.

1.1.1 Field equations

With the goal of describing relativistic phenomena, the $(n+1)-$Minkowski space $\mathbb{R}^{1,n}$ will be considered, which comprises n spatial dimensions and time. Spatial coordinates and time will be denoted as $x^1, \dots, x^n$ and $x^0 = t$ respectively. The Minkowski metric will be chosen so that the associated matrix reads $\eta = \text{Diag}(1, -1, \dots, -1)$. Although later on we shall focus our efforts in a scenario with only one spatial dimension, let us consider the general case for now. In scalar field theory, a real field $\phi(t, \vec{x})$ is a map $\phi : \mathbb{R}^{1,n} \to \mathbb{R}$ that sends each point in the Minkowski space to the real numbers. When multiple fields are considered $\phi^i(t, \vec{x})$ with $i = 1, \dots, N$, these can be expressed collectively by means of another map of the form $\phi : \mathbb{R}^{1,n} \to \mathbb{R}^N$. In this manner, taking coordinates in this space $\mathbb{R}^N$, which receives the name of target space, N fields $\phi^i(t, \vec{x})$ emerge[1]. Once fields ϕ^i with $i = 1, \dots, N$ have been defined, we are in a position to construct particular field theories. This is accomplished through the choice of a Lagrangian density function $\mathcal{L}(\phi, \partial_\mu \phi)$ and the construction of an action $S[\phi]$, which assigns to each field configuration $\phi(t, \vec{x})$ a real number by

[1] A specific notation will be adopted, where an exponentiation of a field ϕ^i shall be written as ϕ_i^n. Since we shall not deal explicitly with the components of the corresponding covectors $\phi_i = g_{ij}\phi^j$ of the position vector $(\phi^1, \dots, \phi^N)$, there will be no risk of confusing one with the other.

the integration of the Lagrangian density on $\mathbb{R}^{1,n}$

$$S[\phi] \equiv \int_{\mathbb{R}^{1,n}} \mathcal{L}(\phi^i, \partial_\mu \phi^i)\ d^n x\, dt\,, \tag{1.1}$$

where the Einstein summation convention is used for the index $\mu = 0, 1, \ldots, n$. Field theories employ Hamilton's principle of stationary action to produce field equations. This is, variational calculus allows us to find a condition for those fields in the form of the Euler-Lagrange equations so that they are stationary configurations

$$\frac{\partial \mathcal{L}}{\partial \phi^i} = \partial_\mu \left(\frac{\partial \mathcal{L}}{\partial \left(\partial_\mu \phi^i\right)} \right) \qquad \forall i\,,$$

where the Einstein summation convenction is used of the index μ. Therefore, different theories, this is, different Lagrangian densities $\mathcal{L}(\phi^i, \partial_\mu \phi^i)$, will produce different solutions. Naturally, fields are defined to be $\phi^i \in \mathcal{C}^2(\mathbb{R}^{1,n}, \mathbb{R})$ so that Euler-Lagrange equations are well-defined. Notice that a Lagrangian density must depend on derivatives, since without this dependence Euler-Lagrange equations would lead to a relation between only coordinates, not a dynamical condition. Also, as it is common, higher order derivatives have not been included in the Lagrangian density. On the other hand, this method allows us to easily include certain symmetries that the physical system exhibits. Indeed, symmetries in the Lagrangian density will be inherited by Euler-Lagrange equations. In particular, Lorentz invariance will be imposed when constructing Lagrangian densities $\mathcal{L}(\phi^i, \partial_\mu \phi^i)$. In fact, the type of Lagrangian densities that will be of our interest will be "natural Lagrangian densities", which can be typically written as

$$\mathcal{L}(\phi^i, \partial_\mu \phi^i) = \frac{1}{2} \sum_{i=1}^{N} \left[\left(\frac{\partial \phi^i}{\partial t} \right)^2 - \sum_{a=1}^{n} \left(\frac{\partial \phi^i}{\partial x^a} \right)^2 \right] - V(\phi^1, \ldots, \phi^N)\,, \tag{1.2}$$

where V is the "potential function", a positive semi-definite function that determines the dynamics of the model. Notice that this Lagrangian density is indeed Lorentz invariant. Finally, Euler-Lagrange equations produce for the above natural Lagrangian density the following field equations

$$\frac{\partial^2 \phi^i}{\partial t^2} - \sum_{a=1}^{n} \frac{\partial^2 \phi^i}{\partial x_a^2} = -\frac{\partial V}{\partial \phi^i} \qquad \forall i\,, \tag{1.3}$$

which are, as mentioned before, Lorentz-invariant.

1.1.2 Noether's theorem and conserved quantities

It is worth noting that apart from the symmetry under Lorentz transformations, other symmetries can appear. As it is well-known, continuous symmetries in the Lagrangian density implies the existence of conserved currents and quantities, result known as Noether's theorem. Let us consider a continuous symmetry of the Lagrangian density $\mathcal{L}(\phi^1, \ldots, \phi^N)$. This is, let us consider a transformation of fields $\phi^a \to \phi^a + \epsilon\ \Delta\phi^a$ with small continuous parameter $\epsilon \in \mathbb{R}$ for which the Lagrangian density experiences a shift given by a divergence

$$\mathcal{L} \to \mathcal{L} + \epsilon\ \partial_\mu K^\mu\,, \tag{1.4}$$

where $K^\mu = K^\mu(\phi^1, \ldots, \phi^N)$ are four differentiable functions $\mu = 0, 1, 2, 3$. The action of the field theory is the integral of the Lagrangian density over the Minkowski space. Given that surface terms do not contribute to this integral, these additional terms of the form of divergences $\partial_\mu K^\mu$ leave the action unaltered. On the other hand, these field transformations lead to a change in the Lagrangian density that can be written as

$$\mathcal{L} \to \mathcal{L} + \epsilon\, \partial_\mu \left(\frac{\partial \mathcal{L}}{\partial\left(\partial_\mu \phi^a\right)} \Delta\phi^a \right) + \epsilon \left(\frac{\partial \mathcal{L}}{\partial \phi^a} - \partial_\mu \left(\frac{\partial \mathcal{L}}{\partial(\partial_\mu \phi^a)} \right) \right) \Delta\phi^a \,.$$

Notice that the last term vanishes when solutions of the Euler-Lagrange equations are considered. Hence, equation (1.4) and this last equation for solutions of the Euler-Lagrange equations lead us to conserved currents

$$\partial_\mu J^\mu = 0\,, \quad \text{where} \quad J^\mu = \frac{\partial \mathcal{L}}{\partial\left(\partial_\mu \phi^a\right)} \Delta\phi^a - K^\mu \,.$$

This implies in turn the existence of conserved quantities, which shall be denoted as Q. These can be constructed by integrating the first component J^0 of each conserved current over the spatial part of the Minkowski space

$$Q = \int_{\mathbb{R}^n} J^0 \; d^n x \,.$$

Indeed, its time derivative can be manipulated when we assume that $\lim_{|x|\to\infty} J^i = 0$ for $i = 1, \ldots, n$ so that it vanishes

$$\frac{dQ}{dt} = \int_{\mathbb{R}^n} \frac{dJ^0}{dt} \; d^n x = -\int_{\mathbb{R}^n} \vec{\nabla} \cdot \vec{J} \; d^n x = 0 \,.$$

Therefore, the identification of continuous symmetries in the Lagrangian density allows us to construct conserved quantities for its field equations. In particular, for Lagrangian densities of the form (1.2), certain conserved quantities are always present due to the continuous symmetries that arise from its form. Let us discuss them briefly.

1. **Time and space translational symmetries**: The type of Lagrangian density (1.2) does not depend explicitly on the spacetime coordinates. The invariance under translations in space and time lead to four conserved currents, assembled in the so-called energy-momemtum tensor T^μ_ν

$$T^\mu_\nu \equiv (J^\mu)_\nu = \frac{\partial \mathcal{L}}{\partial\left(\partial_\mu \phi^a\right)} \partial_\nu \phi^a - \delta^\mu_\nu \mathcal{L} \,,$$

for which the divergence vanishes $\partial_\mu T^\mu_\nu = 0$ for every possible direction $\nu = 0, \ldots, n$. By Noether's theorem, these currents have associated conserved quantities, which are the energy and the momenta:

$$E = \int T^{00} \; d^n x \,, \qquad P^i = \int T^{0i} \; d^n x \,. \tag{1.5}$$

In particular, in models of the form (1.2) the energy can be expressed as follows

$$E = \int_{\mathbb{R}^n} \left\{ \frac{1}{2} \sum_{i=1}^{N} \left[\left(\frac{\partial \phi^i}{\partial t} \right)^2 + \sum_{a=1}^{n} \left(\frac{\partial \phi^i}{\partial x^a} \right)^2 \right] + V(\phi^1, \ldots, \phi^N) \right\} d^n x \,. \tag{1.6}$$

2. **Lorentz symmetry**: The Lorentz group contains rotations in space and boosts, that is, changes between reference frames. Since our Lagrangian density is invariant under the action of this group, rotations and boosts generate respectively nine and three conserved charges

$$Q^{ij} = \int \left(x^i T^{0j} - x^j T^{0i}\right)\, d^n x\,, \qquad Q^{0i} = \int \left(x^0 T^{0i} - x^i T^{00}\right)\, d^n x\,,$$

see [113]. The conserved quantities associated to boosts Q^{0i} reveal interesting information when they are combined with the conservation of momentum. The time derivative of these charges, given the fact that the energy-momentum tensor does not depend explicitly on space-time coordinates, can be arranged as follows

$$\frac{dQ^{0i}}{dt} = P^i + t\frac{dP^i}{dt} - \frac{d}{dt}\int x^i T^{00}\, d^n x = 0\,,$$

which must vanish by definition. Since the momenta are conserved, this last condition reads

$$P^i = \frac{d}{dt}\int x^i T^{00}\, d^n x\,,$$

which implies that the energy centre is travelling with constant velocity.

3. **Internal symmetries**: Apart from the space-time translations and Lorentz symmetries, the action may exhibit other types of internal symmetries. When these symmetries are continuous, described by the action of Lie groups, the action may correspond to a Gauge theory. In fact, this scenario may lead to the emergence of a continuum of zeroes of the potential function. While Gauge theories and their conserved currents and quantities are of paramount importance in physics, we will not explore this type of theories in this thesis. However, discrete internal symmetries will be frequently encountered. These, as we shall see, will relate the positions of the zeroes of the potential and solutions in different regions, simplifying their identification.

1.1.3 Topological charges

Note that the energy density (1.6) for any configuration is a semidefinite positive function, but its integral may diverge for a given solution of the theory. In fact, the behaviour of the energy density at infinities is crucial to prevent this integral from diverging and guarantee its finiteness. Therefore, in order to have a solution $(\phi_s^1, \ldots, \phi_s^N)$ of finite energy, this solution must satisfy for each field $\forall i = 1, \ldots, N$ the following two asymptotic conditions

1. Spatial and time derivatives of fields must vanish at infinities for all fields $i = 1, \ldots, N$

$$\lim_{x\to\pm\infty} \frac{\partial\phi^i}{\partial t} = 0 \qquad \text{and} \qquad \lim_{x\to\pm\infty} \frac{\partial\phi^i}{\partial x^a} = 0 \quad \forall a\,. \tag{1.7}$$

2. Every field must tend to one of the zeros of the potential

$$\lim_{x\to\pm\infty} \phi^i(t,\vec{x}) \in \mathcal{M} \tag{1.8}$$

for $i = 1, \ldots, N$ and where $\mathcal{M} \equiv V^{-1}(0)$ denotes the set of zeroes of the potential V. These points shall be referred to as vacua, while the set that contains them receives the name of vacuum manifold in the literature.

As a consequence of these two conditions, any solution with finite energy must connect, at least asymptotically, two minima of the potential. For the sake of convenience, let us restrict now to the $(1+1)-$dimensional Minkowski space. For a discrete vacuum manifold $\mathcal{M}$, a homotopic classification of solutions leads to the existence of $|\mathcal{M}|^2$ sectors, where $|\mathcal{M}|$ is the number of points in the set $\mathcal{M}$. Indeed, this number $|\mathcal{M}|^2$ is the combinatorial of $|\mathcal{M}|$ possible left ends for solutions with $|\mathcal{M}|$ possible right ends, see Figure 1.1. Any continuous deformation of any solution will not change its sector by definition of homotopy class. These sectors are referred to in the literature as topological sectors, alluding to this homotopic classification. On the other hand, when the vacuum manifold $\mathcal{M}$ is continuous, the arising homotopy classes can be measured by the homotopy group $\pi_0(\mathcal{M})$, which just accounts for the set of path components of $\mathcal{M}$. In that regard, all points inside each path-connected part of the vacuum manifold are identified as if they were the same vacuum point.

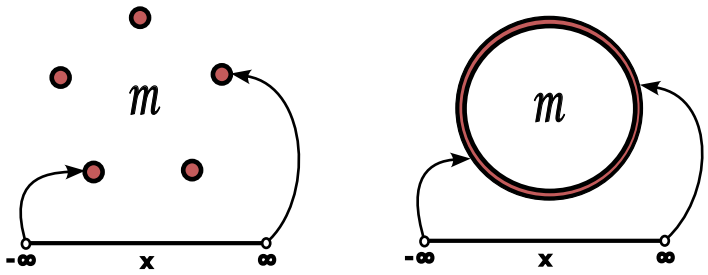

Figure 1.1: When only one spatial dimension is considered, homotopy classes of solutions map the infinities of the spatial line to a discrete and a continuous vacuum manifold respectively.

Now, let us consider the two-dimensional Minkowski space $\mathbb{R}^{1,1}$ and a set of N real scalar fields on it $\phi^i : \mathbb{R}^{1,1} \to \mathbb{R}$ for $i = 1, \ldots, N$. For solutions of finite energy, derivatives of these fields at infinities must vanish (1.7). This allows the construction of another type of conserved quantity, one created from the homotopic constraints of solutions. Let us define for each field ϕ^i the following current

$$j^\mu_{(i)} \equiv \varepsilon_{\mu\nu}\partial_\nu\phi^i \,,$$

where $\varepsilon_{\mu\nu}$ is an antisymmetric symbol that makes its divergence vanish $\partial_\mu j^\mu_{(i)} = 0$ given the commutativity of the partial derivatives. The fact that derivatives vanish in the limit when we approach infinities enables us to define the conserved quantities known as topological charges

$$Q_i = \int j^0_{(i)} dx = \lim_{x\to\infty} \phi^i(t,x) - \lim_{x\to-\infty} \phi^i(t,x) \,, \qquad \forall i \,. \tag{1.9}$$

Indeed, the derivative of any of these charges with respect time vanishes given the conditions at infinities

$$\frac{dQ_i}{dt} = \frac{d}{dt}\int \varepsilon_{0\nu}\partial_\nu\phi^i dx = \int \varepsilon_{j\nu}\partial_j\left(\partial_\nu\phi^i\right) dx = 0 \,,$$

where $\partial_\mu j^\mu_{(i)} = 0$ has been employed. Notice that while these topological charges are conserved, their value depend on the employed coordinate system. The reason for this is that the conserved current $j^\mu_{(i)}$ is constructed locally, that is, it is coordinate-dependent. However, for a fixed reference frame these charges gather important information about the different homotopy classes of solutions. Namely, two solutions that connect asymptotically different points cannot be deformed continuously one into the other without intermediate infinite-energy configurations. This is the reason why solutions are frequently grouped according to their topological charges into the same topological sector. These sectors are commonly denoted as $C^{\alpha\beta}$, where α and β are the vacua that such solution asymptotically joins at $x \to -\infty$ and $x \to \infty$ respectively. Furthermore, it is also common in the literature to encounter a classification of solutions into topological and non-topological solutions:

- **Topological:** We shall say that a solution is topological when not all the corresponding topological charges vanish, this is, $Q_i \neq 0$ for at least one of the i indices.
- **Non-Topological:** Similarly, a solution will be said to be non-topological when all its topological charges vanish $Q_i = 0\ \forall i$.

Making use of these topological charges to label solutions is very convenient to distinguish between topological sectors. However, these charges will not characterise entirely the homotopy class of solutions in certain cases. For instance, solutions in a regular lattice have degeneracy of topological charges. Moreover, notice that if a non-simply connected target space is chosen, labelling the end and final points is not enough to classify solutions homotopically. This matter will be explored in depth later on. Finally, once a synthesis of the necessary foundation for field theories has been presented, we are sufficiently prepared to address the concept of topological defect.

1.2 Topological defects

Different topological properties allow new and interesting scenarios in physics to emerge. One of these breakthroughs in the history of physics was Dirac's monopole [57] in 1931. During several decades magnetic monopoles were thought to be unquestionably precluded by nature. In fact, etched in stone Maxwell's equations in the early 1860s considered the divergence of the magnetic field to be zero based on experimental results. Dirac provided a theoretical environment where the magnetic monopole could arise. The key behind this theory is the topological features of Gauge fields, in which different homotopy classes give rise to physically distinguishable states. In the particular case of Dirac's monopole, these solutions, homotopically different from that of vacua, were given the name of topological defects [134].

In the case under consideration, the topological restrictions arise from the asymptotic conditions imposed on solutions to ensure that their energies are finite. In fact, these topological defects have the distinctive feature that cannot be found perturbatively from other solutions due to this homotopic constraints. Indeed, the ends of this type of solutions are fixed at different points. Now, depending on the number of dimensions in the system and the physical context where these arise they are named differently. Interesting structures like Monopoles, skyrmions or sphalerons can be

found for Gauge theories with three spatial dimensions. Vortices can be identified when two spatial dimensions are considered. While these types of topological defects are remarkably rich structures that enables us to model a wide range of phenomena, this thesis will focus on the study of structures that emerge for only one spatial dimension, known as kinks in the literature.

1.2.1 Solitons in scalar field theory

Observing the propagation of waves on the surface of the water as in Russel's experiment, the notion of soliton comes somewhat intuitively. In field theory, this notion of propagating "heap" is recovered when the energy density profile corresponding to a particle is considered. As described before, the requisite that the energy of a field configuration must be finite makes us impose that limits at the ends of the spatial line of the energy density profile $\varepsilon(x,t)$ must tend to zero

$$\lim_{x\to\pm\infty} \varepsilon(t,\vec{x}) = 0 \tag{1.10}$$

in order to prevent the energy from diverging. Hence, since the energy density is a semidefinite positive function (1.5), this condition induces on the profile of the energy density a "heap-like" form. This is encapsulated in Rajaraman's definition of solitary wave in field theory [117], which can be stated as follows:

Definition 1.2.1 (Rajaraman) *A solitary wave is any non-singular solution of any non-linear field equation (or coupled equations) that satisfies the following two conditions:*

1. *The total energy is finite.*
2. *The energy density has a space-time dependence of the form $\varepsilon(t,x) = \varepsilon(\vec{x}-\vec{v}t)$ where $\vec{v}$ is a velocity vector.*

This type of solution has indeed a localised energy density profile and it is travelling with constant velocity and without losing its form. Notice that the term "localised" refers here to the fact that fields are extended in such a manner that the finiteness of the total energy is ensured. Also, notice that Drazin's condition of preserving the identity of "heaps" is lost. According to the above definition, after a collision of solitons the original energy density profiles may not be necessarily recovered.

Now, in order to find an energy density of the form $\varepsilon(t,x) = \varepsilon(\vec{x}-\vec{v}t)$, the form of fields $\phi^i(t,x) = \phi^i(\vec{x}-\vec{v}t)$ will be considered. This implication can be trivially checked substituting this dependence in equation (1.6). Furthermore, if a field of the form $\phi^i(t,x) = \phi^i(\vec{x}-\vec{v}t)$ exists, one could choose the reference frame where this is a static solution. Indeed, a travelling field configuration with velocity v is related to the corresponding static field configuration by means of a Lorentz transformation $\Lambda_v : \mathbb{R}^{1,n} \to \mathbb{R}^{1,n}$

$$\phi^i_{\vec{v}}(x,t) = \phi^i(\Lambda_v(t,x)) = \phi^i(\vec{x})\,.$$

This static configuration, in turn, leads to a static energy density $\varepsilon_{\vec{v}}(t,x) = \varepsilon(x)$. It is therefore sufficient to search for static solutions to construct this type of solutions, for which the corresponding energy density will be localised and propagating at constant velocity. In practice, this means that instead of trying to solve the general

field equations (1.3), the search of these solutions is tantamount to solving the static field equations

$$\sum_{a=1}^{n} \frac{\partial^2 \phi^i}{\partial x_a^2} = \frac{\partial V}{\partial \phi^i} \qquad \forall i\,, \tag{1.11}$$

which is a system of partial differential equations which do not involve time. Moreover, these equations are precisely those that are found when the following functional in $\mathbb{R}^n$ is extremised

$$E_{\rm st}[\phi] = \int_{\mathbb{R}^n} \left[\frac{1}{2} \sum_{i=1}^{N} |\vec{\nabla}\phi^i|^2 + V(\phi^1, \ldots, \phi^N) \right] d^n x\,, \tag{1.12}$$

where ∇ and $|\ |^2$ are the standard gradient and norm in $\mathbb{R}^n$ respectively. In fact, $E_{\rm st}[\phi]$ is nothing but the energy (1.5) for static configurations $\phi^i(t,x) = \phi^i(x)\ \forall i$.

In conclusion, the problem of finding travelling solutions in Minkowski space $\mathbb{R}^{1,n}$ is equivalent to finding solutions of equations (1.11) in $\mathbb{R}^n$, this is, static configurations of minimal energy that can be set into motion by a boost. Lastly, it is worth noting that static equations (1.11) become considerably simpler when space-times with only one spatial dimension are considered. Indeed, in this scenario these become ordinary differential equations. In fact, this will not be the only particular feature of this scenario with only one spatial dimension. In the following section Derrick's theorem is presented, which will elucidate the correlation between spatial dimensions and the existence of static solutions.

1.2.2 Derrick's theorem

Lorentz invariance allows us to eliminate time from the field equations, simplifying the search of travelling kinks. If this type of solutions can be identified in the static equations, which minimise the static energy functional (1.12), then travelling kinks can be constructed. However, these static solutions cannot be found for any number of spatial dimensions. In this section, we delve into the intricacies of this limitation, referred to as Derrick's theorem [56], uncovering its underlying nuances.

Let us then assume that $\phi_s(x^1, \ldots, x^n)$ is a static solution of a field theory on $\mathbb{R}^{1,n}$ with a Lagrangian density of the type (1.2). With this solution let us construct a one-parameter family of configurations $\phi_\lambda(x)$ by performing a family of spatial dilations on the static solution $\phi_\lambda(x) = \phi_s(\lambda x^1, \ldots, \lambda x^n)$ for $\lambda > 0$. When this family of functions is substituted in (1.12) a real function $E_{\rm st}[\lambda]$ is obtained

$$E_{\rm st}[\lambda] = \int_{\mathbb{R}^n} \left[\frac{1}{2} \sum_{a=1}^{N} \sum_{i=1}^{n} \left(\frac{\partial \phi_\lambda^a}{\partial x^i} \right)^2 + V(\phi_\lambda^1, \ldots, \phi_\lambda^N) \right] d^n x\,,$$

which is extremised only for the value $\lambda = 1$. Now, since the energy functional $E_{\rm st}[\phi]$ is integrating over all $\mathbb{R}^n$, the integration domain is invariant under these dilations $x^i \to \tilde{x}^i = \lambda\, x^i$. However, the integrand is not invariant under spatial dilations

$$E_{\rm st}[\lambda] = \int_{\mathbb{R}^n} \left[\frac{1}{2} \sum_{a=1}^{N} \sum_{i=1}^{n} \lambda^2 \left(\frac{\partial \phi_s^a}{\partial \tilde{x}^i} \right)^2 + V(\phi_s^1, \ldots, \phi_s^N) \right] \frac{d^n \tilde{x}}{\lambda^n}\,,$$

where the arguments of the fields have been rescaled $\phi_s^i = \phi_s^i(\tilde{x}^1, \ldots, \tilde{x}^n)$. Since the actual solution is that with $\lambda = 1$, the following condition must be satisfied

$$\frac{dE_{\text{st}}}{d\lambda}\,[\lambda]\bigg|_{\lambda=1} = 0\,. \tag{1.13}$$

The limits of integration of the above functional are the infinities and therefore any dilation with $\lambda > 0$ leaves them unaltered. Thus, this last extremal condition for the static energy as a function can be written as follows

$$(2-n)\int_{\mathbb{R}^n} \frac{1}{2}\sum_{a=1}^{N}\sum_{i=1}^{n}\left(\frac{\partial\phi_s^a}{\partial\tilde{x}^i}\right)^2 d^n\tilde{x} - n\int_{\mathbb{R}^n} V(\phi_s^1, \ldots, \phi_s^N)d^n\tilde{x} \equiv (n-2)I_1 - nI_2 = 0\,,$$

where both I_1 and I_2 are clearly positive semi-definite since I_1 integrates a sum of squares and I_2 integrates the potential function, which is in turn by definition positive semi-definite. Hence, extremal condition (1.13) imposes a different relation between quantities I_1 and I_2 for each number of spatial dimensions n in the Minkowski space $\mathbb{R}^{1,n}$

$$(2-n)I_1 = nI_2\,. \tag{1.14}$$

Since only configurations for which the energy is finite are considered, asymptotic conditions make both I_1 and I_2 finite. This requirement leaves us with three different scenarios:

1. When only one spatial dimension is considered $n = 1$, equation (1.14) reads $I_1 = I_2$. Since solutions will be curves in $\mathbb{R}$, solving the static equations in this case is conceptually equivalent to solving those of a mechanical problem. Next section will be devoted to studying this in depth.

2. Two spatial dimensions $n = 2$ produce in equation (1.14) condition $I_2 = 0$. This in turn, given that the potential function is positive semi-definite, implies that it is the potential function itself that must vanish $V(\phi_s(x^1, x^2)) = 0$ for the whole image of ϕ_s. Consequently, either the potential function is identically zero or the static configuration $\phi_s(x^1, x^2)$ takes values only inside the vacuum manifold $\mathcal{M}$. Considering that for static field configurations with non-vanishing energy at least one of the field profiles must be non-constant, the existence of these static solutions for the case $n = 2$ requires the vacuum manifold to contain at least a continuum.

3. Cases with $n \geq 3$ are forbidden in equation (1.14) since both I_1 and I_2 are positive semi-definite. As a consequence, under these conditions, no static configuration can exist for more than two spatial dimensions.

In summary, for the considered scalar field theories, Derrick's theorem restricts the existence of static solutions with finite energy outside the vacuum manifold to field theories on the $(1+1)-$dimensional Minkowski space. Nonetheless, this limitation can be evaded by ignoring the condition of finite energy or altering the dependence of the Lagrangian density, so that it includes terms that modify equation (1.14). Lastly, one could consider other alternatives with more profound implications, like a non-local Lagrangian density. That is, a Lagrangian density that depends on spatial coordinates to avoid this scaling invariance lack [106]. Notice that in that scenario,

while more freedom is obtained to find static solutions in theories with more spatial dimensions, the momenta is not conserved anymore since the spatial invariance is lost. In any case, we shall focus on the case with one spatial dimension, which as we shall see, can produce an abundance of analytically solvable theories.

1.2.3 Mechanical analogy

Derrick's theorem is highly restrictive, for the chosen form of the Lagrangian density there exist no static solutions with finite energy for a number of spatial dimension $n > 2$ and when $n = 2$ static fields must take their values inside the vacuum manifold. Consequently, as mentioned, we shall focus on the case when only one spatial dimension is considered $n = 1$. In fact, as has already been implied, a connection appears between the problem of searching for static solutions in $\mathbb{R}^{1,1}$ and mechanical systems. Indeed, solutions that minimise the static energy in $\mathbb{R}^{1,1}$

$$E_{\text{st}}[\phi] = \int \left[\frac{1}{2} \sum_{i=1}^{N} \left(\frac{d\phi^i}{dx} \right)^2 + V(\phi^1, \ldots, \phi^N) \right] dx \,, \tag{1.15}$$

are essentially curves $\phi_s : \mathbb{R} \to \mathbb{R}^n$. If the trick $V = -(-V) \equiv -U$ is performed in the static energy functional, this functional can be interpreted as the action $S_{\text{mec}}[\phi]$ of a mechanical system with mechanical potential $U(\phi^1, \ldots, \phi^N) = -V(\phi^1, \ldots, \phi^N)$

$$S_{\text{mec}}[\phi] \equiv E_{\text{st}}[\phi] = \int \left[\frac{1}{2} \sum_{i=1}^{N} \left(\frac{d\phi^i}{dx} \right)^2 - U(\phi^1, \ldots, \phi^N) \right] dx \,, \tag{1.16}$$

with mechanical coordinates $(\phi^1, \ldots, \phi^N)$ and where x plays the role of time. Thus, solutions $\phi(x)$ of this mechanical system will provide static solutions for the original scalar field theory. Alternatively, the same trick can be implemented in the Euler-Lagrange equations (1.11) for static solutions in $\mathbb{R}^{1,1}$, which are now ordinary differential equations

$$\frac{d^2\phi^i}{dx^2} = \frac{\partial V}{\partial \phi^i} = -\frac{\partial U}{\partial \phi^i} \qquad \forall i \tag{1.17}$$

identical in form to Newton's equations. Note that since the potential of the field theory V is positive semi-definite, the potential function $U = -V$ defined for the analogue mechanical problem is negative semi-definite. That is to say, while solutions in the field theory will asymptotically join minima of the potential, in the mechanical system they will link maxima. On the other hand, this mechanical analogy brings some constrictions to the analogous mechanical system. In order to guarantee that the energy of solutions in the field theory is finite, conditions (1.7) and (1.8) at infinities for the fields are also imposed on the static fields $\phi^i(x)$ as coordinates of the mechanical system. Given the inherited form of the Lagrangian (1.16), the energy i_1 of a given solution of this mechanical system

$$i_1 = \sum_a \frac{1}{2} \left(\frac{d\phi^a}{dx} \right)^2 + U(\phi^1, \ldots, \phi^N) \,, \tag{1.18}$$

is a conserved quantity. Therefore, its value must be the same at any mechanical time x. In particular, the energy must coincide with its value in the asymptotic

limits of the mechanical time x

$$i_1 = \lim_{x\to\pm\infty}\left[\sum_a \frac{1}{2}\left(\frac{d\phi^a}{dx}\right)^2 - V(\phi^1,\ldots,\phi^N)\right] = 0\,, \tag{1.19}$$

which is zero because of the asymptotic conditions. Hence, differentiable solutions $\phi_0(x)$ with zero energy of the mechanical system with equations (1.17) and with potential $U = -V$, correspond to static solutions with finite energy in a field theory with potential V. These, in turn, are set into motion by a boost

$$\phi_0^i(x) \longrightarrow \phi_v^i(t,x) = \phi_0^i\left(\frac{x-vt}{\sqrt{1-v^2}}\right)$$

and therefore transformed into solutions for which the energy density is travelling with constant velocity and without losing their form. This type of solitons that arise in the $n = 1$ scenario are known in the literature as kinks. In fact, the study of this type of solutions in various contexts shall constitute the primary focus of this thesis.

Notice that finding static kinks by solving the equations of motion of a mechanical system presents some advantages. Newton's equations involve total derivatives, while field equations involve partial derivatives. This implies that theorems of existence and uniqueness of solutions will be available in general, unlike in the scenario with differential equations in partial derivatives. Furthermore, from the fact that the mechanical energy is zero (1.18) the Virial theorem immediately follows

$$T = V\,,$$

with T the kinetic part of the action of the field theory. This condition is significantly stronger than that that follows from Derrick's theorem (1.14) for $1+1-$dimensional spacetimes. Now the difference $T - V$ is forced to be identically zero and not only its integral, as Derrick's theorem imposes in $1+1-$dimensions

$$\int (T-V)\,dx = 0\,. \tag{1.20}$$

Furthermore, through this mechanical analogy method, we can employ a range of potent techniques from classical mechanics. In particular, given that the energy vanishes, Hamilton-Jacobi formalism can simplify the search of these static solutions when certain type of potentials are considered. This will be explored in next section.

1.2.4 Integrability in classical mechanics

The search of kinks will lead us to systems of differential equations that correspond to mechanical systems. If these equations can be integrated, then kink-type solutions for the field theory can be obtained. However, multiple definitions of integrability for a mechanical system coexist in the literature. In our case, Arnold-Liouville's definition will be employed. Even if this forces us to step in Hamiltonian terrain, this path will equip us with indispensable tools to construct the type of fields theories we wish to find, that is, those whose solutions can be analytically identified.

Let us denote as M the $n-$dimensional configuration space of a mechanical system and TM its tangent bundle, which will also be referred to as position-velocity

phase space, whose dimension is $2n$. Legendre transformation is, under certain convexity conditions that are satisfied here, an isomorphism between the tangent bundle TM and the cotangent bundle T^*M, which shall be referred to as phase space. In order to make the Legendre transformation $\dot{q}_i \to p_i = \frac{\partial L}{\partial q_i}$ convex, the following condition is imposed on the Lagrangian:

$$\frac{\partial^2 L}{\partial \dot{q}_i \partial \dot{q}_j} \neq 0 \qquad \forall i, j \,.$$

This transformation allows us to deal with functions on T^*M instead of TM without losing any information. The motivation behind this change of scenario is the fact that it is always possible to define a symplectic form on T^*M, that is, a closed and non-degenerate $2-$form ω on M. Given this symplectic form, each function $f : T^*M \to \mathbb{R}$ will define a vector field X_f on M, generating a flow on it

$$i_{X_f}\omega = df \,, \tag{1.21}$$

where i_{X_f} represents the contraction with the vector field X_f and d is the exterior derivative operator. In natural/canonical coordinates $(q_1, \ldots, q_n, p_1, \ldots, p_n)$ on T^*M the symplectic form is written locally simply as

$$\omega = \sum_{i=1}^{n} dp_i \wedge dq_i \,.$$

If a particular function $H : T^*M \to \mathbb{R}$ is chosen, called the Hamiltonian of the system, then equation (1.21) reads in these coordinates as Hamilton's equations

$$\frac{dq_i}{dt} = \frac{\partial H}{\partial p_i} = \{H, q_i\} \,, \qquad \frac{dp_i}{dt} = -\frac{\partial H}{\partial q_i} = \{H, p_i\} \,, \tag{1.22}$$

where t is the parameter of the integral curves of X_H and the Poisson bracket $\{\cdot,\cdot\} : \mathcal{F}(T^*M) \times \mathcal{F}(T^*M) \to \mathcal{F}(T^*M)$ between functions $f, g : T^*M \to \mathbb{R}$ have been defined by means of the symplectic form

$$\{f, g\} \equiv \omega(X_f, X_g) \,.$$

Of course, in canonical coordinates this bracket, which has been constructed from the symplectic form, has the simpler and standard form

$$\{f, g\} = \sum_{i=1}^{n} \left[\frac{\partial f}{\partial p_i}\frac{\partial g}{\partial q_i} - \frac{\partial f}{\partial q_i}\frac{\partial g}{\partial p_i} \right] .$$

Notice that Hamilton's equations are a system of $2n$ first order differential equations, unlike Euler-Lagrange equations, which are n second order differential equations. It is also worth noting that any information about the geometry on M when this is chosen to be a Riemannian manifold, encoded in the metric tensor defined on M, will be encapsulated in the Hamiltonian function H itself. This will be further detailed later on. Now, in this context, from equations (1.22) it follows that conserved quantities are functions F_i for which the Poisson bracket with the Hamiltonian function vanishes $\{F_i, H\} = 0$. This result paves the way for stating the Arnold-Liouville theorem, from which our notion of integrability for mechanical systems will be derived.

Theorem 1 (Arnold-Liouville) *Given the phase space $T^*\mathbb{R}^{2n}$ with coordinates $(q_1,\dots,q_n,p_1,\dots,p_n)$ and Hamiltonian $H(q_1,\dots,q_n,p_1,\dots,p_n,t)$, if n conserved quantities are found, $\{F_i,H\}=0$ for $F_1,\dots,F_n$, functionally independent and in involution $\{F_i,F_j\}=0\ \forall i,j$, then Hamilton's equations can be solved by quadratures.*

In light of this theorem, we shall say that a mechanical system is integrable when these conserved quantities can be found, so that its equations can be solved by quadratures. In a general sense, the implication of having n conserved quantities whose variables are n coordinates q_i and n coordinates p_i, is that all $p_i(q_1,\dots,q_n)$ can be determined as algebraic set of equations. Indeed, this allows us to gather all the information in the phase space. Now, according to this definition of integrability, it follows that all one-dimensional mechanical systems derived from the mechanical analogy will always be integrable. The energy will be conserved and integrability in these cases requires only one conserved quantity. Unfortunately, in general there is no certainty that a complete set of conserved quantities can be found in higher dimensional mechanical systems. Therefore, integrability is not always guaranteed when the dimension of the analogue mechanical system is higher than one, this is, when the field theory has more than one field.

On the other hand, the Hamiltonian formalism grants us access to a particularly successful method known as Hamilton-Jacobi formalism. The first step in this procedure is finding another coordinate system $(q_i,p_i)\to(Q_i,P_i)$ in which Hamilton's equations are easier to solve. However, these coordinate transformations have to respect the structure of the symplectic form ω

$$\omega=\sum_{i=1}^{n}dp_i\wedge dq_i\longrightarrow\omega=\sum_{i=1}^{n}dP_i\wedge dQ_i\,,$$

i.e. they have to be what it is called symplectomorphisms or canonical transformations. Let us now consider the extended phase space $\mathbb{R}^{2n+1}$ with coordinates $(q_1,\dots,q_n,p_1,\dots,p_n,t)$. Given a Hamiltonian function H, the Poincaré-Cartan integral invariant can be defined as the following $1-$form

$$\alpha=p_idq_i-Hdt\,,$$

where the index i is summed. Let us denote as $\mathfrak{X}(M)$ the set of all vector fields on M. For the sake of convenience, let us also define the field of vortex directions $\xi\in\mathfrak{X}(M)$ of a $1-$form β as the vector field that satisfies

$$d\beta(\xi,\eta)=0\qquad\forall\eta\in TM\,,\tag{1.23}$$

which is uniquely determined when $d\beta$ is non-singular. It can be verified that integral curves of the field of vortex directions ξ of α are precisely the trajectories of the phase flow in the extended phase space [29]. That is, these are the trajectories that Hamilton's equations produce. Therefore, changes of coordinates that leave the form of the Poincaré-Cartan integral invariant unaltered will produce the same Hamilton's equations in other coordinates. However, in these transformations a degree of freedom that can be exploited appears. Indeed, an extra term dS can be included since the exterior derivative is a nilpotent operator $d^2\equiv0$

$$\sum_{i=1}^{n}p_idq_i-H(q_i,p_i,t)dt=\sum_{i=1}^{n}P_idQ_i-K(Q_i,P_i,t)dT+dS\,,$$

where K is the Hamiltonian function in the new canonical variables (Q_i, P_i) and S is a generic differentiable function that receives the name of generating function. Now, to obtain the Hamilton-Jacobi equation a particular form of the generating function $S(Q_i, q_i, t)$ is chosen. This type of generating function produces the following relation between coordinates

$$p_i = \frac{\partial S(Q_i, q_i)}{\partial q_i}\,, \qquad P_i = \frac{\partial S(Q_i, q_i)}{\partial Q_i}$$

and a set of Hamilton's equations from which conserved quantities can be directly identified

$$\frac{dQ_i}{dt} = 0 \qquad \frac{dP_i}{dt} = -\frac{\partial K}{\partial Q_i}\,.$$

The use of these generating functions to perform canonical transformations simplifies the resolution of the equations of motion of analogous mechanical systems. These will play a crucial role to find mechanical systems whose solutions can be obtained analytically. Indeed, it allows us to state the following theorem.

Theorem 2 (Jacobi's theorem) *If a general solution of the Hamilton-Jacobi equation*

$$\frac{\partial S}{\partial t} + H\left(q_i, \frac{\partial S}{\partial q_i}, t\right) = 0 \tag{1.24}$$

is found so that it depends on n parameters Q_i and such that

$$\frac{\partial^2 S}{\partial q_i \partial Q_j} \neq 0 \qquad \forall i, j\ , \tag{1.25}$$

then Hamilton's equations of the system can be solved by quadratures and the following quantities are conserved

$$P_i = \frac{\partial S(Q_i, q_i)}{\partial Q_i}\,.$$

Note that condition (1.25) is again required to guarantee the convexity of such transformation. Now, even if this method seems to complicate more the search of solutions given that we are dealing with an equation in partial derivatives, in reality it will reduce the search of solutions to systems in which the integrability is guaranteed. In particular, in the context of analogous mechanical systems, as it had been shown, the energy of any solution must vanish. This implies that Hamilton-Jacobi equation (1.24) reads in this case as follows

$$H\left(q_i, \frac{\partial S}{\partial q_i}\right) = 0\,. \tag{1.26}$$

Let us now be more concrete about the type of theories that will be considered in this thesis. The inherited Lagrangians from the chosen type of field theories will be time-independent and natural, but these will be written in general in the form

$$L\left(q_i, \dot{q}_i\right) = \frac{1}{2} g_{ij}(q)\dot{q}^i\dot{q}^j - U(q)\,,$$

where $g_{ij}(q)$ are the components of the corresponding metric tensor and where U is the mechanical potential. Notice that the form of the Lagrangian density considered

until now (1.2) is recovered when Cartesian coordinates are taken in the Euclidean case $g_{ij} = \delta_{ij}$. Since the momentum conjugate is $p_i = g_{i\alpha}\dot{q}^\alpha$, the Hamiltonian function can be written as

$$H\left(q^i, p_i\right) = \frac{1}{2} g^{ij}(q)\dot{p}_i\dot{p}_j + U(q)\,.$$

Given that the mechanical systems that shall be studied will be derived from a field theory, let us replace the mechanical potential $U = -V$ by that of the field theory V and let us write for convenience $q^i = \phi^i$. Furthermore, given the chosen type of generating function, relation $p_i = \frac{\partial S}{\partial q_i}$ is satisfied and Hamilton-Jacobi equation (1.26) leads to a condition for the potential function

$$\frac{1}{2} g^{ij}(q)\frac{\partial S}{\partial q_i}\frac{\partial S}{\partial q_j} - V(\phi) = 0 \qquad \Rightarrow \qquad V(\phi^1, \ldots, \phi^n) = \frac{1}{2} g^{ij}(q)\frac{\partial S}{\partial \phi^i}\frac{\partial S}{\partial \phi^j}\,, \tag{1.27}$$

where both signs, S and $-S$, produce the same potential function. Therefore, field theories for which the corresponding potentials can be written in terms of derivatives of a differentiable function $S(\phi^1, \ldots, \phi^n)$ as in equation (1.27) have an integrable analogue mechanical system. This is, static solutions of these field theories will be analytically available by quadratures

$$p_i = \frac{\partial S}{\partial q_i} = g_{ik}\dot{q}^k \quad \Rightarrow \quad \dot{q}^j = g^{ji}\frac{\partial S}{\partial q_i} \quad \Rightarrow \quad \frac{d\phi^j}{dx} = g^{ji}\frac{\partial S}{\partial q_i}\,. \tag{1.28}$$

Notice that these are first order differential equations, unlike Newton's equations. This generating function S usually receives the name of superpotential in the context of kinks and it is commonly denoted as W. This terminology is inherited by the supersymmetry context.

1.2.5 Bogomol'nyi arrangement for Euclidean target spaces

In the previous section the notion of integrability in classical mechanics and the Hamilton-Jacobi formalism are summarised. If the form of the potential function of the analogue mechanical system of a field theory allows us to employ the Hamilton-Jacobi formalism, solutions of the Hamilton-Jacobi equation will provide us with static solutions for the original field theory. In this section an alternative approach is summarised, known in the literature as Bogomol'nyi arrangement [46]. In this chapter, the target space of the field theories that shall be considered will be Euclidean $\mathbb{R}^N$. Moreover, for illustration purposes, let us consider Cartesian coordinates in $\mathbb{R}^N$. The type of field theories that shall be considered is restricted to those for which the potential term V can be written as

$$V(\phi^1, \ldots, \phi^N) = \frac{1}{2}\sum_{i=1}^{N}\left(\frac{\partial W}{\partial \phi^i}\right)^2\,, \tag{1.29}$$

where $W : \mathbb{R}^N \to \mathbb{R}$ is a differentiable function called superpotential. Bogomoln'nyi arrangement in this case consists in writing the static energy functional as the sum

of the following terms

$$E[\phi] = \frac{1}{2}\int dx \sum_{i=1}^{N}\left(\frac{d\phi^i}{dx} + (-1)^a \frac{\partial W}{\partial \phi^i}\right)^2 + \left|\int dx \frac{d\phi^i}{dx}\frac{\partial W}{\partial \phi^i}\right|,$$
$$= \frac{1}{2}\int dx \sum_{i=1}^{N}\left(\frac{d\phi^i}{dx} + (-1)^a \frac{\partial W}{\partial \phi^i}\right)^2 + \left|\int dW\right|,$$

where $a = 0, 1$. The second integral is constant when solutions within a particular topological sector are considered, e.g. when the final and initial points of kinks are fixed

$$\left|\int dW\right| = \left|\lim_{x\to\infty} W(\phi) - \lim_{x\to-\infty} W(\phi)\right|. \tag{1.30}$$

This implies that this functional $E[\phi]$ is minimised within a topological sector when the squares in the first integral vanish. Solutions that satisfy these first order differential equations, which receive the name of Bogomol'nyi equations

$$\frac{d\phi^i}{dx} = (-1)^a \frac{\partial W}{\partial \phi^i}, \tag{1.31}$$

will be referred to as BPS-kinks, named after Bogomol'nyi, Prasad and Sommerfield. Note that the global factor $(-1)^a$ could be absorbed in the spatial variable x, which means that kinks and antikinks are obtained for different values of a. If the superpotential $W(\phi)$ and the field profiles of the BPS kinks are smooth functions, then the second integral becomes a topological charge that corresponds to the static energy of these kinks

$$E = \left|\lim_{x\to\infty} W(\phi) - \lim_{x\to-\infty} W(\phi)\right|, \tag{1.32}$$

which depends only on the vacua that are being asymptotically connected by the BPS kinks. Naturally, it can be straightforwardly checked that these BPS kinks are also static solutions of the field equations (1.3). Furthermore, this approach allows us to instantly compute the energy of a kink if the superpotential is differentiable along its path. Conversely, if this is not the case, the curve must be split into different pieces where the procedure (1.30) can be performed. Lastly, it should be highlighted that, as has been advanced, Bogomol'nyi equations (4.6) corresponds to Hamilton-Jacobi equations (1.28) when the mechanical energy vanishes. Even if these equations only seem to be identified for Euclidean target spaces $g_{ij} = \delta_{ij}$, in future chapters the full correspondence will be shown in general.

On the other hand, since Bogomon'nyi's equations are a set of first order differential equations, information about crossings of these solutions follows from the Picard-Lindelöf theorem. If the superpotential W is continuously differentiable, and therefore Lipschitz continuous, then a unique solution exists for this equation at each point. This means, in turn, that solutions of Bogomol'nyi equations, given a superpotential of this type, do not intersect at any point. However, if the superpotential is not continuously differentiable at any point, crossings of solutions of the same differential equation may occur. This is also related to the presence of points in solutions where the tangent vector is not well-defined. Indeed, the existence of

these "conjugate points" where families of kink orbits intersect, implies that these kinks are unstable in the context of Morse theory [14].

Under the condition of differentiability for the superpotential, solutions of Bogomol'nyi equations for a given superpotential are not allowed to cross. Nevertheless, it is worth noting that a potential function may admit more than one superpotential when the Bogomol'nyi arrangement is performed. In such cases, intersections may arise between solutions derived from different systems of differential equations, even if the superpotential of each system is continuously differentiable. See [23] for an example of intersection of solutions in the context of the Wess-Zumino model.

1.2.6 A criterion for stability of kinks

The mechanical analogy is a method that facilitates the identification of kinks. However, the stability of these solutions has not yet been addressed. By definition, a static configuration ϕ_K does not evolve in time

$$\frac{\partial \phi_K^i}{\partial t} = 0 \quad \forall i = 1, \dots, N \,,$$

where N denotes the number of field in the theory. However, if a perturbation is performed on this kink, the resulting configuration may evolve so that it never abandons the vicinity of the static solution or so that it never returns to it. In this sense, static kinks are said to be stable or unstable depending on their behaviour after these perturbations. In particular, among all notions of stability, that against small linear perturbations will be studied. This will be referred to as linear stability under small perturbations. These slightly perturbed solutions $\phi(t,x)$ of a static solution $\phi_K(x)$ can be written in coordinates as

$$\phi^i(t,x) = \phi_K^i(x) + \epsilon\ \psi^i(t,x) \,,$$

where the variation field $\psi(t,x)$ contains the information of how this perturbation is performed and the parameter that controls the intensity of the perturbation ϵ is a small real number. Moreover, we will be interested in a very particular type of small linear perturbation. Those that are solutions of the field equations to the first order in the parameter ϵ will encapsulate the leading markers of its evolution. These are the perturbations for which the evolution must be closely observed. In order to search for these, the field configuration $\phi(t,x)$ is introduced in the field equations (1.11), where only terms up to degree ϵ^1 are kept and the rest ϵ^i with $i > 2$ are neglected. This produces the following condition on the variation field $\psi(t,x)$

$$-\frac{\partial^2 \psi^i}{\partial x^2} + \left.\frac{\partial^2 V}{\partial \phi^i \partial \phi^k}\right|_{\phi_K} \psi^k = -\frac{\partial^2 \psi^i}{\partial t^2} \,, \quad i = 1, \dots, N \,. \tag{1.33}$$

These equations define those perturbations that contain the leading information about the stability of a static solution. However, this is a system of coupled differential equations in partial derivatives where both time and space are involved. Thus, solving these equations analytically is in general highly non-trivial. With the purpose of sidestepping this issue, a Fourier transform for all components ψ^i of the field variation is performed

$$\psi^i(t,x) = \frac{1}{\sqrt{2\pi}} \int_{-\infty}^{\infty} e^{i\omega t} \sigma^a(x,\omega)\ d\omega \,, \tag{1.34}$$

for new functions $\sigma^a(x,\omega)$. When these expressions are introduced in the above condition (1.33), the following spectral equations are obtained

$$-\frac{d^2\sigma^j}{dx^2}+\left.\frac{\partial^2 V}{\partial\phi^j\partial\phi^k}\right|_{\phi_K}\sigma^k=\omega^2\sigma^j \quad j=1,\dots,N. \tag{1.35}$$

Solutions of these spectral equations define small linear perturbations that are solutions of the field equations to the first order in the parameter of the variation ϵ. Perturbations for which $\omega^2>0$ will make the static solution linearly stable, since the integrand in equation (1.34) will be bounded in time. However, when $\omega^2<0$ the kink will be linearly unstable, as the evolution of this perturbation will grow and move away from the static solution. Finally, it is noteworthy to mention that these spectral equations are usually presented in the matricial form

$$\mathcal{H}\sigma=\omega^2\sigma\,,$$

where $\sigma=(\sigma^1,\dots,\sigma^N)^T$ and the operator H, which receives the name of Hessian operator, reads

$$\mathcal{H}=\left.\begin{bmatrix} -\frac{d^2}{dx^2}+\frac{\partial^2 V}{\partial\phi_1^2} & \cdots & -\frac{d^2}{dx^2}+\frac{\partial^2 V}{\partial\phi_N\partial\phi_1} \\ \vdots & \ddots & \vdots \\ -\frac{d^2}{dx^2}+\frac{\partial^2 V}{\partial\phi_1\partial\phi_N} & \cdots & -\frac{d^2}{dx^2}+\frac{\partial^2 V}{\partial\phi_N^2} \end{bmatrix}\right|_{\phi=\phi_K(x)}. \tag{1.36}$$

1.3 Examples of kinks

The last sections establish the foundations for the search of travelling kinks in a wide variety of Lorentz invariant field theories. In summary, static solutions are sought in the field equations, leading to equations that can be interpreted as Newton's equations of a mechanical system. Through this approach, the powerful arsenal of techniques in classical mechanics can be employed to solve these equations and set this static configuration into motion via a boost. This section presents three models of historical importance to offer a more tangible understanding of the concept of kink.

1.3.1 The ϕ^4-model

The ϕ^4-model takes the spotlight as the first model that will be presented, which is arguably one of the most relevant models in field theory. This model was first introduced in 1937 by Landau to describe phase transitions in condensed matter [94, 95]. However, it was not until 1960 that it was employed in particle physics [70, 108] and since then this model has become ubiquitous. The main interest of this model lies in the symmetry breaking mechanism it presents. This can shed light, for instance, on the emergence of preferred directions in materials at low temperatures, leading to the formation of ordered phases. Further examples include ferromagnets, liquid crystals, superconductors and even the simplified version of the Higgs model in high-energy physics [140].

Although this model can be constructed with multiple fields, the simplest version of this model consists in a real scalar field $\phi:\mathbb{R}^{1,1}\to\mathbb{R}$ on the $1+1-$dimensional

Minkowski space, where kinks will be sought. Now, for historical reasons let us write the potential function of this model as

$$V(\phi) = \frac{\lambda}{4}\left(\phi^2 - \frac{m^2}{\lambda}\right)^2 , \tag{1.37}$$

where λ and m are positive real numbers. From the form of this potential immediately follows that the vacuum manifold is discrete and contains two points

$$\mathcal{M} = \left\{-\frac{m}{\sqrt{\lambda}}, \frac{m}{\sqrt{\lambda}}\right\} .$$

Notice that the separation between these minima, represented in Figure 1.2, is simultaneously modulated by both parameters m and λ, while the height of the potential is exclusively controlled by the parameter λ.

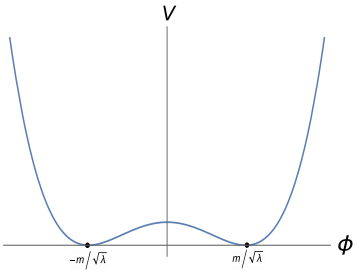

Figure 1.2: The potential function of the ϕ^4-model presents two vacua, whose separation is modulated by the value of $\frac{m}{\sqrt{\lambda}}$. The height of the peak is controlled by the parameter λ.

The dynamics of this model is governed by the differential equation obtained by introducing the above potential into the Euler-Lagrange equation (1.3). This provides the following differential equation in partial derivatives

$$\frac{\partial^2\phi}{\partial t^2} - \frac{\partial^2\phi}{\partial x^2} = -\lambda\phi\left(\phi^2 - \frac{m^2}{\lambda}\right) .$$

Since static solutions are sought to obtain travelling solutions, this last equation is reduced to an ordinary differential equation

$$\frac{d^2\phi}{dx^2} = \lambda\phi\left(\phi^2 - \frac{m^2}{\lambda}\right) . \tag{1.38}$$

It is worth noticing that constant solutions at minima $\phi = \pm\frac{m}{\sqrt{\lambda}}$ are solutions of this equation. However, the energy density and consequently the energy of these solutions

$$E[\phi] = \int_{-\infty}^{\infty} dx \left[\frac{1}{2}\left(\frac{\partial\phi}{\partial t}\right)^2 + \frac{1}{2}\left(\frac{\partial\phi}{\partial x}\right)^2 + \frac{\lambda}{4}\left(\phi^2 - \frac{m^2}{\lambda}\right)^2\right]$$

vanish. The order of equation (1.38) can be reduced by means of the substitution $p = \frac{d\phi}{dx}$. This change of variables $(\phi, x) \to (p, \phi)$ allows us to obtain a first order differential equation

$$p\frac{dp}{d\phi} = \lambda\phi\left(\phi^2 - \frac{m^2}{\lambda}\right)$$

which, given that $p\frac{dp}{d\phi} = \frac{1}{2}\frac{dp^2}{d\phi}$, can be directly integrated resulting in a familiar equation

$$\frac{1}{2}p^2 = \frac{\lambda}{4}\left(\phi^2 - \frac{m^2}{\lambda}\right)^2 + C\,. \tag{1.39}$$

where C is the integration constant. Indeed, the constant C in equation (1.39) is nothing but the energy of the mechanical system. Therefore, since finite energy field configurations are sought, this constant C must vanish due to the asymptotic conditions. This is consistent with a previously shown result, the corresponding mechanical energy of any finite energy solution in a field theory must be zero. Now, the disappearance of this constant C in the expression (1.39) simplifies the search of the explicit solution. Instead of an elliptic integral, an immediate integral is found and the following two solutions are obtained

$$\phi(x) = \pm\frac{m}{\sqrt{\lambda}}\tanh\frac{m(x-x_0)}{\sqrt{2}}\,.$$

These asymptotically connect both minima $\phi = \pm\frac{m}{\sqrt{\lambda}}$, but each trajectory proceeds along a distinct direction, see Figure 1.3. The monotonic increasing field profile shall be referred to as kink, while the monotonic decreasing solution shall be referred to as antikink.

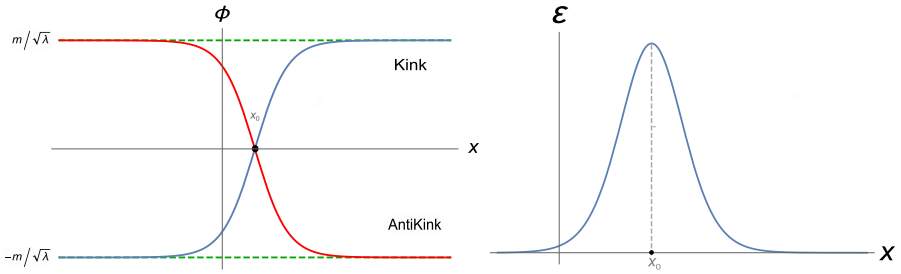

Figure 1.3: Kink and antikink profiles on the left and their energy density profile on the right for the ϕ^4-model. These solutions asymptotically join both minima of the theory and their static energy density is clearly localised around a point.

Moreover, the topological charges of the kink and the antikink will be additive inverses since their field profiles are related by a reflexion $x \to -x$

$$Q_{\text{Kink}} = -Q_{\text{Antikink}} = \frac{2m}{\sqrt{\lambda}}\,.$$

These are therefore topological kinks. On the other hand, the static energy density of both kink and antikink describes the same static heap

$$\varepsilon(x) = \frac{m^4}{2\lambda}\text{sech}^4\frac{m}{\sqrt{2}}(x-x_0)\,.$$

The integration of this energy density provides the energy for both kink and antikink, which are identical

$$E\left[\phi_{\text{Kink}}\right] = E\left[\phi_{\text{Antikink}}\right] = \frac{2\sqrt{2}}{3}\frac{m^3}{\lambda} \equiv M\,.$$

Finally, when a boost is introduced, the energy density describes the same lump but in motion with a constant velocity v while preserving it original form

$$\varepsilon(x,t) = \frac{m^4}{2\lambda(1-v^2)}\text{sech}^4\frac{m}{\sqrt{2}}\left(\frac{x-vt-x_0}{\sqrt{1-v^2}}\right) .$$

Similarly, the energies of the moving kink and antikink will be affected by the velocity at which they propagate

$$E\left[\phi_{\text{Kink,v}}\right] = E\left[\phi_{\text{Antikink,v}}\right] = \frac{M}{\sqrt{1-v^2}} .$$

Lastly, a study can be conducted to assess the stability against small linear perturbations of these kinks. For the vacuum solutions $\phi = \pm\frac{m}{\sqrt{\lambda}}$ the spectral equation (1.35), where the information about this type of stability is encoded, reads

$$-\frac{d^2\sigma}{dx^2} + 2m^2\sigma = \omega^2\ \sigma .$$

This implies that only a continuous spectrum appears, beginning at $\omega^2 = 2m^2$. Since all values of this eigenvalue are positive $\omega^2 > 0$, these solutions are linearly stable as it was expected. On the other hand, information about the linear stability of the non-constant static kinks can also be obtained. Their spectral equation read

$$-\frac{d^2\sigma}{dx^2} + m^2\left(2 - 3\ \text{sech}^2\frac{m(x-x_0)}{\sqrt{2}}\right)\sigma = \omega^2\ \sigma ,$$

which corresponds to that of a Pösch-Teller potential [105], see Appendix A. A continuous spectrum arises at $\omega^2 = 2m^2$ and the discrete spectrum is given by

$$\omega_n^2 = 2m^2 - \frac{m^2(2-n)^2}{2} , \quad \text{with} \quad n = 0, 1, 2 .$$

This implies that apart from a continuous spectrum, three different vibrational modes are found

$$\omega_0^2 = 0 , \qquad \omega_1^2 = \frac{3m^2}{2} , \qquad \omega_2^2 = 2m^2 .$$

Notice that a perturbation given by $\omega_0^2 = 0$ transforms static solutions into static solutions to the first order in the parameter of the variation. This type of perturbation is known in the literature as zero mode and springs from translational invariance of the centre of the kink x_0. In conclusion, since no negative value of ω^2 is found in the spectrum, these kinks are stable against small linear perturbations. Lastly, it should be pointed out that, alternatively, kinks for this model could have been found by employing the superpotential formalism (1.27). Indeed, this function can be chosen as

$$W(\phi) = \sqrt{\lambda}\left(\frac{m^2}{\lambda}\phi - \frac{\phi^3}{3}\right) ,$$

and the same solutions are retrieved by solving the first order differential equations (1.28). This more direct approach will be used in future chapters.

1.3.2 Sine-Gordon model

The Sine-Gordon equation was found in 1862 by Edmond Bour while studying surfaces of constant negative curvature [45]. Subsequently, this equation emerged in various fields of physics, including the current topic of study, field theory. In particular, this equation is a second order equation in partial derivatives which is usually[2] written in the form

$$\frac{\partial^2\phi}{\partial x^2} - \frac{\partial^2\phi}{\partial t^2} = \sin\phi\,.$$

It is worth noting that not only is this equation invariant under Lorentz transformations, but it is also of the same form as Euler-Lagrange equation. Consequently, it seems reasonable to expect this equation to come from a field theory. In fact, as is the case with the KdV equation, this equation is one of the few examples of differential equations in partial derivatives for which an infinite amount of conserved quantities can be found for the associated field theory, a feature for which they are referred to as integrable. In this case, sine-Gordon equation appears when one considers a real scalar field $\phi : \mathbb{R}^{1,1} \to \mathbb{R}$ on the Minkowski space $\mathbb{R}^{1,1}$ and a periodic potential of the form

$$V(\phi) = m^2\,(1 - \cos\phi) = 2m^2 \sin^2\frac{\phi}{2}\,.$$

with a real number $m \in \mathbb{R}$ that modules its height, see Figure 1.4.

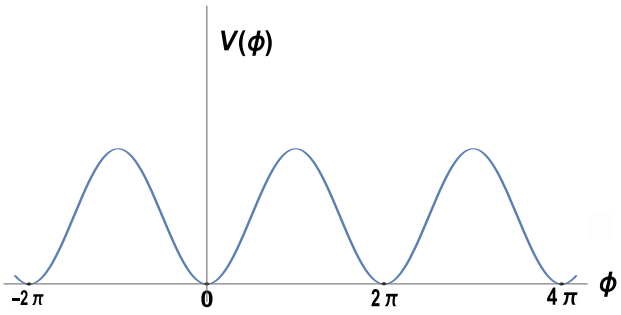

Figure 1.4: Example of potential in field theory that veils a Sine-Gordon equation. In particular, the potential with $m = 1$ has been depicted. This model presents an infinite number of periodically distributed minima.

The periodicity of this potential function implies the existence of an infinite amount of minima distributed periodically

$$\mathcal{M} = \{2\pi k / k \in \mathbb{Z}\}\ ,$$

which kinks could potentially join. Seeking static solutions and subsequently applying a boost is equivalent to directly searching for travelling solutions $\phi(x,t) = f(x - vt)$ with velocity $v \in \mathbb{R}$. Substituting this travelling form in the sine-Gordon equation, an equation equivalent to that for static solutions is obtained in terms of the variable $\varphi = x - vt$

$$\frac{d^2 f}{d\varphi^2}(1 - v^2) = m^2 \sin f(\varphi)\,.$$

[2] A rotation in the $t-x$ plane produces another common form in which this equation is presented $\phi_{xt} = \sin\phi$.

Indeed, the change of variable $\tilde{\varphi} = \frac{\varphi}{\sqrt{1-v^2}}$ retrieves the equation for static solutions

$$\frac{d^2 f}{d\tilde{\varphi}^2} = m^2 \sin f(\tilde{\varphi}) \, .$$

Let us now reduce the differential order $p = \frac{df}{d\varphi}$ exactly as in the ϕ^4-model by making the change of variables $(\phi, x) \to (p, \phi)$. This leaves an equation of the form

$$\frac{(1-v^2)}{2} p^2 = m^2 \left(C - \cos f\right) \, ,$$

where C is the integration constant. Similarly to the previous model, this constant must be determined through conditions at infinities in order to prevent the energy from diverging. However, asymptotic conditions in this case make this constant be set at $C = 1$. Naturally, this must be the case since for static solutions $v = 0$ the mechanical energy can be related to this constant as $E = m^2(C-1)$. This leads us to two solutions between $\phi \in (0, 2\pi)$

$$\phi(x,t) = 4 \arctan e^{\pm \frac{m(x-vt-x_0)}{\sqrt{1-v^2}}} \, ,$$

where x_0 is a constant that represents the centre of the kink. These are topological kink and antikink that asymptotically link the vacua located at $\phi = 0$ and $\phi = 2\pi$, see Figure 1.5.

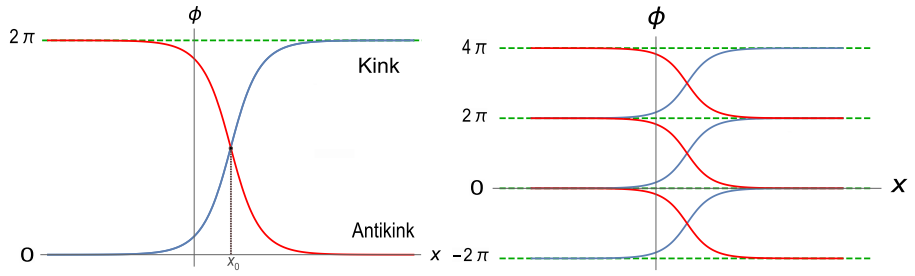

Figure 1.5: Kink profiles that emerge in the sine-Gordon model have been depicted asymptotically connecting a pair of vacua (left). These kinks are replicated between any other pair of vacua (right). Notice that since an infinite amount of vacua emerge in this model, an infinite number of kinks emerge.

Furthermore, even if the above solutions only join these two vacua, symmetries in the potential $V(\phi + 2\pi k) = V(\phi) = V(-\phi)$ for any $k \in \mathbb{Z}$, which are also present in the field equation, replicate these solutions so that they asymptotically connect any other adjacent pair of vacua, see Figure 1.5. This implies in turn that regardless of the pair of vacua that are being connected, the topological charge of any these kinks and antikinks is either $Q = 2\pi$ or $Q = -2\pi$. This case shows how relying solely on topological charges falls short in fully characterising solutions, as an infinite number of solutions share the same topological charge. It is important to emphasise that, as demonstrated in this section, for Lorentz invariant actions the method of the mechanical analogy can be replaced by the travelling condition $f(x - vt)$ to obtain this infinite number of travelling topological kinks and antikinks. Moreover, the energy density of any of these solutions is identical, which once more describes a travelling lump

$$\varepsilon(t,x) = \frac{4\, m^2}{1-v^2} \operatorname{sech}^2 \left(\frac{m(x-vt-x_0)}{\sqrt{1-v^2}} \right) \, ,$$

with a total energy that varies based on the velocity at which it is travelling

$$E[\phi_{\text{Kink}}] = E[\phi_{\text{Antikink}}] = \frac{8\,|m|}{\sqrt{1-v^2}}\,.$$

Similar to the scenario found in the ϕ^4-model, it is noteworthy that these solutions can also be derived by the Hamilton-Jacobi formalism (1.27), for which one can choose a superpotential of the form

$$W(\phi) = 2m \sin\frac{\phi}{2}\,.$$

Lastly, it should be noted that even if the above travelling solutions arise when the form $\phi(x-vt)$ is imposed, other types of solutions of this equation can be found. In [59] other solutions of the form

$$\phi(t,x) = 4\arctan\frac{F(x)}{G(t)}$$

are obtained by Bäcklund transformations for arbitrary functions $F(x)$ and $G(t)$, which represent kink-kink and kink-antikink collisions. Furthermore, the so-called breather soliton solution can be found [128], which maintains their shape while oscillating.

1.3.3 MSTB model

In the two previous models the integrability of the analogue mechanical system was guaranteed by the fact that only one scalar field was being considered. Indeed, the scenario involving only one field corresponds to a one-dimensional mechanical system where a conserved quantity, the energy, is always available. However, as previously indicated, the assurance of integrability does not hold consistently when dealing with field theories involving multiple scalar fields. Amidst this landscape of challenges, the Montonen-Sarker-Trollinger-Bishop model (MSTB model) stands out as an essential example of field theory with more than one scalar field for which the analogue mechanical system is integrable. In 1976, Montonen constructed a model [104] for complex scalar field theories exhibiting a global $U(1)$ symmetry in the search of charged solitons. Subsequently, Rajaraman and Weinsberg partially identified the kink variety of this model [116] and later in 1976 Sarker, Trullinger and Bishop examined the stability of these identified kinks [121]. As a result, the model acquired its name. Even though the entire kink variety had been found in 1976, families of non-topological kinks had only been identified through numerical methods. In 1984 Magyari and Thomas [98] found two conserved quantities for the analogue mechanical system, but it was not until 1985 that implicit expressions for the field profiles were derived by Ito [80, 81]. In this section an overview of the discovered kink variety will be presented, delving into the key details concerning the stability of these solutions.

The original MSTB model is in fact a one-parameter family of field theories with two scalar fields on $\mathbb{R}^{1,1}$ given by a Lagrangian density of the form (1.2), so that the potential can be written in Cartesian coordinates as

$$V(\phi_1,\phi_2) = \frac{1}{2}(\phi_1^2+\phi_2^2-1)^2 + \frac{\sigma^2}{2}\phi_2^2\,, \tag{1.40}$$

where ϕ_1 and ϕ_2 are dimensionless fields. In this wise, every value of the parameter $\sigma \in \mathbb{R}$ corresponds to a particular model. Notice that in absence of the last term $\sigma = 0$, the potential would exhibit a continuous vacuum manifold related by the continuous symmetry $U(1)$. Therefore, this extra term breaks the continuous vacuum manifold to produce a set of only two points that lie in the ϕ_1-axis

$$\mathcal{M} = \left\{v^1 = (-1, 0), v^2 = (1, 0)\right\} .$$

As this parameter σ deviates from zero, the potential function varies accordingly, see Figure 1.6 for a transition from $\sigma^2 = 0$ to $\sigma^2 = 1$. As we shall see, this transition in form of the potential for this range of the parameter σ^2 conceals radical changes in the corresponding kink variety.

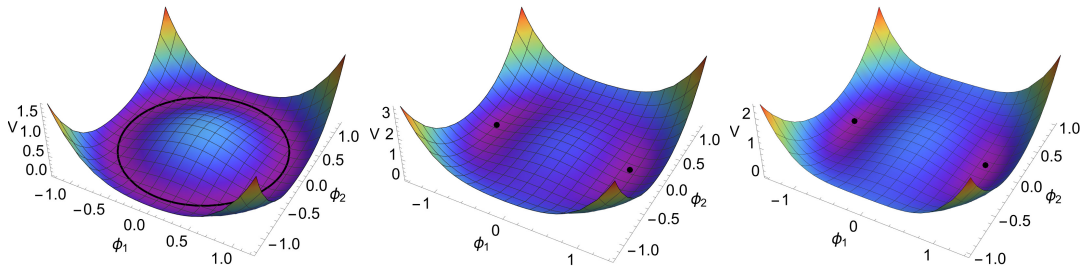

Figure 1.6: Potential functions for values $\sigma = 0$, $\sigma = 0.9$ and $\sigma = 1$ respectively. The continuous vacuum manifold is broken for non-vanishing values of the parameter σ, giving rise to a discrete set of only two points.

Given that these theories with $\sigma \neq 0$ have two vacua, four topological sectors appear C^{11}, C^{12}, C^{21} and C^{22}. Now, as usual, solutions will be grouped according to the vanishingness of their topological charges. This is, employing the topological and non-topological labels:

1. **Non-topological kinks**: These solutions leave v^1 or v^2 at one of the ends of the spatial line to return to the same vacua, v^1 or v^2 respectively, at the other. Therefore, among the four mentioned topological sectors, two could contain kinks of this type. Notice that unlike previous models, non-topological sectors C^{11} and C^{22} may not be empty due to the extra dimension in the target space.

2. **Topological kinks**: Two topological sectors arise when vacua v^1 and v^2 are asymptotically connected. Indeed, when the first end of the spatial line to be assigned is mapped to one of the vacua, two possibilities appear.

Let us try to find these kinks by searching for static solutions of the Euler-Lagrange equations for the potential function (1.40). These are a coupled system of two differential equations in which the parameter σ^2 is inherited

$$\frac{d^2\phi_1}{dx^2} = 2\phi_1(\phi_1^2 + \phi_2^2 - 1) , \qquad \frac{d^2\phi_2}{dx^2} = 2\phi_1(\phi_1^2 + \phi_2^2 - 1) + \sigma^2\phi_2 . \tag{1.41}$$

As mentioned, the first solutions were found by the trial orbit method, and only later the general solution was obtained. Thus, maintaining the historical order in which they were discovered, let us present them accordingly.

1. **TK1 kink**: The first trial orbit that will be discussed, which shall be referred to as TK1 kink, is the one characterised by condition $\phi_2 = 0$. This is in fact, as one can prove [24], the only possible kink-like solution for models given by values of the parameter $\sigma^2 \geq 1$. This trial orbit makes the second Euler-Lagrange equation hold trivially, while causing the first one to transform into that of a ϕ^4 model (1.38). This produces the following two static solutions

$$\phi_1 = \pm \tanh(x - x_0)\,, \qquad \phi_2 = 0\,,$$

that is, a topological kink and its antikink. The kink profiles and the energy densities are, up to constants, those of the ϕ^4-model described in a previous section, see Figures (1.3) and (1.7).

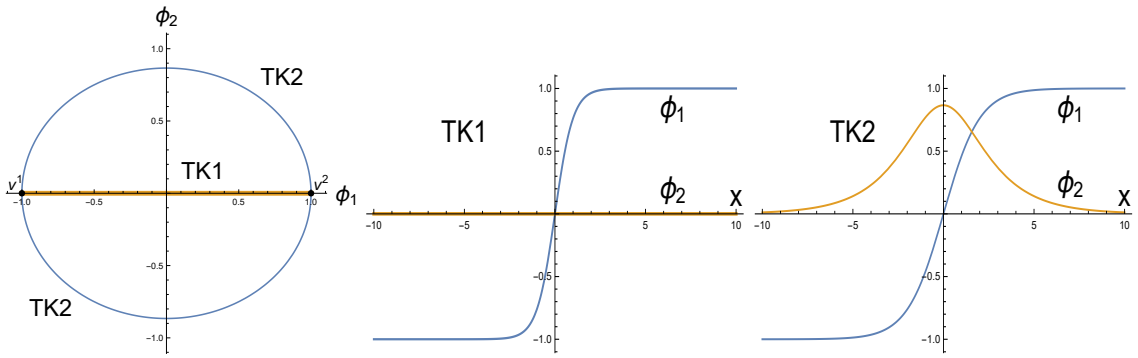

Figure 1.7: Kink orbits and profiles for the $TK1$ and $TK2-$kinks for the particular case of $\sigma = 0.5$ and $\epsilon_1 = \epsilon_2 = 0$.

Interestingly, the energy of these kinks is independent of the parameter σ

$$E[TK1] = \frac{4}{3}\,.$$

Furthermore, the stability of this type of kink can be analysed analytically. The second order differential operator that contains the information about small linear perturbations of these kinks $\mathcal{H}$ can be written as the following pair of equations

$$\begin{aligned} -\frac{d^2\eta^1}{dx^2} + (4 - 6\,\mathrm{sech}^2(x - x_0))\eta^1 &= \omega^2\eta^1\,, \\ -\frac{d^2\eta^2}{dx^2} + (\sigma^2 - 2\,\mathrm{sech}^2(x - x_0))\eta^2 &= \omega^2\eta^2\,, \end{aligned}$$

where the eigenfunctions are denoted as η^i to prevent confusion with the parameter σ. Consequently, the Hessian operator $\mathcal{H}$, written in (1.36), is a diagonal operator and both equations can be analysed separately. Once more, the spectral equations correspond to those of Pösch-Teller potentials, enabling the analytical identification of the spectrum. In particular, the discrete spectrum for each component is

$$\begin{aligned} \omega^2_{n_1} &= 4 - (2 - n_1)^2\,, \qquad n_1 = 0, 1, 2\,, \\ \omega^2_{n_2} &= \sigma - (1 - n_2)^2\,, \qquad n_2 = 0, 1\,. \end{aligned}$$

It should be noted that, regardless of the value of the parameter σ, a zero mode can be found when $n_1 = 0$. Moreover, when $n_2 = 0$ the value of ω_{n_2} is negative $\omega_{n_2}^2 = \sigma^2 - 1 < 0$ when $\sigma^2 - 1 < 0$. Therefore, in the regime where $\sigma^2 < 1$ this kink is unstable, while it remains stable in the regime where $\sigma^2 > 1$. Indeed, if no other kink exists this one must be linearly stable.

2. **TK2 kink**: The second trial orbit corresponds to ellipses with eccentricity depending on the parameter σ^2. Specifically, the equation describing these singular kink orbits is given by

$$\phi_1^2 + \frac{\phi_2^2}{1-\sigma^2} = 1\,.$$

Notice that orbits are closed only within the range of values $\sigma^2 \in [0, 1)$, with foci of the ellipses located at $\phi_2 = -\sigma$ and $\phi_2 = \sigma$. For $\sigma = 0$ this corresponds to a circumference, while for $\sigma^2 > 1$ these curves transition into hyperbolas. As a result, our focus will be seeking ellipses for values $\sigma^2 < 1$. This trial orbit now yields four solutions

$$\phi_1 = (-1)^{\epsilon_1} \tanh\left(\sigma(x - x_0)\right), \qquad \phi_2 = (-1)^{\epsilon_2}\sqrt{1-\sigma^2}\,\mathrm{sech}(\sigma(x - x_0))\,,$$

with $\epsilon_1, \epsilon_2 = 0, 1$, see Figure 1.7. These solutions shall be referred to as $TK2$ kinks. Note that these kink profiles are real only for $\sigma^2 \leq 1$, values for which curves correspond to ellipses. On the other hand, the energy of these kinks depends now on σ

$$E[TK2] = 2\sigma\left(1 - \frac{\sigma^2}{3}\right),$$

and gradually increases as the ellipse tends to the circumference in the limit $\sigma \to 0$. The spectral analysis of the Hessian operator for these kinks is significantly more complicated than that of the previous trial orbit. In fact, the spectrum cannot be identified analytically. However, a numerical analysis can be conducted to verify the absence of negative eigenvalues, leading to the conclusion that these kinks are linearly stable [24].

3. **Families of non-topological kinks NTK**: As previously mentioned, Magyari and Thomas [80] found in 1984 for this analogue mechanical system two conserved quantities in involution and functionally independent, which shall be denoted as K_1 and K_2

$$\begin{aligned} K_1 &= \frac{l_{12}^2}{\sigma^2} + p_1^2 + 2\phi_1^2 - \phi_1^2(\phi_1^2 + \phi_2^2)\,, \\ K_2 &= -\frac{l_{21}^2}{\sigma^2} + p_2^2 + (2-\sigma^2)\phi_2^2 - \phi_2^2(\phi_1^2 + \phi_2^2)\,, \end{aligned} \tag{1.42}$$

where $p_a = \frac{d\phi_a}{dx}$ is the conjugate momentum corresponding to the coordinate ϕ_a and where $l_{ab} = p_a\phi_b - p_b\phi_a$. It is worth noticing that this is not a superintegrable mechanical system, as these quantities are related to the energy as $K_1 + K_2 = 2H + 1$. By Stäckel theorem, due to the quadratic dependence on momenta p_i^2 in these conserved quantities, the mechanical problem is separable. In fact, Hamilton-Jacobi separability becomes evident when this system is expressed in elliptic coordinates (u, v)

$$\phi_1 = \frac{1}{\sigma}uv\,, \qquad \phi_2 = \pm\frac{1}{\sigma}\sqrt{u^2-\sigma^2}\sqrt{\sigma^2-v^2}\,, \tag{1.43}$$

where $u \geq \sigma$ and $-\sigma \leq v \leq \sigma$. This observation was made by Ito [81] in 1985, who found that in these coordinates the Hamiltonian was separable

$$H = \frac{1}{u^2 - v^2}\left(H_u + H_v\right)$$

and could be written, up to a global factor, in terms of the following two terms

$$H_u = \frac{u^2 - \sigma^2}{2}\left(p_u^2 - (u^2-1)^2\right), \qquad H_v = \frac{\sigma^2 - u^2}{2}\left(p_v^2 - (v^2-1)^2\right).$$

This allows Hamilton-Jacobi's formalism to be applied (1.24) with a generating function that will be defined so that it can be separated into two adding terms

$$S = S_u(u) + S_v(v) \tag{1.44}$$

where the missing term $-Ex$ in S vanishes since the energy of the mechanical system must vanish. Then, orbit's equations for families of kinks, which shall be denoted as NTK, are obtained

$$\begin{aligned}
\left(\frac{(1-u)(u+\sigma)^\sigma}{(1+u)(u-\sigma)^\sigma}\right)^{\mathrm{sg}(u')}\left(\frac{(1-v)(v+\sigma)^\sigma}{(1+v)(\sigma-v)^\sigma}\right)^{\mathrm{sg}(v')} &= e^{2(1-\sigma^2)\bar{x}}\,, \\
\left(\frac{(1+u)(u-\sigma)^{\frac{1}{\sigma}}}{(1-u)(u+\sigma)^{\frac{1}{\sigma}}}\right)^{\mathrm{sg}(u')}\left(\frac{(1+v)(\sigma-v)^{\frac{1}{\sigma}}}{(1-v)(\sigma+v)^{\frac{1}{\sigma}}}\right)^{\mathrm{sg}(v')} &= e^{2(1-\sigma^2)\gamma}\,,
\end{aligned} \tag{1.45}$$

where $\bar{x} = x - x_0$ with x_0 being the centre of the kink and γ is a constant of integration that labels each member of this family of kinks. Even though these implicit solutions determine the field profiles in the plane of elliptic coordinates, let us proceed even further and obtain the field profiles in Cartesian coordinates. From the above equations the explicit solutions for $u(x)$ and $v(x)$ can be derived and with them those in Cartesian coordinates [24]

$$\begin{aligned}
\phi_1(x,\gamma,a) &= \pm\frac{\sigma_-\cosh(\sigma_+x_+) - \sigma_+\cosh(\sigma_-x_-)}{\sigma_-\cosh(\sigma_+x_+) + \sigma_+\cosh(\sigma_-x_-)}\,, \\
\phi_2(x,\gamma) &= \frac{2\sigma_+\sigma_-\sinh(\bar{x})}{\sigma_-\cosh(\sigma_+x_+) + \sigma_+\cosh(\sigma_-x_-)}\,,
\end{aligned}$$

with auxiliary constants $\sigma_\pm = 1 \pm \sigma$ and where the two following shifts in the spatial coordinate have been defined

$$x_- = \bar{x} - \gamma\sigma(\sigma+1)\,, \qquad x_+ = \bar{x} - \gamma\sigma(\sigma-1)\,.$$

After expressing these solutions in Cartesian coordinates, it becomes apparent that these correspond to a whole family of non-topological kinks parametrised by γ. These leave one vacuum point, cross a focus of the ellipses and finally return to the initial vacuum, see Figure 1.8.

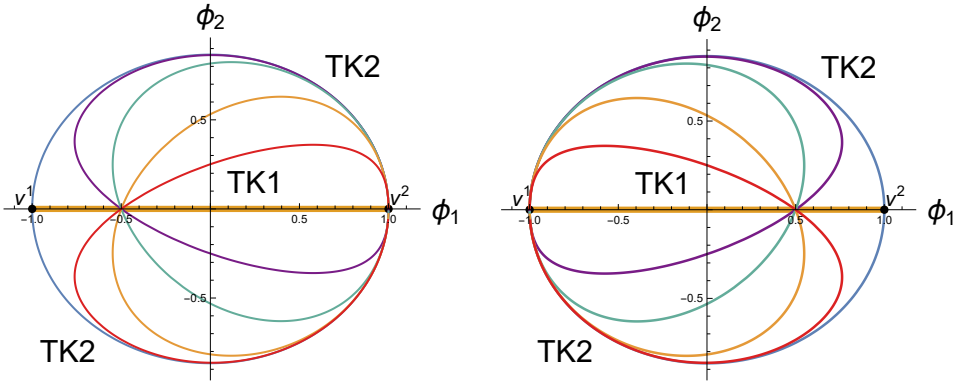

Figure 1.8: Orbits for different members of the family of kinks in Cartesian coordinates are shown when $\sigma = 0.5$. The two possibilities in signs in the solutions originate two subfamilies of non-topological kinks, each one departing from a different vacuum point and crossing a different focus of the ellipse, which are located at points $(\pm\sigma, 0)$.

Limits $\gamma \to \pm\infty$ of this family of kinks coincide with a combination of a $TK1$ and a $TK2$, as can be observed in Figure 1.8. This causes under certain conditions the emergence of an extra peak in the energy density profiles. This also leads to an energy sum rule. Indeed, the energy of all members of this family is

$$E[NTK] = \frac{2}{3}(1+\sigma)^2(2-\sigma)\,,$$

which is precisely the sum of the two previously described singular kinks

$$E[NTK] = E[TK1] + E[TK2]\,.$$

Although it is beyond the scope of this section, it is worth mentioning that this model has been further studied up until the present [8–11, 13, 15, 101, 112]. For instance, Morse theory has been employed to analyse the stability of the emerged non-topological kinks. Indeed, the presence of fixed points in all these orbits where the flow is undefined, which are the foci of the ellipse which are crossed by all members of a subfamily, reveals that these are in fact unstable.

In conclusion, the MSTB model is an example of scalar field theory with two field profiles for which a coordinate system that makes the analogous mechanical system separable can be identified. However, it is important to note that not all field theories that involve multiple fields allow us to find these coordinates. Given the challenges involved in identifying additional conserved quantities in general, field theories are frequently constructed so that the analogue mechanical systems admit the Hamilton-Jacobi formalism in certain coordinates. This, in fact, will be the approach adopted in this and in the subsequent chapters. Only those field theories for which Hamilton-Jacobi formalism can be applied shall be considered.

1.4 Brochosons in the plane

Topological kinks cannot decay into vacuum due to the homotopic impediments that arise from fixing the asymptotic values of the kink profiles. In contrast, non-

topological kinks lack these obstructions and can typically decay into vacuum. However, under specific conditions, a similar impossibility for decaying into vacuum can also appear for non-topological kinks. Indeed, when the target space is non-simply connected, kinks that describe unshrinkable loops may emerge. This type of solution that cannot decay into vacuum will be referred to as "brochoson" from the ancient Greek word "βροχος" (brochos), which can be translated as "loop" or "ring". Notice that brochosons are to be distinguished from "lavions", which only display local stability [25, 73].

According to equation (1.32), the static energy of any static kink depends on the evaluation of the superpotential at the final and initial points. When Cartesian coordinates are employed, the energy of non-topological solutions along which the superpotential is differentiable would vanish. Clearly, this type of solution does not meet the criteria to be considered a kink. In order to avoid this no-go result, one may explore superpotentials in Cartesian coordinates that exhibit non-differentiability at specific points. Alternatively, adhering to the scenario in which the superpotential exhibits differentiability, another coordinate system can be chosen. If a periodic coordinate is introduced, then the static energy (1.32) of a non-topological kink may be different from zero. An example of brochoson can be found in [16, 25], where polar coordinates are employed to construct a model that supports this type of solutions. Building upon this line of work, a different model in which brochosons can be found is presented in this section. In particular, instead of polar coordinates, elliptic coordinates on the Euclidean plane will be employed. Moreover, for the sake of convenience, instead of the version provided in last section, a trigonometric version of these coordinates is chosen here. Indeed, elliptic coordinates can be written as follows

$$\begin{aligned} \phi^1(\mu,\nu) &= a\cosh\mu\cos\nu\,, \\ \phi^2(\mu,\nu) &= a\sinh\mu\sin\nu\,, \end{aligned}$$

where $\mu \geq 0$, $\nu \in [0, 2\pi)$ and the parameter $a > 0$ determines the position of the foci of the ellipses that curves with constant μ describe. Interestingly, in these coordinates the metric tensor can be written as

$$g = \Delta(\mu,\nu)\,(d\mu\otimes d\mu + d\nu\otimes d\nu)\,, \quad \Delta(\mu,\nu) = \frac{a^2}{2}[\cosh 2\mu - \cos 2\nu]\,,$$

which reveals the fact that this plane of coordinates μ and ν is conformally flat. Now, let us construct the action for a field theory in the Euclidean plane but making use of these coordinates. Starting from the action in Cartesian coordinates, a direct change of coordinates leads to

$$\begin{aligned} S &= \int_{\mathbb{R}^{1,1}} \left[\frac{1}{2}\left[\left(\frac{\partial\phi^1}{\partial t}\right)^2 + \left(\frac{\partial\phi^2}{\partial t}\right)^2 - \left(\frac{\partial\phi^1}{\partial x}\right)^2 - \left(\frac{\partial\phi^2}{\partial x}\right)^2\right] - V(\phi^1,\phi^2)\right] dx\ dt \\ &= \int_{\mathbb{R}^{1,1}} \left[\frac{1}{2}\Delta(\mu,\nu)\left[\left(\frac{\partial\mu}{\partial t}\right)^2 + \left(\frac{\partial\nu}{\partial t}\right)^2 - \left(\frac{\partial\mu}{\partial x}\right)^2 - \left(\frac{\partial\nu}{\partial x}\right)^2\right] - V(\mu,\nu)\right] dx\ dt\,, \end{aligned}$$

where the components $g_{ab} = \Delta(\mu,\nu)\delta_{ab}$ of the metric tensor in elliptic coordinates appear as a result of the change of variables. If the type of potential that is being

considered is such that admits the Hamilton-Jacobi formalism, this is, potentials that can be written as

$$V(\mu,\nu)=\frac{1}{2\Delta(\mu,\nu)}\left[\left(\frac{\partial W}{\partial\mu}\right)^2+\left(\frac{\partial W}{\partial\nu}\right)^2\right], \tag{1.46}$$

then solutions of the first order equations (1.28), which read now

$$\frac{d\mu}{dx}=\pm\frac{1}{\Delta(\mu,\nu)}\frac{\partial W}{\partial\mu}, \qquad \frac{d\nu}{dx}=\pm\frac{1}{\Delta(\mu,\nu)}\frac{\partial W}{\partial\nu}, \tag{1.47}$$

are static solutions for the field theory. Notice that the metric factor $\Delta(\mu,\nu)$ appears as denominator in the potential function and in both first order differential equations. Therefore, special care must be taken in the zeros of this factor. Although it vanishes at an infinite number of points in the $\mu-\nu-$plane, $\Delta(0,n\,\pi)=0$ where $n\in\mathbb{Z}$, these infinite number of points correspond to the two foci of the ellipses in the Cartesian plane $(x,y)=((-1)^n a,0)$. Indeed, given that ν is an angular coordinate, all points $(\mu,\nu)=(\mu,\nu+2\pi n)$ with $n\in\mathbb{Z}$ are identified. Furthermore, these points become singularities of the potential unless the numerator vanishes at one of these points, scenario where the limit of the potential at these points must be taken. At this juncture, a paradigm-shifting transformation occurs, as the emergence of singularities replace the Euclidean plane by a non-simply connected space, where not every loop can be contracted to a point. This implies in turn that non-topological kinks in this space may not be able to decay into vacuum. Taking this into consideration, a particular model where this situation emerges is presented in next section.

1.4.1 Example of model with brochosons

As previously noted, elliptic coordinates in the plane potentially introduces two singularities that may be avoided by the choice of the superpotential. Since only one singularity suffices to make the space non-simply connected, in the present model one of these will be removed. In order to achieve this, let us define the superpotential directly in elliptic coordinates:

$$W(\mu,\nu)=m(\alpha+\beta\cos\mu)\sin\frac{\nu}{2},$$

where $m,\alpha,\beta\in\mathbb{R}$. This superpotential leads by (1.46) to a potential function

$$V(\mu,\nu)=\frac{m^2}{2\Delta(\mu,\nu)}\left[\beta^2\sin^2\mu\sin^2\frac{\nu}{2}+\frac{1}{4}(\alpha+\beta\cos\mu)^2\cos^2\frac{\nu}{2}\right], \tag{1.48}$$

for which the number and distribution of vacua will depend on the values of the introduced parameters α and β. Moreover, values of α and β will affect the limits of the potential at the zeroes of the denominator $\Delta(\mu,\nu)=0$. Let us analyse both foci separately.

- **Point** $(-a,0)$**:** The value of the potential $V(\mu,\nu)$ in the vicinity of points $(\mu,\nu)=(0,(2n+1)\pi)$, which correspond in Cartesian coordinates to the focus $(-a,0)$, depends in general on the approaching angle. This is, the limit of this

potential does not exist in general. While all possible values of the potential are finite and positive, the limit will only exist when relations $\alpha = 3\beta$ or $\alpha = 5\beta$ are satisfied. Therefore, regardless of the chosen parameters α and β, this point located at $(\phi^1, \phi^2) = (-a, 0)$ will neither be a singularity nor a vacuum point. Even further, in general this will be a point to avoid in our solutions as we shall see.

- **Point** $(a, 0)$**:** On the other hand, points $(\mu, \nu) = (0, 2\pi n)$ with $n \in \mathbb{Z}$ are maintained as singularities of the potential unless $\alpha = -\beta$, case where they become minima of the potential. This scenario will be avoided, since the presence of at least one singularity in the plane is required to construct this non-simply connected space from the Euclidean plane. Thus, given that ν is an angular variable, only one singularity appears. This corresponds in the Cartesian plane to the point $(\phi_1, \phi_2) = (a, 0)$.

On the other hand, the number of vacua, both in the plane of elliptic coordinates and in the Cartesian plane, is infinite. As suggested, this number and distribution are affected by the relation between these parameters. Excluding the case where no singularity is present $\alpha = -\beta$, three cases emerge for further examination:

- **Case** $|\alpha| > |\beta|$**:** In this scenario points $(\mu, \nu) = (k\pi, \pi)$ with positive integer k are the vacua of the field theory in the $\mu - \nu-$plane, see Figure 1.9. These correspond to the following points in the Cartesian plane

$$(\phi^1, \phi^2) = (-a \cosh k\pi, 0) \, .$$

- **Case** $\alpha = \beta$**:** This relation between parameters enables the potential to vanish not only at the same points as in the previous case, but also at $(\mu, \nu) = ((2k+1)\pi, 0)$ with $k \in \mathbb{Z}$, see Figure 1.9. Note that these extra points are placed in the Cartesian plane at

$$(\phi^1, \phi^2) = (a \cosh (2k+1)\pi, 0) \ ,$$

  where $k \in \mathbb{Z}$. This is, these extra vacua are placed on the positive branch of the ϕ^1-axis.

- **Case** $|\alpha| < |\beta|$**:** In this last scenario instead of just one extra vacuum point within every 2π in μ, two will appear $(\mu, \nu) = \left(2\pi k \pm \arccos \frac{-\alpha}{\beta}, 0\right)$ with $k \in \mathbb{Z}$. These extra points are also on the positive branch of the ϕ^1-axis, two for each integer $k \in \mathbb{Z}$

$$\left(\phi^1, \phi^2\right) = \left(a \cosh \left(2\pi k \pm \arccos \frac{-\alpha}{\beta}\right), 0\right) \, .$$

On a different note, it is also worth noticing that while this potential is periodic in $\nu \in [0, 2\pi)$, the superpotential is not. This aligns with the desired scenario, as it paves the way for the existence of non-topological kinks given that the energy of a solution that revolves once around the singularity does not vanish

$$\begin{aligned} E =& \left| \lim_{x\to\infty} W(\mu(x), \nu(x) \pm 2\pi) - \lim_{x\to-\infty} W(\mu(x), \nu(x)) \right| \\ =& 2 \left| \lim_{x\to\infty} m(\alpha + \beta \cos \mu(x)) \sin \frac{\nu(x)}{2} \right| \, . \end{aligned}$$

The particular energy values for each individual case will be derived later on. Lastly, the first order differential equations (1.47) for the chosen superpotential in elliptic coordinates are of the form

$$\frac{d\mu}{dx} = \mp\frac{2m\beta}{a^2}\frac{\sin\mu\sin\frac{\nu}{2}}{\cosh 2\mu-\cos 2\nu}, \qquad \frac{d\nu}{dx} = \pm\frac{m}{a^2}\frac{(\alpha+\beta\cos\mu)\cos\frac{\nu}{2}}{\cosh 2\mu-\cos 2\nu}. \tag{1.49}$$

Although these equations cannot be directly integrated, some information can be obtained from them. For instance, Rajaraman's trial orbit can be employed to identify solutions for which one of the coordinates remains constant. This will be covered in next section.

1.4.2 Singular kinks

By means of Rajaraman's trial orbit method two types of singular kinks can be found. On one hand, for certain constant values of μ, solutions that describe ellipses in the Cartesian plane are obtained. These will be denoted as N_K-kinks. On the other, fixing certain values of ν produces solutions that correspond to segments in the ϕ^1-axis in the Cartesian plane. These other singular kinks will be denoted as M_K-kinks.

- M_K-**kinks:** If the angular coordinate is fixed at values $\nu = \pi + 2\pi l_2$ where $l_2 \in \mathbb{Z}$, then a differential equation whose solutions are the M_K-kinks is found

$$\frac{d\mu}{dx} = \mp\frac{2m\beta}{a^2}\frac{\sin\mu}{\cosh 2\mu-1}\,.$$

  These solutions, whose expressions will be omitted due to length, will join minima $(\mu_v,\nu_v) = (\pi l_1, \pi+2\pi l_2)$ to minima $(\mu_v,\nu_v) = (\pi(l_1+1), \pi+2\pi l_2)$ for any positive integer $l_1 > 0$, see Figure 1.9. This implies that in the Cartesian plane these kinks will connect minima $(\phi^1,\phi^2) = (-a\cosh\pi l_1, 0)$ to minima $(\phi^1,\phi^2) = (-a\cosh\pi(l_1+1), 0)$. Notice that no solution can cross the region with singularities $\mu = 0$, as the equation above is not well-defined at these points. For the sake of convenience let us denote as M_K^i the kink that joins the vacua located at $\mu_v = \pi i$ to those at $\mu_v = \pi(i+1)$ with positive integer i, so that the nearest kinks to the origin is M_K^1. In addition, the energy of all these topological singular kinks is identical

$$E[M_K^i] = 2m\beta \quad \forall i \in \mathbb{Z}^+\,.$$

  Lastly, it should be noted that these kinks are always present regardless of the values of the parameters α and β.

- N_K-**kinks:** By fixing the other coordinate at values $\mu = \pi l_1$ with integer $l_1 > 0$, the differential equation for the other type of singular kink, N_K-kinks, is derived

$$\frac{d\mu}{dx} = \pm\frac{m}{a^2}\frac{(\alpha+(-1)^{l_1}\beta)}{\cosh 2\pi l_1-\cos 2\nu}\cos\frac{\nu}{2}\,.$$

  In this case solutions join minima $(\mu,\nu) = (\pi l_1, \pi+2\pi l_2)$ with minima $(\mu,\nu) = (\pi l_1, 3\pi+2\pi l_2)$ and $l_2 \in \mathbb{Z}$, see Figure 1.9. In the Cartesian plane these singular kinks correspond to ellipses that connect asymtotically vacua $(\phi_v^1,\phi_v^2) =$

$(-a\cosh\pi l_1, 0)$ with themselves. That is, they are non-topological kinks that revolve around the singularity located at $(\phi^1, \phi^2) = (a, 0)$. This fact makes these singular kinks the first type of brochoson that is identified in this model. For convenience, let us denote as N_K^i with non-negative integer i the singular kink that joins the minimum $\mu_v = \pi(i+1)$ with itself, so that the nearest kink to the origin, which corresponds to the vacuum point $(\phi_v^1, \phi_v^2) = (-a\cosh\pi, 0)$ in the Cartesian plane, is N_K^0. Notice that, given the approximation $\cosh 2\pi l_1 \approx \sinh 2\pi l_1$ when $l_1 > 0$, the eccentricity of these ellipses will be negligible. Also, when $|\alpha| = |\beta|$ half of these singular kinks will be lost. Indeed, these values of parameters lead to a situation where for alternating values of l_1 the equation above holds trivially. Now, in contrast to M_K-kinks, the energy of these singular kinks depends on the minimum they depart from

$$E[N_k^i] = 2m(\alpha - (-1)^i\beta)\,.$$

Due to the existence of two different energetic profiles among these, let us distinguish between two types of N_K-kinks. Those with $i = 0 \bmod 2$ will be denoted as $N_K^{[0]}$ while those with $i = 1 \bmod 2$ will be denoted as $N_K^{[1]}$. Observe that in this notation the following energy sum rule appears

$$E[N_K^{[1]}] = E[N_K^{[0]}] + 2E[M_K]\,.$$

The above described sum energy rule between singular kinks points towards the possibility of the existence of whole families of brochosons. In the next section, the orbit equation that follows from the system of first order differential equations will be integrated in order to find these solutions.

1.4.3 Families of Brochosons

From the first order differential equations (1.49) the following orbit equation is derived

$$\frac{d\mu}{d\nu} = -2\beta\frac{\sin\mu}{\alpha + \beta\cos\mu}\tan\frac{\nu}{2}\,. \tag{1.50}$$

Notice that this equation is valid as long as solutions avoid the foci $(\phi^1, \phi^2) = (\pm a, 0)$. Now, this orbit equation can be easily integrated, leading to the one-parameter family of solutions given by

$$\left|\gamma\cos^{4\beta}\frac{\nu}{2}\right| = \left|\tan^{\alpha}\frac{\mu}{2}\sin^{\beta}\mu\right|,$$

where $\gamma > 0$ is a constant that distinguishes between family members. Note that this orbit equation could allow us to integrate explicitly equations (1.49) in each case, but this direction of research will not be pursued. Instead, among the infinite number of possibilities for the pair of parameters (α, β), three representatives for the three mentioned cases will be chosen to illustrate the behaviour of this family of models. In particular, the pairs of parameters $(\alpha, \beta) = (2, 1)$, $(\alpha, \beta) = (1, 1)$ and $(\alpha, \beta) = (1, 2)$ will be studied. Each of these cases reveals a different kink variety, see Figure 1.9 for a representation of these families of kinks in the elliptic plane.
In spite of the fact that the kink variety can be perfectly identified in the elliptic plane, let us send these solutions to the Cartesian plane, where the behaviour of these kinks can be understood more easily. Since every case unveils a different scenario, let us discuss every case separately.

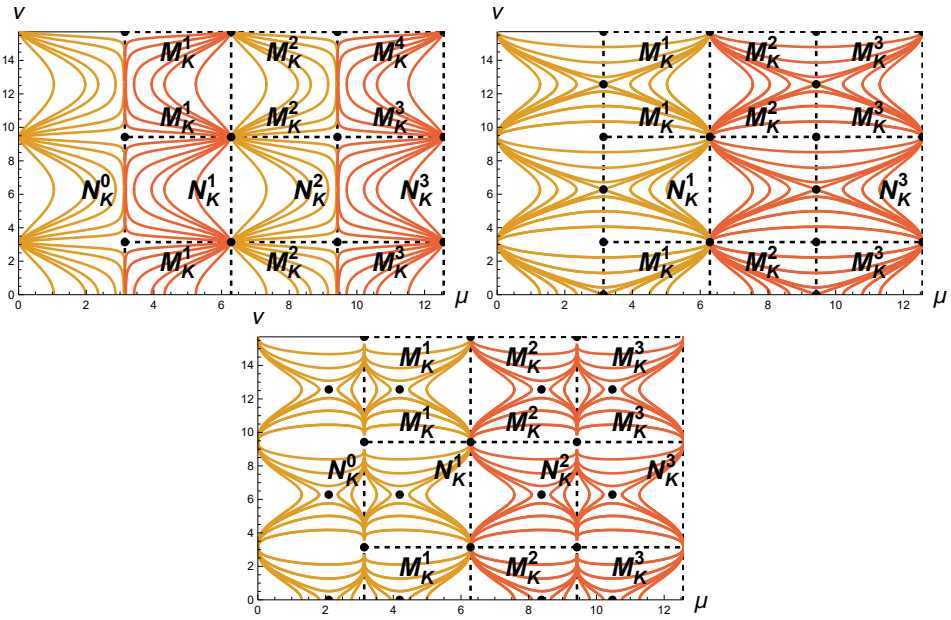

Figure 1.9: Families of kinks that appear as solutions of the orbit equation in the $\mu - \nu-$plane for values $(\alpha, \beta) = (2, 1)$, $(\alpha, \beta) = (1, 1)$ and $(\alpha, \beta) = (1, 2)$ respectively. Vacua are represented with black dots and multiples copies of the same plane have been depicted together so that solutions are continuously represented. Note that while in the first case this family of solutions is comprised exclusively by non-topological kinks, in the rest topological kinks emerge.

- **Case $|\alpha| > |\beta|$:** Once all solutions of the orbit equations and all singular kinks are sent to the Cartesian plane, families of kinks revolving the singularity $(\phi^1, \phi^2) = (a, 0)$ can be easily identified, see Figure 1.10 for the particular case when $(\alpha, \beta) = (2, 1)$. This implies that regardless of their linear stability they cannot decay into vacuum, as the singularity prevents the loop from contracting to a point. These kinks are indeed brochosons. It is also interesting to note that the kink variety's structure repeats itself every two N_K-kinks. This feature can also be observed in the elliptic plane, where N_K-kinks are symmetrically represented, see Figure 1.9. In other words, it replicates itself on larger scales. The only exception in this replication is the central area, which contains solutions of the orbit equations that do not connect any vacua and therefore must be discarded. Indeed, these artificially emerge in the orbit equations.

  Now, the singular kinks that form ellipses N_K^i adopt two different roles depending on the label i. For odd i, they are intermediate members of a subfamily, while for even i these singular kinks are boundaries between two different subfamilies of brochosons, each one based on a different vacua. Notice that only half of the vacua are connected by these families. For convenience, let us split this family of non-topological kinks into subfamilies labelled by the minimum they are asymptotically connecting. In particular, let us denote as $\Sigma_K^{2k}(x; \gamma)$ the subfamily that contains all members of this family that leave and return to the minimum located at $(\phi_v^1, \phi_v^2) = (-a \cosh 2\pi k, 0)$ with $k > 0$. Let us split these subfamilies again and let us employ an additional label ϵ to distinguish between those members that lie inside or outside the area delimited by the

singular kink N_K^{2k-1}. Label $\epsilon = -$ will be employed for those inside while for those outside this ellipse $\epsilon = +$ will be used. In other words, the label ϵ distinguishes between the subfamily $\Sigma_K^{2k,-}(x;\gamma)$ that gets nearer to the origin and that that gets farther from it, denoted as $\Sigma_K^{2k,+}(x;\gamma)$.

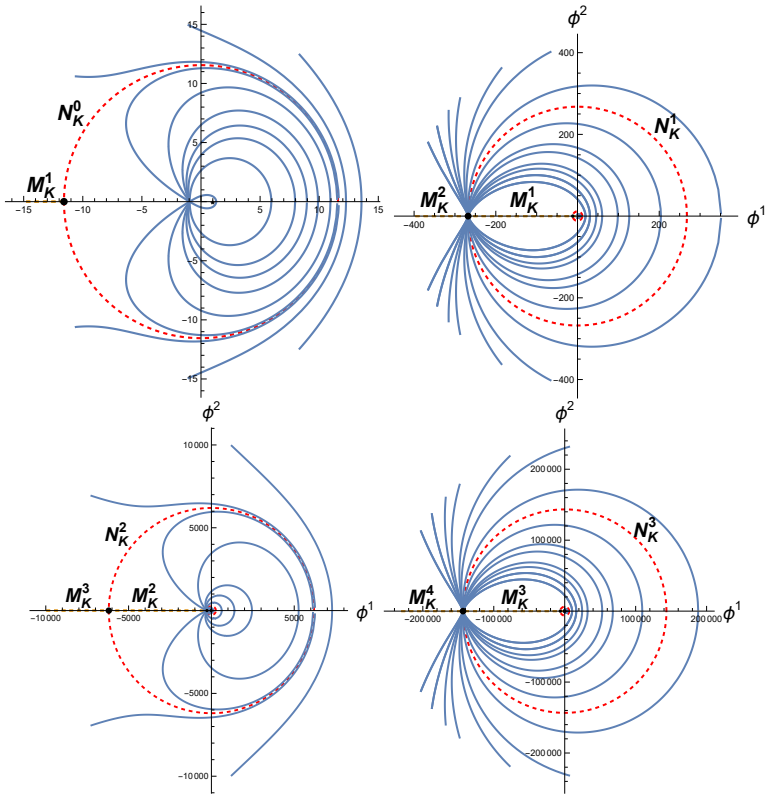

Figure 1.10: Families of brochosons are shown in the Cartesian plane at different scales for the values $(\alpha, \beta) = (2, 1)$. Dots in the negative branch of the ϕ^1-axis represent the vacua. Notice that N_K-kinks appear represented in the last three figures near the origin. This is due to the considerable difference in scale between consecutive N_K-kinks.

On the other hand, the energy of all members is the same regardless of the subfamily they belong to

$$E[\Sigma_K] = E[N_K^{[1]}] = 2m(\alpha + \beta)\,.$$

This result is related to how limits for the parameter γ of these families coincide with the previously discussed singular kinks

$$\begin{aligned}
&\lim_{\gamma\to 0} \Sigma_K^{(2i,+)}(x;\gamma) \equiv \lim_{\gamma\to 0} \Sigma_K^{(2i,-)}(x;\gamma) \equiv N_K^{2i}(x)\,,\\
&\lim_{\gamma\to \infty} \Sigma_K^{(2i,+)}(x;\gamma) \equiv M_K^{2i+1}(x) \cup N_K^{2i}(x) \cup M_K^{2i+1}(x)\,,\\
&\lim_{\gamma\to \infty} \Sigma_K^{(2i,-)}(x;\gamma) \equiv M_K^{2i-1}(x) \cup N_K^{2i-1}(x) \cup M_K^{2i-1}(x)\,.
\end{aligned}$$

Note that this, as it was expected, is consistent with the previously mentioned energy sum rule $E[\Sigma_K] = E[N_K^{[1]}] = E[N_K^{[0]}] + 2E[M_K]$.

- **Case $\alpha = \beta$:** In this scenario the emerging extra vacua give rise to extra topological kinks, which separate different families of brochosons and topological kinks, see Figure 1.11. Once more, solutions that cross the focus of the ellipses located at $(-a, 0)$ must be discarded, as the potential it is not defined at this point. The other focus $(a, 0)$, however, is a singularity which prevents these non-topological kinks from decaying into vacuum.

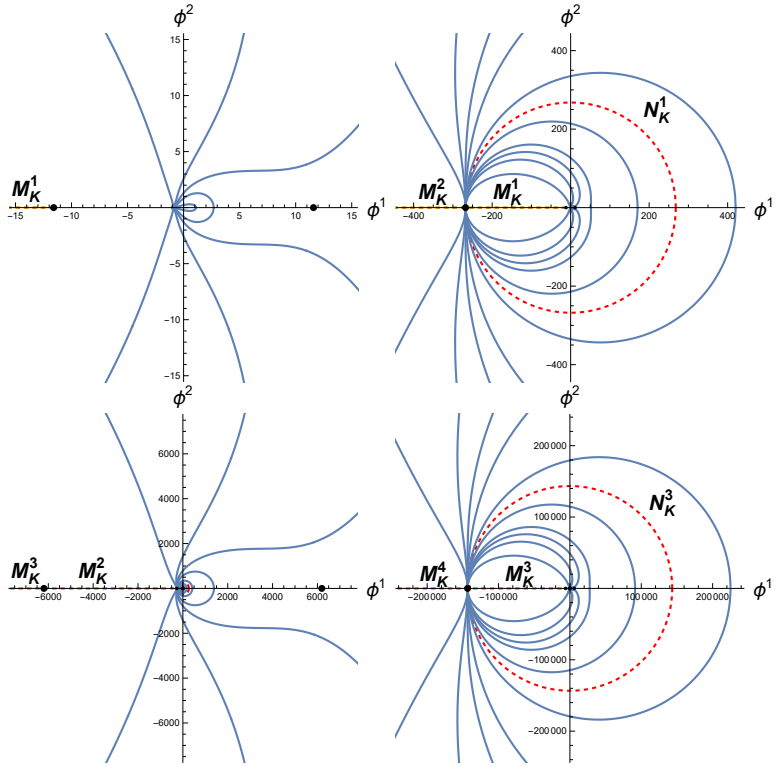

Figure 1.11: Families of brochosons are shown in the Cartesian plane at different scales for the values $(\alpha, \beta) = (1, 1)$. Dots located along both the negative and positive branches of the ϕ^1 axis represent the vacua. Notice that N_K-kinks appear represented in the last three figures near the origin. This is due to the considerable difference in scale between consecutive N_K^1-kinks. Also, new families of topological kinks are formed, making half of the N_k-kinks present in the previous model disappear.

In the previous case, a new N_K-kink were identified after every translation $\nu \to \nu + \pi$ of a N_K-kink. In this case, the replicating structure is given by translations $\nu \to \nu + 2\pi$ instead. Half of the singular kinks of last case disappear as a consequence of the Picard-Lindelöf theorem. This is, because solutions of the first order differential equations cannot intersect and half of these $N_K^{[0]}-$kinks would cross families of solutions, they cannot arise. Moreover, the absence of half of the $N_K^{[0]}-$kinks and the appearence of extra topological kinks motivates us to split these families of kinks into subfamilies of brochosons and subfamilies of topological kinks. These shall be respectively denoted as Σ_K^B and Σ_K^T. Lastly, for this case where $\alpha = \beta$, these families share

the same energy

$$E\left[\Sigma_K^T\right] = 2E\left[M_K\right] = 4m\beta\,,$$
$$E\left[\Sigma_K^B\right] = E\left[N_K^{[1]}\right] = 2m(\alpha+\beta) = 4m\beta\,,$$

which is once again consistent with the energy sum rule.

- **Case $|\alpha| < |\beta|$:** In this last case, additional vacua also emerge. However, they do so in such a way that the $N_K^{[0]}-$kinks are not lost, see Figure 1.12. The count of extra topological kinks observed in the preceding case is now doubled, implying the existence of an even greater number of subfamilies. In particular, three types of subfamilies can be identified based on the energy of their members. One consists of brochosons that tend to a $N_K^{[0]}-$kink, another comprised by brochosons that tend to $N_K^{[1]}-$kink and one final subfamily which contains only topological kinks. These will be denoted as $\Sigma_K^{[0]}$, $\Sigma_K^{[1]}$ and Σ_K^T respectively. Notice that topological kinks serve as boundaries for these three subfamilies.

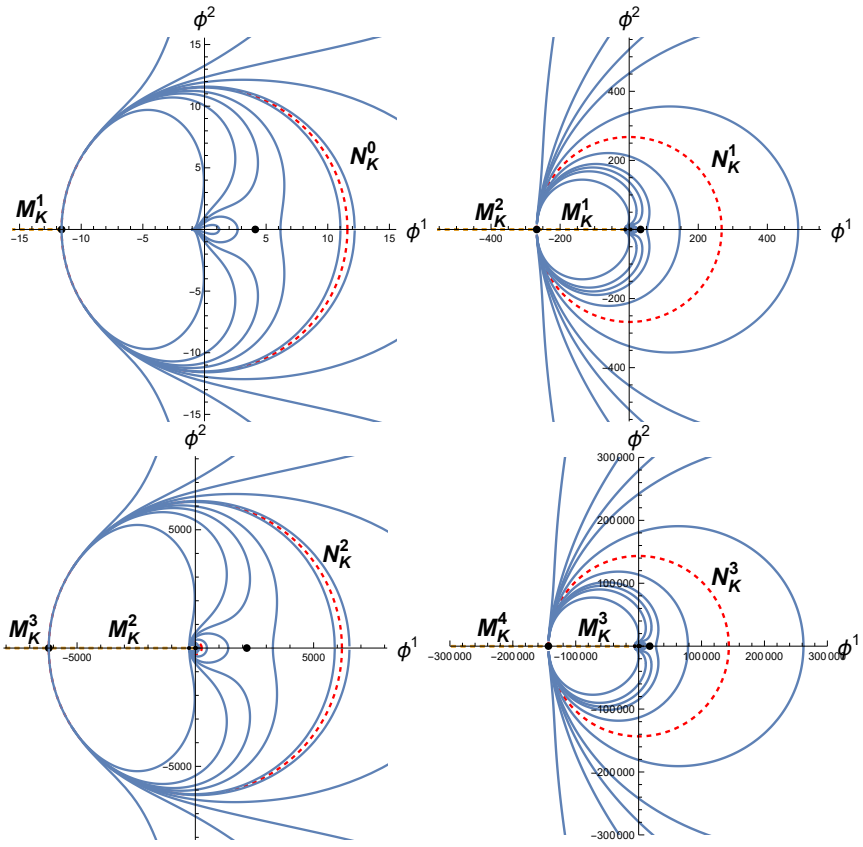

Figure 1.12: Families of brochosons are shown in the Cartesian plane at different scales for the values $(\alpha,\beta) = (1,2)$. Dots located along both the negative and positive branches of the ϕ^1-axis represent the vacua. Notice that N_K-kinks appear represented in the last three figures near the origin. This is due to the considerable difference in scale between consecutive N_K-kinks. With the reappearance of the N_K-kinks in this case, yet another additional subfamily of brochosons arise.

On the other hand, the energy of each subfamily coincides with that of a

different singular kink. These relations can be written as follows

$$E\left[\Sigma_K^T\right] = E\left[M_K\right] = 2m\beta\,,$$
$$E\left[\Sigma_K^{[0]}\right] = E\left[N_K^{[0]}\right] = 2m(\alpha-\beta)\,,$$
$$E\left[\Sigma_{[1]}^B\right] = E\left[N_K^{[1]}\right] = 2m(\alpha+\beta)\,.$$

Thus, with this choice on parameters α and β two families of brochosons and one family of topological kinks emerge replicated at different scales.

In summary, a singularity has been introduced in the potential $p = (\phi^1, \phi^2) = (0, a)$ to replace the Euclidean plane $\mathbb{R}^2$ as target manifold by $\mathbb{R}^2 - p$, which is non-simply connected. The choice of a differentiable superpotential which is not periodic on the angular variable ν, allows the emergence of non-topological kinks that revolve around this singularity. In order to find these solutions, given that the first order differential equations cannot be directly integrated, their orbits are obtained by the derivation of the orbit equation. Since the metric in elliptic coordinates on the plane is conformally flat, information about the metric is lost in the orbit equation. This must be borne in mind, since this orbit equation will produce solutions for the plane in Cartesian coordinates that must be discarded. In other words, it ignores the fact that the original equations are not defined at the focus $(-a, 0)$ of the ellipses. As a result, any solution that crosses this point in the Cartesian plane is not considered. Fortunately, an infinite number of vacua allows an infinite number of singular kinks and families of kinks to arise.

Three different scenarios emerge depending on the chosen values for the parameters introduced in the superpotential α and β. These correpond to cases with $|\alpha| > |\beta|$, $\alpha = \beta$ and $|\alpha| < |\beta|$, being the case $\alpha = -\beta$ excluded as no singularity appears in this case. On one hand, new vacua and topological kinks appear for the last two cases. Instead of just families of non-topological kinks and singular topological kinks, whole families of topological kinks are identified in the last two cases. In the second case $\alpha = \beta$, half of the N_K-kinks disappear to avoid crossings between kinks. This fact substantially affects the kink variety, making families of kinks split differently in each scenario. Also, limits of these families and the sum energy rules between singular kinks are different in each scenario as the distribution of vacua change.

Despite these variations, all these scenarios unveil an infinite number of vacua, singular brochosons and families of brochosons. Indeed, these solutions cannot decay into vacuum due to the presence of the introduced singularity that prevents all loops that revolve it from contracting to a point. Interestingly, the kink variety is periodically replicated at larger scales. Lastly, this idea of employing non-simply connected spaces as target manifolds to search for brochosons can be applied in other scenarios. For instance, contractility of kinks can be study in field theories that employ target spaces with curvature.

1.5 Further comments

In this chapter, a concise overview of scalar field theories have been presented, restricting to those defined on the $(1+1)-$dimensional Minkowski space with the objective of identifying finite-energy static solutions that connect different vacua. The energy density profile of these solutions, known as kinks in the literature, will travel without losing its form and at constant velocity. Examples of historical importance have been shown, where their stability is also analysed. In last sections the abrupt change in complexity that entails constructing field theories with multiple scalar fields becomes apparent. Indeed, the analogue mechanical problem for these theories may not be integrable. The required number of conserved quantities for the analogue mechanical system may not be found, unlike in cases with only one field, where the energy is always available.

Lastly, new examples of scalar field theories where brochosons can be identified are constructed. These non-topological kinks that cannot decay into vacuum emerge when two conditions are satisfied. On one hand, the target space $\mathbb{R}^N$ is replaced by a non-simply connected space by introducing a singularity into the potential. On the other, the superpotential employed to construct these field theories must be non-periodic in one angular variable. This prevents the energy of such a configuration from vanishing. This procedure will be generalised to the context of Sigma models in next chapters, where the notions of kink and stability will adapt to this scenario.

Chapter 2

Kinks on manifolds with curvature

Chapter 1 introduces the notion of kink as a finite energy solution in certain type of field theories defined on the $1+1-$dimensional Minkowski space $\mathbb{R}^{1,1}$. In this chapter, the Euclidean target space is replaced by a more general space, the Riemannian manifold. This gives rise to a more general type of field theories, which are frequently referred to as Sigma models in the literature.

A similar approach to the one used in the preceding chapter will be adopted. First, the field equations for this new context will be derived. Then, static solutions will be sought in our quest to identify kinks. Once more, in order to be able to obtain kinks analytically, the type of potential functions that shall be considered is restricted to a particular type. This is, in order to perform the Bogomol'nyi arrangement, which conceals Hamilton-Jacobi formalism, we shall exclusively concentrate on a specific type of field theory.

The concept of kink smoothly translates into this generalised scenario, where once again, the existence of first order differential equations will aid in searching for solutions. Nevertheless, as this generalization occurs, the notion of linear stability must be similarly adjusted. A similar study will be conducted, so that a generalisation of the spectral equations and the vibrational modes from chapter 1 are obtained when dealing with Riemannian manifolds.

Lastly, a mechanism for inducing geometrical constraints in a continuous manner for kinks and domain walls is presented. The results of this study, published in [30], hold potential for several applications to material science.

2.1 Kinks in Sigma models

In the preceding chapter, the pursuit of kinks led us to the search of static solutions in the field equations. However, for the type of field theories and solutions that were being considered, according to Derrick's theorem these could only be found in $1+1-$dimensional spacetimes. On these spacetimes, scalar fields $\phi^i : \mathbb{R}^{1,1} \to \mathbb{R}$ were defined as differentiable maps to the real numbers. In order to condense notation, fields $\phi : \mathbb{R}^{1,1} \to \mathbb{R}^n$ were constructed, so that each coordinate in this target space $\mathbb{R}^n$ was a real scalar field. Generalising models constructed on Euclidean target spaces, M. Gell-Mann and M. Lévy introduced another type of models called Sigma models in 1960 [68]. Although these were originally created to study spinless mesons denoted as σ, hence the name, they have proven to be useful in modelling many other phenomena. These models introduce Riemannian manifolds (M, g) with Riemannian

metric tensor g to generalise $\mathbb{R}^n$ as target space. This allows us to define fields $\phi : \mathbb{R}^{1,1} \to M$ that send points from Minkowski space $\mathbb{R}^{1,1}$ to points of a Riemannian manifold M. Our primary focus lies on scalar fields ϕ^i, which can be constructed through the use of charts $\{(U_M, \{\lambda^i_M\})\}$ on this manifold as follows:

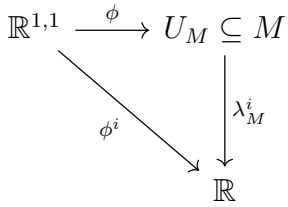

That is, given a chart on M and a field $\phi : \mathbb{R}^{1,1} \to M$, the scalar fields $\phi^i = \lambda^i_M \circ \phi$ with $i = 1, \ldots, \dim M$ are defined by composition. Notice that this generalises the models constructed in Chapter 1 since Euclidean spaces $\mathbb{R}^n$ are examples of Riemannian manifolds. On the other hand, the dynamics of this type of model will be determined not only by the chosen potential functions V, but also by the geometry of the target space encoded in the metric tensor g. Notice that this scenario was already found in last chapter. In Cartesian coordinates, the Euclidean geometry made the coupling of fields in the action appear exclusively in the potential. However, in other coordinates components of the metric are able to introduce dependence on coordinates. In particular, the action of a Sigma model is given in coordinates by the following functional:

$$S = \int_{\mathbb{R}^{1,1}} \left[\frac{1}{2} \eta^{\mu\nu} g_{ab}(\phi(x,t)) \frac{\partial \phi^a}{\partial x^\mu} \frac{\partial \phi^b}{\partial x^\nu} - V(\phi(x,t)) \right] dxdt \,, \tag{2.1}$$

where the Einstein summation convention has been employed for both space-time coordinates x^μ and internal space coordinates ϕ^i. This functional has a form similar to that of the previously considered scalar field theories. In fact, when the Riemnannian manifold is $M = \mathbb{R}^n$ with the Euclidean metric, both actions coincide. Note that the action is still of the form (1.1), which implies that the same conserved currents and quantities will be present. In particular, the energy of a certain configuration will be a direct generalisation of the previous one

$$E = \int_{-\infty}^{\infty} \left[\frac{1}{2} g_{ab}(\phi(x,t)) \frac{\partial \phi^a}{\partial t} \frac{\partial \phi^b}{\partial t} + \frac{1}{2} g_{ab}(\phi(x,t)) \frac{\partial \phi^a}{\partial x} \frac{\partial \phi^b}{\partial x} + V(\phi^1, \ldots, \phi^N) \right] dx \,. \tag{2.2}$$

Of course, the finite energy requirement for kinks in this context will lead to similar conditions to those for Euclidean spaces. The distinction lies within the inclusion of components of the metric tensor in this functional as functions of coordinates in general. Indeed, in order to guarantee the finiteness of the energy, solutions must satisfy the following asymptotic conditions

$$\lim_{x \to \pm\infty} \frac{1}{2} g_{ab}(\phi(x,t)) \frac{\partial \phi^a}{\partial t} \frac{\partial \phi^b}{\partial t} = \lim_{x \to \pm\infty} \frac{1}{2} g_{ab}(\phi(x,t)) \frac{\partial \phi^a}{\partial x} \frac{\partial \phi^b}{\partial x} = 0 \,.$$

For now, let us assume the absence of zeroes and singularities in the metric, cases that shall be discussed later on. Under these considerations, the same asymptotic conditions that emerged in the Euclidean case to obtain kinks are recovered, namely:

- Derivatives of all fields must vanish at infinities

$$\lim_{x\to\pm\infty}\frac{\partial\phi^i}{\partial t}=\lim_{x\to\pm\infty}\frac{\partial\phi^i}{\partial x}=0\,.$$

- Fields must tend to one of the zeroes of the potential at infinities

$$\lim_{x\to\pm\infty}\phi^i(t,\vec{x})\in\mathcal{M}\,.$$

On the other hand, topological charges Q_i are also conserved in these theories. However, the interpretation of these quantities may depend on the topological properties of the target manifold. This will be thoroughly explored in Chapter 4. Just as in the previous chapter, the search for kinks will involve seeking static solutions in the field equations. Before diving into the task, one must check whether Derrick's theorem still holds in the context of Sigma models with one spatial dimension. Following a similar approach to that used in the case with Euclidean target space, let us consider a static solution $\phi_s(x^1,\ldots,x^n)$ of a Sigma model on a Riemannian manifold (M,g) with potential function V and on the $(1+n)-$dimensional Minkowski space. Let $\phi_\lambda(x)=\phi_s(\lambda x^1,\ldots,\lambda x^n)$ with $\lambda>0$ be a one-parameter family of configurations which is only a solution when $\lambda=1$. Once again, a spatial dilation has been performed on this solution. The energy of any static configuration it is according to equation (2.2) the following functional

$$E_{st}[\lambda]=\int\left[\frac{1}{2}g_{ab}(\phi_\lambda)\frac{\partial\phi^a_\lambda}{\partial x}\frac{\partial\phi^b_\lambda}{\partial x}+V(\phi_\lambda(x))\right]\,d^nx\,, \tag{2.3}$$

where n is the number of spatial dimensions of the Minkowski space. Now, if the dilation in the spatial coordinates $x^i\to\tilde{x}^i=\lambda x^i$ is performed for a positive real number λ, the static energy reads

$$E[\lambda]=\int\left[\lambda^2 g_{ab}(\phi_s)\eta^{ij}\frac{\partial\phi^a_s(\tilde{x})}{\partial\tilde{x}^i}\frac{\partial\phi^b_s(\tilde{x})}{\partial\tilde{x}^j}+V(\phi_s)\right]\frac{d^nx}{\lambda^n}\,. \tag{2.4}$$

The static energy is therefore a function of the parameter of the dilation λ, whose derivative must vanish at $\lambda=1$, when the original solution is recovered. This generates formally the same condition as that which was found in the Euclidean case

$$\frac{dS}{d\lambda}[\lambda]\bigg|_{\lambda=1}=0\quad\Rightarrow\quad(2-n)I_1=nI_2\,, \tag{2.5}$$

allowing static solutions only in these scalar field theories when $1+1-$dimensional spacetimes are considered. Thus kinks, as static solutions of the field equations, are also allowed to emerge in the context of Sigma models. The next section will focus on deriving these field equations.

2.1.1 Field equations

In the previous section the action that governs the dynamics of a Sigma model is introduced and the energy of a given configuration obtained. However, the derivation of the field equations resulting from this action remains pending. This will lead us to a point where, similarly to the Euclidean case, the isometries in the Minkowski

space will enable us to identify kinks by seeking static solutions with finite energy of these equations. This is the aim of this section, where a similar differential geometry approach to that in classical mechanics will be employed [69,71,84,102]. A summary of this geometrical approach can be found in Appendix B. While a configuration in mechanics is a curve $c : \mathbb{R} \to M$, in $1+1-$dimensional scalar field theories each field profile describes a surface $\phi^i : \mathbb{R}^{1,1} \to M$. This observation leads us to include not just one tangent vector field, but two in the field theory action. In particular, let us consider a chart $(U_M, \{\phi^i\})$, where ϕ^i denote the coordinates on the open set U_M with $i = 1, \ldots, \dim M$ and let us consider the Levi-Civita connection. In order to write the action of a Sigma model (2.1) in terms of the metric tensor acting on vector fields, let us define the following vector fields

$$\phi_t(t,x,\xi) = \frac{\partial \phi^i(t,x,\xi)}{\partial t}\frac{\partial}{\partial \phi^i}\,, \quad \phi_x(t,x,\xi) = \frac{\partial \phi^i(t,x,\xi)}{\partial x}\frac{\partial}{\partial \phi^i}\,, \tag{2.6}$$

where Einstein summation notation is employed. This allows to write the action of a Sigma model on a Riemannian manifold (M,g) as follows

$$S = \int_{\mathbb{R}^{1,1}} \left[\frac{1}{2}g(\phi_t,\phi_t) - \frac{1}{2}g(\phi_x,\phi_x) - V(\phi)\right] dxdt\,, \tag{2.7}$$

where the potential function of the field theory has been denoted as V. When the action is extremised in classical mechanics, those variations of a given solution curve that leave its ends unaltered are considered. This is, proper variations of solutions are sought. In the context of $(1+1)-$dimensional field theories, where surfaces arise instead of curves, this asymptotic condition must be generalised. Instead of two ends of a curve, a proper variation must leave unmodified all values of these fields ϕ^i at infinities. In particular, a proper variation of a reference surface $\phi : \mathbb{R}^{1,1} \to M$ will be defined as any differentiable map

$$\begin{array}{rccc} \varphi\colon & \mathbb{R}^{1,1}\times(-\epsilon,\epsilon) & \longrightarrow & M \\ & (t,x,\xi) & \longmapsto & \varphi(t,x,\xi) \end{array} \tag{2.8}$$

where ϵ is small enough to make the surface well-defined, such that $\varphi(t,x,0) = \phi(t,x)$ and such that values at infinities are fixed

$$\lim_{t\to\pm\infty}\frac{\partial}{\partial\xi}\varphi^i(t,x,\xi) = \lim_{x\to\pm\infty}\frac{\partial}{\partial\xi}\varphi^i(t,x,\xi) = 0\,, \qquad \forall i,\xi\,.$$

Note that these derivatives must vanish at infinities for every proper variation and therefore for every value of ξ. In a two-dimensional spacetime the concept of variation naturally leads to the definition of three distinct vector fields. On one hand, a vector field arises for each direction in the spacetime

$$\varphi_t(t,x,\xi) = \frac{\partial \varphi^i(t,x,\xi)}{\partial t}\frac{\partial}{\partial \phi^i}\,, \quad \varphi_x(t,x,\xi) = \frac{\partial \varphi^i(t,x,\xi)}{\partial x}\frac{\partial}{\partial \phi^i}\,. \tag{2.9}$$

On the other, the parameter of variations generates another vector field, which will be denoted as

$$\psi(t,x,\xi) = \frac{\partial \varphi^i(t,x,\xi)}{\partial \xi}\frac{\partial}{\partial \phi^i}\,. \tag{2.10}$$

Notice that this variation field ψ must, by definition of proper variation, vanish at infinities in all directions

$$\lim_{t\to\pm\infty} \psi^i(t,x,\xi) = \lim_{x\to\pm\infty} \psi^i(t,x,\xi) = 0 \qquad \forall \xi, i\,. \tag{2.11}$$

With all the necessary components prepared, we can now proceed to derive the field equations by following the same steps employed in the mechanical case. Let us denote now as ϕ a configuration that extremises the Sigma model action (2.7) and as φ a proper variation of this solution, see Figure 2.1.

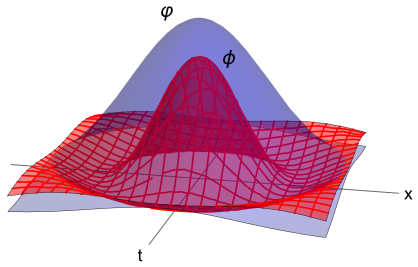

Figure 2.1: Visual representation of a proper variation φ of a field configuration ϕ.

It is worth noting that any proper variation is in fact a family of configurations, labelled by the parameter ξ. Hence, the action for any of these families of configurations is a function of this parameter, reaching its extremal value when $\xi = 0$. This implies that the following condition must be satisfied

$$\left.\frac{dS}{d\xi}\right|_{\xi=0} = 0\,.$$

Let us first obtain an expression for this derivative with respect to the parameter of the variation. Since the limits of integration of the action $S[\phi]$ are independent of this parameter, the position of the derivative and integral symbols can be interchanged. Employing that the connection is compatible with the metric, that the metric tensor is symmetric and the definition of the gradient on Riemannian manifolds, the derivative of the action with respect to ξ can be written in terms of covariant derivatives as follows

$$\frac{dS}{d\xi} = \int_{\mathbb{R}^{1,1}} \left[g\left(\frac{D\varphi_t}{\partial\xi}, \varphi_t\right) - g\left(\frac{D\varphi_x}{\partial\xi}, \varphi_x\right) - g\left(\text{grad } V, \psi\right)\right] dx\ dt\,.$$

The fact that Levi-Civita connection is torsionless allows us to write $\frac{D\varphi_z}{\partial\xi} = \frac{D\psi}{\partial z}$ for both time and the spatial coordinate $z = t, x$. After introducing this in the action one obtains

$$\frac{dS\,[\xi]}{d\xi} = \int_{\mathbb{R}^{1,1}} \left[g\left(\frac{D\psi}{\partial t}, \varphi_t\right) - g\left(\frac{D\psi}{\partial x}, \varphi_x\right) - g\left(\text{grad } V, \psi\right)\right] dx\ dt\,. \tag{2.12}$$

As in the mechanical case, the compatibility condition of the connection with the metric provides an "integration by parts" or "distributive property" formula that reads for both space and time $z = t, x$

$$g\left(\frac{DX_1}{\partial z}, X_2\right) = \frac{\partial}{\partial z} g(X_1, X_2) - g\left(X_1, \frac{DX_2}{\partial z}\right)\,, \tag{2.13}$$

for any vector fields $X_1, X_2 \in \mathfrak{X}(M)$. As has been shown, the proper variation condition forces the variation vector field to vanish at infinities (2.11). This result can be exploited to further simplify equation (2.12) when the integration by parts is performed. Indeed, terms that evaluate this field ψ at infinities vanish, resulting in

$$\frac{dS}{d\xi} = \int_{\mathbb{R}^{1,1}} \left[g\left(-\frac{D\varphi_t}{\partial t} + \frac{D\varphi_x}{\partial x} - \text{grad } V, \psi \right) \right] dx\ dt\,. \tag{2.14}$$

Because this holds true for any proper variation, it also applies to the unaltered configuration $\xi = 0$, which by construction is a solution of the field theory. Consequently, the following integral must be zero

$$\left.\frac{dS}{d\xi}\right|_{s=0} = \int_{\mathbb{R}^{1,1}} \left[g\left(-\frac{D\phi_t}{\partial t} + \frac{D\phi_x}{\partial x} - \text{grad } V, \psi \right) \right] dx\ dt\ = 0.$$

By the fundamental theorem of the variational calculus, the condition above holds for any possible proper variations only when the integrand vanishes identically. This yields the field equations of the field theory

$$-\frac{D\phi_t}{\partial t} + \frac{D\phi_x}{\partial x} = \text{grad } V(\phi)\,. \tag{2.15}$$

It is worth noting that this equation is identical in form to the one found in the mechanical case, see Appendix B, with the addition of a term involving the temporal covariant derivative. In coordinates, this equation produces $\dim M$ equations

$$-\frac{\partial^2\phi^k}{\partial t^2} + \frac{\partial^2\phi^k}{\partial x^2} - \Gamma^k_{ij}\left[\frac{\partial\phi^i}{\partial t}\frac{\partial\phi^j}{\partial t} - \frac{\partial\phi^i}{\partial x}\frac{\partial\phi^j}{\partial x}\right] = g^{mk}\frac{\partial V}{\partial\phi^m} \qquad k = 1, \ldots, \dim M\,, \tag{2.16}$$

where the Einstein summation convention is employed, Γ^k_{ij} denote the Christoffel symbols and g^{mk} are the components of the dual metric. Notice that the coupling of fields may be present now not only in the potential function, but also in the metric tensor and Christoffel symbols. Furthermore, when static solutions $\phi(x)$ are sought, these equations are those of a mechanical system with potential $U = -V$ and with mechanical time x. This is, the same scenario found for Euclidean target spaces appears for Riemannian manifolds. However, solving Newton's equations on Riemannian manifolds becomes more challenging due to the presence of the metric and the Christoffel symbols. Fortunately, the same procedure described in chapter 1 can be applied to derive first order differential equations for specific types of potentials. This will be discussed in next section.

2.1.2 Superpotential and Bogomol'nyi arrangement

The endeavour of integrating Newton's equations on Riemannian manifolds represents a formidable challenge. Indeed, the presence of the metric and Christoffel symbols introduces additional layers of complexity to the resolution of coupled second order differential equations. In this section, the Bogomol'nyi arrangement for Euclidean target spaces presented in Chapter 1 is generalised to the context of Sigma models. When the potential of the field theory can be written in terms of a differentiable function $W : M \to \mathbb{R}$ on the Riemannian manifold (M, g) as follows

$$V(\phi(x)) = \frac{1}{2}g\left(\text{grad } W(\phi(x)), \text{grad } W(\phi(x))\right) = \frac{1}{2}g^{ij}\frac{\partial W}{\partial\phi^i}\frac{\partial W}{\partial\phi^j}\,, \tag{2.17}$$

with grad $W \in \mathfrak{X}(M)$ its gradient, then a similar procedure, also known as Bogomol'nyi arrangement, can be employed. As mentioned in the previous chapter, this function is referred to as superpotential in the literature. In particular, this arrangement is performed in the functional of energy for static configurations or, equivalently, in the action of the analogue mechanical system. More specifically, this procedure consists in manipulating these functionals so that they can be written as the sum of two terms

$$\begin{aligned} S_{mec}[\phi(x)] = E_{st}[\phi(x)] = &\int_{-\infty}^{\infty} ||\dot{c}(x) + \epsilon \text{ grad } W(c(x))||^2 \, dx \\ &- \epsilon \int_{-\infty}^{\infty} g\left(\dot{c}(x), \text{grad } W(c(x))\right) \, dx \,, \end{aligned}$$

where $\epsilon = \pm 1$ and $||\cdot||^2$ is the squared norm induced by the metric tensor defined on the target space

$$||\dot{c}(x) + \epsilon \text{ grad } W(c(x))||^2 = g\left(\dot{c}(x) + \epsilon \text{ grad } W(c(x)), \dot{c}(x) + \epsilon \text{ grad } W(c(x))\right) \,.$$

Finally, the use of coordinates in the integrand in the second term of the action above simplifies the expression significantly

$$\begin{aligned} S_{mec}[\phi(x)] &= \int_{-\infty}^{\infty} ||\dot{c}(x) + \epsilon \text{ grad } W(c(x))||^2 \, dx - \epsilon \int_{-\infty}^{\infty} \frac{dW}{dx}(c(x)) \, dx \\ &= \int_{-\infty}^{\infty} ||\dot{c}(x) + \epsilon \text{ grad } W(c(x))||^2 \, dx - \epsilon \left[\lim_{x\to\infty} W(c(x)) - \lim_{x\to-\infty} W(c(x)) \right] . \end{aligned}$$

Kinks are solutions that asymptotically link two vacuum points of the field theory. Consequently, the last term is fixed by the topological sector the kink belongs to. This is, it is path-independent within a topological sector. On the other hand, the integrand of the first term is non-negative. As a consequence, configurations that minimise this functional within a topological sector must satisfy

$$\dot{c}(x) + \epsilon \text{ grad } W(c(x)) = 0 \,,$$

which in coordinates produces a number of equations equal to the dimension of M

$$\frac{d\phi^i}{dx} = \pm g^{ji} \frac{\partial W}{\partial \phi^j} \qquad \forall i = 1, \ldots, \dim M \,. \tag{2.18}$$

These equations, referred to as Bogomol'nyi equations, establish the lower bound of energy for static configurations within a specific topological sector, also known as BPS-kinks. In particular, for BPS-kinks the only term that does not vanish in the static energy functional corresponds to the lower bound of the energy

$$E_{st}[\phi(x)] = \left| \lim_{x\to\infty} W(\phi(x)) - \lim_{x\to-\infty} W(\phi(x)) \right| \,, \tag{2.19}$$

which is fixed for a topological sector. As previously noted, kinks cannot be continuously deformed to change their topological sector and energy. This limitation arises because any intermediate configuration would asymptotically connect non-vacuum points, and such a transition would require an infinite amount of energy. On the

other hand, the energy i_1 of any of these solutions in the analogue mechanical system must vanish due to the asymptotic conditions. This is guaranteed for solutions of Bogomol'nyi equations since $\forall x$

$$i_1 = \frac{1}{2} g\left(\dot{c}(x), \dot{c}(x)\right) + U(c(x)) = \frac{1}{2}\left[\epsilon^2 - 1\right] g\left(\text{grad } W(c(x)), \text{grad } W(c(x))\right) = 0\,.$$

Once again, the primary advantage of restricting the types of theories under consideration (2.17) is that instead of a set of second order different equations which involve Christoffel symbols, a set of much simpler first order differential equations are obtained. In the process, however, solutions of the Newton equations are lost, but those that remain must asymptotically join by construction two vacua, which guarantees the finiteness of their energy.

Lastly, it is important to emphasise that this procedure is equivalent to the Hamilton-Jacobi formalism presented in chapter 1 for mechanical systems with vanishing energy. Indeed, the dependence in coordinates that the components of the metric tensor introduces does not alter the form of the Hamiltonian that was being considered for the analogue mechanical system

$$H = \frac{1}{2} g^{ij} p_i p_j - V(\phi)\,.$$

In this context, imposing Hamilton-Jacobi separability leads to a Hamilton principal function with zero energy that can be identified with the superpotential found in the Bogomol'nyi arrangement when the potential function in the field theory is of the form (2.17)

$$S = -i_1 t + W(\phi) = W(\phi)\,.$$

Thus, while the Bogomol'nyi arrangement will take the spotlight playing a key role in finding kinks in future chapters, it is important to keep in mind its connection with the Hamilton-Jacobi formalism. Indeed, Bogomol'nyi equations are a particular case of Hamilton-Jacobi's equations in disguise.

2.1.3 Alternative asymptotic conditions for kinks

In previous sections, the finite energy requirement was forced by imposing two conditions. On one hand, field profiles must tend at infinities to one of the zeroes of the potential. On the other, derivatives of the field profiles had to vanish at infinities. However, this last condition can be ignored in certain situations if the metric tensor defined on the target manifold vanishes at zeroes of the potential function. In order to illustrate this, let us construct an example for the simplest case, which is a field theory with only one field ϕ. In this example, a non-Euclidean geometry is chosen for the target manifold $\mathbb{R}$, which will be given by the following metric tensor

$$g = \frac{1}{\phi^2 + 1} d\phi \otimes d\phi\,.$$

Notice that this metric tensor vanishes at infinities. Accordingly, let us define a potential function that also vanishes at infinities. For instance, the following family of potentials is proposed

$$V = \frac{1}{2} \frac{1}{(\phi^2 + 1)^{2n-1}}\,,$$

with positive integer n. This family of potentials is compatible with the Bogomol'nyi arrangement, for which a family of superpotentials can be derived. This family is given by differential equations

$$\frac{dW}{d\phi} = \pm \frac{1}{(\phi^2+1)^n} \,,$$

whose solutions in general are hypergeometric functions. However, for the first members the analytical expression is simple. For instance, member $n = 1$ leads to a superpotential $W = \arctan\phi$. On the other hand, these potentials generate solutions whose profiles can be analytically obtained

$$\sum_{k=0}^{n-1} \binom{n-1}{k} \frac{\phi^{2k+1}}{2k+1} = \pm(x - x_0) \,, \tag{2.20}$$

with a constant x_0 that represents the centre of the kink. Notice that all cases correspond to diverging curves given that all coefficients are positive and that only odd potencies of ϕ are present, see Figure 2.2.

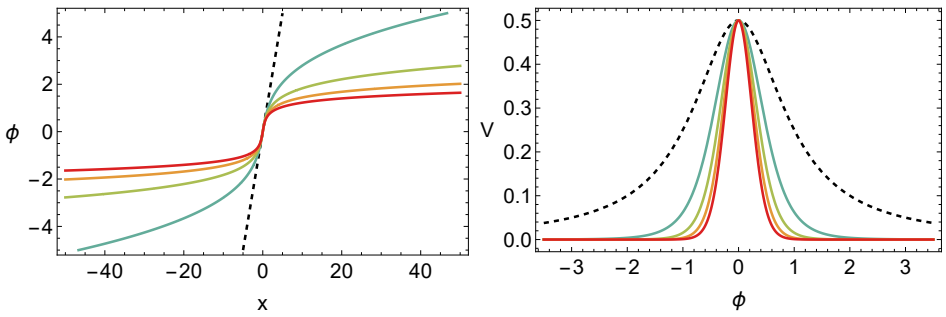

Figure 2.2: Field profiles on the left and corresponding potential functions on the right when n takes the values of the first five natural numbers. Case $n = 1$ has been depicted with a black dashed curve as a reference.

In fact, for the case $n = 1$ the profile is just a line $\phi = \pm(x - x_0)$. Both signs represent the kink-antikink symmetry. On the other hand, the energy of a solution in the analogue mechanical system is zero given that the metric tensor vanishes at infinities. This allows us to write the energy density as $\epsilon_n = 2V$ for each case n, as it was the case in the scenario of vanishing derivatives at infinities. Given that the profile of the solution when $n = 1$ can be explicitly derived $\phi(x) = \pm(x - x_0)$, so can its energy density

$$\epsilon_1(x) = \frac{1}{(x - x_0)^2 + 1} \,.$$

Clearly, this describes a lump centred around a point x_0. However, in order to be a kink the finiteness of the energy must be checked. Equation (2.19) provides the energy of all these solutions, which is finite for any member. Alternatively, integrating the energy density $\epsilon = 2V$ in all domain will provide us with an expression for any member

$$E = \sqrt{\pi}\, \frac{\Gamma\left[n - \frac{1}{2}\right]}{\Gamma\left[n\right]} \,,$$

where $\Gamma[n]$ is the Euler gamma function. Computing the energy of the first members one obtains

$$E = \pi, \frac{\pi}{2}, \frac{3\pi}{8}, \frac{15\pi}{48}, \frac{105\pi}{384}, \dots ,$$

This is, the energy diminishes as the parameter n increases, tending to zero as n approaches infinity, see Figure 2.3.

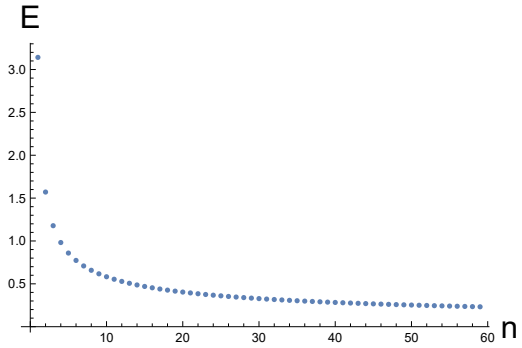

Figure 2.3: Representation of the energy of solutions for the first members of the family of solutions. The energy tends to zero as n approaches infinity.

In conclusion, these families of field theories support solutions for which the energy is finite. This is, even if the derivatives of the field profiles do not vanish at infinities, these are indeed kinks. It is worth noticing that in this example with only one field a change of variables can be performed so that a new model can be obtained for which the above solutions satisfy the original asymptotic conditions. However, this may not be the case when field theories with more fields are considered, where the freedom of choosing the geometry of the internal space also allows us to find this type of kink with alternative asymptotic conditions.

2.2 Stability of kinks

It is of great interest not only to obtain analytically solutions in classical field theory but also assessing their stability. In this section the analysis of linear stability under small perturbations presented in chapter 1 for Euclidean spaces is generalised to admit general Riemannian manifolds as target manifolds. The field equations that correspond to a Sigma model (2.16) include terms with second derivatives of fields with respect both time and space, but also with first derivatives. However, exactly as in the Euclidean case, while static solutions will not evolve by construction, perturbations of these may. Indeed, as the perfectly static configuration is abandoned, time derivatives in the field equation will generate changes in the field profiles. The same two scenarios are contemplated. It may occur that after this perturbation the kink profiles are bound and start oscillating around the static solution, reflecting the property of stability. Or, on the contrary, if the perturbation starts growing leaving completely behind the original configuration, we shall say that such a solution is unstable. While the same notion of linear stability under small perturbation is employed, it is worth studying the effect of the curvature of the target manifold in it. Undoubtedly, the presence of the Christoffel symbols will significantly augment the complexity of the stability analysis. Lastly, other criteria for stability will be explored.

2.2.1 Linear stability in field theory

In field theory, one can conduct a stability analysis analogous to the study of linear stability in mechanics [71]. A summary of this approach is presented in Appendix C. By following similar steps, the second derivative of the action will be evaluated at a reference static solution ϕ. This will allow us to identify variations that are also solutions to the first order in the parameter of the variation. Finally, adopting again a procedure similar to that employed in Chapter 1, Fourier transformations will be used to linearise the equations and derive spectral equations that encapsulate the information regarding the linear stability. The initial step is then to differentiate equation (2.12) with respect to the parameter of the variation ξ, resulting in the following expression for the second derivative

$$\frac{d^2S}{d\xi^2}[\varphi] = \int_{\mathbb{R}^{1,1}} \left[g\left(\frac{D}{\partial\xi}\frac{D\psi}{\partial t}, \varphi_t\right) + g\left(\frac{D\psi}{\partial t}, \frac{D\varphi_t}{\partial\xi}\right) - g\left(\frac{D}{\partial\xi}\frac{D\psi}{\partial x}, \varphi_x\right) \right.$$
$$\left. - g\left(\frac{D\psi}{\partial x}, \frac{D\varphi_x}{\partial\xi}\right) - g\left(\frac{D}{\partial\xi}(\text{grad } V), \psi\right) - g\left(\text{grad } V, \frac{D\psi}{\partial\xi}\right) \right] dx\, dt\,.$$

Notice that the derivative has been moved inside the integral again. This is possible because the limits of integration are independent of the variable with respect to which differentiation is being performed. Additionally, Levi-Civita connection is compatible with the metric, and as a result, the previously shown "distributive" property has been employed. Now, in the context of field theory, the variation $\varphi(t, x, \xi)$ involves an additional variable when it is compared to the mechanical case. Consequently, two separate relations for the Riemannian curvature tensor will be required

$$\frac{D}{\partial\xi}\frac{D\psi}{\partial z} - \frac{D}{\partial z}\frac{D\psi}{\partial\xi} = R(\varphi_z, \psi)\psi\,,$$

one for space and one for time $z = t, x$. This allows us to manipulate the second derivative to change the order in which covariant derivatives act

$$\frac{d^2S}{d\xi^2}[\varphi] = \int_{\mathbb{R}^{1,1}} \left[g\left(R(\varphi_t, \psi)\psi, \varphi_t\right) + g\left(\frac{D}{\partial t}\frac{D\psi}{\partial\xi}, \varphi_t\right) - g\left(R(\varphi_x, \psi)\psi, \varphi_x\right) \right.$$
$$- g\left(\frac{D}{\partial x}\frac{D\psi}{\partial\xi}, \varphi_x\right) + g\left(\frac{D\psi}{\partial t}, \frac{D\varphi_t}{\partial\xi}\right) - g\left(\frac{D\psi}{\partial x}, \frac{D\varphi_x}{\partial s}\right)$$
$$\left. - g\left(\frac{D}{\partial\xi}\left(\text{grad } V\right), \psi\right) - g\left(\text{grad } V, \frac{D\psi}{\partial\xi}\right) \right] dx\, dt\,. \tag{2.21}$$

Let us apply now the integration by parts (2.13) to the second and fourth terms. Through this process, certain terms vanish given that proper variation fields ψ also vanish at infinities

$$\lim_{t\to\pm\infty} \frac{D\psi}{\partial\xi} = \lim_{x\to\pm\infty} \frac{D\psi}{\partial\xi} = 0\,.$$

Finally, let us evaluate this second derivative for the reference solution. This is, for the member of this family of variation with $\xi = 0$

$$\left.\frac{d^2S}{d\xi^2}[\varphi]\right|_{\xi=0} = \int_{\mathbb{R}^{1,1}} \left[g\left(R(\phi_t, \psi)\psi, \phi_t\right) - g\left(R(\phi_x, \psi)\psi, \phi_x\right) \right.$$
$$\left. + g\left(\frac{D\psi}{\partial t}, \frac{D\phi_t}{\partial t}\right) - g\left(\frac{D\psi}{\partial t}, \frac{D\phi_x}{\partial x}\right) - g\left(\frac{D}{\partial\xi}\left(\text{grad } V\right), \psi\right) \right] dx\, dt\,.$$

When the integration by parts (2.13) is employed in the last three terms, certain terms vanish because configurations are fixed at infinities. Moreover, using in the first two terms the Riemannian curvature tensor's property

$$g(R(u,v)w,z) = -g(R(u,v)z,w) \quad \forall u,v,w,z \in \mathfrak{X}(M)\,,$$

the second derivative of the action for a given solution ϕ can be written as

$$\frac{d^2S}{d\xi^2}[\varphi]\Big|_{\xi=0} = \int_{\mathbb{R}^{1,1}} g\left(-\frac{D^2\psi}{\partial t^2} + \frac{D^2\psi}{\partial x^2} - R(\phi_t,V)(\phi_t) + R(\phi_x,\psi)(\phi_x) \right.$$
$$\left. -\nabla_\psi \text{grad } V,\psi\right) dx\; dt\,.$$

For static fields $\phi(x)$, the term involving the time derivative of the field vanishes. However, variation fields are time-dependent and the resulting operator is therefore also time-dependent

$$\frac{d^2S}{d\xi^2}[\varphi]\Big|_{\xi=0} = \int_{\mathbb{R}^{1,1}} g\left(-\frac{D^2\psi}{\partial t^2} + \frac{D^2\psi}{\partial x^2} + R(\phi_x,\psi)(\phi_x) - \nabla_\psi \text{grad } V,\psi\right) dx\,dt\,. \quad (2.22)$$

Variations of interest for studying linear stability under small perturbations are those that transform the reference solution into another solution of the field equations to the first order in the parameter of the variation. As will be demonstrated in next section, this implies that the second derivative above must vanish.

2.2.2 First order solution variations

Thus far, the only limitation that has been imposed on variations is that they must be proper variations. This is, variations must be fixed at infinities to ensure that the energy of the perturbation is finite. However, not every variation of a solution is a solution of the field equations. Consequently, among all possible proper variations of static solutions, we shall focus on those which are solutions at least to the first order in the parameter of the variation. This restricts the type of variations to small linear perturbations

$$\varphi^a = \phi^a_K(x) + \xi\;\psi^a(x,t) + O(\xi^2) \quad a = 1,\ldots,\dim M\,, \quad (2.23)$$

where ϕ^a_K and ψ^a denote the components of a static field configuration and those of the variation vector field respectively. The study of the time evolution for these variations will reveal information about how stable these static configurations are. Now, when introducing this form of the variation φ^a into the fields equations of a Sigma model (2.16) and subsequently truncating these equations while retaining terms up to the first degree, the equation governing the evolution of this type of variations in the field theory is derived

$$-\partial_t^2\psi^a + \partial_x^2\psi^a + 2\Gamma^a_{ij}\partial_x\psi^i\frac{d\phi^j_K}{dx} + \left.\frac{\partial\Gamma^a_{ij}}{\partial\phi^m}\right|_{\phi_K}\frac{d\phi^i_K}{dx}\frac{d\phi^j_K}{dx}\psi^m \quad (2.24)$$
$$= g^{ma}(\phi_K)\left.\frac{\partial U}{\partial\phi^m\partial\phi^n}\right|_{\phi_K}\psi^n + \left.\frac{\partial U}{\partial\phi^m}\right|_{\phi_K}\left.\frac{\partial g^{ma}}{\partial\phi^n}\right|_{\phi_K}\psi^n\,,$$

These equations can be expressed without coordinates so that a familiar form can be obtained. In order to achieve this, the following three ingredients will be required:

1. First, the covariant derivative of the variation vector field with respect to both time and spatial coordinate $z = t, x$ reads in coordinates as

$$\frac{D^2\psi}{\partial z^2} = \Big[\partial_z^2\psi^i + \partial_z\psi^b\partial_z\phi^a\Gamma^i_{ab} + \psi^b\partial_z^2\phi^a\Gamma^i_{ab} + \psi^b\partial_z\phi^a\partial_z\phi^m\frac{\partial\Gamma^i_{ab}}{\partial\phi^m} + \\ +\Gamma^i_{mj}\partial_z\phi^m\left(\partial_z\psi^j + \psi^b\partial_z\phi^a\Gamma^j_{ab}\right)\Big]\frac{\partial}{\partial\phi^i}\,.$$

2. Secondly, once the components of the Riemannian curvature tensor are written in terms of the Christoffel symbols, the following result can be readily verified

$$R(\phi_x,\psi)(\phi_x) = \partial_x\phi^a\psi^b\partial_x\phi^c\left[\partial_b\Gamma^i_{ac} - \partial_a\Gamma^i_{bc} + \Gamma^i_{b\lambda}\Gamma^\lambda_{ac} - \Gamma^i_{a\lambda}\Gamma^\lambda_{ab}\right]\frac{\partial}{\partial\phi^i}\,.$$

3. Lastly, the covariant derivative of the gradient of the potential V along the variation field ψ is written in coordinates as

$$\nabla_\psi\text{grad }V = \psi^b\left[\frac{\partial g^{\mu i}}{\partial\phi^b}\frac{\partial V}{\partial\phi^\mu} + g^{\mu i}\frac{\partial^2 V}{\partial\phi^b\partial\phi^\mu} + g^{\mu\nu}\Gamma^i_{b\nu}\frac{\partial V}{\partial\phi^\mu}\right]\frac{\partial}{\partial\phi^i}\,.$$

By taking into consideration these three key points, the evolution equation for these variations can be seen as a more concise equation when second and higher order terms in the parameter of the variation are neglected

$$-\frac{D^2\psi}{\partial t^2} + \frac{D^2\psi}{\partial x^2} + R(\phi_x,\psi)\phi_x - \nabla_\psi\text{grad }V = 0\,.$$

Notice that the left-hand side of this equation is precisely the operator found in the integrand of the second derivative of the action for static field configurations (2.22). Therefore, for linear perturbations of static solutions that produce solutions of the field theory to the first order in the parameter of the variation, the second derivative evaluated at the reference solution vanishes

$$\left.\frac{d^2S}{d\xi^2}\right|_{\xi=0} = 0\,.$$

This was expected, as the vanishing second derivative indicates that these variations deform solutions into other solutions to the first order in ξ. Notice that the evolution equation is an approximation, as higher order terms are not considered. However, these linear perturbations will highlight the most relevant information about the stability. Indeed, once these variations for a given solution have been identified, their time-evolution must be studied to obtain information about their stability. This objective guides the next section, where, following an analogously approach to that employed in Chapter 1, spectral equations that define vibrational modes are sought.

2.2.3 Spectral equation and vibrational modes

The evolution equations of small linear perturbations (2.24) are second order differential equations in partial derivatives. Therefore, the direct identification of solutions is a formidable task. To extract information, without any loss of generality the

components of the variation vector field ψ^a will be written in terms of its Fourier's transform σ^a

$$\psi^a(x,t) = \frac{1}{\sqrt{2\pi}} \int_{-\infty}^{\infty} e^{i\omega t} \sigma^a(x,\omega)\, d\omega\,, \tag{2.25}$$

replacing time by the new variable ω. Introducing this form of the variation vector field ψ in equations (2.24) we obtain $\dim M$ equations

$$\frac{1}{\sqrt{2\pi}} \int_{-\infty}^{\infty} e^{i\omega t} F^a(\omega,x)\, d\omega = 0 \quad a = 1,\ldots,\dim M\,, \tag{2.26}$$

one for each dimension of the target manifold, where functions $F^a(\omega,x)$ of the new variable ω and the spatial coordinate x are given by

$$F^a(\omega,x) = -\partial_x^2\sigma^a - 2\Gamma^a_{ij}\partial_x\sigma^i \frac{d\phi^j_K}{dx} - \left.\frac{\partial\Gamma^a_{ij}}{\partial\phi^m}\right|_{\phi_K} \frac{d\phi^i_K}{dx}\frac{d\phi^j_K}{dx}\sigma^m +$$

$$+ g^{ma}(\phi_K) \left.\frac{\partial V}{\partial\phi^m\partial\phi^n}\right|_{\phi_K} \sigma^n + \left.\frac{\partial V}{\partial\phi^m}\right|_{\phi_K} \left.\frac{\partial g^{ma}}{\partial\phi^n}\right|_{\phi_K} \sigma^n - \omega^2\sigma^a\,.$$

Since the Fourier transform of the zero function is the zero function again, it follows from equation (2.26) that $F^a(\omega) = 0$ holds for every coordinate $a = 1,\ldots,\dim M$. Therefore, the information regarding this type of variations is encoded in the functions $\sigma^a(x,\omega)$, which are defined by equations

$$-\partial_x^2\sigma^a - 2\Gamma^a_{ij}\partial_x\sigma^i \frac{d\phi^j_K}{dx} - \left.\frac{\partial\Gamma^a_{ij}}{\partial\phi^m}\right|_{\phi_K} \frac{d\phi^i_K}{dx}\frac{d\phi^j_K}{dx}\sigma^m \tag{2.27}$$

$$+ g^{ma}(\phi_K) \left.\frac{\partial V}{\partial\phi^m\partial\phi^n}\right|_{\phi_K} \sigma^n + \left.\frac{\partial V}{\partial\phi^m}\right|_{\phi_K} \left.\frac{\partial g^{ma}}{\partial\phi^n}\right|_{\phi_K} \sigma^n = \omega^2\sigma^a\,.$$

These are spectral equations whose spectra contain the information about the time evolution and whose eigenvalues define the form of such variations. For the sake of simplicity, let us express this spectral equation more compactly by defining the Hessian operator $\mathcal{H}$ as the matrix differential operator that encompasses all the left hand sides of the equation (2.27), so that they can be equivalently written as

$$\mathcal{H}\sigma = \omega^2\sigma\,, \tag{2.28}$$

with $\sigma = (\sigma^1,\ldots,\sigma^{\dim M})^T$. Note that when the variation field ψ is time-independent, equation $\mathcal{H}\sigma = 0$ is obtained. This is precisely the equation that describes in mechanics small linear perturbation that are also solutions of the Euler-Lagrange equations. This is only natural, since perturbing a static solution with a time-independent variation is equivalent to restricting to the mechanical analogy. As mentioned in Chapter 1, these variations defined by zero eigenvalue $\omega^2 = 0$, receive the name of zero modes and will appear as a result of certain symmetries as we shall see.

On the other hand, it is worth noting that these equations are a generalisation of the spectral equations derived in Chapter 1 for Euclidean target spaces in Cartesian coordinates. Indeed, for the type of field theories discussed in last chapter, the first derivatives terms $\partial_x\sigma^i$ disappear as the Christoffel symbols vanish. This is another

consequence of generalising to field theories that take values in general Riemannian manifolds, the analysis of small linear perturbations becomes more intricate.

Now, to study the behaviour of these variations we must realise that eigenvalues ω^2 define the frequencies that remain in the exponentials in the Fourier transform of the vector field variation (2.25). This implies that any negative eigenvalue in the spectrum $Spec(\mathcal{H})$ will lead to a non-bounded exponential $e^{i\omega t}$ in the integrand. If at least one negative eigenvalue ω^2 is found, then there exists a variation that will grow indefinitely. Exactly as in the previous chapter, in such a case, the static solution is said to be linearly unstable. If, on the contrary, the discrete spectrum of this operator is non-negative then we will say that the static solution will be stable.

While each static solution in each Sigma model may give rise to distinct spectral equations, vacuum solutions will always lead to a spectral equation of the same form. If a vacuum solution $\phi^i(x) = \phi_0^i$ with $\phi_0^i \in \mathbb{R}$ for $i = 1, \ldots, \dim M$ is chosen to be analysed, the spectral equation reads

$$-\partial_x^2 \sigma^a + C_n^a \sigma^n = \omega^2 \sigma^a \,,$$

where since the vacuum point is a minimum all the derivatives of the potential evaluated at that point vanish and C_n^a is defined as follows

$$\left.\frac{\partial V}{\partial \phi^m}\right|_{\phi_0} = 0 \,, \qquad C_n^a = g^{ma}(\phi_0) \left.\frac{\partial V}{\partial \phi^m \partial \phi^n}\right|_{\phi_0} > 0 \,.$$

Notice that since the metric tensor is symmetric, a basis for which it is diagonal can be chosen. This implies that in these coordinates this constant matrix C_n^a is also diagonal and its components positive because it is a Riemannian metric tensor and any second derivative of the potential must be positive since it is a minimum. A spectral problem of this type cannot have negative spectrum and therefore any vacuum point of a Sigma model is linearly stable.

On the other hand, the analysis of the spectrum of a Hessian operator for a general static solution of a Sigma model is highly non-trivial. In general, numerical methods will be needed for identifying it. Examples of these analysis will be presented in future chapters, where the spectra will be thoroughly discussed.

Lastly, it is important to emphasise that the linear stability of only static solutions are analysed. However, this is the only type of solution in which we are interested, as it leads to kinks. One may consider studying the stability of a kink in motion. However, this formalism should ensure that variations, as solutions, are Lorentz-invariant.

2.2.4 Other criteria of stability

Last section establishes the foundations for studying the linear stability of static solutions of a Sigma model under small perturbations. However, it is important to note that other arguments may reveal different types of stability or instability. First, whether an energetic argument can be employed to extract information regarding the stability will be discussed. Secondly, the possibility of decaying into vacuum and its connection with the topology of the target manifold will be explored.

If a potential admits only one superpotential, solutions of Bogomol'nyi equations for this superpotential minimise the static energy (2.19) within their respective topological sectors. However, if more than one differentiable superpotential

$W(\phi^1,\dots,\phi^m)$ with $m=\dim M$ can be found as solution of the equation

$$g^{ij}\frac{\partial W}{\partial \phi^i}\frac{\partial W}{\partial \phi^j}=2V(\phi^1,\dots,\phi^m)\,, \tag{2.29}$$

up to signs and constants, then a solution of one superpotential may not be the absolute minimum of the energy in its topological sector. Indeed, given a solution $\phi_A(x)$ of a superpotential, another superpotential for the same potential may yield another solution $\phi_B(x)$ in the same topological sector with lower energy

$$E_{st}[\phi_A(x)]>E_{st}[\phi_B(x)]\,.$$

In this sense, another criterion for stability arises, one that considers whether there exist other solutions in the same topological sector to which it may decay. Thus, it is necessary to compare the energy of all solutions that belongs to the same topological sector, even if they originate from different superpotentials. This is, more energetic solutions can be promptly identified as unstable solutions. Conversely, when no other superpotential with a solution in that topological sector can be found or the energy for those other superpotentials is the same, that solution will be regarded as stable from an energetic point of view.

In general, determining whether a potential admits more than one superpotential is not possible since equation (2.29) is a differential equation in partial derivatives. This problem is avoided when the dimension of the target manifold is $\dim M=1$, as the uniqueness of the superpotential follows from the fact that it is an ordinary differential equation. However, in general the dimension of the target manifolds will be higher than one. Nevertheless, when the superpotential is additively separable, this uniqueness, up to signs and additive constants, is retrieved regardless of the dimension of the target manifold. In order to see this, let us consider a field theory with fields $\phi^1,\dots,\phi^m$ with $m=\dim M$. Moreover, let us consider differentiable functions $f_1(\phi),\dots,f_m(\phi)$ and the following potential

$$V(\phi)=\sum_{i=1}^{m}\frac{1}{2}g^{ii}(\phi)f_i^2(\phi)\,.$$

Identification of terms with those of the potential (2.29) leads to m uncoupled differential equations

$$\frac{\partial W}{\partial \phi^i}=f^i(\phi^i)\quad i=1,\dots,m\,.$$

This implies that, up to additive constants, instead of just one, 2^m additively separable superpotentials emerge as solutions

$$W(\phi^1,\dots,\phi^m)=\sum_{i=1}^{m}\int(-1)^{\epsilon_i}f^i(\phi^i)d\phi^i+K$$

where $K\in\mathbb{R}$ and $\epsilon_i=0,1$. Despite this multiplicity of superpotentials, the signs ϵ_i are irrelevant when computing the energy since they are compensated with those in Bogomol'nyi equations. Naturally, this must occur since the energy is always positive (2.2). The energy of a solution that asymptotically joins two vacua is independent of the chosen member of this family of superpotentials. This scenario where only

one potential function can arise leads to a stability from the energetic perspective. This will be further discussed with an example in chapter 4.

On the other hand, instead of analysing the stability under small linear perturbations or through energetic arguments, among all solutions to which a solution may decay into, let us now direct our attention to the possibility of decay into vacuum. This was explored for Euclidean target spaces in Chapter 1, leading to the notion of brochoson, a non-topological kink that cannot decay into vacuum because of topological constraints. This type of solution can be found not only for Euclidean target spaces, but also when the target manifold is a Riemannian manifold in general. Their inability for decaying into vacuum resembles that of topological kinks due to the fixed ends, see Figure 2.4.

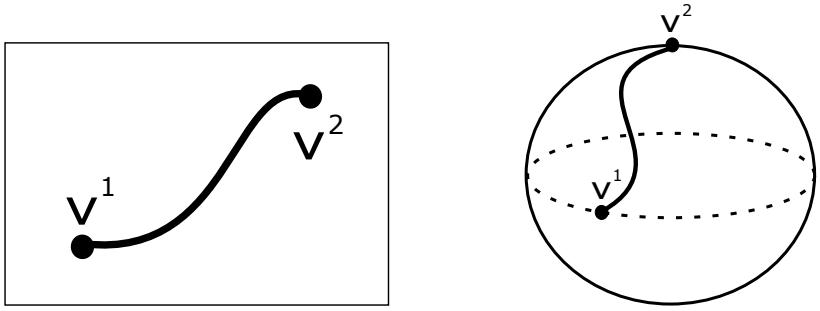

Figure 2.4: Topological kinks in the Euclidean plane and in the sphere. These cannot decay into vacuum because displacing any end from a vacuum point would require an infinite amount of energy.

Since non-topological are loops, these do not have in general a topological impediment to decay, see Figure 2.5. Elastic forces that appear in the field equations may cause these loops to contract into points.

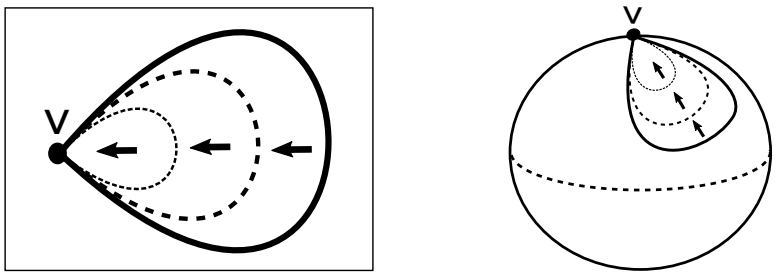

Figure 2.5: Elastic forces will tend to cause non-topological kinks to shrink. Graphical examples of contractions of non-topological kinks into vacuum in the Euclidean plane and in the sphere have been depicted.

However, this topological protection can be achieved by considering, instead of a simply connected manifold as the target space, for example the Euclidean space $\mathbb{R}^n$ or the sphere $\mathbb{S}^n$, a non-simply connected manifold. There are several approaches through which this can be accomplished. One possibility is removing points from an Euclidean space, as it was the case in the model in elliptic coordinates presented in Chapter 1. Another, far more interesting, is to directly consider a non-simply connected target manifold. For instance, one may consider the $2-$dimensional torus, see Figure 2.6. These scenarios will be studied in future chapters.

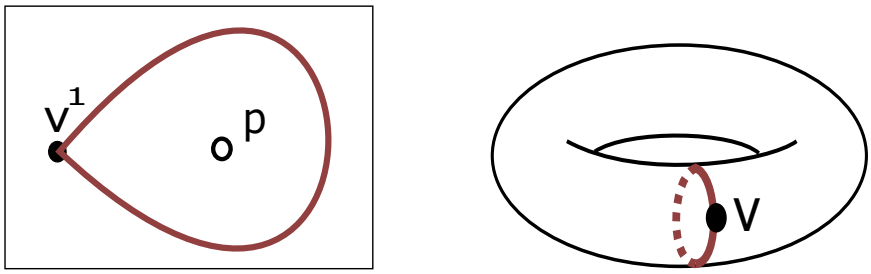

Figure 2.6: Non-topological kinks can be stable if the target manifold is non-simply connected manifolds. Examples of non-contractible loops in $\mathbb{R}^2 - \{p\}$ and in the torus $\mathbb{S}^1 \times \mathbb{S}^1$ have been depicted.

2.3 Mechanism for geometrical constriction

In this chapter the Sigma models have been introduced, which allows us to deal with field theories with a broader range of target spaces. In this section, particular Sigma models on $\mathbb{R}^n$ with different geometries are constructed. In particular, the results published in [30] are summarised, where a mechanism to mimic and modulate geometrical constraints in ferromagnetic materials is described. This will be accomplished by extending both the target space and the superpotential of a given model, changing the geometry of the target space in the process.

The main motivation of this section is based on the experimental results described in [85] and the techniques developed in [40]. In [85] the authors prove that the magnetisation distribution in a wall structure can be controlled in geometrically constricted magnetic materials. In [40] a method to modify the internal structure of kinks in the two-dimensional ϕ^4-model is presented. In the present section, this method is generalised not only allowing to control continuously the internal structure, but also including the possibility of transforming a configuration asymmetrically. This generalised method is applied to two models, a ϕ^4 model and the two-dimensional model described in [33].

2.3.1 Extended target space

The main idea in [40] is to induce a change in the profiles and energy density for a Sigma model on an Euclidean space $\mathbb{R}^n$ that admits a superpotential. This is accomplished by replacing the original target space $\mathbb{R}^n$ by a bigger one $\mathbb{R}^{n+1}$. Instead of assigning a physical meaning to this extra dimension, the extra field that arises will modulate the other field profiles. This is, the emerging kinks in the extended target space are projected to the original target space, creating a change in the original profiles in the process. In order to do this, the extended space $\mathbb{R}^{n+1}$ is endowed with a metric tensor which is not Euclidean in general. Let us denote as $(\phi^1, \ldots, \phi^n)$ the coordinates of the original target space $\mathbb{R}^n$ and $(\phi^1, \ldots, \phi^n, \psi)$ the coordinates on the extended target space $\mathbb{R}^{n+1}$. Let us once again restrict to models that admit the Bogomol'nyi arrangement and let us denote as $W_0(\phi^1, \ldots, \phi^n)$ the superpotential from which the original Sigma model is constructed. Moreover, the n kink profiles that arise in the original model will be denoted as $\phi^i(x)$. In these coordinates, the geometry for the extended space, determined by the metric tensor,

is defined as

$$g = f(\psi)\left[d\phi^1 \otimes d\phi^1 + \cdots + d\phi^n \otimes d\phi^n\right] + d\psi \otimes d\psi\,, \tag{2.30}$$

where $f(\psi)$ is a non-negative function. This extension equally alters the distances in the first n directions, now affected by the coordinate ψ. Since potential functions for which the Bogomol'nyi arrangement can be performed are sought, the form of the metric tensor produces the following form for potentials (2.17) in these coordinates

$$V(\phi^1, \ldots, \phi^n, \psi) = \frac{1}{2f(\psi)}\left[\sum_{i=1}^{n}\left(\frac{\partial W}{\partial \phi^i}\right)^2\right] + \frac{1}{2}\left(\frac{\partial W}{\partial \psi}\right)^2 . \tag{2.31}$$

Furthermore, if the new superpotential is constructed adding to the original one a term that depends exclusively on ψ

$$W = W_0(\phi^1, \ldots, \phi^n) + h(\psi)\,, \tag{2.32}$$

then the extra field profile can be isolated in Bogomol'nyi equations (2.18). Indeed, these equations are partially decoupled

$$\frac{d\phi^i}{dx} = \pm\frac{1}{f(\psi)}\frac{\partial W_0}{\partial \phi^i} \quad i = 1, \ldots, n, \qquad \frac{d\psi}{dx} = \pm\frac{dh}{d\psi}\,. \tag{2.33}$$

When the integral of the last equation exists and the explicit profile $\psi(x)$ can be analytically obtained, the rest of the equations can be reparametrised

$$\frac{d\phi^i}{d\xi} = \pm\frac{\partial W_0}{\partial \phi^i} \quad i = 1, \ldots, n\,,$$

in terms of a new spatial coordinate $\xi(x)$ that will receive the name of geometrical coordinate, which is defined as

$$\xi = \xi_0 + \int \frac{dx}{f(\psi(x))}\,, \tag{2.34}$$

where $\xi_0 \in \mathbb{R}$ is an integration constant. Notice that this reparametrisation depends on the geometry of the extended target space, encoded in the function $f(\psi)$ of the metric and in the function $h(\psi)$ of the superpotential. Solving the reparametrised equations produce modified profiles $\phi^i(\xi(x))$ for the n original fields $\phi^i(x)$. Obviously, the original unaltered case is recovered when $f(\psi) = 1$ since this leads to $\xi = x$ up to a constant. On the other hand, the energy densities of these solutions are also affected by the change in their field profiles. The new energy density will be split into two contributions that shall be denoted as $\epsilon = \epsilon_1 + \epsilon_2$. On one hand, the first contribution ϵ_1 is generated by the n fields ϕ^i

$$\epsilon_1(x) = \frac{1}{f(\psi(x))}\left[\sum_{i=1}^{n}\left(\frac{\partial W_0}{\partial \phi^i}\right)^2\right]\Bigg|_{\phi(\xi(x))} = \frac{2V_0(\phi(\xi(x)))}{f(\psi(x))}\,, \tag{2.35}$$

where V_0 is the potential of the original field theory. The second one ϵ_2, which emerges due to the extra field ψ, will be given by

$$\epsilon_2(x) = \left.\frac{dh}{d\psi}\right|_{\psi(x)}\,. \tag{2.36}$$

Note that if $f(\psi) = 1$ and $h(\psi)$ is a constant function, the same field and energies profiles from the original model are recovered. Now, the change in the geometry can be performed so that singularities are introduced in the metric tensor, see [40]. In this scenario, any singularity in the component g_{ii} of the metric tensor at a point prevents solutions from advancing along that direction i at that point. Indeed, if the tangent vector in that direction at that point is not zero the contribution to the energy (2.2) is infinite. This places significant geometrical constraints on solutions. In our case, alternative geometries will be proposed so that these singularities are avoided, only recovering this scenario as a limit. This will be discussed in next section.

2.3.2 Two families of geometrical constrictions

In [40] kink profiles and their energy density profiles are modulated by defining two singular metric tensors on the extended target space. In particular, these are determined by functions

$$f_1(\psi) = \frac{1}{\psi^2}\,, \quad f_2(\psi) = \frac{1}{\cos^2 n\pi\psi}\,,$$

where n is a positive integer. While the first function implies the existence of singular points when $\psi = 0$, function $f_2(\psi)$ has an infinite number of zeroes, which are periodically distributed at $\psi = \frac{2k+1}{2n}$ with $k \in \mathbb{Z}$. In order to avoid an infinite energy, constricted solutions in [40] must cross orthogonally continua of singularities. For instance, when constricting the ϕ^4-model, curves must cross orthogonally the lines of singular points given by constant values of ψ. In the case at hand, these singular metric tensors will be replaced by two families of metric tensors that will serve as a bridge connecting the original Euclidean model with the completely constricted case that includes singularities in the metric. This is, the following two one-parameter families of functions are considered

$$f_1(\psi) = \frac{1+\lambda}{1+\lambda\psi^2}\,, \quad f_2(\psi) = \frac{1+\lambda}{1+\lambda\cos^2 n\pi\psi}\,,$$

with parameter $\lambda \in [0, \infty)$. Notice how both limits of this parameter are precisely the Euclidean case $\lambda = 0$ and the completely constrained one $\lambda \to \infty$. This avoids singularities in the metric while allowing distances to be arbitrarily big so that minimum energy curves cross the singularities with increasing angle, being orthogonal in the limit $\lambda \to \infty$. Intermediate values of λ will modify the core of these profiles, transitioning continuously from one case to the other. Let us fix for both geometries, given by functions f_1 and f_2 respectively, the same function $h(\psi)$ in the superpotential

$$h(\psi) = \alpha\left(\psi - \frac{\psi^3}{3}\right)\,,$$

with positive constant $\alpha > 0$. This choice of $h(\psi)$, which corresponds to a superpotential of a ϕ^4-model, will produce the following profile and energy density for the extra field

$$\psi(x) = \pm\tanh\left(\alpha(x - x_0)\right)\,, \quad \epsilon_2 = \alpha^2\,\mathrm{sech}^4(\alpha(x - x_0))\,,$$

where x_0 is an integration constant that determines the centre of the kink. The integration of its energy density $\epsilon_2(x)$ provides the energetic contribution of this field $\psi(x)$, which is $E_2 = \frac{4\alpha}{3}$. On the other hand, this profile engenders for both functions f_1 and f_2 by equation (2.34) the following two geometrical coordinates

$$\xi_1(x) = \xi_0 + x - x_0 - \frac{\lambda}{\alpha(1+\lambda)} \tanh\left(\alpha(x-x_0)\right), \tag{2.37}$$

$$\xi_2(x) = \xi_0 + \frac{2+\lambda}{2(1+\lambda)}(x-x_0) + \frac{\lambda}{4\alpha(1+\lambda)}\left(Ci\left(\zeta_n^+\right) - Ci\left(\zeta_n^-\right)\right), \tag{2.38}$$

where ξ_0 is a constant of integration that will play an important role in the asymmetrisation of solutions, Ci is the cosine integral function and

$$\zeta_n^{\pm}(x) = 2n\pi(1 \pm \tanh\alpha(x-x_0)),$$

Once more, notice how the parameter λ interpolates the geometrical coordinates in the original Euclidean case and that of the full constrained one. The geometrical coordinate ξ_1 forms a plateau at $x = 0$ as λ approaches the limit $\lambda \to \infty$. The other one ξ_2, forms $2n$ plateaux in the same limit of λ, see Figure 2.7.

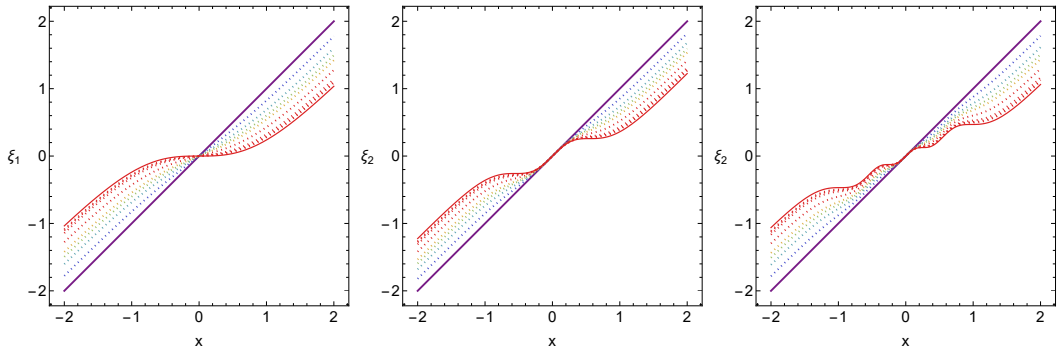

Figure 2.7: Geometrical coordinate ξ_1 on the left, ξ_2 with $n = 1$ in the centre and with $n = 2$ on the right for different values of λ. Parameters $\alpha = 1$ and $\xi_0 = 0$ have been employed. The case $\lambda = 0$ is represented by a thick line while cases with $\lambda > 0$ are represented with dotted lines.

It is important to highlight that limits of these geometrical coordinates correspond to minus infinity and infinity. This implies that the constrained profiles $\phi^i(\xi(x))$ will tend to the same values as the original ones $\phi^i(x)$. Since the potential has been constructed from a superpotential and these geometrical coordinates are differentiable, the contribution to the energy of the n fields $\phi^i(\xi(x))$ must be the same as their energy in the original model

$$\begin{aligned} E_1 = \int_{-\infty}^{\infty} \epsilon_2(x)\,dx &= \lim_{x\to\infty} W_0(\phi^i(\xi(x))) - \lim_{x\to-\infty} W_0(\phi^i(\xi(x))) \\ &= \lim_{x\to\infty} W_0(\phi^i(x)) - \lim_{x\to-\infty} W_0(\phi^i(x)) = E_0\,. \end{aligned}$$

However, the contribution of the extra field ψ to the energy depends on the parameter introduced in the superpotential α. Therefore, the total energy of these constrained solutions also depends on this parameter α

$$E = E_0 + \frac{4}{3}\alpha \geq E_0\,.$$

Finally, these two families of geometrical constrictions will be applied to two particular models. The first one, which shall be referred to as Case A, will be the ϕ^4-model with one field. In the other model, which will correspond to Case B, this mechanism of continuous geometrical constriction will be employed for solutions of a particular field theory with two fields [33].

2.3.3 Extensions of the ϕ^4-model

The ϕ^4-model, among various other applications, can mimic magnetic transitions. For instance, Néel walls can be modelled. Since this model also admits a superpotential, it is a good candidate to illustrate how this mechanism of continuous geometrical constriction works. In particular, as described in Chapter 1, the superpotential and potential functions can be written as follows

$$W_0(\phi) = \phi - \frac{\phi^3}{3}\,, \quad V = \frac{1}{2}\left(1-\phi^2\right)^2\,.$$

Solving Bogomol'nyi equations, a kink and an antikink are easily derived. For the sake of simplicity, let us consider the unshifted kink $x_0 = 0$ as profile to geometrically constrain

$$\phi(x) = \tanh(x)\,, \quad \epsilon(x) = \operatorname{sech}^4 x\,,$$

where $\epsilon(x)$ is the corresponding energy density. When this mechanism is applied to this solution, it leads to a new field profile and a new energy density for each chosen geometry, given by f_1 and f_2.

- **Function** f_1: For f_1 we find a field profile and an energy density profile

$$\phi_{f_1}(x) = \tanh\left[\xi_0 + x - x_0 - \frac{\lambda}{\alpha(1+\lambda)}\tanh\left(\alpha(x-x_0)\right)\right],$$
$$\epsilon_{1,f_1}(x) = \frac{1+\lambda\tanh^2(x-x_0)}{1+\lambda}\left(1-\phi_{f_1}^2(x)\right)^2\,,$$

  which are depicted in Figure 2.8. Notice how an incipient plateau in the geometrical coordinate $\xi_1(x)$ generates an incipient plateau in the field profile, which is only a true plateau in the limit $\lambda \to \infty$. On the other hand, in the energy density profile $\epsilon_1(x)$ a new minimum is formed for a certain value of λ. Indeed, from equation (2.35) follows that for any $x_s \in \mathbb{R}$ for which $\psi(x_s)$ tends to a singularity of f_1 for high values of λ, the energy density also tends to zero due to the factor $\frac{1}{f(\psi(x))}$. In particular, this transition from maximum to minimum occurs at a value $\lambda = \lambda_*(\alpha)$ that depends on the parameter α

$$\lambda_* = \frac{\beta^{1/3}}{\alpha} + \frac{\alpha}{3\beta^{1/3}} - \frac{2}{3}\,, \quad \text{where} \quad \beta = \alpha\left(\alpha^2 + 27 + 3 + \sqrt{3(2\alpha^2+27)}\right)\,.$$

  Lastly, it is worth noticing that a non-vanishing integration constant ξ_0 produces an asymmetry in both the field profile and in the energy density profile, see Figure 2.8. The plateau is shifted upwards or downwards in the field profile and two lumps of different heights appear in the energy density.

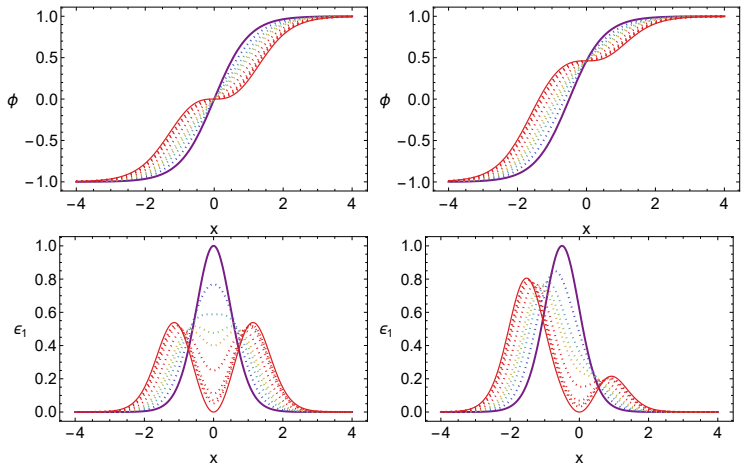

Figure 2.8: Solution $\phi(x)$ and its energy density profile $\epsilon_1(x)$ for different values of the parameter λ that controls the constraint. On the left the symmetric case $\xi_0 = 0$ is presented and on the right the asymmetry of the case with $\xi_0 = \frac{1}{2}$ is shown. The original case $\lambda = 0$ is represented by the thick purple line while that corresponding to $\lambda \to \infty$ by a thin red line. Intermediate values are represented by dotted lines. The value of the parameter $\alpha = 1$ has been employed.

- **Function** f_2: For the second geometry in $\mathbb{R}^2$ that has been proposed, which is given by the above defined function f_2, the field and energy density profiles read

$$\phi_{f_2}(x) = \tanh \xi_0 + \frac{2+\lambda}{2(1+\lambda)}(x - x_0) + \frac{\lambda}{4\alpha(1+\lambda)} \left(Ci\left(\zeta_n^+\right) - Ci\left(\zeta_n^-\right)\right),$$

$$\epsilon_{1,f_2}(x) = \frac{1 + \lambda \cos^2 n\pi \tanh^2 (x - x_0)}{1+\lambda} \left(1 - \phi_{f2}^2(x)\right)^2 .$$

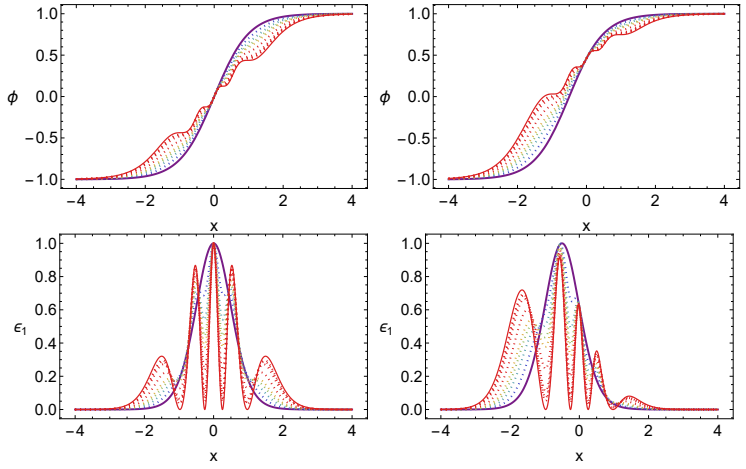

Figure 2.9: Solution $\phi(x)$ and its energy density profile $\epsilon_1(x)$ for different values of the parameter λ that controls the constraint when $n = 2$ is chosen. On the left the symmetric case $\xi_0 = 0$ is presented and on the right the asymmetry of the case with $\xi_0 = \frac{1}{2}$ is shown. The original case $\lambda = 0$ is represented by the thick purple line while that corresponding to $\lambda \to \infty$ by a thin red line. Intermediate values are represented by dotted lines. The value of the parameter $\alpha = 1$ has been employed.

Naturally, $\phi_{f_2}(x)$ presents now $2n$ incipient plateaux instead of just one incipient minimum, inherited from $\xi_2(x)$. Similarly to the case of f_1, in the energy density will appear $2n$ minima for the same reason, see Figure 2.9.

2.3.4 Extensions of a field theory with two fields

With the introduction of multiple fields more interesting structures emerge. For instance, it becomes possible to model the degrees of freedom of Bloch walls by this mechanism, where geometrical constrictions are simulated. As a two-dimensional representative to apply this procedure, the model described in [33] is employed. This model, like the previous one, can be constructed from a superpotential

$$W_0(\phi,\chi) = \phi - \frac{\phi^3}{3} - r\phi\chi^2\,, \quad V_0(\phi,\chi) = \frac{1}{2}\left[(1-\phi^2-r\chi^2)^2 + 4r^2\phi^2\chi^2\right]\,, \tag{2.39}$$

where $r \in \mathbb{R}$ and fields will be denoted as $\phi^1 \equiv \phi$ and $\phi^2 \equiv \chi$ following the original notation. This model has been profusely studied [12, 33] and both singular and families of kinks have been found. However, for the sake of simplicity let us apply this method to a particular solution which is obtained by considering elliptic orbits

$$\phi(x) = \tanh(2rx)\,, \quad \chi(x) = \sqrt{\frac{1-2r}{r}}\,\operatorname{sech}(2rx)\,, \tag{2.40}$$

where the parameter r must be within the range of values $r \in \left(0, \frac{1}{2}\right)$. This chosen solution joins minima located at $(\phi,\chi) = (-1,0)$ and $(\phi,\chi) = (1,0)$. By construction, the geometrical constriction will leave both ends of the kink unaltered, since both geometrical coordinates have the same limits at infinity than x. For the geometry in the extended target space $\mathbb{R}^2$ that f_1 defines, we obtain

$$\begin{aligned}
\phi_{f_1}(x) &= \tanh\left[2r\left(\xi_0 + x - x_0 - \frac{\lambda}{\alpha(1+\lambda)}\tanh\left(\alpha(x-x_0)\right)\right)\right]\,,\\
\chi_{f_1}(x) &= \sqrt{\frac{1-2r}{r}}\,\operatorname{sech}\left[2r\left(\xi_0 + x - x_0 - \frac{\lambda}{\alpha(1+\lambda)}\tanh\left(\alpha(x-x_0)\right)\right)\right]\,,\\
\epsilon_{1,f_1}(x) &= \frac{1+\lambda\tanh^2\left[\alpha(x-x_0)\right]}{1+\lambda}\left[(1-\phi_{f_1}^2(x)-r\chi_{f_1}^2(x))^2 + 4r^2\phi_{f_1}^2(x)\chi_{f_1}^2(x)\right]\,.
\end{aligned}$$

These field and energy density profiles have been depicted in Figure 2.10. The effect of this mechanism is identical to that in the ϕ^4-model, but it is simultaneously applied to both fields ϕ and χ. An incipient plateau is inherited in the origin from the geometrical coordinates for both fields and a minimum appears in the energy density for high values of λ. The integration constant ξ_0 creates again an asymmetry in both field and energy density profiles.

Notice that in this procedure the orbits in the projection to $\mathbb{R}^2$ coincide with those of the original model. Indeed, Bogomol'nyi equations (2.33) lead to the same flow orbit equation in the projected plane

$$\frac{d\phi^2}{d\phi^1} = \frac{\frac{\partial W_0}{\partial \phi^1}}{\frac{\partial W_0}{\partial \phi^2}}\,,$$

as the common global factor $f(\psi)$ disappears, see Figure 2.11.

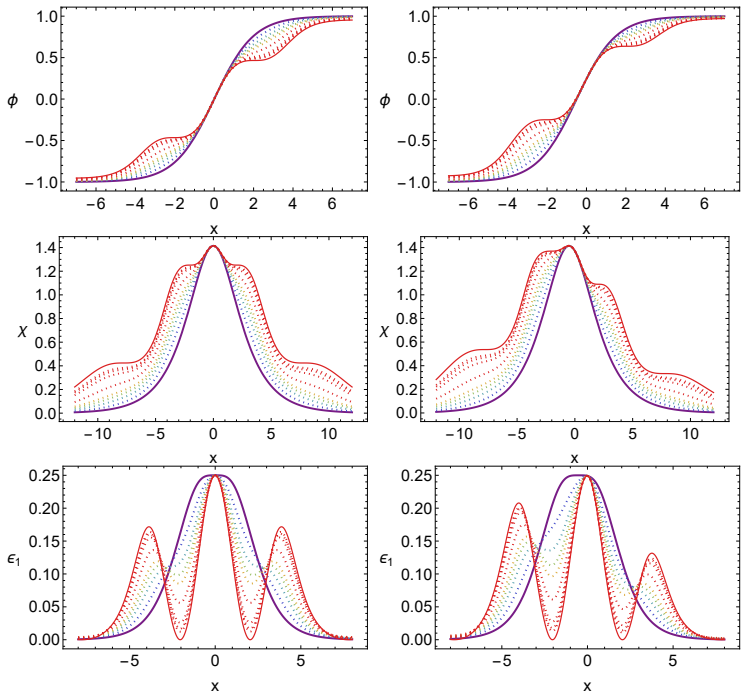

Figure 2.10: Solutions $\phi(x)$ and $\chi(x)$ and their energy density profile $\epsilon_1(x)$ for different values of the parameter λ that controls the constraint. On the left the symmetric case $\xi_0 = 0$ is presented and on the right the asymmetry of the case with $\xi_0 = \frac{1}{2}$ is shown. The original case $\lambda = 0$ is represented by the thick purple line while that corresponding to $\lambda \to \infty$ by a thin red line. Intermediate values are represented by dotted lines. Values of the parameters $\alpha = 1$ and $r = \frac{1}{4}$ have been employed.

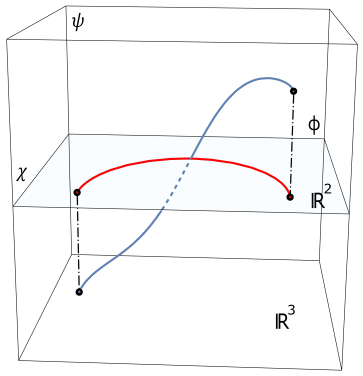

Figure 2.11: The projection of the new kink to the original target space results in the same orbit than that of the original kink. This detour through the extra dimension alters the parametrisation of the projected curve, which does not coincide with the original one except for the trivial case when $\lambda = 0$. Solutions has been displaced from the origin to improve the clarity of the figure.

However, even though the new projected orbits are the same as the original, the parametrisation changes significantly. The new curve is allowed to move in the extra dimension, reducing the velocity with which it advances along the projected orbit.

On the other hand, for f_2 the analogue constrained profiles are of the form

$$\phi_{f_2}(x) = \tanh\left[2r\left(\xi_0 + \frac{2+\lambda}{2(1+\lambda)}(x-x_0) + \frac{\lambda}{4\alpha(1+\lambda)}\delta_n(x)\right)\right],$$

$$\chi_{f_2}(x) = \sqrt{\frac{1-2r}{r}}\,\mathrm{sech}\left[2r\left(\xi_0 + \frac{2+\lambda}{2(1+\lambda)}(x-x_0) + \frac{\lambda}{4\alpha(1+\lambda)}\delta_n(x)\right)\right],$$

$$\epsilon_{1,f_2}(x) = \frac{1+\lambda\cos^2\left[\tanh\left(\alpha(x-x_0)\right)\right]}{1+\lambda}\left[(1-\phi^2_{f_2}(x)-r\chi^2_{f_2}(x))^2 + 4r^2\phi^2_{f_2}(x)\chi^2_{f_2}(x)\right],$$

where the auxiliary function $\delta_n(x) \equiv Ci\left(\zeta_n^+\right) - Ci\left(\zeta_n^-\right)$ has been defined. Once more, the incipient plateau is replicated $2n$ times in the field profiles. Similarly, $2n$ holes appear in the energy density and a non-vanishing ξ_0 introduces asymmetry in all profiles, see Figure 2.12.

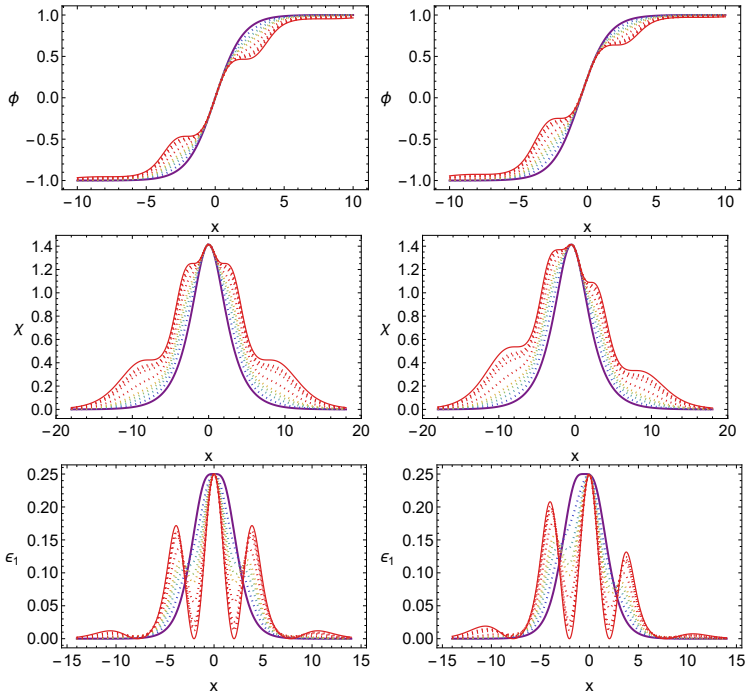

Figure 2.12: Solutions $\phi(x)$ and $\chi(x)$ and their energy density profile $\epsilon_1(x)$ for different values of the parameter λ that controls the constraint when $n = 2$ is chosen. On the left the symmetric case $\xi_0 = 0$ is presented and on the right the asymmetry of the case with $\xi_0 = \frac{1}{2}$ is shown. The original case $\lambda = 0$ is represented by the thick purple line while that corresponding to $\lambda \to \infty$ by a thin red line. Intermediate values are represented by dotted lines. Values of the parameters $\alpha = 1$ and $r = \frac{1}{4}$ have been employed.

2.4 Further comments

In the mechanism of continuous geometrical constriction introduced in this chapter, the target space of a Sigma model with values in $\mathbb{R}^n$ has been extended by introducing an extra field ψ as it is shown in (2.30) for superpotentials of the form (2.32). Different geometries encoded in different functions $f(\psi)$ and different forms

of the superpotential give rise to different kinks in the extended target space. Once solutions are projected to the target space of the original field theory, different geometrical constrictions of the kinks of the original field theory are constructed through the parameter λ. Therefore, this mechanism allows us to smoothly build an internal structure and asymmetry in field and energy density profiles for kinks and Domain walls.

In particular, this method allows a fixed number of plateaux to be continuously constructed in the field profiles and that same number of minima to be continuously formed in the energy density. One-parameter families of metric tensors are considered so that when $\lambda = 0$ the Euclidean case is recovered and in the limit $\lambda \to \infty$ the completely constrained case, described in [40], is also obtained. By altering the original distances in the extended target space in certain directions, minimum energy configurations are modified to adjust to the new values of the metric tensor. Because distances in all directions of the original target space are changed by the same function $f(\psi)$, a reparametrisation of the spatial coordinate in Bogomol'nyi equations is possible so that the original form of the Bogomol'nyi equations is retrieved. Indeed, the orbit flow equation restricted to the original target space is identical to the original one. The geometrical coordinate $\xi(x)$ that contains the information about the reparametrisation, which absorbs the effect of the change of geometry, not only depends on the chosen geometry $f(\psi)$, but also on the function $h(\psi)$, present in the superpotential W. This enables us to write the constrained kinks as the original ones but as functions of this new spatial coordinate $\phi^i(\xi(x))$. This reparametrisation is due to the fact that the kink in the new target space is also moving through the extra dimension, decelerating the advancement of the projected curve. The integration constant ξ_0 generates not only asymmetry in the field profiles, shifting the centre of the structure, but also in the energy density, where lumps can now be modulated to have different heights. This may be of great interest in high energy physics. On the other hand, as the parameter that modulates the constriction λ increases, the energy density profiles become increasingly distinct. Nevertheless, the total energy associated to the constrained fields ϕ^i, for the selected functions $f(\psi)$ and $h(\psi)$, remains identical to the original energy. This is because the derived geometrical coordinates, $\xi_1(x)$ and $\xi_2(x)$, are continuous functions with an image that covers the entire real number line. It is worth mentioning, however, that even though the contribution to the energy from the corresponding original fields is the same, an additional energy $\Delta E = \frac{4\alpha}{3}$ arises as contribution from the extra field ψ.

In particular, this mechanism has been applied in two scenarios. In the first one, a solution of the ϕ^4-model is geometrically constricted. In the second one, this procedure is applied to a solution of the model with two fields described in [33]. The extended target spaces are therefore $\mathbb{R}^2$ and $\mathbb{R}^3$ respectively. The extra function $h(\psi)$, added in the superpotential, has been chosen so that the extra field profile $\psi(x)$ corresponds to a solution of a ϕ^4 model.

On the other hand, it is worth highlighting that the scope of this procedure exceeds that of the field theories considered in this sections. For instance, similar geometrical constraints can be applied to other models, such as sine-Gordon's. Moreover, this mechanism can be extended to cases where the target manifold is a general Riemannian manifold. Indeed, as long as the function f equally affects all original dimensions, the same reparametrisation can be performed.

Lastly, this technique has several applications in ferromagnetic and ferrimagnetic materials. For instance, in [48] a mechanism to manipulate magnetic domain walls in ferrimagnetic or ferromagnetic multiferroics using electric fields is proposed. On the other hand, in [115] an interlayer Dzyaloshinkii-Moriya interation at interfaces causes chiral symmetry breaking between Bloch wall components. In [47] the effect of the domain wall chirality induced by these interfaces is modulated. Furthermore, more applications can be found in the scattering of topological kinks in the constricted scenario in mono-graphene, bilayer graphene and in other graphene-like classical wave systems [41].

Chapter 3

Kinks on the sphere $\mathbb{S}^2$

Previous chapters set the foundations for the study of certain types of Sigma models on general Riemannian manifolds. Indeed, the Bogomol'nyi arrangement provides a method for constructing Sigma models, enabling the analytical identification of kinks when the associated set of first order differential equations is solvable. Furthermore, criteria for assessing the stability of solutions of these equations have been introduced. In Chapter 2, kinks are found when the target space $\mathbb{R}^2$ is endowed with geometries different from the Euclidean. In this chapter, all these tools and notions will be extended to the case where the target manifold is the two-dimensional sphere $\mathbb{S}^2$. This transition is noteworthy, as the topology of the sphere will reveal a completely new scenario.

Two primary objectives will be addressed in this chapter. The first objective will involve calculating exact kinks of a Ginzburg-Landau non-linear $\mathbb{S}^2$-Sigma hybrid model, results that can be found in [22]. Homogeneous quartic polynomial potentials in Cartesian coordinates will be chosen to control the dynamics of these Sigma models. This construction will prompt the analogous mechanical system to exhibit Hamilton-Jacobi separability in some coordinates. Families of kinks on the sphere shall be sought and their stability studied. The second objective of this chapter is to investigate the emergence of brochosons in Sigma models on the sphere $\mathbb{S}^2$. A similar procedure to that introduced in Chapter 1 will be employed, where the presence of singularities in the potential will enable the existence of brochosons in this context.

3.1 Homogeneous quartic potentials on the sphere

In the first part of this chapter, the rich moduli space of kinks in a hybrid of the non-linear $\mathbb{S}^2$ Sigma model and the Ginzburg-Landau theory of phase transitions shall be investigated. This model can be interpreted as a low-energy limit of an effective field theory of a modified Heisenberg model for magnetic crystals with simple cubic structure. Electronic interaction between neighbour atoms can cause a weak anisotropy, breaking the O(3) symmetry of the ground state in the classical Heisenberg model. The inclusion in the Heisenberg Hamiltonian of anisotropy terms of the form $h_{\text{an}} = \frac{1}{2}BM_z^2$, with magnetisation vector field $M = (M_x, M_y, M_z)$ and a parameter B that modulates the anisotropy, has allowed the description of the behaviour of chiral magnetic soliton lattices, see [92]. As a result, a sine-Gordon equation is obtained in the continuum limit under certain assumptions, for which

analytical solutions can be used to analyse spin configurations in chiral helimagnets. Notably, Lorentz microscopy and small-angle electron diffraction reveals experimentally the existence of these solitonic configurations in these materials, see [129]. Converserly, a term of the form $h_{\text{an}} = \frac{1}{2}\sum_{i=1}^{3} B_{ij} M_i^2 M_j^2$ with $i, j = x, y, z$, describes the anisotropy contributions in simple cubic magnetic crystals by breaking the $O(3)$ symmetry while preserving the $\mathbb{Z}_2 \times \mathbb{Z}_2 \times \mathbb{Z}_2$ symmetry. In the continuum limit, a potential of the form $V(\phi) = \frac{1}{2}\sum_{i=1}^{3} B_{ij}\phi_i^2\phi_j^2$ is retrieved. This is, a non-negative homogeneous quartic polynomial in the fields. In particular, in order to derive analytical solutions, the anisotropy parameters will be chosen so that $B_{23} = B_{13} - B_{12}$.

In contrast to the approach followed until now, let us derive the field equations of a Sigma model by restricting fields in $\mathbb{R}^3$ to the sphere $\mathbb{S}^2$ and see how this is equivalent. Let us start then by considering a one-parameter family of $(1+1)$-dimensional $O(3)$ non-linear sigma models, whose dynamics is governed by the action

$$S[\phi] = \int \left[\frac{1}{2}\sum_{i=1}^{3} \left(\frac{\partial \phi^i}{\partial t}\right)^2 - \frac{1}{2}\sum_{i=1}^{3} \left(\frac{\partial \phi^i}{\partial x}\right)^2 - V(\phi;\sigma) \right] dx\, dt \ , \tag{3.1}$$

with scalar fields $\phi^1(t,x), \phi^2(t,x), \phi^3(t,x) : \mathbb{R}^{1,1} \to \mathbb{R}$ and where $V(\phi;\sigma)$ is a one-parameter family of potential functions labelled by parameter σ. In order to restrict the dynamics to the two-dimensional sphere $\mathbb{S}^2$ of radius R, the following function of the field profiles must vanish

$$f(\phi) = \phi_1^2(t,x) + \phi_2^2(t,x) + \phi_3^2(t,x) - R^2 \ . \tag{3.2}$$

Thus, in order to impose this constraint, the following Lagrange multiplier λ is introduced in the action

$$S[\phi] = \int \left[\frac{1}{2}\sum_{i=1}^{3} \left(\frac{\partial \phi^i}{\partial t}\right)^2 - \frac{1}{2}\sum_{i=1}^{3} \left(\frac{\partial \phi^i}{\partial x}\right)^2 - V(\phi;\sigma) - \lambda f(\phi) \right] dx\, dt \ ,$$

The introduction of a Ginzburg-Landau type potential energy density $V(\phi;\sigma)$ in the action functional (3.1) breaks the $O(3)$ symmetry of the system and leads to a spontaneous symmetry breaking scenario where kinks can emerge. An interesting choice of the function $V(\phi,\sigma)$ is given by the non-negative homogeneous quartic polynomial

$$V(\phi_1,\phi_2,\phi_3;\sigma) = \frac{1}{2}\Big[\phi_1^2\,\phi_3^2 + \sigma^4\,\phi_2^2\,\phi_3^2 + \bar{\sigma}^4\,\phi_1^2\,\phi_2^2\Big] \ , \tag{3.3}$$

where the restriction $\sigma \in (0,1)$ and the change in parameter $\bar{\sigma}^2 = 1 - \sigma^2$ have been performed for the sake of convenience. The action functional (3.1) is now invariant under the symmetry group $\mathbb{G} = \mathbb{Z}_2 \times \mathbb{Z}_2 \times \mathbb{Z}_2$, generated by transformations $\pi_i : \phi_i \to -\phi_i$ with $i = 1,2,3$. Moreover, a duality in the family of models can be constructed by simultaneously swapping the parameter values $\sigma \leftrightarrow \bar{\sigma}$ and the field components $\phi_1 \leftrightarrow \phi_3$. This allows us to restrict the study to the parameter interval $\sigma^2 \in (0, \frac{1}{2}]$, extending to the rest of cases by using this duality.

The field equations of the model, obtained from the action (3.1), are given by

the non-linear system of coupled differential equations

$$\begin{aligned}\frac{\partial^2\phi_1}{\partial t^2}-\frac{\partial^2\phi_1}{\partial x^2} &= \phi_1(\lambda-\bar{\sigma}^4\phi_2^2-\phi_3^2) \quad ,\\ \frac{\partial^2\phi_2}{\partial t^2}-\frac{\partial^2\phi_2}{\partial x^2} &= \phi_2(\lambda-\bar{\sigma}^4\phi_1^2-\sigma^4\phi_3^2)\,, \\ \frac{\partial^2\phi_3}{\partial t^2}-\frac{\partial^2\phi_3}{\partial x^2} &= \phi_3(\lambda-\phi_1^2-\sigma^4\phi_2^2) \quad .\end{aligned} \tag{3.4}$$

These equations enable us to determine the Lagrange multiplier λ associated with the constraint (3.2), which reads

$$\lambda=\frac{1}{R^2}\sum_{a=1}^{3}\left[-\left(\frac{\partial\phi_a}{\partial t}\right)^2+\left(\frac{\partial\phi_a}{\partial x}\right)^2+\frac{4}{R^2}V(\phi_1,\phi_2,\phi_3,\sigma)\right] \quad .$$

The spatial integral of the energy density for a configuration restricted to the sphere

$$\epsilon[\phi]=\frac{1}{2}\sum_{i=1}^{3}\left(\frac{\partial\phi^i}{\partial t}\right)^2+\frac{1}{2}\sum_{i=1}^{3}\left(\frac{\partial\phi^i}{\partial x}\right)^2+V(\phi;\sigma)\,, \tag{3.5}$$

provides the total energy E of that configuration $\phi(t,x)$, i.e.,

$$E[\phi(t,x)]=\int_{-\infty}^{\infty}\epsilon[\phi(t,x)]\,dx \quad . \tag{3.6}$$

It is clear from (3.3) that the set of vacua $\mathcal{M}$ of our model, which contains the zero energy static homogeneous solutions, comprises the six absolute minima of the potential $V(\phi;\sigma)$

$$\mathcal{M}=\left\{v_{1a}=\Big((-1)^aR,0,0\Big),\ v_{2b}=\Big(0,(-1)^bR,0\Big),\ v_{3c}=\Big(0,0,(-1)^cR\Big)\right\} \quad , \tag{3.7}$$

where $a,b,c=0,1$. These vacuum points are located at the intersection between the Cartesian axes and the sphere $\mathbb{S}^2$. This is, the six vacua of the system are maximally separated on the sphere. The plane wave expansion around the vacua $v_{i\pm}$ lets us identify the particle spectra in the corresponding quantum theory, which are determined by the mass matrices

$$M^2(v_{1a})=R^2\begin{pmatrix}\bar{\sigma}^4 & 0\\ 0 & 1\end{pmatrix}\,,\quad M^2(v_{2b})=R^2\begin{pmatrix}\bar{\sigma}^4 & 0\\ 0 & \sigma^4\end{pmatrix}\,,\quad M^2(v_{3c})=R^2\begin{pmatrix}1 & 0\\ 0 & \sigma^4\end{pmatrix}\,.$$

Our main goal is to identify the explicit expressions of the kinks that asymptotically connect these vacua. For the sake of efficiency, those whose energy density describes a single lump will be referred to as *single kinks*, while the term *composite kink* will be used when referring to solutions which can be interpreted as a combination of several single kinks. Exactly as in previous chapters, the Lorentz invariance of the model implies that it suffices to identify the static solutions $\phi(x)$ in order to obtain kinks. Indeed, a Lorentz transformation will set into motion any static kink $\phi(t,x)=\phi(x-vt)$. Bearing this in mind, the search of kinks for our model is tantamount to identifying the stationary solutions of the energy functional (3.6) that belong to the configuration space

$$\mathcal{C}=\{\phi:\mathrm{Maps}(\mathbb{R},\mathbb{S}^2)/\mathrm{Maps}(\mathbb{R},\mathrm{point}):E(\phi)<+\infty\}\,.$$

These requirements lead to the need of solving the following system of three ordinary differential equations:

$$\begin{aligned} \frac{d^2\phi_1}{dx^2} &= -\phi_1(\lambda - \bar{\sigma}^4\phi_2^2 - \phi_3^2) \quad , \\ \frac{d^2\phi_2}{dx^2} &= -\phi_2(\lambda - \bar{\sigma}^4\phi_1^2 - \sigma^4\phi_3^2) \, , \\ \frac{d^2\phi_3}{dx^2} &= -\phi_3(\lambda - \phi_1^2 - \sigma^4\phi_2^2) \quad , \end{aligned} \tag{3.8}$$

under the constraint (3.2). Given the finite energy condition, which imposes the asymptotic conditions

$$\lim_{x\to\pm\infty} \frac{d\phi^i}{dx} = 0 \quad \text{and} \qquad \lim_{x\to\pm\infty} \phi \in \mathcal{M} \, , \tag{3.9}$$

for $i = 1, 2$, the configuration space $\mathcal{C}$ is comprised of the union of 36 disconnected sectors determined by the elements of $\mathcal{M}$ reached by each configuration at $x \to -\infty$ and $x \to \infty$. Now, field equations can be simplified if the system of spherical coordinates

$$\phi_1 = \rho \sin\theta \cos\varphi \, , \quad \phi_2 = \rho \sin\theta \sin\varphi \, , \quad \phi_3 = \rho \cos\theta \, , \tag{3.10}$$

with $\theta \in [0, \pi]$ and $\varphi \in (-\pi, \pi]$, is used to address this problem. Indeed, the constraint (3.2) is immediately satisfied by imposing the restriction $\rho = R$. In particular, the evolution equations (3.4) read in these coordinates

$$\frac{\partial^2\theta}{\partial t^2} - \frac{\partial^2\theta}{\partial x^2} + \frac{1}{2}\sin(2\theta)\left[\left(\frac{\partial\varphi}{\partial x}\right)^2 - \left(\frac{\partial\varphi}{\partial t}\right)^2\right] = f_1(\theta, \varphi; \sigma) \, , \tag{3.11}$$

$$\frac{\partial^2\varphi}{\partial t^2} - \frac{\partial^2\varphi}{\partial x^2} + 2\cot\theta\left(\frac{\partial\theta}{\partial t}\frac{\partial\varphi}{\partial t} - \frac{\partial\theta}{\partial x}\frac{\partial\varphi}{\partial x}\right) = f_2(\theta, \varphi; \sigma) \, , \tag{3.12}$$

where the following auxiliary functions have been introduced

$$\begin{aligned} f_1(\theta, \varphi; \sigma) &= -\frac{R^2}{2}\sin(2\theta)\left(\sigma^4 + (1 - \sigma^4)\cos^2\varphi - 2\sin^2\theta\left(\sigma^2 + \bar{\sigma}^2\cos^2\varphi\right)^2\right) \, , \\ f_2(\theta, \varphi; \sigma) &= \frac{R^2}{2}\sin(2\varphi)\left(1 - \sigma^4 - 2\bar{\sigma}^2\sin^2\theta\left(\sigma^2 + \bar{\sigma}^2\cos^2\varphi\right)\right) \, . \end{aligned}$$

These equations, in turn, lead to the static field equations, which can be written as

$$\begin{aligned} -\frac{\partial^2\theta}{\partial x^2} + \frac{1}{2}\sin(2\theta)\left(\frac{\partial\varphi}{\partial x}\right)^2 &= f_1(\theta, \varphi; \sigma) \, , \\ -\frac{\partial^2\varphi}{\partial x^2} - 2\cot\theta\frac{\partial\theta}{\partial x}\frac{\partial\varphi}{\partial x} &= f_2(\theta, \varphi; \sigma) \, . \end{aligned}$$

Thus, solutions of these equations will provide static kinks of the model on the sphere $\mathbb{S}^2$. In next sections the kink variety arising as solutions of these equations will be identified. In particular, singular kinks and families of kinks will be sought.

Lastly, it is worth noting that these results can also be derived by directly considering as target manifold the two-dimensional sphere in spherical coordinates. Indeed, taking a chart $(U_{\mathbb{S}^2}, (\theta, \varphi))$ on the sphere with these coordinates, the metric tensor takes the form

$$g = R^2 d\theta \otimes d\theta + R^2 \sin^2\theta d\varphi \otimes d\varphi \,. \tag{3.13}$$

This allows to directly construct the Sigma model on the sphere in these coordinates as in previous chapters when $\phi^1 = \theta$ and $\phi^2 = \varphi$

$$S[\phi] = \int_{\mathbb{R}^{1,1}} \left[\frac{1}{2} g_{ab} \left(\frac{\partial \phi^a}{\partial t} \frac{\partial \phi^b}{\partial t} - \frac{\partial \phi^a}{\partial x} \frac{\partial \phi^b}{\partial x} \right) - V(\phi; \sigma) \right] dx\, dt \,, \tag{3.14}$$

and therefore derive the same field equations that have been obtained by restricting $\mathbb{R}^3$ to the sphere $\mathbb{S}^2$.

3.1.1 Singular kinks

The form of the field equations suggests that singular solutions may be found when one of the coordinates remains constant. In particular, the possibility of orbits of kinks describing pieces of principal great circles, defined by the intersection between the principal planes and the sphere $\mathbb{S}^2$, are investigated in this section. In order to obtain these, Rajaraman's trial orbit method [117] will be employed in equations (3.11) and (3.12). These singular kinks will be the only solutions in their respective topological sectors modulo the translational symmetry in certain cases. In others, they will be a limit member of a continuous family of solutions. These singular kinks will be classified into three types:

1. **Equatorial singular kinks**: This type of singular kink connects the four vacua v_{1a} and v_{2b} $(a, b = 0, 1)$ following the equator of the sphere $\mathbb{S}^2$. If the condition $\theta = \frac{\pi}{2}$ is substituted into equations (3.11) and (3.12), the resulting sine-Gordon equation

$$\frac{\partial^2 \varphi}{\partial t^2} - \frac{\partial^2 \varphi}{\partial x^2} = -\bar{\sigma}^4 \frac{R^2}{4} \sin(4\varphi) \tag{3.15}$$

provides us with the profile of this type of solutions. The one-soliton solution of (3.15) characterises the following eight kinks

$$\theta(x) = \frac{\pi}{2} \,, \quad \varphi(x) = (-1)^b \left[a\pi + (-1)^a \arctan\left(e^{qR\bar{\sigma}^2 \frac{\bar{x} - vt}{\sqrt{1-v^2}}} \right) \right] \,,$$

where $q = \pm 1$ and $a, b = 0, 1$. As stated, Lorentz invariance allows us to consider only the static case $v = 0$ without any loss of generality. Although these solutions have been derived in spherical coordinates, these can be expressed in terms of the original Cartesian coordinates. These can be written as follows

$$\phi_1(x) = \frac{(-1)^a R}{\sqrt{1 + e^{2R\bar{\sigma}^2 q\bar{x}}}} \,, \quad \phi_2(x) = \frac{(-1)^b R}{\sqrt{1 + e^{-2R\bar{\sigma}^2 q\bar{x}}}} \,, \quad \phi_3(x) = 0 \,, \tag{3.16}$$

where $a, b = 0, 1$ indicates the quadrant of the equator where the topological defect is and $\bar{x} = x - x_0$ is a shift of the spatial axis, being $x_0 \in \mathbb{R}$ the centre of the kink. Notice that the two values of q distinguish between kinks

and antikinks. Depending on the quadrant, solutions asymptotically join the vacuum points v_{1a} and v_{2b}. The translational symmetries and spatial parity underlie the presence of the parameters x_0 and q in (3.16). For the sake of conciseness the equatorial kinks will be denoted as $K_1^{(q,a,b)}(\overline{x})$. As it was expected, the energy density of these $K_1^{(q,a,b)}(\overline{x})$ solutions is a localised function

$$\epsilon[K_1^{(q,a,b)}(\overline{x})] = \frac{R^4\bar{\sigma}^4}{4}\,\mathrm{sech}^2\left(R\,q\,\overline{\sigma}^2\,\overline{x}\right)\,,$$

this is, it is primarily confined to a small region, see Figure 3.1. Therefore, solutions $K_1^{(q,a,b)}(\overline{x})$ describe single kinks. This fact is purposefully highlighted in the employed notation by means of the subscript 1. Now, given that the energy density profile is known, the total energy of these kinks can be computed. In fact, the energy of all these kinks is identical and amounts to

$$E[K_1^{(q,a,b)}(\overline{x})] = \frac{1}{2}\,R^3\,\overline{\sigma}^2\,\,.$$

In addition to the solutions previously described, the multisoliton and breather solutions of the equations (3.15) can be exploited to construct complex evolving kinks. However, this type of solutions will not be exploited here.

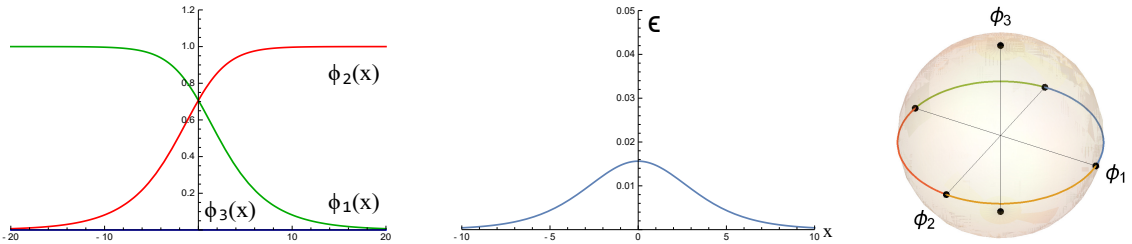

Figure 3.1: Profile of the Cartesian field profiles (left), energy density (middle) and orbits for the $K_1^{(q,a,b)}(\overline{x})$ kinks (right).

2. **$(\pm\frac{\pi}{2})$-Meridian singular kinks**: In this case the trial orbit will be the great circle formed by the meridians with longitude $\varphi = \pm\frac{\pi}{2}$. Once this condition is inserted into equations (3.11) and (3.12), the polar variable θ is free to vary and the resulting sine-Gordon equation

$$\frac{\partial^2\theta}{\partial t^2} - \frac{\partial^2\theta}{\partial x^2} = -\frac{R^2\sigma^4}{4}\sin(4\theta)\,\,, \tag{3.17}$$

leads to eight topological kinks whose profile in spherical coordinates are given by expressions

$$\theta(x) = c\,\pi + (-1)^c\arctan\left(e^{R\,\sigma^2\,q\,\bar{x}}\right)\,,\quad \varphi(x) = \frac{(-1)^b\pi}{2}\,,$$

where $q = \pm 1$ and $b, c = 0, 1$. These topological defects, which join the vacuum points v_{2b} and v_{3c} with $b, c = 0, 1$, read in Cartesian coordinates

$$\phi_1(x) = 0\quad,\quad \phi_2(x) = \frac{(-1)^b R}{\sqrt{1+e^{-2R\sigma^2\,q\bar{x}}}}\quad,\quad \phi_3(x) = \frac{(-1)^c R}{\sqrt{1+e^{2R\sigma^2 q\bar{x}}}}\,\,.$$

These solutions will be denoted as $\overline{K}_1^{(q,b,c)}(\overline{x})$, where parameters q, b and c play the same role as in the previous case. The total energy carried by all these solutions is identical

$$E[\overline{K}_1^{(q,b,c)}(\overline{x})] = \frac{1}{2}R^3\sigma^2 \,,$$

which is obtained by integrating along the spatial coordinate x any of their energy density profiles

$$\epsilon[\overline{K}_1^{(q,b,c)}(\overline{x})] = \frac{R^4\sigma^4}{4}\,\mathrm{sech}^2\left(Rq\sigma^2\bar{x}\right) \,,$$

which read the same. The distribution of this energy density implies that the $\overline{K}_1^{(q,b,c)}(\overline{x})$-kinks are once again single kinks, see Figure 3.2.

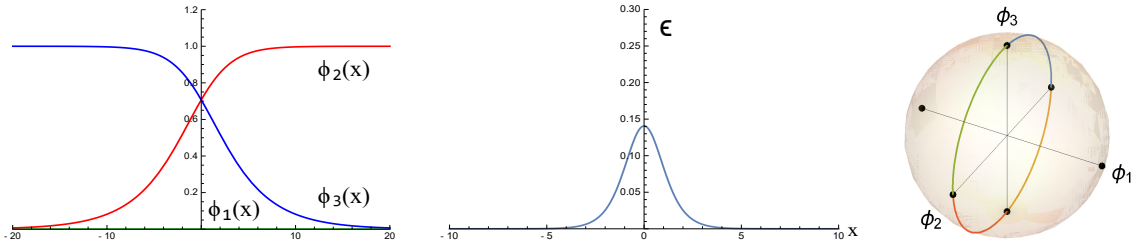

Figure 3.2: Profile of the Cartesian field profiles (left), energy density (middle) and orbits for the $\overline{K}_1^{(q,b,c)}(\overline{x})$ kinks (right).

Mirroring the situation found for equatorial kinks, multisoliton kinks can also be identified in this context by using different solutions of the sine-Gordon equation.

3. **Prime Meridian kinks**: The orbits of this type of solutions are defined on the orthodrome composed of the meridian with azimuthal angle $\varphi = 0$ and its antimeridian. These trial orbits lead again to a sine-Gordon equation

$$\frac{\partial^2\theta}{\partial t^2} - \frac{\partial^2\theta}{\partial x^2} = -\frac{R^2}{4}\sin(4\theta) \,, \tag{3.18}$$

which provides us with the eight similar kinks with profiles in spherical coordinates

$$\theta(x) = c\pi + (-1)^c \arctan\left(e^{R\,q\,\bar{x}}\right) \quad , \quad \varphi(x) = a\pi, \qquad a, c = 0, 1 \,\,.$$

In Cartesian coordinates these topological defects follow the form

$$\phi_1 = \frac{(-1)^a R}{\sqrt{1+e^{-2Rq\,\overline{x}}}}, \qquad \phi_2 = 0, \qquad \phi_3 = \frac{(-1)^c R}{\sqrt{1+e^{2Rq\overline{x}}}} \,\,. \tag{3.19}$$

Exactly as before, while $q = \pm 1$ distinguishes between kinks and antikinks, parameters $a, c = 0, 1$ determine whether a solution belongs to the Northern or Southern Hemisphere and to the Western or Eastern Hemisphere, respectively. These singular kinks (3.19) connect now the four vacua v_{1a} and v_{3c}. These kinks, which complete the set of singular kinks asymptotically joining every

adjacent vacuum point, will be denoted by the symbol $K_2^{(q,a,c)}(\overline{x})$. On the other hand, the energy density of the $K_2^{(q,a,c)}(\overline{x})-$kinks

$$\epsilon[K_2^{(q,a,c)}(\overline{x})] = \frac{R^4}{4}\,\mathrm{sech}^2\,(R\,q\,\overline{x}) \tag{3.20}$$

is again concentrated around the kink centre $x = x_0$ and leads to a total energy

$$E[K_2^{(q,a,c)}(x)] = \frac{1}{2}\,R^3\,.$$

In fact, a relation between the energy of the three types of singular kinks can be found

$$E[K_2^{(q,a,c)}(x)] = E[K_1^{(q,a,b)}(\overline{x})] + E[\overline{K}_1^{(q,b,c)}(\overline{x})]\,. \tag{3.21}$$

This suggests that the prime Meridian kinks are limit members of a continuous family of composite kinks and that it can be interpreted as the overlap of the two previously described solitary lumps $K_1^{(q,a,b)}(\overline{x})$ and $\overline{K}_1^{(q,b,c)}(\overline{x})$, see Figure 3.3. This will be explored and analytically justified in next sections.

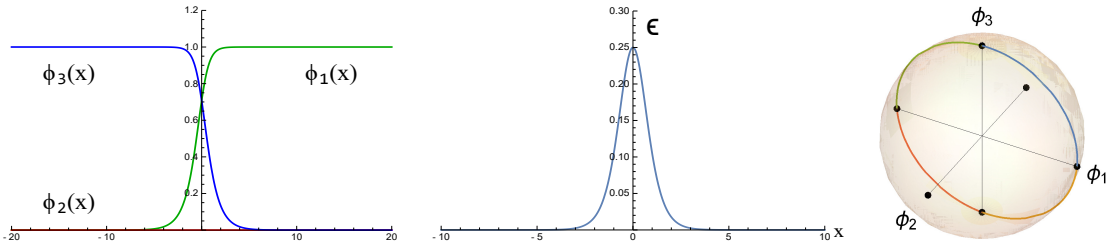

Figure 3.3: Profile of the Cartesian field profiles (left), energy density (middle) and orbits for the $K_2^{(q,a,c)}(\overline{x})$ kinks (right).

3.1.2 Families of composite kinks

In last section, the singular kinks that arise in this model asymptotically connecting every adjacent vacua are identified by Rajaraman's trial orbit. In this section, the description of the kink variety for this non-linear $\mathbb{S}^2$-sigma model is completed. This will be accomplished by introducing coordinates in which the mechanical analogue system is Hamilton-Jacobi separable. Let us search then coordinates on the sphere for which the Bogomol'nyi arrangement can be performed in the potential. These coordinates are the sphero-conical coordinates (λ_1, λ_2) on the sphere, defined as

$$\phi_1^2 = \frac{R^2}{\bar{\sigma}^2}\lambda_1\lambda_2 \;\;,\;\; \phi_2^2 = \frac{R^2}{\sigma^2\bar{\sigma}^2}(\bar{\sigma}^2 - \lambda_1)(\lambda_2 - \bar{\sigma}^2) \;\;,\;\; \phi_3^2 = \frac{R^2}{\sigma^2}(1-\lambda_1)(1-\lambda_2)\,, \tag{3.22}$$

where the range of these coordinates λ_1 and λ_2 is given by the rectangle

$$C \equiv \{(\lambda_1, \lambda_2) : 0 < \lambda_1 < \bar{\sigma}^2 < \lambda_2 < 1\}\,.$$

Notice that the map (3.22) is a coordinate chart between C and an octant of the $\mathbb{S}^2$. The change of coordinates is eight-to-one and eight charts are required to cover the whole sphere. Nevertheless, piecewise solutions can be constructed by demanding smoothness in the transitions between octants. Since sphero-conical coordinates will

be employed to obtain solutions, the form of the metric tensor on the sphere in these coordinates must be derived

$$g = \frac{R^2(\lambda_2-\lambda_1)}{4}\left[\frac{1}{\lambda_1(\bar{\sigma}^2-\lambda_1)(1-\lambda_1)}d\lambda_1\otimes d\lambda_1 + \frac{1}{\lambda_2(\lambda_2-\bar{\sigma}^2)(1-\lambda_2)}d\lambda_2\otimes d\lambda_2\right].$$

On the other hand, the four vertices of the rectangle C are distinguished points in our model. On one hand, the corner $(\lambda_1,\lambda_2)=(0,\bar{\sigma}^2)$ corresponds to the vacua v_{3c}, the point $(\lambda_1,\lambda_2)=(0,1)$ is mapped to the vacua v_{2b} and $(\lambda_1,\lambda_2)=(\bar{\sigma}^2,1)$ goes to the points v_{1a}, where $a,b,c=0,1$. On the other, the remaining vertex $(\lambda_1,\lambda_2)=(\bar{\sigma}^2,\bar{\sigma}^2)$ represents the four points

$$F_{ac} = ((-1)^a\, R\,\bar{\sigma}, 0, (-1)^c\, R\,\sigma) \qquad a,c=0,1$$

in Cartesian coordinates. These are the foci of the "elliptical" curves defined by the sphero-conical coordinate isolines. In summary, the vacua of our model and the foci of the coordinate curves of the sphero-conical coordinate system are mapped to the vertices of C. It is worth highlighting that the principal great circles of the sphere become straight lines in the sphero-conical coordinate plane. In particular, the equator, the $(\pm\frac{\pi}{2})$ meridians and the Prime meridian and its antimeridian are represented respectively by segments

$$\begin{aligned}
&L_{Eq} = \{(\lambda_1,1) : 0<\lambda_1<\bar{\sigma}^2\},\\
&L_{m} = \{(0,\lambda_2) : \bar{\sigma}^2<\lambda_2<1\},\\
&L_{Pm} = L_{aPm} = \{(\lambda_1,\bar{\sigma}^2) : 0<\lambda_1<\bar{\sigma}^2\}\cup\{(\bar{\sigma}^2,\lambda_2) : \bar{\sigma}^2<\lambda_2<1\},
\end{aligned}$$

where the last two are defined by concatenation. Once the action is expressed in these coordinates, it immediately follows that the energy of a given configuration can be written as follows

$$E(\lambda_1,\lambda_2) = \int\left[\frac{1}{2}\,g_{11}(\lambda_1,\lambda_2)\left(\frac{d\lambda_1}{dx}\right)^2 + \frac{1}{2}\,g_{22}(\lambda_1,\lambda_2)\left(\frac{d\lambda_2}{dx}\right)^2 + V(\lambda_1,\lambda_2)\right]dx.$$

This form of the potential unveils the reason behind the use of the sphero-conical coordinates. When the potential is written in terms of these variables

$$V(\lambda_1,\lambda_2) = \frac{R^4}{2(\lambda_2-\lambda_1)}\Big[\lambda_1(1-\lambda_1)(\bar{\sigma}^2-\lambda_1)+\lambda_2(1-\lambda_2)(\lambda_2-\bar{\sigma}^2)\Big],$$

Bogomolny arrangement can now be performed in the functional of energy $E(\lambda_1,\lambda_2)$. As explained in Chapter 2, this requires writing the potential function in terms of a superpotential W, which is chosen as

$$W(\lambda_1,\lambda_2) = \frac{1}{2}R^3(-1)^\alpha[\lambda_1+(-1)^\beta\lambda_2] \qquad \text{with} \qquad \alpha,\beta=0,1.$$

Notice that the separability of this superpotential in these coordinates allows not two but four different superpotentials. Even if a global sign is inconsequential, the relative sign will have an impact on the behaviour of solutions as we shall see. In these coordinates on the sphere, the same procedure described in previous chapters

is followed for the Bogomol'nyi arrangement. Writing this potential in terms of a superpotential leads to

$$\begin{aligned} E(\lambda_1,\lambda_2) &= \int \Big[\frac{1}{2}\sum_{i=1}^{2} g_{ii}\Big(\frac{d\lambda_i}{dx}\Big)^2 + \frac{1}{2}\sum_{i=1}^{2} g^{ii}\Big(\frac{\partial W}{\partial \lambda_i}\Big)^2\Big]dx \\ &= \int \frac{1}{2}\sum_{i=1}^{2} g_{ii}\Big(\frac{d\lambda_i}{dx} - g^{ii}\frac{\partial W}{\partial \lambda_i}\Big)^2 dx + \Big|\int \sum_{i=1}^{2}\frac{\partial W}{\partial \lambda_i}\frac{\partial \lambda_i}{dx}\,dx\Big|\,. \end{aligned}$$

For configurations that belong to the space $\mathcal{C}$, the last term in (3.23)

$$T = \Big|\int dx \sum_{i=1}^{2}\frac{\partial W}{\partial \lambda_i}\frac{\partial \lambda_i}{dx}\Big|$$

is a topological charge, which is conserved during the evolution of the configuration. Accordingly, the energy is minimised when Bogomol'nyi equations are satisfied. These are the first order differential equations

$$\frac{d\lambda_1}{dx} = g^{11}\frac{\partial W}{\partial \lambda_1} = (-1)^{\alpha}\,\frac{2R\,\lambda_1(1-\lambda_1)(\bar{\sigma}^2-\lambda_1)}{\lambda_2-\lambda_1}\quad, \tag{3.23}$$

$$\frac{d\lambda_2}{dx} = g^{22}\frac{\partial W}{\partial \lambda_2} = (-1)^{\alpha+\beta}\frac{2R\,\lambda_2(1-\lambda_2)(\lambda_2-\bar{\sigma}^2)}{\lambda_2-\lambda_1}\quad, \tag{3.24}$$

which can be solved for the values $\alpha,\beta = 0,1$. The integration of the equations (3.23) and (3.24) leads to the expressions

$$\frac{\bar{\sigma}^2-\lambda_1}{\lambda_1^{\sigma^2}(1-\lambda_1)^{\bar{\sigma}^2}}\cdot\Big[\frac{\lambda_2-\bar{\sigma}^2}{\lambda_2^{\sigma^2}(1-\lambda_2)^{\bar{\sigma}^2}}\Big]^{(-1)^{\beta}} = e^{2R\sigma^2\gamma}\quad, \tag{3.25}$$

$$\frac{\bar{\sigma}^2-\lambda_1}{1-\lambda_1}\cdot\Big[\frac{\lambda_2-\bar{\sigma}^2}{1-\lambda_2}\Big]^{(-1)^{\beta}} = e^{(-1)^{\alpha}2R\sigma^2\overline{x}}\quad. \tag{3.26}$$

Depending on the value of $\beta = 0,1$, the pair of relations (3.25) and (3.26) determine a distinct family of kinks $\phi(\overline{x},\gamma)$, which is parameterised by the value of the integration constant $\gamma\in\mathbb{R}$. Note that relation (3.25) define the kink orbits whereas equation (3.26) determines the spatial dependence of the solution. Moreover, kinks or antikinks are obtained as solutions of these equations depending on the value of α. A direct manipulation of the equations (3.25) and (3.26) allows us to write them in a simpler form:

$$\frac{\bar{\sigma}^2-\lambda_1}{1-\lambda_1}\cdot\Big[\frac{\lambda_2-\bar{\sigma}^2}{1-\lambda_2}\Big]^{(-1)^{\beta}} = e^{(-1)^{\alpha}2R\sigma^2\overline{x}} = A(x)\,, \tag{3.27}$$

$$\frac{\lambda_1}{1-\lambda_1}\cdot\Big[\frac{\lambda_2}{1-\lambda_2}\Big]^{(-1)^{\beta}} = e^{2R[(-1)^{\alpha}\overline{x}-\gamma]} = B(x)\,, \tag{3.28}$$

where for sake of simplicity in subsequent expressions, the functions $A(x)$ and $B(x)$ are introduced to denote the exponentials in (3.27) and (3.28). In summary, these two relations define two one-parameter families of composite kinks distinguished by the value of β, whose orbits are dense in the sphere $\mathbb{S}^2$. Let us discuss separately each family.

Family of two-lump composite kinks

Let us commence by examining the family of kinks that arises when the value $\beta = 0$ is taken in equations (3.27) and (3.28). As it is straightforward to check, from these equations an explicit solution for the sphero-conical coordinates can be derived

$$\lambda_i(x) = \frac{1}{2(A(x)+\bar{\sigma}^2+B(x)\sigma^2)}\Big(A(x)+\bar{\sigma}^4+(1-\bar{\sigma}^4)B(x)+ \\ +(-1)^i\sqrt{A(x)^2+2A(x)\bar{\sigma}^4+\bar{\sigma}^8+2A(x)B(x)\sigma^4-2B(x)\bar{\sigma}^4\sigma^4+B(x)^2\sigma^8}\Big) \ ,$$

where $i = 1, 2$. In Figure 3.4 the corresponding kink orbits in the sphero-conical plane have been depicted for several values of γ together with the field profiles.

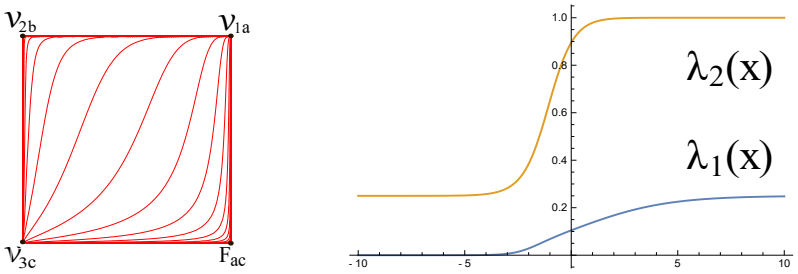

Figure 3.4: Orbits for several members of the family $K_2^{(q,a,b,c)}(\bar{x},\gamma)$ (left) and field profiles (right) represented in sphero-conical coordinates.

By definition of these coordinates, this type of solutions asymptotically connects the vacua v_{3c} and v_{1a} with $a, c = 0, 1$ and are confined to a sphere octant. Notice that components $\lambda_1(x)$ and $\lambda_2(x)$ take values on the corresponding ranges of the sphero-conical coordinates. Finally, these kink profiles can be written in Cartesian coordinates, adopting the following concise form

$$\begin{aligned}
\phi_1^{(a,b,c)}(x,\gamma) &= (-1)^a R\sigma\sqrt{\frac{B(x)}{A(x)+\bar{\sigma}^2+B(x)\sigma^2}} \ , \\
\phi_2^{(a,b,c)}(x,\gamma) &= (-1)^b R\sqrt{\frac{A(x)}{A(x)+\bar{\sigma}^2+B(x)\sigma^2}} \ , \\
\phi_3^{(a,b,c)}(x,\gamma) &= (-1)^c R\bar{\sigma}\frac{1}{\sqrt{A(x)+\bar{\sigma}^2+B(x)\sigma^2}} \ ,
\end{aligned} \tag{3.29}$$

where parameters $a, b, c = 0, 1$ determine the sphere octant where these kinks are confined. Orbits of several members of this family have been plotted on the sphere $\mathbb{S}^2$ in Figure 3.5. In this figure, the graphics of the Cartesian field profiles and the energy densities have also been included.

Let us denote these one-parameter families of kinks as $K_2^{(q,a,b,c)}(\bar{x},\gamma)$, where $q = \pm 1$ will once again distinguish between kinks and antikinks. On the other hand, the distribution of the energy densities for members of this family shows that these can be interpreted as the combination of two separated single kinks $K_1^{(q,a,b)}(\overline{x})$ and $\overline{K}_1^{(q,b,c)}(\overline{x})$, where the parameter γ measures the distance between these energy density lumps.

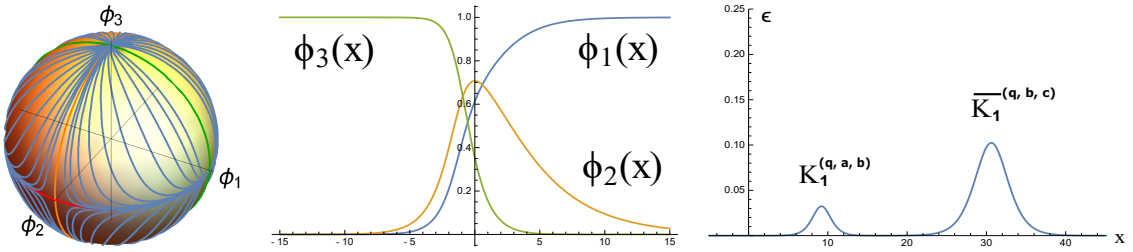

Figure 3.5: Orbits for several members of the family $K_2^{(q,a,b,c)}(\bar{x},\gamma)$ (left), field profiles in Cartesian coordinates (middle) and energy density (right).

Furthermore, the single kinks can be obtained from the family (3.29) by taking specific limits in the parameter space (γ, x_0). Indeed, one can check the following

$$\lim_{\substack{\gamma\,\to\,-\infty \\ \gamma+(-1)^{\alpha}\bar{\sigma}^2 x_0\,\equiv\,\text{constant}}} K_2^{(q,a,b,c)}(x,\gamma) = K_2^{(q,a,c)}(x)\,,$$

which means that the singular kinks $K_2^{(q,a,c)}(x)$ introduced in the previous section are limit members of the one-parameter family $K_2^{(q,a,b,c)}(x,\gamma)$. Similarly, the other two singular kinks are recovered as limits

$$\lim_{\substack{\gamma\,\to\,\infty \\ x_0\ \text{constant}}} K_2^{(q,a,b,c)}(x,\gamma) = \overline{K}_1^{(q,b,c)}(x)\,,$$

$$\lim_{\substack{\gamma\,\to\,\infty \\ \gamma+(-1)^{\alpha}x_0\,\equiv\,\text{constant}}} K_2^{(q,a,b,c)}(x,\gamma) = K_1^{(q,a,b)}(x)\,.$$

These limits are compatible with the energy sum rule (3.21), since the energy of these families are related to those of the singular kinks as follows

$$E[K_2^{(q,a,b,c)}(\bar{x},\gamma)] = E[K_2^{(q,a,c)}(\bar{x})] = E[K_1^{(q,a,b)}(\overline{x})] + E[\overline{K}_1^{(q,b,c)}(\overline{x})] = \frac{1}{2}\,R^3\,.$$

Thus, the family of $K_2^{(q,a,b,c)}(\bar{x},\gamma)$-kinks can be understood as two kinks that are separated by a distance fixed by the value of the family parameter γ. The singular member $K_2^{(q,a,c)}(\bar{x})$ arises when the two previously mentioned kinks are maximally overlapped.

Family of four-lump composite kinks

If the value $\beta = 1$ is substituted into the orbit equations (3.27) and (3.28), the remaining family of kinks on the sphere is identified. Once more, the spatial dependence of the kink profiles in sphero-conical coordinates can be obtained analytically, which is given by the expressions

$$\lambda_1(x) = \frac{B(x)(1+A(x))\bar{\sigma}^2}{B(x)+A(x)B(x)\bar{\sigma}^2+A(x)\sigma^2}\,,\qquad \lambda_2(x) = \frac{(1+A(x))\bar{\sigma}^2}{A(x)+\bar{\sigma}^2+B(x)\sigma^2}\,.$$

The trajectories and the field profiles of this type of solutions are depicted in the sphero-conical plane for several values of γ in Figure 3.6. Notice how curves in the sphero-conical plane must be properly glued to guarantee the differentiability of solutions.

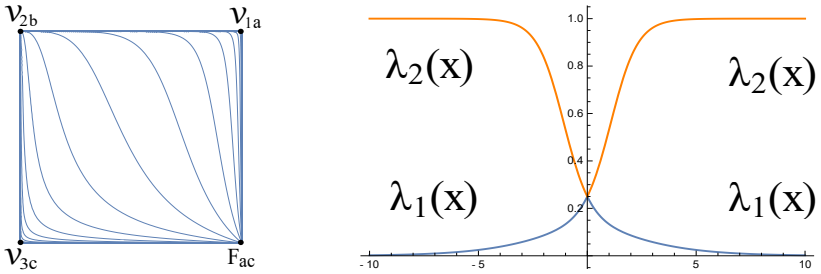

Figure 3.6: Orbits for several members of the family $K_4^{(q,a,b,c)}(\bar{x},\gamma)$ (left) and field profiles (right) depicted in sphero-conical coordinates.

In the sphero-conical rectangle C all the orbits begin at the vertex v_{2b} and monotonically reach the foci F_{ac}. Indeed, a particular solution arrives at F_{ac} when $\overline{x} = (-1)^{\alpha}\gamma$, where the label α distinguishes between kinks and antikinks. It is worth noting that in the original fields the tangent vector at the foci F_{ac} can be written as

$$\frac{d\vec{\phi}}{dx} = (-1)^{\alpha} R^2 \sigma\bar{\sigma}\Big((-1)^{a}\sigma\tanh(\sigma^2 R\gamma), -\mathrm{sign}(\phi_2)\,\mathrm{sech}(\bar{\sigma}^2 R\gamma), -(-1)^{c}\tanh(\sigma^2 R\gamma)\Big)\,,$$

where $\vec{\phi} = (\phi_1,\phi_2,\phi_3)$. At this point in C, solutions carry non-vanishing potential energy density and continue to the next sphere octant represented by the same rectangle C. In order to complete the kink orbit, this curve must be glued in a differentiable manner to a new piece of trajectory. From the previous expression it is clear that this can be achieved by concatenating the previous solution with the one obtained from the equations (3.25) and (3.26) with the opposite value of α and γ. Despite the need of gluings when these coordinates are employed, a global expression can be found for the field profiles in Cartesian coordinates

$$\begin{aligned}
\phi_1^{(a,b,c)}(x,\gamma) &= (-1)^{a} R\bar{\sigma}(1+A(x))\sqrt{\frac{B(x)}{F(x)}},\\
\phi_2^{(a,b,c)}(x,\gamma) &= (-1)^{b} R\sigma\bar{\sigma}(1-B(x))\sqrt{\frac{A(x)}{F(x)}},\\
\phi_3^{(a,b,c)}(x,\gamma) &= (-1)^{c} R\sigma\frac{A(x)+B(x)}{\sqrt{F(x)}}\,,
\end{aligned}$$

where the auxiliary function $F(x)$ has been defined as follows

$$F(x) = (B(x)+A(x)B(x)\bar{\sigma}^2+A(x)\sigma^2)(A(x)+\bar{\sigma}^2+B(x)\sigma^2)\,.$$

All these orbits asymptotically start at a vacuum point v_{2b} $(b=0,1)$, cross the Prime Meridian, passing to a new sphere octant through one of the foci F_{ac} and asymptotically arrive at the antipodal vacuum, see Figure 3.7. Notation $K_4^{(q,a,b,c)}(\overline{x},\gamma)$ will be used to denote this family of topological defects. Four energy density lumps, also illustrated in Figure 3.7, appear in their energy density distribution. In particular, the $K_4^{(q,a,b,c)}(\overline{x},\gamma)$ solutions consist of a non-linear combination of a single $\overline{K}_1^{(q,b,c)}(\overline{x})-$kink and a single $K_1^{(q,a,\bar{b})}(\overline{x})-$kink with $\bar{b} = (b+1)\mathrm{mod}\,2$, which are separated by a $K_2^{(q,a,c)}(\overline{x})$-meridian kink in the middle, see Figure 3.7. In addition, the central lump $K_2^{(q,a,c)}(\overline{x})$ can be understood as the overlapping of the two single

walls $\overline{K}_1^{*(q,b,c)}(\overline{x})$ and $K_1^{(q,a,b)}(\overline{x})$ or $\overline{K}_1^{*(q,\bar{b},c)}(\overline{x})$ and $K_1^{(q,a,\bar{b})}(\overline{x})$, where the asterisk as a superscript in the previous notation stands for the antikink of the involved solution. Notice that the configuration of four single kinks that conform the $K_4^{(q,a,b,c)}(\overline{x},\gamma)$-solutions always involves the presence of a kink and its antikink.

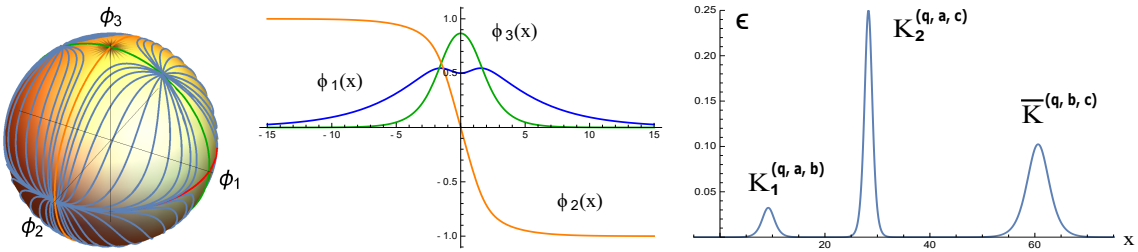

Figure 3.7: Orbits for several members of the family $K_4^{(q,a,b,c)}(\bar{x},\gamma)$ (left), field profiles in Cartesian coordinates (middle) and energy density (right).

Given that members of this family lie in two octants in the sphere, the energy sum rules will be significantly different

$$\begin{aligned} E[K_4^{(q,a,b,c)}(\bar{x},\gamma)] &= E[K_1^{(q,a,b)}(\overline{x})] + E[K_2^{(q,a,c)}(x)] + E[\overline{K}_1^{(q,b,c)}(\overline{x})] = \\ &= 2\,E[K_1^{(q,a,b)}(\overline{x})] + 2\,E[\overline{K}_1^{(q,b,c)}(\overline{x})] = R^3 \end{aligned}$$

In summary, unlike the previous family $K_2^{(q,a,b,c)}(\bar{x},\gamma)$, the family of $K_4^{(q,a,b,c)}(\bar{x},\gamma)$-kinks can be understood as four singular kinks. This is, two different singular kinks equally separated from a superposition of the other two, being the distance fixed by the value of the family parameter γ. Lastly, also in this case the singular kinks can be found as certain limits of this family of kinks. Indeed, it can be checked that $\gamma \to \infty$ limits

$$\begin{aligned} \lim_{\substack{\gamma\to\infty \\ x_0 \text{ constant}}} & K_4^{(q,a,b,c)}(x,\gamma) = \overline{K}_1^{(-q,b,c)}(x)\,, \\ \lim_{\substack{\gamma\to\infty \\ \gamma+x_0 \equiv \text{constant}}} & K_4^{(q,a,b,c)}(x,\gamma) = K_2^{(q,a,c)}(x)\,, \\ \lim_{\substack{\gamma\to\infty \\ \gamma+\overline{\sigma}^2 x_0 \text{ constant}}} & K_4^{(q,a,b,c)}(x,\gamma) = K_1^{(q,a,(b+1)\bmod 2)}(x)\,, \end{aligned}$$

provide us with the singular kinks. Similarly, the $\gamma \to -\infty$ limits lead to

$$\begin{aligned} \lim_{\substack{\gamma\to-\infty \\ x_0 \text{ constant}}} & K_4^{(q,a,b,c)}(x,\gamma) = \overline{K}_1^{(q,(b+1)\bmod 2,c)}(x)\,, \\ \lim_{\substack{\gamma\to-\infty \\ \gamma+x_0 \equiv \text{constant}}} & K_4^{(q,a,b,c)}(x,\gamma) = K_2^{(-q,a,c)}(x)\,, \\ \lim_{\substack{\gamma\to-\infty \\ \gamma+\overline{\sigma}^2 x_0 \text{ constant}}} & K_4^{(q,a,b,c)}(x,\gamma) = K_1^{(-q,a,b)}(x)\,. \end{aligned}$$

3.1.3 Linear stability of the kinks

In this section the linear stability under small perturbations of the kinks described in the previous sections is explored. Since the singular solutions were described

by using spherical coordinates, the Hessian operator will be also constructed in these coordinates. Let us write for convenience kinks as $\Theta(x) = (\theta(x), \varphi(x))$ and as $\eta(x) = (\eta_1(x), \eta_2(x))$ the fluctuations around these. The approach will be similar to that in previous chapters and others found in the literature, see for instance [17,18,20]. In order to study the stability, the analysis of the second-order differential operator

$$H\eta \;=\; -\nabla_{\Theta'}\nabla_{\Theta'}\eta - R(\Theta',\eta)\Theta' - \nabla_\eta \operatorname{grad} U\,, \tag{3.30}$$

will be necessary, which has been written in terms of covariant derivatives and the curvature tensor. Specifically, in the standard basis $\{\frac{\partial}{\partial\theta}, \frac{\partial}{\partial\varphi}\}$ for the tangent space to the sphere along the kink, the vector fields are written as

$$\Theta'(x) = \theta'(x)\frac{\partial}{\partial\theta} + \varphi'(x)\frac{\partial}{\partial\varphi}\,, \quad \eta(x) = \eta_1\frac{\partial}{\partial\theta} + \eta_2\frac{\partial}{\partial\varphi}$$

and $\nabla_\eta \operatorname{grad} U$ leads to the Hessian of the potential function. In general, the explicit form of this operator for a given kink makes the analysis of its spectrum very complex. However, the special geometry of the singular kink orbits allows us to determine the complete spectrum for these singular solutions. Let us explore separately the stability of each singular kink.

- **Equatorial kinks**: Introducing the expressions of Equatorial kinks into equation (3.30), the following small fluctuation operator is obtained

$$\begin{aligned} H_{\mathrm{Eq}}\eta = &\left[-\tfrac{d^2\eta_1}{dx^2} + \tfrac{R^2}{2}\left(1+\sigma^4 - \tfrac{3\bar\sigma^4}{2\cosh^2(R\bar\sigma^2 x)} - (1-\sigma^4)\tanh(R\bar\sigma^2 x)\right)\eta_1\right]\tfrac{\partial}{\partial\theta} \\ &+\left[-\tfrac{d^2\eta_2}{dx^2} + R^2\bar\sigma^4\left(1-\tfrac{2}{\cosh^2(R\bar\sigma^2 x)}\right)\eta_2\right]\tfrac{\partial}{\partial\varphi}\,. \end{aligned}$$

  which can be decomposed into two spectral problems associated to modified Poschl-Teller potentials. The first component of the Hessian operator

$$\mathcal{H}_{11} = -\frac{d^2}{dx^2} + \frac{R^2}{2}\left[1+\sigma^4 - \frac{3\bar\sigma^4}{2\cosh^2(R\bar\sigma^2 x)} - (1-\sigma^4)\tanh(R\bar\sigma^2 x)\right]$$

  governs the behaviour of the orthogonal fluctuations around the $K_1^{(q,a,b)}(\overline{x})$-kinks. The spectrum of $\mathcal{H}_{11}$ consists of a continuous spectrum which is simply degenerate in the range $[\sigma^4R^2, R^2]$ and doubly degenerate for eigenvalues in the interval (R^2,∞). On the other hand, the small longitudinal fluctuation operator

$$\mathcal{H}_{22} = -\frac{d^2}{dx^2} + R^2\bar\sigma^4\left(1-\frac{2}{\cosh^2(R\bar\sigma^2 x)}\right)$$

  involves the presence of a zero mode $\omega_0^2 = 0$ and a doubly degenerate continuous spectrum emerging on the threshold value $\omega^2 = R^2\bar\sigma^4$. The existence of a longitudinal zero mode establishes that the kink centre can be set at any spatial point $x_0 \in \mathbb{R}$. In conclusion, the lack of negative eigenvalues implies that the $K_1^{(q,a,b)}(\overline{x})$-kinks are linearly stable.

- **Meridian kinks**: The $\left(\pm\frac{\pi}{2}\right)$-Meridian kink fluctuation operator is given by the expression

$$\begin{aligned} H_{\mathrm{Mer}}\eta = &\left(-\tfrac{d^2\eta_1}{dx^2} + R^2\sigma^4\left(1-\tfrac{2}{\cosh^2(R\sigma^2 x)}\right)\eta_1\right)\tfrac{\partial}{\partial\theta} \\ &+\left(-\tfrac{d^2\eta_2}{dx^2} - R\sigma^2\left(1-\tanh(R\sigma^2 x)\right)\tfrac{d\eta_2}{dx} + R^2\bar\sigma^2\left(1-\sigma^2\tanh(R\sigma^2 x)\right)\eta_2\right)\tfrac{\partial}{\partial\varphi}\,. \end{aligned}$$

The form of this operator can be simplified if a basis for the tangent space that is transported in a parallel way along the kink is considered [18, 20]. The parallel transport equations along Meridian solutions for a generic vector field $v(x) = v^1(x)\frac{\partial}{\partial\theta} + v^2(x)\frac{\partial}{\partial\theta}$ read as $\frac{dv^1}{dx} = 0$ and $\frac{dv^2}{dx} = -\frac{R\sigma^2 v^2}{e^{2R\sigma^2 x}+1}$, which leads to solution $v^1(x) = 1$ and $v^2(x) = \sqrt{1+e^{-2R\sigma^2 x}}$. Therefore,

$$\left\{v_1 = \frac{\partial}{\partial\theta}, v_2 = \sqrt{1+e^{-2R\sigma^2 x}}\,\frac{\partial}{\partial\varphi}\right\}$$

is a parallel frame along $\left(\pm\frac{\pi}{2}\right)$-Meridian solutions. Writing the perturbation field in this basis $\bar\eta = \bar\eta_1\, v_1 + \bar\eta_2\, v_2$, the Hessian operator reads:

$$\begin{aligned} H_{\rm Mer}\bar\eta = &\left[-\tfrac{d^2\eta_1}{dx^2} + R^2\sigma^4\left(1 - \tfrac{2}{\cosh^2(R\sigma^2 x)}\right)\eta_1\right] v_1 + \\ + &\left[-\tfrac{d^2\eta_2}{dx^2} + \tfrac{R^2}{2}\left(\sigma^4 - 2\sigma^2 + 2 - \tfrac{3\sigma^4}{2\cosh^2(R\sigma^2 x)} - \sigma^2(2-\sigma^2)\tanh(R\sigma^2 x)\right)\bar\eta_2\right] v_2\,. \end{aligned}$$

For these solutions the longitudinal fluctuation operator

$$\mathcal{H}_{11} = -\frac{d^2}{dx^2} + R^2\sigma^4\Big(1 - \frac{2}{\cosh^2(R\sigma^2 x)}\Big)$$

comprises a zero mode $\omega_0^2 = 0$ and a doubly degenerate spectrum $\omega^2 \in (R^2\sigma^4, \infty)$. On the other hand, the spectrum of the second component

$$\mathcal{H}_{22} = -\frac{d^2}{dx^2} + \frac{R^2}{2}\Big(\sigma^4 - 2\sigma^2 + 2 - \frac{3\sigma^4}{2\cosh^2(R\sigma^2 x)} - \sigma^2(2-\sigma^2)\tanh(R\sigma^2 x)\Big)$$

is simply degenerate in the interval $\omega^2 \in [\bar\sigma^4 R^2, R^2]$ and doubly degenerate in $\omega^2 \in (R^2, \infty)$. From the previous analysis, we conclude that the $\overline{K}_1^{(q,b,c)}(\overline{x})$-solutions are also stable topological kinks.

- **Prime Meridian kinks**: This case is similar to the previous one, the $K_2^{(q,a,c)}(\overline{x})$-fluctuation operator extracted from (3.30) is given by

$$\begin{aligned} \Delta_{\rm PMer}\eta = &\left(-\frac{d^2\eta_1}{dx^2} + R^2\left(1 - \frac{2}{\cosh^2(Rx)}\right)\eta_1\right)\frac{\partial}{\partial\theta} \\ &+\left(-\frac{d^2\eta_2}{dx^2} - R\left(1-\tanh(Rx)\right)\frac{d\eta_2}{dx} - R^2\bar\sigma^2\left(\sigma^2 - \tanh(Rx)\right)\eta_2\right)\frac{\partial}{\partial\varphi} \end{aligned}$$

in the standard frame. If the parallel frame is defined by the system

$$\left\{v_1 = \frac{\partial}{\partial\theta}, v_2 = \sqrt{1+e^{-2Rx}}\,\frac{\partial}{\partial\varphi}\right\},$$

which is obtained by solving the parallel transport equations $\frac{dv^1}{dx} = 0$ and $\frac{dv^2}{dx} = -\frac{Rv^2}{e^{2Rx}+1}$, then in this frame the previous operator reads

$$\begin{aligned} H_{\rm PMer}\bar\eta = &\left[-\tfrac{d^2\eta_1}{dx^2} + R^2\left(1 - \tfrac{2}{\cosh^2(Rx)}\right)\eta_1\right] v_1 \\ + &\left[-\tfrac{d^2\eta_2}{dx^2} + \tfrac{R^2}{2}\left(2\sigma^4 - 2\sigma^2 + 1 - \tfrac{3}{2\cosh^2(Rx)} + (1-2\sigma^2)\tanh(Rx)\right)\bar\eta_2\right] v_2\,. \end{aligned}$$

The spectrum of this operator comprises two zero modes, each of them associated with the two different components of Δ_{PMer}. A doubly degenerate continuous spectrum emerges at the threshold value $\omega^2 = R^2$ for the first component. For the second component a simply and doubly degenerate spectra in the intervals $[\min\{\bar{\sigma}^4R^2, \sigma^4R^2\}, \max\{\bar{\sigma}^4R^2, \sigma^4R^2\}]$ and $(\max\{\bar{\sigma}^4R^2, \sigma^4R^2\}, \infty)$ arise. As a consequence the $K_2^{(q,a,c)}(\overline{x})$-kinks are stable, although a new neutral stability channel is open for these solutions.

Finally, even if the spectral equations that the Hessian operator defines for any member of the families are beyond analytical analysis, Morse Theory can be applied to the kink orbit space. Indeed, Morse theory allows us to unveil the stability of the families of kinks $K_2^{(q,a,b,c)}(\overline{x}, \gamma)$ and $K_4^{(q,a,b,c)}(\overline{x}, \gamma)$. In the first case, $K_2^{(q,a,b,c)}(\overline{x}, \gamma)$-kink orbits lack conjugate points, which implies that these solutions are stable. Therefore, every member of this family, which can be interpreted as a non-linear combination of the single walls $K_1^{(q,a,b)}(\overline{x})$ and $\overline{K}_1^{(q,b,c)}(\overline{x})$, form a stable configuration. On the other hand, all the $K_4^{(q,a,b,c)}(\overline{x}, \gamma)$ orbits cross through the conjugate point F_{ac}. This allows us to conclude that these solutions are unstable. This is only natural, since as it was noted, solutions that belong to this family involve the presence of a kink and its antikink, which obviously is a source of unstability. Thus, Morse theory merely confirms in this last case what had already been suspected.

3.2 Brochosons on the sphere $\mathbb{S}^2$

In last section a rich variety of topological kinks is found in the sphere $\mathbb{S}^2$. All these kinks cannot decay into vacuum given that their ends are fixed at different points in space. However, no non-topological kink is found in that model. Since the sphere is a simply connected manifold, non-topological kinks could, in principle, decay into vacuum due to elastic forces. Indeed, in principle every loop in the sphere can be contracted to a point. The objective of this section is the construction of a model on the sphere that supports brochosons, this is, non-topological kinks that cannot decay into vacuum.

In Chapter 1 a model in $\mathbb{R}^2$ where brochosons arise was constructed. The procedure was based on two conditions. The first one is that the potential must have a singularity. On the other hand, the second one is that the potential can be derived from a superpotential which is not periodic in an angular coordinate. This allowed us to find non-topological kinks in the Euclidean plane revolving the singularity, or more precisely, the Euclidean point except for one point p, the singularity. This meant in practice that the target space $\mathbb{R}^2$ was replaced by the non-simply connected target space $\mathbb{R}^2 - p$ and therefore brochosons could emerge.

In this chapter, dedicated to the sphere $\mathbb{S}^2$, an analogue procedure will be followed. A singularity in the potential function of a Sigma model on the sphere can be included so that it makes us exclude a point from the target manifold. However, the topological properties of the sphere allow loops revolving this singularity to be contracted in the other direction, this is, avoiding this singularity. Therefore, two singularities will be necessary to prevent non-topological kinks from decaying into vacuum on the sphere. In fact, this is only natural, if a point is removed from the sphere $\mathbb{S}^2$ the resulting target space is topologically equivalent to a plane. If another point is removed, a space topologically identical to that of Chapter 1 is obtained.

3.2.1 Models involving singularities in spherical coordinates

As mentioned, this method for finding brochosons requires a chart on the manifold with at least one periodic coordinate. In this case, the two-dimensional sphere $\mathbb{S}^2$, this coordinate appears naturally when the spherical coordinates (θ, φ) are considered. In particular, coordinate φ will be the angular variable with which the non-periodicity trick in the superpotential will be performed. Indeed, the identification of points $(\theta, -\pi)$ and (θ, π) is made for all values of θ. Therefore, given that these coordinates are the same as those of previous sections, the same metric tensor and the same action (3.14) will be considered. Now, the idea is to construct the potential from a superpotential $W(\theta, \varphi)$. This is, only potentials that admit the Bogomol'nyi arrangement will be addressed. This implies that the potential must be in spherical coordinates of the form

$$V(\theta,\varphi) = \frac{1}{2}\left[\frac{1}{R^2}\left(\frac{\partial W}{\partial \theta}\right)^2 + \frac{1}{R^2\sin^2\theta}\left(\frac{\partial W}{\partial \varphi}\right)^2\right]. \tag{3.31}$$

Notice that the second term presents two singularities at $\theta = 0, \pi$ unless they are eliminated by the derivative of the superpotential. This corresponds to the north pole N and the south pole S of the sphere. This is the minimum number of singularities required in this procedure. Hence, the superpotential will be chosen so that these singularities are not washed away. In particular, for the sake of simplicity, an additively separable superpotential will be considered

$$W(\theta,\varphi) = f(\theta) + h(\varphi)\,. \tag{3.32}$$

This simplifies the integration of Bogomol'nyi equations, as they are partially decoupled

$$\frac{d\theta}{dx} = \pm\frac{1}{R^2}\frac{df(\theta)}{d\theta}\,, \qquad \frac{d\varphi}{dx} = \pm\frac{1}{R^2\sin^2\theta}\frac{dh(\varphi)}{d\varphi}\,. \tag{3.33}$$

Integration of the first equation provides profiles $\theta_\pm(x)$, which depend on the chosen function $f(\theta)$. This, in turn, allows us to perform a reparametrisation in the second equation so that it reads

$$\frac{d\varphi}{d\xi} = \pm\frac{dh(\varphi)}{d\varphi}\,, \tag{3.34}$$

where this new spatial coordinate is defined as

$$\xi = \xi_0 + \int \frac{dx}{R^2\sin^2\theta(x)}\,. \tag{3.35}$$

Let us denote as $\varphi_\pm(\xi)$ the kink profiles that equation (3.34) produces and as $(\theta_\pm(x), \varphi_\pm(\xi(x)))$ the corresponding solutions of the model. It is worth noting that in order to make this reparametrisation well-defined, solution $\theta(x)$ must not vanish. This must be taken into consideration when choosing the particular function $f(\theta)$, as this function determines this profile $\theta(x)$. Lastly, as in previous models, the energy of these kinks, solutions of Bogomol'nyi equations, will not depend on the path the kink follows, but only on the evaluation of the superpotential at the initial and final point

$$E = \left|\lim_{x\to\infty} W(\theta(x),\varphi(x)) - \lim_{x\to-\infty} W(\theta(x),\varphi(x))\right|\,.$$

Exactly as in the model presented in Chapter 1, the fact that the superpotential is not periodic in an angular coordinate allows non-topological kinks to have non-vanishing energy. This is, it enables the existence of non-topological kinks.

3.2.2 A particular family of models with singularities

Because of the definition of the parameter $\xi(x)$, the profiles $\theta_\pm(x)$ must not vanish. In order to prevent this, a shifted ϕ^4-model will be constructed for the variable θ. Let us consider as the function $f(\theta)$ that appears in the superpotential the following function

$$f(\theta) = m_1 \frac{(b-a)^2}{4} \left[\frac{2\theta - a - b}{b-a} - \frac{1}{3} \left(\frac{2\theta - a - b}{b-a} \right)^2 \right] , \tag{3.36}$$

where $m_1, a, b \in \mathbb{R}$. This function produces by the first Bogomol'nyi equation a ϕ^4-model-like solution

$$\theta_\pm(x) = \frac{a+b}{2} \pm \frac{b-a}{2} \tanh \left[\frac{m_1(x-x_0)}{R^2} \right] , \tag{3.37}$$

where x_0 is an integration constant that represents the kink centre. Note that this solution connects values $\theta = a$ and $\theta = b$. Therefore, in order to avoid the zero, values a and b must be both positive or both negative. Since this coordinate is defined in the interval $\theta \in [0, \pi]$, condition $\pi > b > a > 0$ will be imposed. Now, these profiles $\theta_\pm(x)$ define the reparametrisation ξ, for which $\frac{d\xi}{dx}$ does not vanish and therefore it is well-defined, see Figure 3.8.

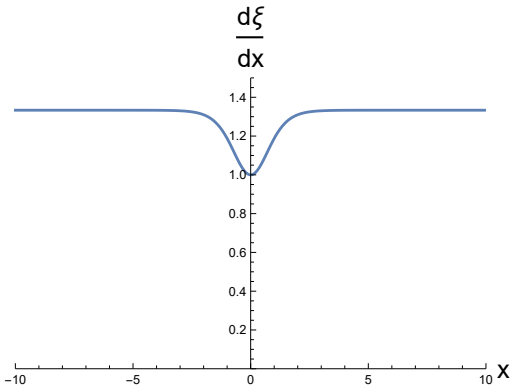

Figure 3.8: The reparametrisation is well-defined for a non-vanishing profile of a shifted ϕ^4-model type. Values of the parameters $a = \frac{\pi}{3}$ and $b = \frac{2\pi}{3}$ have been used.

On the other hand, as has been advanced, for the other coordinate φ a non-periodic function $h(\varphi)$ in $\varphi \in [-\pi, \pi]$ must be chosen. Otherwise the energy would vanish. In particular, a function that complies with this property is

$$h(\varphi) = m_2 \sin \frac{\varphi}{2} , \tag{3.38}$$

where m_2 is a real number. This function produces a profile in φ

$$\varphi(x) = \pm \mathrm{Gd}[\xi(x)] , \tag{3.39}$$

where Gd denotes the Gudermannian function. This field profile performs a whole revolution between π and $-\pi$ given that $\xi(x)$ has the same limits than x at infinities by construction. Now, by combining both functions $f(\theta)$ and $h(\varphi)$, the following family of superpotentials emerges

$$W(\theta,\varphi) = m_1 \frac{(b-a)^2}{4}\left[\frac{2\theta-a-b}{b-a} - \frac{1}{3}\left(\frac{2\theta-a-b}{b-a}\right)^3\right] + m_2 \sin\frac{\varphi}{2}\,, \tag{3.40}$$

which is modulated by parameters m_1, m_2, a and b. While different values of paramaters a and b will produce different kink orbits, m_1 and m_2 will affect their energy. This superpotential leads by equation (3.31) to the following family of potential functions

$$V(\theta,\varphi) = \frac{1}{2}\left[\frac{m_1^2(b-a)^2}{4R^2}\left[1-\left(\frac{2\theta-a-b}{b-a}\right)^2\right]^2 + \frac{m_2^2}{4R^2\sin^2\theta}\cos^2\frac{\varphi}{2}\right]\,, \tag{3.41}$$

which is periodic in $\varphi \in [-\pi,\pi]$ even if the superpotential W is not. Notice as well that the singularities at $\theta = 0$ and $\theta = \pi$ remain as it was required, see Figure 3.9. Given the identification of points $(\theta,\pi) = (\theta,-\pi)$ for all θ, the vacuum manifold in this model is comprised by only two points

$$\mathcal{M} = \left\{v^1 = (a,\pi), v^2 = (b,\pi)\right\}\,.$$

Indeed, parameters a and b controls the position of the vacua of the model, which will be asymptotically connected by kinks.

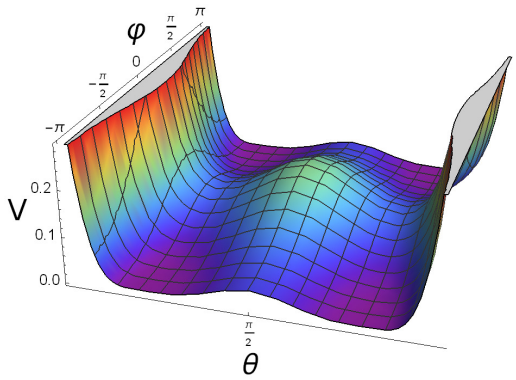

Figure 3.9: Potential function in the $\theta-\varphi-$plane for the values of the parameters $a = \frac{\pi}{3}$ and $b = \frac{2\pi}{3}$. Two vacua appear at (a,π) and (b,π) while two singularities appear in the limits $\theta \to 0$ and $\theta \to \pi$.

3.2.3 Kink variety of the model

In last section a particular family of models has been constructed, hoping that brochosons emerge as solutions. However, their kink variety remains unexplored. This is the aim of this section, where solutions of Bogomol'nyi equations will be identified. These are, for the chosen superpotential, of the form

$$\frac{d\theta}{dx} = \pm\frac{m_1}{R^2}\frac{b-a}{2}\left[1-\left(\frac{2\theta-a-b}{b-a}\right)^2\right]\,, \qquad \frac{d\varphi}{dx} = \pm\frac{m_2}{2R^2\sin^2\theta}\cos\frac{\varphi}{2}\,. \tag{3.42}$$

Four types of solutions will appear as solutions of these equations. The first one is vacuum solutions, that is, $(\theta(x), \varphi(x)) = (a, \pi)$ or $(\theta(x), \varphi(x)) = (b, \pi)$. The second and third types are singular solutions where one of the coordinates is constant along the curve. Rajaraman's trial orbit method will be employed to derived these. Lastly, a whole family of solutions neither constant in θ nor in φ is found as general solutions of Bogomol'nyi equations. Let us describe in detail these non-vacuum solutions.

- Θ_K-**kinks**: The first type of singular kink will be that with constant φ and shall be denoted as Θ_K-kink. In particular, condition $\varphi = \pi$ makes the second equation in (3.42) hold trivially and the orbit will travel only in the $\theta-$direction

$$\Theta_K(x) = \left(\frac{a+b}{2} \pm \frac{b-a}{2} \tanh\left[\frac{m_1(x-x_0)}{R^2} \right], \pi \right) . \tag{3.43}$$

  These solutions, both kink and antikink, are topological, since they asymtotically join both vacua v^1 and v^2, see Figure 3.10. The energy of these kinks is modulated not only by the parameter m_1, but also by the separation between vacua $b-a$

$$E\left[\Theta_K(x)\right] = \frac{(b-a)^2}{3}|m_1| .$$

- Φ_K-**kinks**: If $\theta-$constant solutions are sought, two options arise since two vacua emerge in this model. Let us denote as $\Phi_{K,a}$ and $\Phi_{K,b}$ the profiles that emerge when trial orbits $\theta = a$ and $\theta = b$ are respectively considered. When these are imposed, the first equation in (3.42) holds trivially and we obtain the profiles

$$\Phi_{K,a}(x) = (a, \pm \mathrm{Gd}[\xi(x)]) ,$$
$$\Phi_{K,b}(x) = (b, \pm \mathrm{Gd}[\xi(x)]) .$$

  These are non-topological kinks and antikinks that asymptotically connect a vacuum with itself after revolving once around the sphere, see Figure 3.10. Notice that these kinks are not allowed to decay into vacuum since due to the existence of singularities in both north and south poles. Therefore, the topology of the target space makes these solutions brochosons. On the other hand, their energies depend only on the parameter m_2

$$E\left[\Phi_{K,a}(x)\right] = E\left[\Phi_{K,b}(x)\right] = |2m_2| .$$

- **Family of kinks**: The last type of solutions is the one comprised by a combination of the other two, with no constant coordinate. These are general solutions of Bogomol'nyi equations (3.42), which shall be denoted as $\Sigma(x, \xi_0)$. The kink profiles read

$$\Sigma(x, \xi_0) = \left(\frac{a+b}{2} \pm \frac{b-a}{2} \tanh\left[\frac{m_1(x-x_0)}{R^2} \right], \pm \mathrm{Gd}[\xi(x, \xi_0)] \right) ,$$

  where ξ_0 is the parameter that distinguishes between different members of the family. These solutions describe kinks that connect both vacua while revolving once around the sphere, see Figure 3.10.

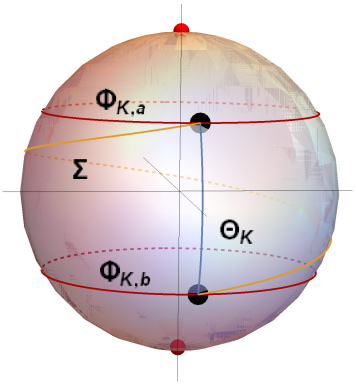

Figure 3.10: Solutions on the sphere for the values of the parameters $a = \frac{\pi}{3}$ and $b = \frac{2\pi}{3}$. Vacua are represented by black points while singularities are represented by red points located in the poles. The Θ_K-kink, depicted in blue, asymptotically connects both vacua in a trajectory with φ constant. The two different Φ_K-kinks, depicted in red, are non-topological kinks which cannot decay into vacuum due to the existence of the two singularities in the sphere. Lastly, one representative member of the one-parameter family of kinks is depicted in yellow, as a combination of two singular kinks.

Note that the rotation of these topological kinks is performed in two different directions depending on the sign that appears in the solution. On the other hand, the energy of all members of this family is identical and is simultaneously modulated by the distance $b-a$ and parameters m_1 and m_2

$$E\left[\Sigma\right] = \frac{(b-a)^2}{3}|m_1| + |2m_2| \,.$$

This is to be expected, since limits of this family of kinks must coincide with a combination of a Θ_K-kink and a Φ_K-kink as the sum energy rule suggests

$$E\left[\Sigma\right] = E\left[\Theta_K\right] + E\left[\Phi_K\right] \,.$$

3.3 Further comments

In this chapter two objectives have been accomplished. In the first part, the kink variety that arises in a non-linear $\mathbb{S}^2$-sigma model with a particular homogeneous quartic polynomial potential has been analytically calculated and the stability of solutions analysed. This model has been constructed so that the vacuum manifold in this model is comprised by six maximally separated vacuum points on the sphere. This, in turn, leads to singular kinks as pieces of great circles joining these points. These singular kink orbits, denoted as Equatorial, $(\pm\frac{\pi}{2})$-Meridian and Primer Meridian kinks, split the sphere in eight octants. The first two types describe two simple kinks, whose energy densities are localised around a point. In contrast, the Prime Meridian kinks appear when a Equatorial kink and a $(\pm\frac{\pi}{2})$-Meridian kink are exactly overlapped. Indeed, these solutions are singular members of the $K_2^{(q,a,b,c)}(\overline{x},\gamma)$-kink families, characterised as a non-linear combination of the two previously mentioned simple kinks. The energy density of these solutions are condensed around two points, which are separated by a distance parameterised by the value of γ. Note that no

interaction appears between these two singular static kinks. In fact, all these solutions have been proved to be stable kinks. A similar equilibrium configuration is obtained when four simple kinks (two of each type) are alternately disposed along the space if the two kinks in the middle are exactly overlapped and equally separated of the other two. These static solutions constitute the $K_4^{(q,a,b,c)}(\overline{x},\gamma)$-kink families. However, their complex internal structure make these topological defects unstable.

In the second part of this chapter, a family of models that admit brochosons is constructed on the sphere. Although the sphere is a simply connected manifold, a similar strategy to that employed in Chapter 1 has been followed. This consists in imposing two separate requirements. On one hand, a potential function with singularities in the poles will allow us to exclude two points from the target manifold, transforming it into a non-simply connected manifold. Indeed, the sphere without the north and south poles is topologically equivalent to the target space employed in Chapter 1. This is, from a topological point of view, the target manifold is replaced by a cylinder. Nevertheless, from a geometrical point of view they are not equivalent, as distances are those on the sphere. On the other hand, the superpotential is defined so that it is not periodic in the angular variable φ, preventing the energy of certain configurations that correspond to non-topological kinks from vanishing. Moreover, the superpotential is defined in such a way that Bogomol'nyi equations can be partially decoupled.

In particular, a family of Sigma model on the sphere $\mathbb{S}^2$ with two vacua and two singularities has been constructed. The potential of these models can be interpreted as a combination of a that of a ϕ^4-model and that of a sine-Gordon model for each angular variable. In order to introduce singularities in the poles, these models are constructed in spherical coordinates, where these naturally appear. This implies, however, that the poles of the sphere must be avoided. This is accomplished by shifting the ϕ^4-model, so that the corresponding profile $\theta(x)$ never reaches the poles. As a result, only one type of singular kink Θ_K with $\varphi-$constant orbit is found, which is topological. Indeed, only one can be found due to the fact that the vacua are aligned in the θ coordinate and both north and south poles are inaccessible. Interestingly, its energy is not only modulated by the parameter m_1 introduced in the superpotential, but also by the distance between the vacua on the sphere. On the other hand, two different non-topological kinks Φ_K are identified with constant variable θ. These are brochosons, since these loops cannot be contracted because of the singularities located at both poles. Notice that the energy of these singular kinks, unlike that of Θ_K-kinks, is exclusively modulated by the parameter m_2. This is only natural, since separation between vacua does not affect orbits given by $\theta-$constant circles. Lastly, as general solutions of Bogomol'nyi equations, a whole family of topological kinks revolving the sphere once is found connecting asymptotically both vacua. Since limits of this one-parameter family must be identified with a combination of a Θ_K-kink and a Φ_K-kink, the energy of any member of this family is the sum of the energies of these two singular kinks, which is then simultaneously modulated by m_1 and m_2. In fact, the existence of this family of kinks was already suggested by an emerging energy sum rule between singular kinks.

In conclusion, this procedure of introducing singularities in the potential to make the target manifold non-simply connected, which had been employed for the Euclidean plane, has now been extended for the two-dimensional sphere. Furthermore, this method can be applied to any Riemannian manifold. Now, instead of relying

on the existence of singularities in the potential, Sigma models with differentiable potentials could be constructed on a non-simply connected Riemannian manifold. For instance, the two-dimensional torus could be considered. This will be the main objective in Chapter 4, where brochosons will be sought in Sigma models on the torus.

Chapter 4

Kinks on the torus $\mathbb{S}^1 \times \mathbb{S}^1$

Topological kinks asymptotically connect different vacua, which implies that the decay of this type of solutions into vacuum would require an infinite amount of energy. Therefore, topological kinks cannot decay into vacuum. In contrast, this topological protection is lost in general when non-topological kinks are considered. Indeed, in general elastic forces will contract these loops into points that belong to the vacuum manifold. Nevertheless, the local behaviour of the potential of a Sigma model can make non-topological kinks linearly stable against small fluctuations. An example of this possibility in the plane can be found in reference [25], where a deformation of the MSTB model comprises a linearly stable non-topological kink. However, these solutions may decay into vacuum if a large enough fluctuation is applied. As has been shown in previous chapters, the topological protection against decaying into vacuum can be recovered for non-topological solutions when the potential term involves a singularity surrounded by the kink, see [16]. This is, brochosons may arise when the target manifold of a Sigma model is non-simply connected. Models presented in previous chapters employed target manifolds that were originally simply connected, that is, for which any loop could be shrunk into a point. In order to allow the emergence of brochosons, singularities in the potential function were introduced, removing in the process these points from the target space. In a nutshell, this procedure replaced the original target space by a non-simply connected manifold.

In this chapter, instead of employing this method, a non-simply connected Riemannian manifold will be directly considered as target manifold for Sigma models. This will allow us to consider differentiable potential functions while still being able of identifying brochosons. Even if non-linear Sigma models on Riemannian manifolds of genus zero are vastly employed in the literature, see for example [17, 18, 20, 74], Riemannian surfaces with genus at least one are more exotic. In this chapter this rich scenario will be explored. In precise detail, analytical expressions of kinks in $\mathbb{S}^1 \times \mathbb{S}^1$-Sigma models will be sought. In other words, a two-dimensional torus will be chosen as target manifold, which makes this study have an intrinsic mathematical interest with physical repercussions. Now, although brochosons cannot decay into vacuum, it is worth noting that brochosons may decay into other solutions. For this reason, the analysis of the linear stability will also be important for this type of solutions.

As previously stated, this chapter aims to provide further analytical insight within the context of a torus as a target manifold. First, the general framework

of a Sigma model on the torus is presented. Then, two very different families of this type of Sigma models with different numbers of vacua are presented, studying their kink varieties and hoping that brochosons emerge among their solutions. The main results presented in this chapter can be found published in [26] and [27].

4.1 Non-linear $(\mathbb{S}^1 \times \mathbb{S}^1)$-Sigma models in (1+1)-dimensions

We shall deal with non-linear Sigma models on the $2-$dimensional torus $\mathbb{S}^1 \times \mathbb{S}^1$, which shall be embedded in $\mathbb{R}^3$. In this type of theory two scalar fields will be employed to represent the poloidal-toroidal coordinates on the torus. These two scalar fields $\theta, \varphi : \mathbb{R}^{1,1} \to \mathbb{S}^1$, defined on the $(1+1)-$dimensional Minkowski space $\mathbb{R}^{1,1}$, can be defined by their relation with the corresponding Cartesian coordinates ϕ^1, ϕ^2, ϕ^3 of the embbeding in $\mathbb{R}^3$

$$\begin{aligned} \phi^1(\theta,\varphi) &= (R + r\sin\theta)\cos\varphi\,, \\ \phi^2(\theta,\varphi) &= r\cos\theta\,, \\ \phi^3(\theta,\varphi) &= (R + r\sin\theta)\sin\varphi\,, \end{aligned} \tag{4.1}$$

with poloidal $\theta \in [0, 2\pi)$ and toroidal $\varphi \in [0, 2\pi)$ coordinates and where R and r are the major and minor radii of the torus $R > r > 0$, see Figure 4.1.

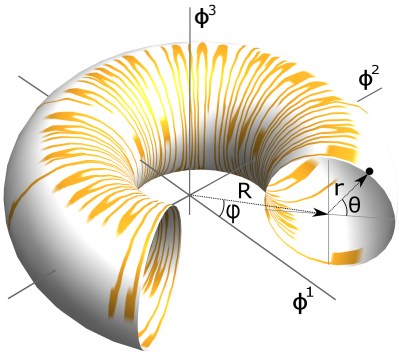

Figure 4.1: Poloidal-toroidal coordinates (θ, φ) on the two-dimensional torus.

Moreover, a metric tensor on the torus is inherited from the ambient space, which in these coordinates is of the form

$$g = r^2 d\theta \otimes d\theta + (R + r\sin\theta)^2 d\varphi \otimes d\varphi\,.$$

Let us construct a non-linear Sigma model with these fields. Since the metric tensor in these coordinates is diagonal, the corresponding action reads just as

$$S[\theta,\varphi] = \int_{\mathbb{R}^{1,1}} \left[\frac{1}{2} r^2 \left[\left(\frac{\partial\theta}{\partial t}\right)^2 - \left(\frac{\partial\theta}{\partial x}\right)^2 \right] + \frac{1}{2}(R + r\sin\theta)^2 \left[\left(\frac{\partial\varphi}{\partial t}\right)^2 - \left(\frac{\partial\varphi}{\partial x}\right)^2 \right] - V(\theta,\varphi) \right] dx\ dt\,,$$

where once again $V : \mathbb{S}^1 \times \mathbb{S}^1 \to \mathbb{R}$ is a potential function. Notice that this functional could have been derived following a procedure similar to that in Chapter 3. This is, employing a Lagrange multiplier in a Sigma model on the Euclidean space $\mathbb{R}^3$ with constraint

$$f(\phi_1, \phi_2, \phi_3) = \left(R - \sqrt{\phi_1^2 + \phi_3^2}\right)^2 + \phi_2^2 - r^2 = 0\,,$$

the same functional is retrieved. This action, in turn, will lead us to the following field equations

$$\eta^{\mu\nu}\frac{\partial^2 u^i}{\partial x^\mu \partial x^\nu} + \eta^{\mu\nu}\Gamma^i_{jk}\frac{\partial u^j}{\partial x^\mu}\frac{\partial u^k}{\partial x^\nu} + g^{ij}\frac{\partial V}{\partial u^j} = 0\,, \quad u^1 = \theta\,,\, u^2 = \varphi\ ,\ \ i,j = 1,2\,. \tag{4.2}$$

where Einstein summation convention is used for both latin and greek indices and Γ^i_{jk} denote the Christoffel symbols associated to the metric tensor g defined by coordinates (4.1)

$$\Gamma^1_{22} = -\frac{1}{r}\cos\theta(R + r\sin\theta), \qquad \Gamma^2_{12} = \Gamma^2_{21} = \frac{r\cos\theta}{R + r\sin\theta}\,,$$
$$\Gamma^1_{11} = \Gamma^1_{12} = \Gamma^1_{21} = \Gamma^2_{11} = \Gamma^2_{22} = 0.$$

Among all solutions $\Sigma(t,x) \equiv (\theta(t,x), \varphi(t,x))$ of the field equations (4.2), we shall focus on kinks. This implies that we shall be focusing on solutions that belong to the configuration space defined by the finite energy condition

$$E[\theta,\varphi] = \int_{-\infty}^{\infty}\left\{\frac{1}{2}r^2\left[\left(\frac{\partial\theta}{\partial t}\right)^2 + \left(\frac{\partial\theta}{\partial x}\right)^2\right] + \frac{1}{2}(R + r\sin\theta)^2\left[\left(\frac{\partial\varphi}{\partial t}\right)^2 + \left(\frac{\partial\varphi}{\partial x}\right)^2\right] + V(\theta,\varphi)\right\}dx\,.$$

This condition forces solutions to tend asymptotically to a zero of the potential function $V(\theta,\varphi)$ and their derivatives to zero at the ends of the spatial line. The vacuum manifold $\mathcal{M}$, which is the set of zeroes of the potential $V(\theta,\varphi)$, will be comprised by pairs of values for both angles

$$\mathcal{M} = \{v_j = (\theta_j, \varphi_j) \in \mathbb{S}^1 \times \mathbb{S}^1 \mid V(\theta_j,\varphi_j) = 0,\ j = 1,2,\dots\}\,.$$

Now, travelling solutions can be identified by applying a Lorentz boost to static configurations, which are solutions of the static field equations

$$\frac{d^2\theta}{dx^2} - \frac{1}{r}\cos\theta(R + r\sin\theta)\frac{d\varphi}{dx}\frac{d\varphi}{dx} - \frac{1}{r^2}\frac{\partial V}{\partial\theta} = 0\,, \tag{4.3}$$
$$\frac{d^2\varphi}{dx^2} + \frac{2r\cos\theta}{R + r\sin\theta}\frac{d\theta}{dx}\frac{d\varphi}{dx} - \frac{1}{(R + r\sin\theta)^2}\frac{\partial V}{\partial\varphi} = 0\,. \tag{4.4}$$

The same strategy is followed to derive the energy density profiles of kinks. Since these field theories are Lorentz invariant, it suffices to obtain the static energy profile $\varepsilon(x)$ and subsequently the static energy for a given static solution $(\theta(x), \varphi(x))$

$$E[\theta(x),\varphi(x)] = \int_{-\infty}^{\infty}\varepsilon(x)dx\,,$$

to identify the topological structure in motion. Furthermore, in order to perform Bogomoln'nyi's procedure, the type of potential term V considered in the action shall be restricted to those that can be written in terms of the superpotential as

$$V(\theta,\varphi) = \frac{1}{2r^2}\left(\frac{\partial W}{\partial \theta}\right)^2 + \frac{1}{2\left(R + r\sin\theta\right)^2}\left(\frac{\partial W}{\partial \varphi}\right)^2 . \tag{4.5}$$

By applying Bogomoln'nyi's arrangement, configurations that minimise the energy functional $E[\theta,\varphi]$ in the configuration space $\mathcal{C}$, that is BPS kinks, are obtained as solutions of the following first order differential equations

$$\frac{d\theta}{dx} = (-1)^a \frac{1}{r^2}\frac{\partial W}{\partial \theta}\,, \qquad \frac{d\varphi}{dx} = (-1)^a \frac{1}{(R + r\sin\theta)^2}\frac{\partial W}{\partial \varphi}\,. \tag{4.6}$$

These are also solutions of the field equations (4.3)-(4.4). Note that the global factor $(-1)^a$ could be absorbed in the spatial variable x, which means that kinks and antikinks are obtained for different values of a. If the superpotential $W(\theta,\varphi)$ and the profiles of the BPS kinks are smooth functions, then the energy becomes a topological charge

$$E = \left| \lim_{x\to\infty} W[\theta(x),\varphi(x)] - \lim_{x\to-\infty} W[\theta(x),\varphi(x)] \right|, \tag{4.7}$$

which depends exclusively on the vacua that the BPS kinks are asymptotically connecting. It is worth highlighting the fact that, unlike in simply connected spaces, labelling the minima that the kink is asymptotically joining is not enough to distinguish between topological sectors. Indeed, even if these two minima are fixed, kinks revolving a different number of times around any direction on the torus will not belong to the same homotopy class. Now, since an infinite number of topological sector arise, these will be grouped into "topological clusters" in which solutions link the same minima. The term topological will then be used for kinks that belong to clusters in which solutions connect different minima and non-topological for kinks that belong to clusters that connect a minimum with itself.

Lastly, the stability of these kinks must be analysed. The study of the linear stability of a solution $\Sigma(x) = (\theta(x),\varphi(x))$, i.e. the analysis of small fluctuations around a kink, leads to the spectral problem associated to the operator

$$\mathcal{H}_\Sigma \eta = -\left(\nabla_{\Sigma'}\nabla_{\Sigma'}\eta + R(\Sigma',\eta)\Sigma' + \nabla_\eta \mathrm{grad}V\right),$$

where the covariant derivative of $\eta(x)$ and the action of the curvature tensor on $\eta(x)$ will be written in coordinates as

$$\nabla_{\Sigma'}\eta = \left(\eta'^i(x) + \Gamma^i_{jk}\eta^j u'^k\right)\frac{\partial}{\partial u^i}\,, \qquad R(\Sigma',\eta)\Sigma' = u'^i\eta^j(x)u'^k R^l_{ijk}\frac{\partial}{\partial u^l}\,,$$

with $u^1 = u^1(x) = \theta(x)$, $u^2 = u^2(x) = \varphi(x)$ and where $\eta(x)$ is a vector field along the kink solution $\Sigma(x)$ in the torus. The Hessian of the potential function, evaluated at $\Sigma(x)$, reads

$$\nabla_\eta \mathrm{grad}V = \eta^i\left(\frac{\partial^2 V}{\partial u^i \partial u^j} - \Gamma^k_{ij}\frac{\partial V}{\partial u^k}\right) g^{jl}\frac{\partial}{\partial u^l}\,.$$

Particularising the previous expressions to the case of the torus, see Appendix D, the spectral equation for the second-order small fluctuation operator is written in matrix form as

$$\mathcal{H}[\Sigma(x)]\,\Psi_n(x) = \omega_n^2\Psi_n(x)\,, \tag{4.8}$$

where $\mathcal{H}[\Sigma(x)]$ is a (2×2)-matrix operator, whose components are expressed as

$$\begin{aligned}
\mathcal{H}_{11} =& -\frac{d^2}{dx^2}+\left[\cos^2\theta-\frac{\sin\theta(R+r\sin\theta)}{r}\right]\left(\frac{d\varphi}{dx}\right)^2+\frac{1}{r^2}\frac{\partial^2 V}{\partial\theta^2}\,,\\
\mathcal{H}_{12} =& \frac{2\cos\theta(R+r\sin\theta)}{r}\frac{d\varphi}{dx}\,\frac{d}{dx}+\frac{1}{r^2}\frac{\partial^2 V}{\partial\theta\partial\varphi}\,,\\
\mathcal{H}_{21} =& -\frac{2r\cos\theta}{R+r\sin\theta}\frac{d\varphi}{dx}\frac{d}{dx}+\frac{2r(r+R\sin\theta)}{(R+r\sin\theta)^2}\frac{d\varphi}{dx}\frac{d\theta}{dx}\\
&+\frac{1}{(R+r\sin\theta)^2}\frac{\partial^2 V}{\partial\theta\partial\varphi}-\frac{2r\cos\theta}{(R+r\sin\theta)^3}\frac{\partial V}{\partial\varphi}\,,\\
\mathcal{H}_{22} =& -\frac{d^2}{dx^2}-\frac{2r\cos\theta}{R+r\sin\theta}\frac{d\theta}{dx}\frac{d}{dx}+\frac{1}{(R+r\sin\theta)^2}\frac{\partial^2 V}{\partial\varphi^2}
\end{aligned}$$

and $\Psi_n(x)=(\psi_n^1(x),\psi_n^2(x))^T$ stands for the two-component eigenfunctions. The lack of negative eigenvalues in the spectral problem (4.8) implies that the solution $\Sigma(x)=(\theta(x),\varphi(x))$ is stable.

4.2 A family of models with different vacuum manifold

In this section a family of superpotentials is proposed to construct a family of massive non-linear Sigma models on the torus $\mathbb{S}^1\times\mathbb{S}^1$. While singular kinks can be identified in general asymptotically joining vacua in all these models, the whole kink variety must be separately calculated in each case. In particular, in next sections three different models that involve a different number of vacua shall be thoroughly explored. Hopefully, the topological constraints obtained by the non-simply connectedness of the target space will allows us to identify brochosons in the torus. On the other hand, solving Bogomol'nyi equations analytically will allow us to study the linear stability for some basic kinks, similarly to the case of the sphere studied in Chapter 3. Here we shall be interested in investigating the kink variety of the set of non-linear $(\mathbb{S}^1\times\mathbb{S}^1)$-Sigma models defined by the following set of superpotentials

$$W_{n_1,n_2}(\theta,\varphi)=m(R+r\sin n_1\theta)\sin(n_2\varphi)\,, \tag{4.9}$$

where $m\in\mathbb{R}$, $n_1\in\mathbb{Z}$ and n_2 is an integer or a half-integer. Note that these conditions on n_i are chosen to guarantee the periodicity on the torus of the potentials (4.5)

$$V_{n_1,n_2}(\theta,\varphi)=\frac{m^2}{2}\left[n_1^2\cos^2(n_1\theta)\sin^2(n_2\varphi)+\frac{n_2^2\cos^2(n_2\varphi)(R+r\sin(n_1\theta))^2}{(R+r\sin(\theta))^2}\right] \tag{4.10}$$

associated to the superpotencials (4.9) defined on the torus. From (4.5) it is clear that the set of vacua $\mathcal{M}$ (zeroes of V) must comply with conditions

$$\begin{aligned}
\frac{\partial W_{n_1,n_2}}{\partial\theta} &= mn_1r\cos(n_1\theta)\sin(n_2\varphi)=0\,,\\
\frac{\partial W_{n_1,n_2}}{\partial\varphi} &= mn_2\cos(n_2\varphi)[R+r\sin(n_1\theta)]=0\,,
\end{aligned}$$

which lead to a total of $|4n_1n_2|$ vacuum points distributed on the torus

$$\mathcal{M}_{n_1,n_2} = \left\{ \Sigma_{k_1,k_2} = (\theta_{k_2}, \varphi_{k_1}) = \left(\frac{\pi}{2n_1} + \frac{k_1\,\pi}{n_1}\,,\, \frac{\pi}{2n_2} + \frac{k_2\,\pi}{n_2} \right) \quad | \quad k_i \in \mathbb{Z} \right\}.$$

Indeed, the number of vacuum points and kinks connecting them in this set of superpotentials will depend on n_1 and n_2, see Figure 4.2.

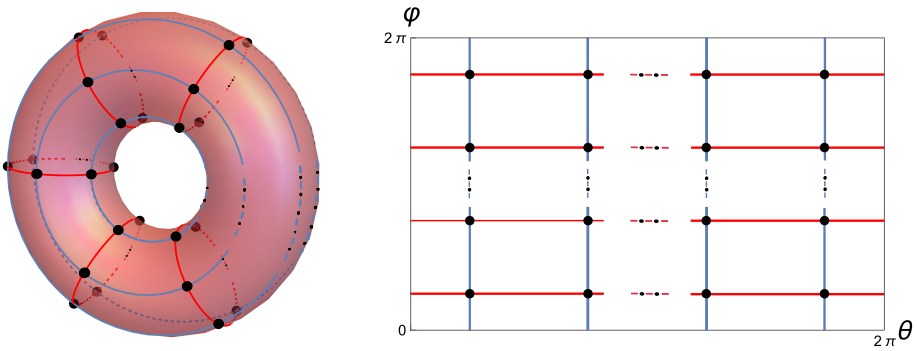

Figure 4.2: Set of vacua for an arbitrary member of this family of potentials (4.10). While in the $\theta - \varphi-$plane an infinite number of minima appear, on the torus these correspond to a finite number of vacua for fixed n_1 and n_2.

On the other hand, the BPS kinks must comply with the first order differential equations (4.6), which for this family of superpotentials read

$$\frac{d\theta}{dx} = (-1)^a\,\frac{m\,n_1}{r}\cos(n_1\theta)\sin(n_2\varphi)\,, \qquad \frac{d\varphi}{dx} = (-1)^a\,m\,n_2\frac{\cos(n_2\varphi)(R + r\sin(n_1\theta))}{(R + r\sin\theta)^2}\,. \tag{4.11}$$

From these equations the kink orbit flow in the phase plane can be determined. It is given by the equation

$$\frac{d\theta}{d\varphi} = \frac{n_1\cos(n_1\theta)(R + r\sin\theta)^2\tan(n_2\varphi)}{n_2 r(R + r\sin(n_1\theta))}\,. \tag{4.12}$$

Despite the fact that equation (4.12) is a separable first order differential equation, the analytical identification of the whole kink orbit variety is not possible for general values of n_1 and n_2. In contrast, singular kinks, for which one of its angular coordinates remains constant, can be analytically obtained for any n_1 and n_2. As a consequence, two different classes of singular kinks can be distinguished:

1. **Φ-kinks**: Loops traced on the torus with the θ-variable fixed as $\theta = \frac{\pi}{2n_1} + \frac{k_1}{n_1}$ cross at least one vacuum point. Depending on the number of vacua that it encounters in its path, a different number of kinks will emerge as pieces of this loop. Each of these curves between vacua will correspond to a Φ-kink. If we substitute the previously fixed value of θ into the first order equations (4.11), the analytical expression for $\Phi_K^{(k_1,k_2)}(x) = (\theta_K(x), \varphi_K(x))$ is obtained

$$\Phi_K^{(k_1,k_2)}(x) = \left(\frac{2k_1 + 1}{2n_1}\pi\,,\, \frac{k_2 + 1}{n_2}\pi + \frac{1}{n_2}\mathrm{Gd}\left[(-1)^{a+k_2+1}\,n_2^2\,A_{k_1}\bar{x}\right] \right), \tag{4.13}$$

where $\bar{x} = x - x_0$, $\mathrm{Gd}\,[y] = -\frac{\pi}{2} + 2\arctan e^y$ denotes the Gudermannian function and where the following constant has been introduced

$$A_{k_1} = \frac{m\,\left(R + (-1)^{k_1} r\right)}{(R + r\sin\frac{2k_1+1}{2n_1}\pi)^2}\,.$$

The integration constant x_0 can be understood as the kink centre. In particular, these kinks trace pieces of loops around the torus center, travelling between vacua located at $\varphi_K = \frac{2k_2+1}{2n_2}$ and $\varphi_K = \frac{2k_2+3}{2n_2}$. The total energy of the kinks (4.13) is given by the relation

$$E[\Phi_K^{(k_1,k_2)}] = 2m\left[R + (-1)^{k_1}\, r\,\right]\,. \tag{4.14}$$

The formula (4.14) suggests the existence of two different groups of Φ-kinks determined by the value of the magnitude $k_1 \bmod 2$ in the formula (4.13). That is, two different groups of solutions are found depending on whether k_1 is even or odd. To distinguish these two kink subtypes, we shall employ the notation $\Phi_K^{[0]}(x)$ and $\Phi_K^{[1]}(x)$ based on the modular arithmetic $[k_1] = k_1 \bmod 2$. Lastly, note that $\Phi_K^{[0]}(x)$-kinks are more energetic than $\Phi_K^{[1]}(x)$-kinks

$$E[\Phi_K^{[0]}] \;>\; E[\Phi_K^{[1]}]\,.$$

2. **Θ-kinks**: Vacuum points can also be connected by pieces of loops defined by the condition $\varphi = \frac{\pi}{2n_2} + \frac{k_2}{n_2}\pi$. In this case, the second equation in (4.11) holds trivially and the first one provides us with kink profiles $\Theta_K^{(k_1,k_2)}(x) = (\theta_K(x), \varphi_K(x))$ that asymptotically link vacua located at $\theta_K = \frac{2k_1+1}{2n_1}$ and $\theta_K = \frac{2k_1+3}{2n_1}$

$$\Theta_K^{(k_1,k_2)}(x) = \left(\frac{k_1+1}{n_1}\pi + \frac{1}{n_1}\mathrm{Gd}\left[\frac{(-1)^{a+k_1+k_2+1}\, m n_1^2}{r}\,\bar{x}\right], \frac{2k_2+1}{2n_2}\pi\right)\,, \tag{4.15}$$

whose total energy is k_i-independent

$$E[\Theta_K] = 2mr\,.$$

It should be noted that the energies of the previous singular kinks comply with the following sum rule

$$E[\Phi_K^{[0]}] \;=\; E[\Phi_K^{[1]}] \;+\; 2E[\Theta_K]\,. \tag{4.16}$$

While $\Phi_K^{[0]}$ is always the most energetic singular kink, the second most energetic one will be $\Phi_K^{[1]}$ or Θ_K depending on the radii of the torus R and r. In particular, $E[\Phi_K^{[1]}] \geq E[\Theta_K]$ when $R \geq 2r$ and $E[\Phi_K^{[1]}] < E[\Theta_K]$ when $R < 2r$. As previously mentioned, in order to describe more thoroughly the structure of the kink varieties in different non-linear $(\mathbb{S}^1 \times \mathbb{S}^1)$-Sigma models with a distinct disposition of vacua on the torus, the following cases of the potential (4.10) shall be studied in detail:

- **Case** 1: Values $n_1 = 1$ and $n_2 = 2$ are chosen to construct a potential with eight vacuum points. Sixty four disjoint topological clusters arise in the configuration space, but as we shall see, only twenty four will contain kinks.

- **Case** 2: Seeking to reduce the number the vacuum points of the model, the values $n_1 = n_2 = 1$ are taken into the potential (4.10). Four vacua and sixteen topological clusters appear, eight of which will be empty.

- **Case** 3: Lastly, the minimum number of vacua present in a model of the type (4.10) is sought while ensuring its physical meaning on the torus. This number is two and it can be found for example when $n_1 = 1$ and $n_2 = \frac{1}{2}$. For this choice of n_1 and n_2, four topological clusters arise, which will be non-empty. By the distribution of Φ_K-kinks described in (4.13), this combination of values of n_1 and n_2 should lead to a scenario where brochosons could emerge. Indeed, in this case these loops will only contain one vacuum point.

In all these scenarios the singular kinks that arise are identified and their linear stability analysed. Additionally, the orbit equation in each case will produce a family of kinks, each exhibiting significantly different behaviours.

4.2.1 Kink variety for a model with eight vacua

In this section the previously mentioned Case 1 will be thoroughly explored, which is defined by the specific values $n_1 = 1$ and $n_2 = 2$ in the general framework introduced in the previous section. The superpotential in this case is of the form

$$W_{1,2}(\theta, \varphi) = m(R + r\sin\theta)\sin 2\varphi\,. \tag{4.17}$$

The fact that the value $n_1 = 1$ has been chosen simplifies significantly the expression of the potential term, as one of the factors of the metric tensor is canceled out

$$V_{1,2}(\theta, \varphi) = \frac{m^2}{2}\left[\cos^2\theta \sin^2 2\varphi + 4\cos^2 2\varphi\right]\,. \tag{4.18}$$

The set of vacua $\mathcal{M}$ contains eight points symmetrically separated on the torus

$$\begin{aligned}\mathcal{M}_{1,2} = \big\{ & v^1 = \left(\tfrac{\pi}{2}, \tfrac{\pi}{4}\right); v^2 = \left(\tfrac{\pi}{2}, \tfrac{3\pi}{4}\right); v^3 = \left(\tfrac{\pi}{2}, \tfrac{5\pi}{4}\right); v^4 = \left(\tfrac{\pi}{2}, \tfrac{7\pi}{4}\right); \\ & v^5 = \left(\tfrac{3\pi}{2}, \tfrac{\pi}{4}\right); v^6 = \left(\tfrac{3\pi}{2}, \tfrac{3\pi}{4}\right); v^7 = \left(\tfrac{3\pi}{2}, \tfrac{5\pi}{4}\right); v^8 = \left(\tfrac{3\pi}{2}, \tfrac{7\pi}{4}\right)\big\}\,,\end{aligned}$$

whose distribution in the target space $\mathbb{S}^1 \times \mathbb{S}^1$ can be seen in Figure 4.3. The fluctuation operator associated to these constant solutions contain no negative eigenvalue

$$\mathcal{H}[v^1, v^2, v^3, v^4] = \begin{pmatrix} \frac{m^2}{r^2} & 0 \\ 0 & \frac{16m^2}{(R+r)^2} \end{pmatrix}\,, \qquad \mathcal{H}[v^5, v^6, v^7, v^8] = \begin{pmatrix} \frac{m^2}{r^2} & 0 \\ 0 & \frac{16m^2}{(R-r)^2} \end{pmatrix}\,,$$

as it is expected of the minima of the potential (4.18). Notice that potential $V_{1,2}(\theta, \varphi)$ involves the angular symmetries $\theta \to \theta + \pi$ and $\varphi \to \varphi + \frac{\pi}{2}$, leaving this potential invariant. These two discrete translations generate the symmetry group of the action $G = \mathbb{Z}_2 \otimes \mathbb{Z}_4$. This implies that the torus can be divided into eight regions where the structure of the kink variety is the same. Kinks defined in one of these regions can be identified with other kinks in other regions by applying the previously shown symmetries. Given this replication, in this model the kink variety will include eight singular topological kinks and antikinks. Furthermore, the family of kinks that will emerge from the orbit equation will also be replicated in all previously mentioned equivalent regions. Let us discuss in more detail these solutions:

• **Φ-kinks**: These singular kinks can be identified from the general expression (4.13). In particular, these solutions will connect different vacua depending on the values $k_1 = 0, 1$ and $k_2 = 0, 1, 2, 3$

$$\Phi_K^{(k_1,k_2)}(x) = \left(\frac{2k_1+1}{2}\pi \ , \ \frac{k_2+1}{2}\pi + \frac{1}{2}\,\mathrm{Gd}\left[(-1)^{a+k_2+1} \frac{4m\bar{x}}{R+(-1)^{k_1} r} \right] \right) . \quad (4.19)$$

The first component clearly reveals that $\Phi_K^{[0]}$-kinks and $\Phi_K^{[1]}$-kinks belong to different topological sectors, see Figure 4.3. While $[k_1]$ distinguishes between "outer" and "inner" circumferences on the torus, different values of k_2 mod 4 discriminate between pieces of these circumferences. Explicitly, these kinks connect the vacuum point v^i to vacua $v^{[i+1]_4}$ and $v^{[i-1]_4}$ and vacuum point v^{i+4} to vacua $v^{[i+1]_4+4}$ and $v^{[i-1]_4+4}$ where $i = 1, 2, 3, 4$, and $[\cdot]_4$ stands for module 4. The kink energy densities are all localised around a point describing a single lump, even though their total energies are different. From the previous section, the following relations hold

$$E[\Phi_K^{[0]}] = 2m(R+r)\,, \qquad E[\Phi_K^{[1]}] = 2m(R-r)\,.$$

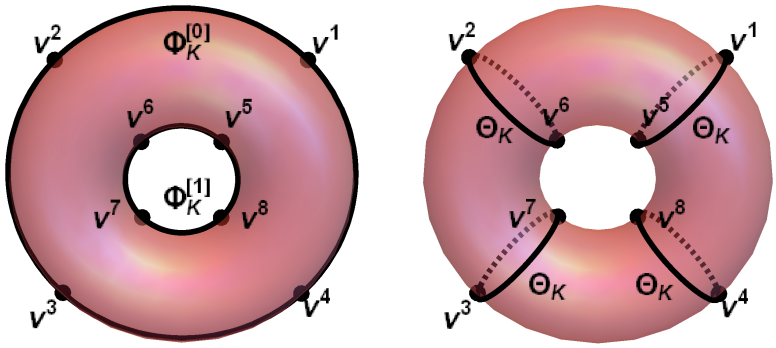

Figure 4.3: Orbits of $\Phi_K^{[0]}$ and $\Phi_K^{[1]}$−kinks (left) and those of Θ−kinks (right). Dotted lines represent curves on the hidden side of the torus. Notice how Φ_K and Θ−kink orbits split the torus into eight regions, which are equivalent by symmetry.

On the other hand, given the explicit expressions of these singular kinks, a study of the linear stability can be performed. For the Φ-kinks the Hessian operator (4.8) leads to the spectral problem

$$\mathcal{H}[\Phi_K^{[k_1]}(x)]\,\Psi_n(z) = \frac{\left(R+(-1)^{k_1}r\right)^2}{16m^2}\,\omega_n^2\,\Psi_n(z)\,, \qquad k_1 = 0, 1\,, \quad (4.20)$$

where the non-null components of the second order small kink fluctuation $\mathcal{H}[\Phi_K^{[k_1]}(x)]$ read as

$$\begin{aligned} \mathcal{H}_{11}[\Phi_K^{[k_1]}(x)] &= -\frac{d^2}{dz^2} + \frac{\left(R+(-1)^{k_1}r\right)^2}{16r^2}\left(1 - \frac{R+(-1)^{k_1}5r}{R+(-1)^{k_1}r}\,\mathrm{sech}^2 z\right)\,, \\ \mathcal{H}_{22}[\Phi_K^{[k_1]}(x)] &= -\frac{d^2}{dz^2} + \left(1 - 2\,\mathrm{sech}^2 z\right)\,. \end{aligned}$$

Notice that these expressions read the same for any kink orbit with different k_2. This was expected given the present symmetries and the distribution of these Φ−kinks.

This spectral problem arises from the general form (4.8) after a change in the space variable

$$z = \frac{4m\,\overline{x}}{R + (-1)^{k_1} r}\,.$$

The spectral problem (4.20) reduces to two one-dimensional problems associated with Schrödinger type differential operators with two different Pösch-Teller potential wells. Fortunately, these spectral equations are exactly solvable:

- Spectrum of $\mathcal{H}_{22}[\Phi_K^{[k_1]}(x)]$: The discrete spectrum of the operator $\mathcal{H}_{22}[\Phi_K^{[k_1]}(x)]$ consists only of a zero mode (whose eigenvalue is zero) and the continuous spectrum emerges on the threshold value 1.

- Spectrum of $\mathcal{H}_{11}[\Phi_K^{[0]}(x)]$: The structure of the spectrum associated to the operator $\mathcal{H}_{11}[\Phi_K^{[k_1]}(x)]$ is more complex. For the case $k_1 = 0$, the operator $\mathcal{H}_{11}[\Phi_K^{[0]}(x)]$ has the discrete spectrum $\omega_n^2 = \frac{n}{2}(\frac{R}{r}+1) - n^2$ for non-negative integers that satisfy $n < \frac{1}{4}\left(\frac{R}{r}+1\right)$. Hence, $\lceil \frac{1}{4}\left(\frac{R}{r}+1\right)\rceil$ discrete states appear, where $\lceil x \rceil \equiv \min\{n \in \mathbb{Z} \mid n \geq x\}$ stands for x if $x \in \mathbb{Z}$ or the immediate integer value above otherwise. Therefore, the number of discrete states grows as the ratio between the major and minor radii increases. The lowest of these modes is a zero mode, that is, the lowest eigenvalue of $\mathcal{H}_{11}[\Phi_K^{[0]}(x)]$ is zero. The continuous spectrum emerges on the threshold value $\frac{1}{16}(\frac{R}{r}+1)^2$.

- Spectrum of $\mathcal{H}_{11}[\Phi_K^{[1]}(x)]$: For the case $k_1 = 1$, the operator $\mathcal{H}_{11}[\Phi_K^{[1]}(x)]$ has a discrete spectrum $\omega_n^2 = \frac{n+1}{2}(\frac{R}{r} - 3 - 2n)$ for non-negative integers that satisfy $n < \frac{1}{4}\left(\frac{R}{r} - 5\right)$ and a continuous spectrum rising at the value $\frac{1}{16}(\frac{R}{r}-1)^2$. Notice that it only exhibits discrete spectrum if $\frac{R}{r} > 5$, in particular $\lceil \frac{1}{4}\left(\frac{R}{r} - 5\right)\rceil$ discrete states.

In conclusion, the operator $\mathcal{H}[\Phi_K^{[k_1]}(x)]$ has no negative eigenvalues and therefore $\Phi_K(x)$-kinks are linearly stable. In addition, the $\Phi_K^{[0]}(x)-$kink has two zero modes. One of them is associated with a translational symmetry but the other one suggests the existence of a kink family in the same topological cluster. This possibility is investigated below.

• **Θ-kinks**: Trial orbits with constant coordinate φ produce in the first order equations (4.11) of the current model four topological kinks together with their antikinks

$$\Theta_K^{(k_1,k_2)}(x) = \left((k_1+1)\pi + \mathrm{Gd}\left[(-1)^{a+k_1+k_2+1}\frac{m\bar{x}}{r}\right]\ ,\ \frac{2k_2+1}{4}\pi\right)\,, \tag{4.21}$$

where $k_1 = 0, 1$ and $k_2 = 0, 1, 2, 3$. Kink orbits correspond to circular arcs associated to the minor radius of the torus. Given that two vacua are present in each circumference, eight topological kinks and anti-kinks will link "exterior" and "interior" vacuum points, see Figure 4.3. While k_1 mod 2 distinguishes between the visible and hidden side of the torus in the picture, k_2 mod 4 differentiates between circumferences. Vacua v^i will be doubly connected to $v^{[i+4]_8}$ with $i = 1, \ldots, 8$, where $[\cdot]_8$ stands now for module 8. As it has been shown, the energy of all the $\Theta_K(x)$-kinks is identical

$$E[\Theta_K] = 2mr\,.$$

In this case, the analysis of the linear stability for the Θ-kinks leads to the spectral problem

$$\mathcal{H}[\Theta_K(x)]\,\Psi_n(z) = \frac{r^2}{m^2}\,\omega_n^2\,\Psi_n(z)\,, \tag{4.22}$$

where the non-null components of the second order small kink fluctuation $\mathcal{H}[\Theta_K(x)]$ read more complicated now

$$\begin{aligned}
\mathcal{H}_{11}[\Theta_K(x)] &= -\frac{d^2}{dz^2} + \left(1 - 2\,\mathrm{sech}^2 z\right)\,, \\
\mathcal{H}_{22}[\Theta_K(x)] &= -\frac{d^2}{dz^2} - \frac{2r\,\mathrm{sech}^2 z}{R + r\tanh z}\frac{d}{dz} + \frac{4r^2\left(4 - \mathrm{sech}^2 z\right)}{\left(R + r\tanh z\right)^2}
\end{aligned}$$

and where the change of variable $z = (-1)^{a+k_2}\frac{m\bar{x}}{r}$ has been employed. Once again, the spectral problem (4.22) reduces to two independent one-dimensional problems associated with the diagonal components of $\mathcal{H}[\Theta_K(x)]$. The first component $\mathcal{H}_{11}[\Theta_K(x)]$ involves the presence of a zero mode and a continuous spectrum arising at the threshold value 1. On the other hand, the analysis of the spectrum for the second component $\mathcal{H}_{22}[\Theta_K(x)]$ is notably more intricate. Since it is not analytically solvable, numerical methods have been used to extract the spectral information of this operator. No negative eigenvalues of ω^2 are found and therefore $\Theta_K(x)-$kinks are linearly stable.

• **Families of kinks**: As previously stated, the fact that the $\Phi_K^{[0]}(x)$-kinks have a second zero mode suggests that these kinks are limit members of a family of kinks. If this family exists, it must be identified by solving the orbit equation (4.12) for the values of parameters n_1 and n_2 that have been chosen in this case. Members of this family shall be denoted as $\Sigma_K^{(k_1,k_2)}(x;\gamma)$, where γ is employed to label every kink member. In this case, the kink orbits can be obtained by solving the orbit flow equation

$$\frac{d\theta}{d\varphi} = \frac{\cos\theta(R + r\sin\theta)\tan(2\varphi)}{2r}\,, \tag{4.23}$$

derived as mentioned from the general equation (4.12). Their analytical expression is given by

$$|\cos 2\varphi| = \frac{1}{\gamma}\frac{\left|1 - \sin\theta\right|^{\frac{2r}{(R+r)}}\cdot\left|R + r\sin\theta\right|^{\frac{4r^2}{R^2-r^2}}}{|1 + \sin\theta|^{\frac{2r}{(R-r)}}}\,, \tag{4.24}$$

where the parameter $\gamma \in (0,\infty)$ is constant. All these kinks connect any "outer" vacuum point to the two adjacent outer vacua. This is, vacuum point v^i is linked to vacua $v^{[i+1]_4}$ and $v^{[i-1]_4}$ where $i = 1,2,3,4$. The energy of all members of these families is the same $E\left[\Sigma_K\right] = 2m(R + r)$. In Figure 4.4 several kinks belonging to this family have been depicted on the torus and on the $\theta - \varphi-$plane.

As it was implied, singular kinks are recovered as certain limits of this family. The limit $\gamma \to 0$ demands $\theta = \frac{\pi}{2}$, letting φ vary freely between the outer vacua, which precisely defines the $\Phi_K^{[0]}(x)$-kink orbits. On the other hand, when $\gamma \to \infty$ two possible solutions of (4.24) arise. One of the possibilities is that φ takes one of the values $\varphi = \frac{\pi}{4}, \frac{3\pi}{4}, \frac{5\pi}{4}, \frac{7\pi}{4}$ whereas the variable θ is free to vary with x. This description leads to the $\Theta_K(x)$-kinks. The second possibility corresponds to the condition $\theta = \frac{3\pi}{2}$, which annihilates the denominator in equation (4.24). This takes

us to the indeterminate form $\frac{\infty}{\infty}$, letting φ vary with x. This is the $\Phi_K^{[1]}(x)$-kink orbit. Symbolically, these limit cases can be written as follows

$$\lim_{\gamma\to 0}\Sigma_K^{(k_1,k_2)}(x;\gamma)\equiv\Phi_K^{[0]}(x)\,,\qquad \lim_{\gamma\to\infty}\Sigma_K^{(k_1,k_2)}(x;\gamma)\equiv\Theta_K(x)\cup\Phi_K^{[1]}(x)\cup\Theta_K(x)\,. \tag{4.25}$$

Note that these limits comply with the previously found energy sum rule for singular kinks (4.16)

$$E[\Sigma_K]=E[\Phi_K^{[0]}] \;=\; E[\Phi_K^{[1]}] \;+\; 2E[\Theta_K]\,.$$

In sum, a family of topological kinks is replicated on the eight regions of the torus. Limits of this family coincide with the previously identified singular kinks, which delimit these eight regions. Lastly, while the linear stability of the singular kinks have been shown, this study has not been performed for members of the family of kinks. Indeed, the emerging spectral problems prove too intricate to solve. Nevertheless, the absence of intermediate points in these kinks where the flow is undefined indicates that there exist no other conjugate points where the kink orbits intersect. This fact ensures, according to the Morse index theorem, that all these kinks are stable, see [14].

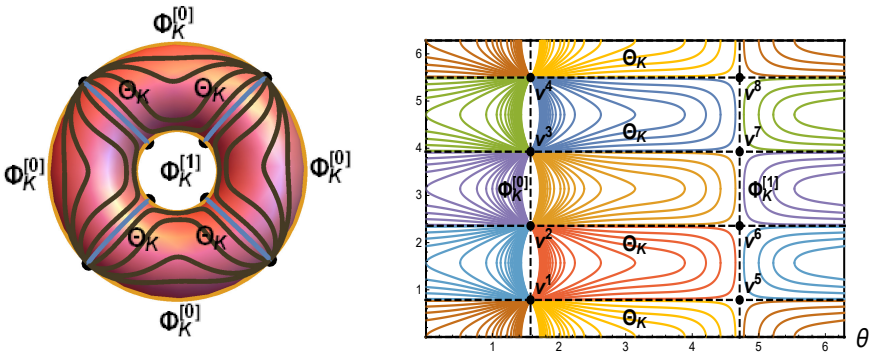

Figure 4.4: Several orbits of the family $\Sigma_K^{(k_1,k_2)}(x;\gamma)$ have been depicted on the torus and on the $\theta-\varphi-$plane. Orbits on the hidden side have been omitted in the first picture. Note in both representations how singular kinks are recovered as limits of this family according to (4.25).

4.2.2 Kink variety for a model with four vacua

In this section Case 2 will be explored, where parameters $n_1 = n_2 = 1$ are chosen to fix the number of vacua of the model to four. This choice of n_i leads us to a superpotential which is once more $2\pi-$periodic in both angles

$$W_{1,1}(\theta,\varphi)=m(R+r\sin\theta)\sin\varphi\,, \tag{4.26}$$

whereas the potential term is $\pi-$periodic and is expressed as

$$V_{1,1}(\theta,\varphi)=\frac{m^2}{2}\left[\cos^2\theta\sin^2\varphi+\cos^2\varphi\right]\,. \tag{4.27}$$

Indeed, the set of vacua $\mathcal{M}$ consists now of only four points

$$\mathcal{M}_{1,1} \;=\; \{v^1=(\tfrac{\pi}{2},\tfrac{\pi}{2});v^2=(\tfrac{3\pi}{2},\tfrac{\pi}{2});v^3=(\tfrac{3\pi}{2},\tfrac{3\pi}{2});v^4=(\tfrac{\pi}{2},\tfrac{3\pi}{2})\}\,,$$

whose distribution in the target space $\mathbb{S}^1 \times \mathbb{S}^1$ can be seen in Figure 4.9. Similarly to Case 1, the fact that these points are minima of the potential (4.27) is manifested in the fluctuation operator associated to these points, which are given by

$$\mathcal{H}[v^1, v^4] = \begin{pmatrix} \frac{m^2}{r^2} & 0 \\ 0 & \frac{m^2}{(R+r)^2} \end{pmatrix}, \qquad \mathcal{H}[v^2, v^3] = \begin{pmatrix} \frac{m^2}{r^2} & 0 \\ 0 & \frac{m^2}{(R-r)^2} \end{pmatrix}.$$

As expected, reducing the number of vacua also affects the symmetries of the new potential (4.27). π-translations in now both angles, $\theta \to \theta + \pi$ and $\varphi \to \varphi + \pi$, leave invariant $V_{1,1}(\theta, \varphi)$. These generate the symmetry group of the action $G = \mathbb{Z}_2 \otimes \mathbb{Z}_2$, which implies that in this case the torus can be divided into four regions with identical kink variety. The singular kinks and the emerging family of kinks arising in the kink variety of this model will be examined separately.

• **Φ-kinks**: In this case these singular kinks will connect v^1 to v^4 or v^3 to v^2 depending on the value $k_1 = 0, 1$

$$\Phi_K^{k_1}(x) = \left(\frac{2k_1 + 1}{2} \,,\; (k_2 + 1)\pi + (-1)^{a+k_2+1} \mathrm{Gd}\left[\frac{m\bar{x}}{R + (-1)^{k_1} r} \right] \right), \tag{4.28}$$

where different values of $k_2 = 0, 1$ shift solutions in the $\theta - \varphi-$plane. This means that $\Phi_K^{[0]}$-kinks and $\Phi_K^{[1]}$-kinks also belong to different topological sectors in this case, see Figure 4.9. Note that while k_1 discriminate between the outer and inner arcs, k_2 distinguishes between the two pieces of the circumferences. The kink energy densities are localised describing a single lump, with energies

$$E[\Phi_K^{[0]}] = 2m(R + r)\,, \qquad E[\Phi_K^{[1]}] = 2m(R - r)\,.$$

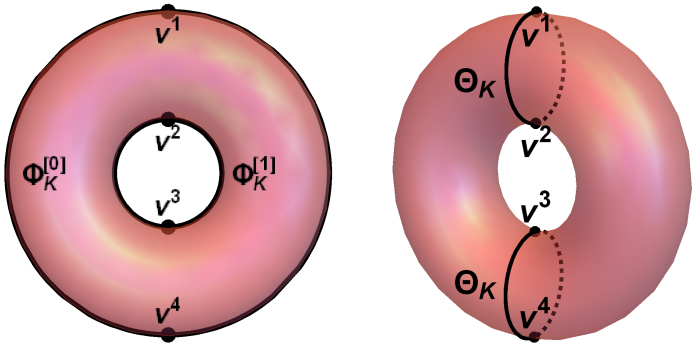

Figure 4.5: Orbits of $\Phi_K^{[0]}$ and $\Phi_K^{[1]}-$kinks (left) and those of $\Theta-$kinks (right). Dotted lines represent curves on the hidden side of the torus. Notice how Φ_K and $\Theta-$kink orbits split the torus into four regions, which are equivalent by symmetry.

The linear stability under small perturbations of the Φ-kinks can be analytically analysed. Similarly to Case 1, the spectral problem matches that of the general form (4.8) when the following space variable change is used

$$z = \frac{m\,\overline{x}}{R + (-1)^{k_1} r}\,.$$

Indeed, this change leads to the following spectral problem

$$\mathcal{H}[\Phi_K^{[k_1]}(x)]\,\Psi_n(z) = \frac{[R+(-1)^{k_1}r]^2}{m^2}\,\omega_n^2\,\Psi_n(z)\,, \qquad k_1 = 0,1\,, \tag{4.29}$$

where the non-null components of this operator $\mathcal{H}[\Phi_K^{[k_1]}(x)]$ have the form

$$\begin{aligned}
\mathcal{H}_{11}[\Phi_K^{[k_1]}(x)] &= -\frac{d^2}{dz^2} + \frac{(R+(-1)^{k_1}r)^2}{r^2} - \frac{(R+(-1)^{k_1}2r)(R+(-1)^{k_1}r)}{r^2}\,\mathrm{sech}^2 z\,,\\
\mathcal{H}_{22}[\Phi_K^{[k_1]}(x)] &= -\frac{d^2}{dz^2} + 1 - 2\,\mathrm{sech}^2 z\,.
\end{aligned}$$

The study of the two arising one-dimensional spectral problems is summerised as follows:

- Spectrum of $\mathcal{H}_{22}[\Phi_K^{[k_1]}(x)]$: Exactly as in the previous case with eight vacua, the discrete spectrum of the operator $\mathcal{H}_{22}[\Phi_K^{[k_1]}(x)]$ contains exclusively a zero mode and the continuous spectrum threshold appears at 1.

- Spectrum of $\mathcal{H}_{11}[\Phi_K^{[0]}(x)]$: Similarly, two cases for $\mathcal{H}_{11}[\Phi_K^{[k]}(x)]$ are considered depending at the value of $[k_1]$. For the case $k_1 = 0$, $\lceil(1+\frac{R}{r})\rceil$ discrete states are found, since the operator $\mathcal{H}_{11}[\Phi_K^{[0]}(x)]$ has a discrete spectrum $\omega_n^2 = 2n\left(\frac{R}{r}+1\right) - n^2$ for non-negative integers that satisfy $n < \frac{R}{r}+1$. Again, amongst these states a zero mode is found. The continuous spectrum threshold is now at the value $(1+\frac{R}{r})^2$.

- Spectrum of $\mathcal{H}_{11}[\Phi_K^{[1]}(x)]$: For the case $k_1 = 1$, the discrete spectrum $\omega_n^2 = (n+1)(\frac{2R}{r} - 3 - n)$ emerges only when $\frac{R}{r} > 2$ and for non-negative integers that satisfy $n < \frac{R}{r} + 2$. $\lceil\frac{R}{r} - 2\rceil$ states arise until the continuous spectrum at the value $(\frac{R}{r} - 1)^2$ is reached. Notice that the number of discrete states is again proportional to the ratio $\frac{R}{r}$ in all cases.

Once more, no negative value of ω_n^2 is found and therefore these kinks are linearly stable. The second zero mode suggests again the existence of a family of kinks, possibility that will be again explored below.

• **Θ-kinks**: Four topological kinks together with their antikinks are found when the φ-constant condition is imposed in the first order equations (4.11)

$$\Theta_K^{(k_1,k_2)}(x) = \left((k_1+1)\pi + (-1)^{a+k_2+1}\mathrm{Gd}\left[\frac{m\bar{x}}{r}\right]\,,\ \frac{\pi}{2} + k_2\pi\right)\,, \tag{4.30}$$

with $k_1, k_2 = 0, 1$. These kink orbits correspond to circular arcs associated with the minor radius, see Figure 4.9. These topological kinks and anti-kinks will link v^1 to v^2 and v^3 to v^4. Note that the $\Theta^{(k_1,0)}$-kinks asymptotically connect the vacua v^1 and v^2 whereas the $\Theta^{(k_1,1)}$-kinks join the points v^3 and v^4. On the other hand, the $\Theta^{(0,0)}$-kinks and $\Theta^{(1,0)}$-kinks are related by the Cartesian coordinate transformation $\phi_2 \leftrightarrow -\phi_2$. In sum, label k_2 distinguishes between the upper and lower circumference while k_1 differentiates between the kinks on one side of the torus and the kinks on the opposite side. Once again, the energy of all the $\Theta_K(x)$-kinks is identical:

$$E[\Theta_K] = 2mr\,.$$

The second order small kink fluctuation operator for the Θ-kinks leads to the spectral problem

$$\mathcal{H}[\Theta_K(x)]\,\Psi_n(z) = \frac{r^2}{m^2}\,\omega_n^2\,\Psi_n(z)\,. \tag{4.31}$$

The non-null components that must be analysed to determine the linear stability of these kinks are again those of the diagonal

$$\begin{aligned}
\mathcal{H}_{11}[\Theta_K(x)] &= -\frac{d^2}{dz^2} + 1 - 2\,\mathrm{sech}^2 z\,,\\
\mathcal{H}_{22}[\Theta_K(x)] &= -\frac{d^2}{dz^2} - \frac{2\,r\,\mathrm{sech}\,z}{R\cosh z + r\sinh z}\frac{d}{dz} + \frac{r^2\sinh^2 z}{(R\cosh z + r\sinh z)^2}\,,
\end{aligned}$$

where the variable change $z = \frac{m\bar{x}}{r}$ has been performed in the original spectral problem (4.8). Again, the spectral problem (4.31) reduces to two independent one-dimensional problems associated with the diagonal components of $\mathcal{H}[\Theta_K(x)]$. The first component $\mathcal{H}_{11}[\Theta_K(x)]$ involves the presence of a zero mode and a continuous spectrum arising at the threshold value 1. Exactly like the previous case with eight vacua, the analysis of the spectral problem for $\mathcal{H}_{22}[\Theta_K(x)]$ will be numeric since it is not analytically solvable. Numerical methods reveal the absence of negative eigenvalues of ω^2, which implies the linear stability of these kinks.

• **Kink families**: As in the previous section, the existence of a second zero mode for $\Phi_K^{[0]}(x)$-kinks prompts us to search for families of kinks in the four previously mentioned equivalent regions of the torus. These families of kink orbits $\Sigma_K^{(k_1,k_2)}(x;\gamma)$ are obtained by solving the orbit flow equation

$$\frac{d\theta}{d\varphi} = \frac{\cos\theta(R + r\sin\theta)\tan(\varphi)}{r}\,, \tag{4.32}$$

derived again from the general equation (4.12). Their analytical expression is

$$|\cos\varphi| = \frac{1}{\gamma}\frac{\left|1-\sin\theta\right|^{\frac{r}{2(R+r)}}\cdot\left|R+r\sin\theta\right|^{\frac{r^2}{R^2-r^2}}}{\left|1+\sin\theta\right|^{\frac{r}{2(R-r)}}}\,, \tag{4.33}$$

where $\gamma \in (0,\infty)$ is constant. All these kinks asymptotically connect the vacua v^1 and v^4 as shown in Figure 4.6. The energy of all members of these families is the same $E[\Sigma_K] = 2m(R+r)$. The asymptotic analysis of the kink orbits carried out in the previous section is valid in this case almost unaltered. The limit $\gamma \to 0$ corresponds to $\Phi_K^{[0]}(x)$-kink orbits and $\gamma \to \infty$ to a combination of $\Theta_K(x)$-kinks and $\Phi_K^{[1]}(x)$-kinks. These limits coincide formally with those of the previous case. However, the distribution and number of kinks connecting vacua is different. In that sense, the same symbolic limits hold

$$\lim_{\gamma\to 0}\Sigma_K^{(k_1,k_2)}(x;\gamma) \equiv \Phi_K^{[0]}(x)\,, \qquad \lim_{\gamma\to\infty}\Sigma_K^{(k_1,k_2)}(x;\gamma) \equiv \Theta_K(x)\cup\Phi_K^{[1]}(x)\cup\Theta_K(x)\,, \tag{4.34}$$

which is again consistent with the energy sum rule $E[\Sigma_K] = E[\Phi_K^{[0]}] = E[\Phi_K^{[1]}] + 2E[\Theta_K]$. Same analysis as in the previous model reveals the stability of these kinks due to the absence of intermediate conjugate points along these curves.

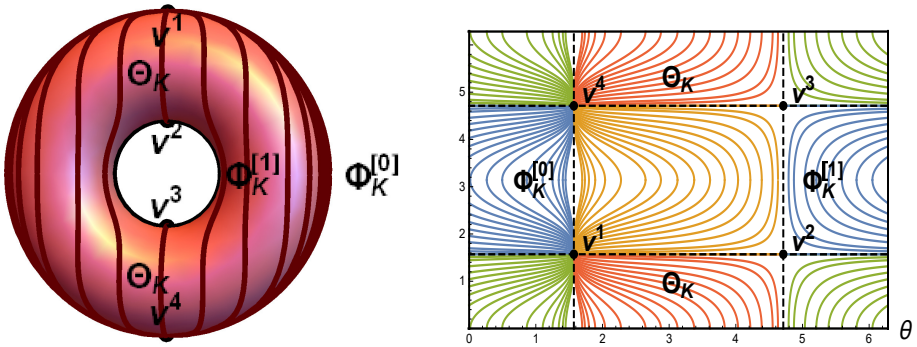

Figure 4.6: Several orbits of the family $\Sigma_K^{(k_1,k_2)}(x;\gamma)$ have been depicted on the torus and on the $\theta-\varphi-$plane. Orbits on the hidden side have been omitted in the first picture. Note in both representations how singular kinks are recovered as limits of this family according to (4.34).

4.2.3 Kink variety for a model with two vacua

In Case 2 the number of vacua had been reduced, but no non-topological kinks were found. Circumferences around the torus passing through vacua consist of two singular kinks. One method for searching for non-topological kinks within this family of potentials is making sure that some of these circumferences contain only one vacuum point. This can be achieved by making an appropriate choice of values for n_1 and n_2. Indeed, the number of vacua $|4n_1n_2|$ is minimised when $|n_1| = 1$ and $|n_2| = \frac{1}{2}$, resulting in a total of two vacua. This is precisely the aim of Case 3, where the kink variety for models whose potential is given by the general expression (4.10) with $n_1 = 1$ and $n_2 = \frac{1}{2}$ shall be studied. This choice of n_i produces the following potential on the torus

$$V_{1,\frac{1}{2}}(\theta,\varphi) = \frac{m^2}{2}\left[\frac{1}{4}\cos^2\left(\frac{\varphi}{2}\right) + \cos^2\theta\sin^2\left(\frac{\varphi}{2}\right)\right], \tag{4.35}$$

which can be derived from a superpotential

$$W_{1,\frac{1}{2}}(\theta,\varphi) = m(R + r\sin\theta)\sin\left(\frac{\varphi}{2}\right) \tag{4.36}$$

which is not periodic on the torus. This fact is precisely what will allow the existence of BPS non-topological kinks. The new set of vacua $\mathcal{M}$ contains only two vacuum points

$$\mathcal{M}_{1,\frac{1}{2}} = \left\{v^1 = \left(\frac{\pi}{2},\pi\right)\ ,\ v^2 = \left(\frac{3\pi}{2},\pi\right)\right\},$$

as it can be observed in Figure 4.7. Moreover, the vacuum fluctuation operator is

$$\mathcal{H}[v^1] = \begin{pmatrix} \frac{m^2}{r^2} & 0 \\ 0 & \frac{m^2}{16(R+r)^2} \end{pmatrix}, \qquad \mathcal{H}[v^2] = \begin{pmatrix} \frac{m^2}{r^2} & 0 \\ 0 & \frac{m^2}{16(R-r)^2} \end{pmatrix}.$$

By further reducing the number of vacua, one of the symmetries that was present in previous cases has been removed. Only the angular symmetry $\theta \to \theta + \pi$ remains, which generates the symmetry group of the action $G = \mathbb{Z}_2$. Therefore, two equivalent regions where the structure of the kink variety is the same will emerge. More specifically, such a kink variety will include two singular non-topological kinks,

two singular topological kinks and a family of non-topological kinks. A thorough description of these kinks is as follows:

• **Φ-kinks**: Finally, non-topological singular kinks are found from the general expression (4.13). In fact, not one but two types of non-topological kinks appear depending on the value $[k_1]$

$$\Phi_K^{[k_1]}(x) = \left(\frac{\pi}{2} + k_1\pi \ , \ 2\pi + (-1)^{a+1} \ 2 \ \text{Gd} \left[\frac{m\overline{x}}{(R + (-1)^{k_1} r)} \right] \right) . \tag{4.37}$$

Indeed, this expression characterises singular non-topological kinks and their antikinks, which asymptotically connect the vacua v^1 and v^2 with themselves, see Figure 4.7.

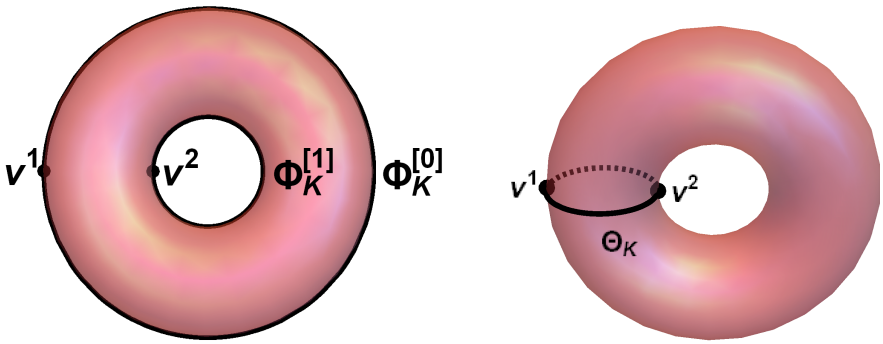

Figure 4.7: Orbits of $\Phi_K^{[0]}$ and $\Phi_K^{[1]}-$kinks (left) and those of $\Theta-$kinks (right). Dotted lines represent curves on the hidden side of the torus. Notice how Φ_K and $\Theta-$kink orbits split the torus into two regions, which are equivalent by symmetry.

Unlike in previous cases, the splitting of these circumferences into more than one solution disappears since $2(k_2 + 1)\pi$ can only take one value in $[0, 2\pi)$ for integers k_2. Notice that these kinks have been progressively absorbing adjacent kinks in all these three cases until only one remains. Naturally, only one can emerge now in each circumference since these cross only one vacuum point. The discussion of the energy is no different from the previous cases, the total energy of these solutions is given by

$$E[\Phi_K^{[k_1]}] = 2m(R + (-1)^{k_1} \ r) \, .$$

The analysis of the linear stability for the $\Phi_K^{[k_1]}(x)$-kinks for this case is analogous to previous $\Phi_K^{[k_1]}(x)$-kinks. The spectral problem reads almost identical

$$\mathcal{H}[\Phi_K^{[k_1]}(x)] \ \Psi_n(z) = \frac{16[R + (-1)^{k_1} \ r]^2}{m^2} \, \omega_n^2 \ \Psi_n(z) \, , \qquad k_1 = 0, 1 \, , \tag{4.38}$$

where once again only diagonal components of the operator $\mathcal{H}[\Phi_K^{[k_1]}(x)]$ do not vanish

$$\begin{aligned} \mathcal{H}_{11}[\Phi_K^{[k_1]}(x)] &= -\frac{d^2}{dz^2} + \frac{16(R + (-1)^{k_1} \ r)^2}{r^2} \left[1 - \frac{(4R + (-1)^{k_1} \ 5r)}{4(R + (-1)^{k_1} \ r)} \text{sech}^2 z \right] , \\ \mathcal{H}_{22}[\Phi_K^{[0]}(x)] &= -\frac{d^2}{dz^2} + \left(1 - 2 \ \text{sech}^2 z \right) \end{aligned}$$

and the change of variable $z = \frac{m\bar{x}}{4(R+(-1)^{k_1} \ r)}$ has been included in (4.8). The study of their stability is summarised in the following points:

- Spectrum of $\mathcal{H}_{22}[\Phi_K^{[k_1]}(x)]$: As before, a zero mode is all the discrete spectrum of $\mathcal{H}_{22}[\Phi_K^{[k_1]}(x)]$ consists of and the continuous spectrum starts at 1.

- Spectrum of $\mathcal{H}_{11}[\Phi_K^{[0]}(x)]$: On one hand, the operator $\mathcal{H}_{11}[\Phi_K^{[0]}(x)]$ has now a discrete spectrum $\omega_n^2 = 8n\left(\frac{R}{r}+1\right) - n^2$ for non-negative integers that satisfy $n < 4\left(\frac{R}{r}+1\right)$. $\lceil 4\left(\frac{R}{r}+1\right)\rceil$ discrete states appear before the continuous spectrum emerges at the threshold value $16\left(1+\frac{R}{r}\right)^2$.

- Spectrum of $\mathcal{H}_{11}[\Phi_K^{[1]}(x)]$: On the other hand, for $\mathcal{H}_{11}[\Phi_K^{[1]}(x)]$ the discrete spectrum $\omega_n^2 = (n+1)\left(\frac{8R}{r} - 9 + n\right)$ is found only when $\frac{R}{r} > \frac{5}{4}$ and for non-negative integers that satisfy $n < \frac{4R}{r} - 5$. $\lceil \frac{4R}{r} - 5\rceil$ discrete states are found before the continuous threshold appears at $16(\frac{R}{r}-5)^2$ in this case.

Same argument as in the previous cases guarantees the linear stability of these kinks. Moreover, the homotopy of curves on the torus prevents these solutions from decaying into vacuum, regardless of the perturbation. This is, brochosons are finally found on the torus.

• **Θ-kinks**: The other circumference that crosses vacua in this model contains two vacua. This corresponds to singular solutions (4.15)

$$\Theta_K^{(k_1)}(x) = \left((k_1+1)\,\pi + (-1)^{a+k_1+k_2+1}\mathrm{Gd}\left[\frac{m\bar{x}}{2r}\right]\ ,\ \pi\right)\,,$$

which describe a pair of topological kinks and their antikinks asymptotically connecting the two vacua v^1 and v^2. The two values of $[k_1]$ give rise to two different orbits, one in each side of the torus, see Figure 4.7. As stated before, the total energy of these kinks is

$$E[\Theta_K] = 2mr\,.$$

Similarly, the spectral problem that must be analysed in this case has the form

$$\mathcal{H}[\Theta_K(x)]\,\Psi_n(z) = \frac{r^2}{m^2}\,\omega_n^2\,\Psi_n(z)\,, \tag{4.39}$$

where the non-null components of the operator $\mathcal{H}[\Theta_K(x)]$ are diagonal

$$\begin{aligned}
\mathcal{H}_{11}[\Theta_K(x)] &= -\frac{d^2}{dz^2} + \left(1 - 2\,\mathrm{sech}^2 z\right)\,,\\
\mathcal{H}_{22}[\Theta_K(x)] &= -\frac{d^2}{dz^2} - \frac{2r\,\mathrm{sech}^2 z}{R + r\tanh z}\frac{d}{dz} + \frac{r^2(1-4\,\mathrm{sech}^2 z)}{16(R+r\tanh z)^2}
\end{aligned}$$

and the change of variable $z = \frac{m\bar{x}}{r}$ has been made in (4.8). Again, for $\mathcal{H}_{11}[\Theta_K(x)]$ a zero mode is found and the continuous spectrum emerges at the threshold value 1. Numerical analysis is once again necessary for the $\mathcal{H}_{22}[\Theta_K(x)]$ operator, for which no negative eigenvalue of ω^2 is found. This ensures the linear stability of $\Theta_K(x)-$kinks.

• **Families of kinks**: In Case 3 the orbit flow equation (4.12) is almost identical to those of previous cases

$$\frac{d\theta}{d\varphi} = \frac{2\,\cos\theta\,(R + r\sin\theta)\tan(\frac{\varphi}{2})}{r} \tag{4.40}$$

and can be integrated as well. The orbits for the resulting family of kinks are given by equation

$$\left|\cos\frac{\varphi}{2}\right| = \frac{1}{\gamma}\frac{\left|1-\sin\theta\right|^{\frac{r}{8(R+r)}}\cdot\left|R+r\sin\theta\right|^{\frac{r^2}{4(R^2-r^2)}}}{\left|1+\sin\theta\right|^{\frac{r}{8(R-r)}}}\,, \tag{4.41}$$

where $\gamma \in (0,\infty)$ is again a constant that labels different kink orbits. All these kinks depart from v^1 and return to the same vacuum point, see Figure 4.8. Therefore, this family, replicated in each side of the torus, is comprised of non-topological kinks. Moreover, all its members are brochosons, as these loops cannot be contracted to a vacuum point. The energy of all members of these families is the same $E\left[\Sigma_K\right] = 2m(R+r)$. When the parameter limit $\gamma \to 0$ is considered, the singular $\Phi_K^{[0]}(x)$-kink is recovered whereas the limit $\gamma \to \infty$ leads to the concatenation of three singular kinks following the general form $\Theta_K(x) \cup \Phi_K^{[1]}(x) \cup \Theta_K(x)$. These are the same symbolic limits that were found in previous sections (4.25), which are obviously compatible with the energy sum rule $E[\Sigma_K] = E[\Phi_K^{[0]}] = E[\Phi_K^{[1]}] + 2E[\Theta_K]$. Finally, the lack of intermediate conjugate points along the orbits implies the linear stability of these kinks. However, as stated, the stability of these kinks goes beyond linear stability, for these loops on the torus are not contractible to a point and hence these kinks are globally stable.

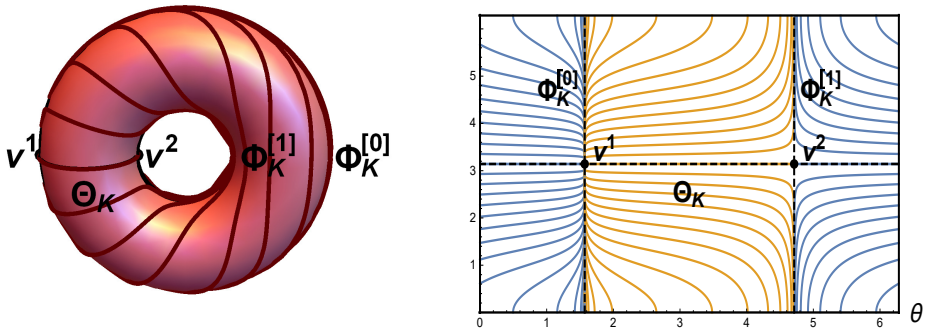

Figure 4.8: Several orbits of the family $\Sigma_K^{(k_1,k_2)}(x;\gamma)$ have been depicted on the torus and on the $\theta-\varphi-$plane. Orbits on the hidden side have been omitted in the first picture. Note in both representations how singular kinks are recovered as limits of this family.

4.3 A family of separable models with different vacuum manifold

In the first part of this chapter a family of non-linear $(\mathbb{S}^1\times\mathbb{S}^1)$-Sigma models is constructed and its kink variety identified for representative cases. Among its solutions, brochosons are found for the case of only two vacua. Indeed, non-contractible loops appear as solutions. However, that family of Sigma models does not include the scenario with only one vacuum point. This situation is extremely interesting since every kink in the model is forced to be non-topological. Therefore, further developing this line of research, another family of potentials for a non-linear $(\mathbb{S}^1\times\mathbb{S}^1)$-Sigma model is constructed. Hopefully, a similar rich kink variety for each member of this family can be analytically obtained, including now this missing case with only one

vacuum point. Furthermore, the potential of the family of Sigma models that shall be constructed in this second part of the chapter will be separable. Specifically, it will be constructed so that it allows us to analytically solve Bogomol'nyi equations instead of the orbit flow equation. This will have two main consequences. First, the identification of the explicit field profiles will enable us to derive the explicit energy density profiles. On the other hand, instead of just one family of kinks, two will emerge as a result of the two signs in Bogomol'nyi equations. In particular, this family of potentials will be of the form

$$V_{n_1,n_2}(\theta,\varphi) = \frac{1}{2}\Big[\frac{m_1^2 n_1^2}{r^2}\cos^2(n_1\theta) + \frac{m_2^2 n_2^2}{(R+r\sin(\theta))^2}\cos^2(n_2\varphi)\Big]\,, \tag{4.42}$$

where m_1, m_2 are positive real numbers and n_1 and n_2 are integers or half-integers so that these potential functions are periodic on the torus. This implies that the set of vacua $\mathcal{M}$ of each potential also contains a total of $|4n_1n_2|$ points distributed on the torus

$$\mathcal{M}_{n_1,n_2} = \Big\{\Sigma_{k_1,k_2} = (\theta_{k_2},\varphi_{k_1}) = \Big(\frac{\pi}{2n_1} + \frac{k_1\,\pi}{n_1}\,,\,\frac{\pi}{2n_2} + \frac{k_2\,\pi}{n_2}\Big) \quad | \quad k_i \in \mathbb{Z}\Big\}\,,$$

which is again exactly the same number of regions on the torus where the kink variety will be the identical. Notice that unlike the previous family of Sigma models, both n_1 and n_2 are allowed to be half integers. Indeed, these new potential functions are well-defined in these cases. Particular cases of potentials (4.42) with four, two and one vacua will be thoroughly explored, where the emergence of brochosons is expected. Once again, each member of this family of potential functions can derived (4.5) from a superpotential W. This leads to the following family of superpotentials

$$W_{n_1,n_2}(\theta,\varphi) = (-1)^{\epsilon_1} m_1 \sin(n_1\theta) + (-1)^{\epsilon_2} m_2 \sin(n_2\varphi)\,, \tag{4.43}$$

with $\epsilon_1, \epsilon_2 = 0, 1$. Indeed, since the potential is separable in these coordinates, the Bogomol'nyi arrangement for the potential family can be made by four superpotentials. Furthermore, this leads to Bogomol'nyi equations (4.6) where the poloidal coordinate θ is decoupled

$$\frac{d\theta}{dx} = (-1)^{\epsilon_1}\,\frac{m_1\,n_1}{r^2}\cos(n_1\theta)\,, \qquad \frac{d\varphi}{dx} = (-1)^{\epsilon_2}\,\frac{m_2\,n_2}{(R+r\sin\theta)^2}\cos(n_2\varphi)\,. \tag{4.44}$$

Notice that since W is a bounded differentiable function, the energy (4.7) of any solution of Bogomol'nyi equations is finite. It is worth noting that the potential functions (4.10) exhibit the symmetries $\varphi \to \varphi + \frac{k_2}{n_2}\pi$ for any $k_2 \in \mathbb{Z}$. As expected, these are also present in Bogomol'nyi equations. However, even though transformations $\theta \to \theta + \frac{k_1}{n_1}\pi$ with $k_1 \in \mathbb{Z}$ are not symmetries of the potentials, they allow us to identify solutions in different pairs of Bogomol'nyi equations. If (θ_s, φ_s) is a solution for a given choice of ϵ_1 and ϵ_2, then the following identification of solutions can be made

$$(\theta_s, \varphi_s, \epsilon_1, \epsilon_2) \longleftrightarrow \Big(\theta_s + \frac{k_2}{n_2}\pi, \varphi_s, (-1)^{k_1}\epsilon_1, \epsilon_2\Big) \tag{4.45}$$

That is, solutions that belong to different families of superpotentials will also be related. These two types of identifications combined, both in θ and in φ, will split the torus into $|4n_1n_2|$ regions where the kink variety will be replicated. In next section the solutions of Bogomol'nyi equations will be analytically calculated.

4.3.1 Singular kinks and families of energy degenerate kinks

Let us classify solutions of Bogomol'nyi equations according to the number of coordinates that remain constant. This leaves us with four types of solutions. The first one is comprised by constant solutions in both coordinates θ and φ. This is, solutions that correspond to the set of vacua that was presented in last section. The second and third types correspond to singular kinks, whose orbits will be constant in θ or in φ respectively. Lastly, the fourth one will contain families of solutions with neither θ nor φ constant. The same terminology used in the first part of the chapter to refer to these kinks will also be employed here.

- **Singular Φ-kinks**: The $|2n_1|$ *toroidal* trajectories defined by $\theta = \frac{\pi}{2n_1} + \frac{k_1}{n_1}\pi$ that cross at least one minimum will be referred to as Φ-kink orbits. First order equations (4.44) with this condition explicitly provide these solutions $\Phi_K^{(k_1,k_2)}(x) = (\theta_K(x), \varphi_K(x))$

$$\Phi_K^{(k_1,k_2)}(x) = \left(\frac{2k_1+1}{2n_1}\pi \ , \ \frac{k_2+1}{n_2}\pi + \frac{1}{n_2}\mathrm{Gd}\left[(-1)^{k_2+\epsilon_2+1}\, n_2^2\, A_{k_1}\bar{x})\right] \right) , \quad (4.46)$$

  where $\bar{x} = x - x_0$ and the following constant is introduced

$$A_{k_1} = \frac{m_2}{(R + r\sin\frac{2k_1+1}{2n_1}\pi)^2} .$$

  Once again, notice that x_0 can be considered the kink centre. In this case, kinks revolve around the torus centre, connecting minima located at $\varphi = \frac{2k_1+1}{2n_1}\pi$ and $\varphi = \frac{2k_1+3}{2n_1}\pi$. Lastly, for this family of potential functions the energy density profiles can be explicitly derived. In fact, different energy density profiles associated with solutions (4.13) will appear depending on k_1

$$\varepsilon\left(\Phi_K^{(k_1,k_2)}(x)\right) = \frac{m_2^2 n_2^2}{\left(R + r\sin\left(\frac{2k_1+1}{2n_1}\pi\right)\right)^2}\ \mathrm{sech}^2 \frac{n_2^2 m_2 \bar{x}}{\left(R + r\sin\left(\frac{2k_1+1}{2n_1}\pi\right)\right)^2} , \quad (4.47)$$

  which describe different single lumps with the same total energy

$$E[\Phi_K^{(k_1,k_2)}] = E[\Phi_K^{[k_1]}] = 2m_2 . \quad (4.48)$$

  Their kink profiles depend on k_1 and k_2, but the energy density profile of all these singular kinks depend only on k_1. Taking this into consideration, notation $\Phi_K^{[k_1]}$ with $[k_1] \equiv [k_1]_{|2n_1|}$ is employed, where the identification $[k_1] = [k_1 + 2n_1]$ is made. Notice that only n_1 or $n_1 + 1$ different energy density profiles emerge for even or odd n_1 respectively.

- **Singular Θ-kinks**: The $|2n_2|$ *poloidal* kink orbits that cross any vacuum v_i defined by condition $\varphi = \frac{\pi}{2n_2} + \frac{k_2}{n_2}\pi$ (orthogonal to toroidal trajectories) will be referred to as singular Θ-kink orbits. Equations (4.44) with this condition produce their kink profile $\Theta_K^{(k_1,k_2)}(x) = (\theta_K(x), \varphi_K(x))$

$$\Theta_K^{(k_1,k_2)}(x) = \left(\frac{k_1+1}{n_1}\pi + \frac{1}{n_1}\mathrm{Gd}\left[\frac{(-1)^{k_1+\epsilon_1+1}\, m_1 n_1^2}{r^2}\,\bar{x}\right] , \frac{2k_2+1}{2n_2}\pi \right) . \quad (4.49)$$

The total energy of these singular kinks is independent of any k_i. In fact, only one energy density profile is obtained, which describes a single lump

$$E[\Theta_K^{(k_1,k_2)}] = E[\Theta_K] = 2m_1\,, \qquad \varepsilon\left(\Theta_K^{(k_1,k_2)}\right) = \frac{m_1^2 n_1^2}{r^2}\,\mathrm{sech}^2\left(\frac{n_1^2 m_1 \bar{x}}{r^2}\right)\,,$$

for all k_1, k_2. Given that the energy density is independent of k_1 and k_2, notation Θ_K is employed. Unlike Φ_K-kinks, these solutions describe only one type of extended particle. It is worth noticing that for both Φ_K and Θ_K-kinks, parameter m_2 and m_1 respectively modulates not only their energy but also the maximum height of the peak in their energy density.

- **Families of energy degenerate kinks**: Equations (4.44) can also be analytically solved when neither of the variables are constant in the general case. The first equation can be directly integrated and the resulting solution $\theta(x)$ can be plugged into the second one. This leads to the following kink profiles for both angles

$$\begin{aligned}\theta(x) &= \frac{k_1+1}{n_1}\pi + \frac{1}{n_1}\mathrm{Gd}\left[(-1)^{\epsilon_1+k_1+1}\frac{m_1 n_1^2}{r^2}(x-x_0)\right]\,,\\ \varphi(x) &= \frac{k_2+1}{n_2}\pi + \frac{1}{n_2}\mathrm{Gd}\left[(-1)^{\epsilon_2+k_2+1} m_2 n_2^2(\xi(x)-\xi_0)\right]\,,\end{aligned}$$

where $\xi_0 \in \mathbb{R}$ and $\xi(x)$ is a new spatial parameter defined by

$$\xi(x) = \int \frac{dx}{(R + r\sin\theta(x))^2}\,. \tag{4.50}$$

Notice that x_0 represents a shift in x, while ξ_0 is a parameter that changes the orbit of the solution. On the other hand, from (4.44) the kink orbit flow in the phase plane can be determined by the equation

$$\frac{d\theta}{d\varphi} = (-1)^{\epsilon}\,\frac{m_1\,n_1}{m_2\,n_2}\,\frac{(R + r\sin(\theta))^2}{r^2}\,\frac{\cos(n_1\theta)}{\cos(n_2\varphi)}\,, \tag{4.51}$$

where $\epsilon = \epsilon_1 - \epsilon_2$. The integration constant that will appear when integrating the orbit flow equation will have the same role as ξ_0 in discriminating members in these families. Unlike the orbit flow equation in the first part of the chapter (4.12), two possible signs $(-1)^{\epsilon}$ appear in this one. It is clear from the expression above that this leads to two families of orbits, denoted as $\Sigma_K^{(k_1,k_2,\epsilon)}(x;\gamma)$, one for each value of ϵ modulo 2 and where γ is the integration constant. Notice that the family label can change $\epsilon \to \epsilon + 1$ if a shift $\epsilon_i \to \epsilon_i + 1$ is performed in one of these parameters. This transformation can be accomplished by applying to a superpotential (4.43) one of the following transformations:

$$(\theta,\varphi) \to \left(\theta, \varphi + \frac{2l+1}{n_2}\pi\right)\,, \qquad (\theta,\varphi) \to \left(\theta, \frac{2\pi l}{n_2} - \varphi\right)\,, \tag{4.52}$$

for $l \in \mathbb{Z}$. These will lead to another of the four possible superpotentials, being then a symmetry of the potential function. These symmetries can relate different families of solutions, including those that belong to different topological sectors. On the other hand, note that these symmetries disappear when

$n_i = \frac{1}{2}$ in the corresponding variable, since the shift becomes 2π. This can be seen in the poloidal-toroidal plane when more copies of the same torus are represented. The kink energy (4.7) will be identical for any member of this family since the initial and final points coincide. Furthermore, employing the symmetries described above between superpotentials, it can be easily proven that members of even different families share the same energy and it is independent of k_1 and k_2. In fact, it is solely modulated by parameters m_1 and m_2, giving rise to the energy sum rule:

$$E\left[\Sigma_K^{(k_1,k_2,0)}\right] = E\left[\Sigma_K^{(k_1,k_2,1)}\right] = 2(m_1+m_2) = E[\Phi_K^{(k_1,k_2)}] + E[\Theta_K^{(k_1,k_2)}]\,. \quad (4.53)$$

In principle, parameters n_1 and n_2 are allowed to be negative, but the sign that appears in reflections $n_i \to -n_i$ in any or both cases $i = 1, 2$ can be absorbed by $\theta \to -\theta$ or/and $\varphi \to -\varphi$. Consequently, only positive n_i will be considered from now on, since symmetries will generate the negative cases. The kink variety for the different members of the family of potentials (4.42) with different number of vacua will be very different. The following four particular cases of the potential (4.10) are chosen to be studied in detail:

- **Case** 1: Aiming for four minima, the potential with values $n_1 = n_2 = 1$ is chosen as representative. This implies the existence of sixteen disjoint topological clusters in the configuration space.

- **Case** 2: Values $n_1 = 1$ and $n_2 = \frac{1}{2}$ in the potential (4.10) make the number of minima decrease down to two. Once again, given the distribution of the Φ_K-kinks, non-topological kinks are expected to emerge.

- **Case** 3: If the values of the parameters are swapped with respect to Case 2, $n_1 = \frac{1}{2}$ and $n_2 = 1$, another potential with two minima is obtained. Even though the same number of topological and non-topological kinks are expected to arise, the kink variety shall be different.

- **Case** 4: Finally, when $n_1 = n_2 = \frac{1}{2}$ every kink must be non-topological, as only one minimum is present in the potential. Consequently, only one topological cluster can exist. However, it must be checked that the emerging solutions in this topological cluster are not contractible to the vacuum point. This is, whether these are brochosons.

Lastly, solutions of Bogomol'nyi equations for a given superpotential minimise the energy in the corresponding topological cluster. The fact that the Bogomol'nyi arrangement can only be performed by one smooth superpotential up to signs, guarantees the linear stability of all these energy degenerate kinks. Indeed, there is no other superpotential for which the energy of kinks in a topological cluster could be lower. This is another consequence of constructing a separable potential function.

4.3.2 Kink variety for a model with four vacua

Case 1 involves a potential function with four minima. This implies that the choice of parameters n_1 and n_2 must be made such that $|4n_1n_2| = 4$. Among the existing

three positive possibilities, $n_1 = \frac{1}{2}$ and $n_2 = 2$, $n_1 = 2$ and $n_2 = \frac{1}{2}$ and $n_1 = 1$ and $n_2 = 1$, the latter will be chosen to be studied. Notice that a similar analysis can be performed for the rest of the cases. The potential function (4.10), which has the form in this case

$$V_{1,1}(\theta,\varphi) = \frac{1}{2}\left[\frac{m_1^2}{r^2}\,\cos^2\theta + \frac{m_2^2}{(R+r\sin\theta)^2}\,\cos^2\varphi\right], \tag{4.54}$$

has four minima symmetrically distributed on the torus

$$\mathcal{M}_{1,1} \;=\; \{v^1 = (\tfrac{\pi}{2},\tfrac{\pi}{2}); v^2 = (\tfrac{3\pi}{2},\tfrac{\pi}{2}); v^3 = (\tfrac{3\pi}{2},\tfrac{3\pi}{2}); v^4 = (\tfrac{\pi}{2},\tfrac{3\pi}{2})\},$$

see Figure 4.9. The four superpotentials that this potential function admits are periodic on the torus

$$W_{1,1}(\theta,\varphi) = (-1)^{\epsilon_1}\, m_1\, \sin\theta + (-1)^{\epsilon_2}\, m_2\, \sin\varphi\,. \tag{4.55}$$

Translations $\theta \to \theta+\pi$ and $\varphi \to \varphi+\pi$ relate solutions from superpotentials with different ϵ_1 and ϵ_2, even if only translation $\varphi \to \varphi+\pi$ is a symmetry of the potential $V_{1,1}(\theta,\varphi)$. This implies that any orbit is replicated in the other three regions of the torus. The torus is therefore split into four regions where the structure of the kink variety is identical. Bogomol'nyi equations provide four singular topological kinks and antikinks as well as two families of topological kinks in each region:

- **Singular Φ_K-kinks**: General expression (4.46) provides solutions that link minimum v^1 to v^4 and minimum v^2 to v^3

$$\Phi_K^{(k_1,k_2)}(x) = \left(\frac{2k_1+1}{2}\pi\;,\;(k_2+1)\pi + \;\mathrm{Gd}\left[(-1)^{\epsilon_2+k_2+1}\frac{m_2\bar{x}}{(R+(-1)^{k_1}r)^2}\right]\right). \tag{4.56}$$

  Employing notation $\Phi_K^{[k_1]}$, the $\Phi_K^{[0]}-$kinks will correspond to exterior singular kinks on the torus while $\Phi_K^{[1]}-$kinks to interior kinks, see Figure 4.9. Label $k_2 = 0,1$ will distinguish beetween the two pieces of each circumference. As expected, the energy density is concentrated around a single point. However, even if the energy of all these singular kinks is the same $E[\Phi_K] = 2m_2$, two different energy density profiles arise depending on the label $[k_1] = 0,1$

$$\varepsilon\left(\Phi_K(x)\right) = \frac{m_2^2}{\left(R+(-1)^{k_1}r\right)^2}\;\mathrm{sech}^2\left(\frac{m_2\bar{x}}{\left(R+(-1)^{k_1}r\right)^2}\right). \tag{4.57}$$

  This means that two different types of extended particles are found as Φ_K-kinks. Note that the peak in the energy density of kinks with $[k_1] = 1$ will be more pronounced.

- **Singular Θ_K-kinks**: Four topological kinks and antikinks in the poloidal direction are obtained when φ-constant orbits are sought in the first order equations (4.44)

$$\Theta_K^{(k_1,k_2)}(x) = \left((k_1+1)\pi + \mathrm{Gd}\left[(-1)^{\epsilon_1+k_1+1}\frac{m_1\bar{x}}{r^2}\right]\;,\;\frac{2k_2+1}{2}\pi\right), \tag{4.58}$$

  where $k_1 = 0,1$ and $k_2 = 0,1$ are enough to represent all these kinks on the torus. While $\Theta^{(k_1,0)}$-kinks connect points v^1 and v^2, $\Theta^{(k_1,1)}$-kinks join minima

v^3 and v^4, see orbits in Figure 4.9. This means that k_2 selects between the upper and lower circumference while k_1 distinguishes between the front and back side of the torus. All the $\Theta_K(x)$-kinks share the same energy density profile and energy:

$$\varepsilon\left(\Theta_K(x)\right) = \frac{m_1^2}{r^2}\,\mathrm{sech}^2\left(\frac{m_1\bar{x}}{r^2}\right), \qquad E[\Theta_K] = 2m_1\,.$$

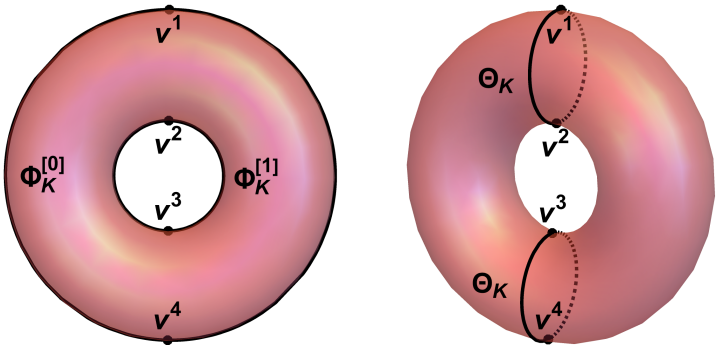

Figure 4.9: Φ_K and Θ_K-kink orbits are represented on the torus, where dotted lines represent kinks on the back side. See how these singular kinks combined split the torus into four regions related by symmetries of the potential.

- **Families of kinks**: The two possible values of ϵ in (4.51) give rise to two families of kinks in each region on the torus. Even if it is possible to obtain the explicit form of the parameter (4.50) for the families when $n_1 = 1$, due to its length it is omitted. Instead, let us give explicitly the kink orbits by solving equation (4.51), whose solution in this case reads

$$\sin\varphi = \tanh\left[\gamma + (-1)^{\epsilon}\,\frac{m_2}{2m_1}\,\frac{r^2}{(R+r)^2}\,\ln\left|\frac{(1+\sin\theta)^{\left(\frac{R+r}{R-r}\right)^2} e^{\left(\frac{R+r}{R-r}\,\frac{2r}{R+r\sin\theta}\right)}}{(1-\sin\theta)(R+r\sin\theta)^{\frac{4rR}{(R-r)^2}}}\right|\right], \tag{4.59}$$

where the parameter $\gamma \in (-\infty, \infty)$ is an integration constant that labels every kink member $\Sigma_K^{(k_1,k_2,\epsilon)}(x;\gamma)$ in each family. Let us briefly discuss both families, which, as stated before, have the same energy:

  - Kink family with $\epsilon = 0$: Minima v^1 and v^3 are connected in the four equivalent regions of the torus by curves that densely fill each region, see Figure 4.10. The limit when $\gamma \to -\infty$ in the orbit equation leads either to $\varphi = \frac{3\pi}{2} + 2\pi l_1$ with $l_1 \in \mathbb{Z}$ or to $\theta = \frac{\pi}{2} + 2\pi l_2$ with $l_2 \in \mathbb{Z}$. These correspond to a $\Phi_K^{[0]}-$kink and a Θ_K-kink respectively, which will be different for different regions labelled by k_1 and k_2. On the other hand, the limit $\gamma \to \infty$ forces either $\varphi = \frac{\pi}{2} + 2\pi l_1$ or $\theta = \frac{3\pi}{2} + 2\pi l_2$. These correspond to different Θ_K-kinks and $\Phi_K^{[1]}-$kinks.

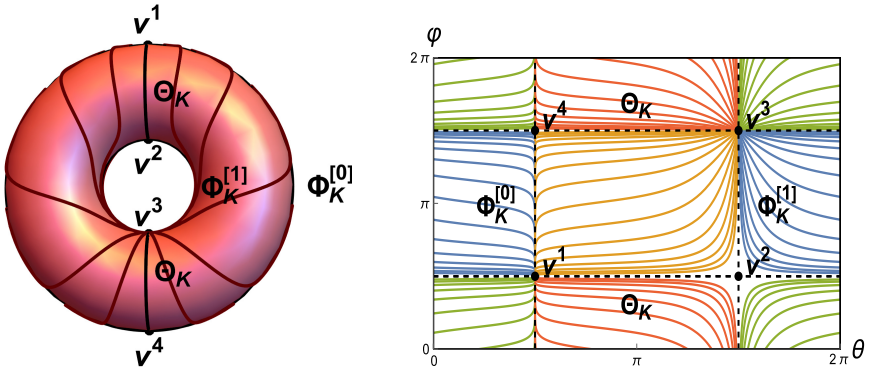

Figure 4.10: Family $\Sigma_K^{(k_1,k_2,0)}(x;\gamma)$ connects minima v^1 and v^3 on the torus and in the $\theta-\varphi-$plane. Even if only kinks on the front of the torus have been shown in the first figure, the kink variety on the back is identical by symmetries.

– Kink family with $\epsilon = 1$: For these solutions minima v^2 and v^4 are now connected in each region of the torus, see Figure 4.11. In this family the limits for the parameter γ are swapped from the previous family. A $\Phi_K^{[1]}-$kink and a Θ_K-kink are obtained for $\gamma \to -\infty$ while a Θ_K-kink and a $\Phi_K^{[0]}$ are found for $\gamma \to \infty$. Of course, this is due to the fact that solutions of this family can be obtained by applying the symmetries that relate the four superpotentials to the previous family

$$(\theta,\varphi) \to (\theta,\varphi+(2l+1)\pi)\ , \qquad (\theta,\varphi) \to (\theta,2\pi l-\varphi)\ , \tag{4.60}$$

for $l \in \mathbb{Z}$, which change their topological cluster. Indeed, members $\Sigma_K^{(k_1,k_2,0)}(x;\gamma)$ are related to members $\Sigma_K^{(k_1,k_2+1,1)}(x;-\gamma)$.

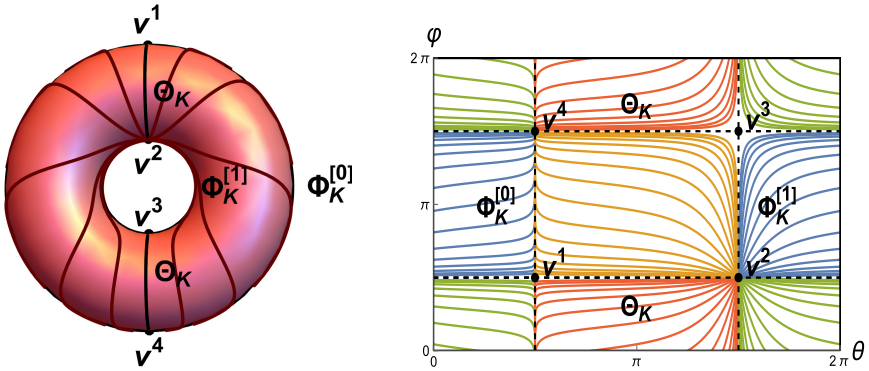

Figure 4.11: Family $\Sigma_K^{(k_1,k_2,1)}(x;\gamma)$ connects minima v^2 and v^4 on the torus and in the $\theta-\varphi-$plane. Even if only kinks on the front of the torus have been shown in the first figure, the kink variety on the back is identical by symmetries.

The limits $\gamma \to \pm\infty$ of these families are combinations of singular kinks that respect the previously found energy sum rules (4.53). Let us write symbolically those for the two families that emerge in the region determined by $k_1 = k_2 = 0$

$$\lim_{\gamma\to-\infty} \Sigma_K^{(0,0,0)}(x;\gamma) \equiv \Phi_K^{[0]}(x) \cup \Theta_K(x)\ , \qquad \lim_{\gamma\to\infty} \Sigma_K^{(0,0,0)}(x;\gamma) \equiv \Theta_K(x) \cup \Phi_K^{[1]}(x)\ , \tag{4.61}$$

$$\lim_{\gamma\to-\infty}\Sigma_K^{(0,0,1)}(x;\gamma)\equiv\Phi_K^{[1]}(x)\cup\Theta_K(x),\qquad \lim_{\gamma\to\infty}\Sigma_K^{(0,0,1)}(x;\gamma)\equiv\Theta_K(x)\cup\Phi_K^{[0]}(x)\,. \tag{4.62}$$

This behaviour can be observed in Figure 4.12, where in each picture the corresponding energy density profiles with two lumps are recovered when $|\gamma|$ is large enough.

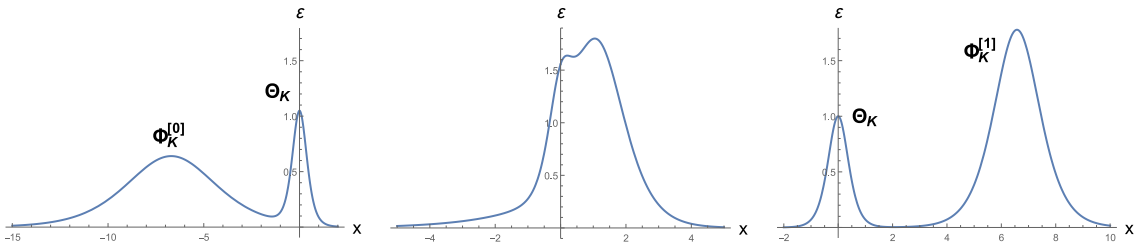

Figure 4.12: Energy densities for three members of the family $\Sigma_K^{(0,0,0)}(x;\gamma)$ given by $\gamma=1$, $\gamma=4.5$ and $\gamma=10$ respectively. Values of parameters $(R,r,m_1,m_2)=(2,0.5,0.5,2)$ have been used. Notice how combinations of singular kinks are obtained as limits. Since orbits of both families $\epsilon=\pm1$ and in different regions are related by symmetries, these are also the energy densities for the family $\epsilon=1$ and for other regions for certain values of γ.

Notice that among these pairs of lumps the three different lumps $\Phi_K^{[0]}$, $\Phi_K^{[1]}$ and Θ_K can be identified. Indeed, they can be interpreted as three different extended particles. In sum, two related families of topological kinks are replicated in the four regions of the torus. Furthermore, the limits of both families coincide with combinations of singular kinks, which delimit these four regions. Since there is no points in these kinks where the flow is undefined, there are no conjugate points where the kink orbits intersect and all these kinks are stable, see [14].

Lastly, it is worth noticing that while this model possess the same number of vacua than Case 2 of the first family of superpotentials, the kink variety is completely different.

4.3.3 Kink variety for a model with two vacua (Case 2)

Models with two vacua can be obtained when condition $|4n_1n_2|=2$ holds. Only two possibilities are available for positive parameters, $n_1=1$, $n_2=\frac{1}{2}$ and $n_1=\frac{1}{2}$, $n_2=1$. These configurations correspond to Case 2 and Case 3 respectively. Let us explore the first choice of n_i, which produces a potential function of the form

$$V_{1,\frac{1}{2}}(\theta,\varphi)=\frac{1}{2}\left[\frac{m_1^2}{r^2}\cos^2\theta+\frac{m_2^2}{4(R+r\sin\theta)^2}\cos^2\frac{\varphi}{2}\right], \tag{4.63}$$

for which the set of vacua $\mathcal{M}$ is distributed in one side of the torus

$$\mathcal{M}_{1,\frac{1}{2}} \;=\; \{v^1=(\tfrac{\pi}{2},\pi);v^2=(\tfrac{3\pi}{2},\pi)\}\,,$$

see Figure 4.13. Unlike the previous model, the four superpotentials are not periodic in the torus

$$W_{1,\frac{1}{2}}(\theta,\varphi)=(-1)^{\epsilon_1}m_1\sin\theta+(-1)^{\epsilon_2}m_2\sin\frac{\varphi}{2}\,. \tag{4.64}$$

This non-periodicity of the superpotential in the torus is precisely what allows the existence of BPS non-topological kinks, just like in the previous family of Sigma models. Indeed, if it were periodic, the energy (4.7) of non-topological BPS kinks would vanish, and it could not describe a kink. Now, as expected, reducing the number of vacua of the potential (4.63) also affects the symmetries between solutions of the superpotential. Only translations $\theta \to \theta + \pi$ relate solutions from different superpotentials now. These split the torus into two regions where the kink variety has the same structure. In particular, the kink variety in each region will include four singular topological kinks and antikinks and two families of topological kinks:

- **Singular Φ_K-kinks**: In this case toroidal loops will cross exclusively v^1 or v^2. This implies that depending on $k_1 = 0, 1$, solutions

$$\Phi_K^{(k_1,k_2)}(x) = \left(\frac{2k_1+1}{2}\pi \ , \ 2\pi(k_2+1) + 2\mathrm{Gd}\left[(-1)^{\epsilon_2+1} \frac{m_2 \bar{x}}{4(R+(-1)^{k_1} r)^2} \right] \right) . \tag{4.65}$$

  describe two types of non-topological kinks on the torus. Here k_2 labels solutions under and above the value $\varphi = \pi$ and k_1 will distinguish between those kinks in the "exterior" and "interior" circumferences. Two types of Φ_K-kinks are identified depending on k_1, each one with different energy density profile

$$\varepsilon\left(\Phi_K(x)\right) = \frac{m_2^2}{4\left(R+(-1)^{k_1} r\right)^2} \operatorname{sech}^2\left(\frac{m_2 \bar{x}}{4\left(R+(-1)^{k_1} r\right)^2} \right) , \tag{4.66}$$

  while the energy remains the same $E[\Phi_K] = 2m_2$ for all values of k_1. Same notation as in the previous section $\Phi_K^{[k_1]}$ will be used to distinguish between different energy density profiles. The $\Phi_K^{[0]}-$kink, whose energy density peak is more pronounced, corresponds to the "exterior" kink while the $\Phi_K^{[1]}-$kink corresponds to the "interior" one, see Figure 4.13. Therefore, these singular kinks describe two different brochosons, as they cannot decay to a vacuum solution.

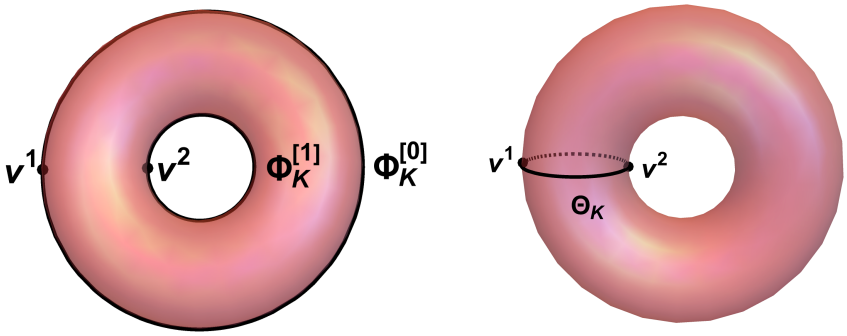

Figure 4.13: Φ_K and Θ_K-kink orbits are represented on the torus, where dotted lines represent kinks on the back side. See how these singular kinks combined split the torus into two regions related by symmetries of the potential.

- **Singular Θ_K-kinks**: φ-constant orbits produce in the first order equations (4.44) two topological kinks and antikinks

$$\Theta_K^{(k_1,k_2)}(x) = \left((k_1+1)\pi + \mathrm{Gd}\left[(-1)^{k_1+\epsilon_1+1}\frac{m_1\bar{x}}{r^2}\right], \pi\right) \quad , \qquad k_1 = 0, 1\,, \tag{4.67}$$

which correspond to half-circumferences associated with the minor radius, see Figure 4.9. These poloidal curves will connect asymptotically the two minima v^1 and v^2. The two values of $[k_1]$ distinguish between the kink on the front of the torus and the kink on the back, see Figure 4.13. Once again, both the energy density and the energy of all these $\Theta_K(x)$-kinks are identical

$$\varepsilon\left(\Theta_K(x)\right) = \frac{m_1^2}{r^2}\,\mathrm{sech}^2\left(\frac{m_1\bar{x}}{r^2}\right) , \qquad E[\Theta_K] = 2m_1\,.$$

- **Families of kinks**: The value n_1 has not changed in comparison to the previous case and therefore the same reparametrisation $\xi(x)$ as in Case 1 is obtained. Alternatively, the explicit orbit equation is shown, which provides the following family of topological kinks

$$\sin\frac{\varphi}{2} = \tanh\left[\gamma + (-1)^{\epsilon}\frac{m_2}{8m_1}\frac{r^2}{(R+r)^2}\ln\left|\frac{(1+\sin\theta)^{\left(\frac{R+r}{R-r}\right)^2} e^{\left(\frac{R+r}{R-r}\frac{2r}{R+r\sin\theta}\right)}}{(1-\sin\theta)(R+r\sin\theta)^{\frac{4rR}{(R-r)^2}}}\right|\right] , \tag{4.68}$$

where the parameter $\gamma \in (-\infty, \infty)$ is an integration constant, see Figure 4.14. Notice that in this case both values $\epsilon = 0, 1$ describe the same orbits on the torus since they complete a whole revolution along the toroidal direction. Members of these families shall be denoted as $\Sigma_K^{(k_1,k_2,\epsilon)}(x;\gamma)$, where the parameter γ is again employed to label every kink member in each family.

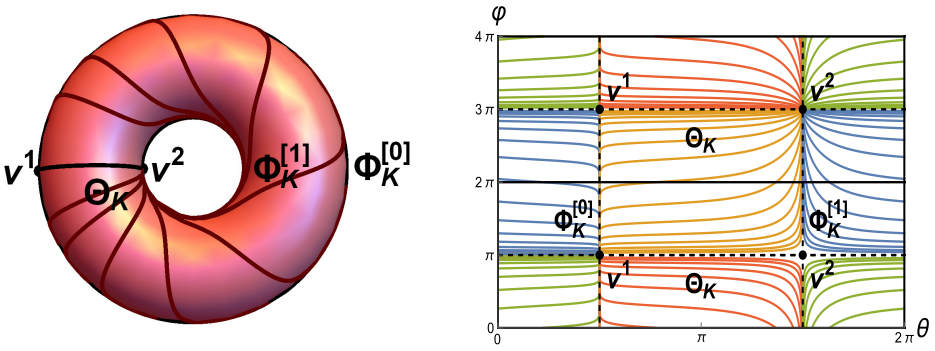

Figure 4.14: Family $\Sigma_K^{(k_1,k_2,0)}(x;\gamma)$ connects minima v^1 and v^2 on the torus and in the $\theta-\varphi-$plane. Even if only kinks on the front of the torus have been shown in the first figure, the kink variety on the back is identical by symmetries. Given the identification between members of both families, orbits for the family $\Sigma_K^{(k_1,k_2,1)}(x;\gamma)$ coincide with those of $\Sigma_K^{(k_1,k_2+1,0)}(x;\gamma)$.

In this case all these solutions connect the same minima v^1 and v^2 in both regions of the torus. In fact, solutions with different ϵ describe the same kink orbits and therefore only one family is found in each region. Indeed, a symmetry between superpotentials:

$$(\theta,\varphi) \to (\theta, \varphi + (2l+1)2\pi)\,, \qquad (\theta,\varphi) \to (\theta, 4\pi l - \varphi)\,, \tag{4.69}$$

for $l \in \mathbb{Z}$, allows us to make an identification between members $\Sigma_K^{(k_1,k_2,0)}(x;\gamma) = \Sigma_K^{(k_1,k_2+1,1)}(x;-\gamma)$, which in this case belong to the same topological cluster. Two copies of the same torus have been represented in the $\theta-\varphi-$plane so that both related solutions can be seen in the $\theta-\varphi-$plane. On the other hand, limits of the orbit equation for $\gamma \to \pm\infty$ are almost identical to those of the previous model. Let us restrict to the region $k_1 = k_2 = 0$. The obtained limit values for φ have been doubled, that is $\varphi = \pi + 4\pi l_1$ and $\varphi = 3\pi + 4\pi l_1$, and so has been its periodicity in this direction. These limits, of course, correspond to the analogue Θ_K-kinks in this model. In sum, for $\epsilon = 0$ a $\Phi_K^{[1]}-$kink and a Θ_K-kink are recovered for $\gamma \to -\infty$ while another Θ_K-kink and a $\Phi_K^{[0]}-$kink are obtained for $\gamma \to \infty$. Hence, the same formal limits as in the previous case for this family of kinks emerge. This is, they correspond to the same combinations of singular kinks, which obviously abide by the energy sum rules. These combinations are symbolically written the same way as before

$$\lim_{\gamma\to-\infty} \Sigma_K^{(0,0,0)}(x;\gamma) \equiv \Phi_K^{[0]}(x) \cup \Theta_K(x)\,, \qquad \lim_{\gamma\to\infty} \Sigma_K^{(0,0,0)}(x;\gamma) \equiv \Theta_K(x) \cup \Phi_K^{[1]}(x)\,. \tag{4.70}$$

$$\lim_{\gamma\to-\infty} \Sigma_K^{(0,0,1)}(x;\gamma) \equiv \Phi_K^{[1]}(x) \cup \Theta_K(x)\,, \qquad \lim_{\gamma\to\infty} \Sigma_K^{(0,0,1)}(x;\gamma) \equiv \Theta_K(x) \cup \Phi_K^{[0]}(x)\,. \tag{4.71}$$

and can be visualised in Figure 4.15, where two extended particles can be identified for each limit of γ. Notice that while in the model with two vacua in the first family of potentials the emerging family of kinks was comprised by brochosons, in this case only the Φ_K-kinks are. Lastly, same analysis as in the previous model reveals that, due to the absence of intermediate conjugate points, these families of kinks are stable.

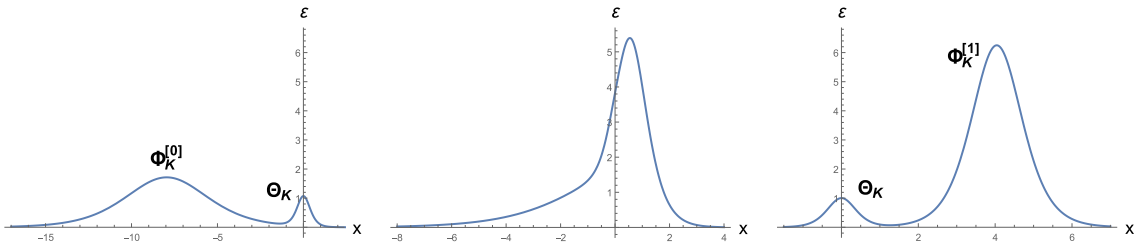

Figure 4.15: Energy densities for three members of the family $\Sigma_K^{(0,0,0)}(x;\gamma)$ given by $\gamma = -3$, $\gamma = 1$ and $\gamma = 5$ respectively. Values of parameters $(R, r, m_1, m_2) = (1.6, 0.5, 0.5, 5.5)$ have been used. Notice how combinations of singular kinks are obtained as limits. Since orbits of both families $\epsilon = \pm 1$ and in different regions are related by symmetries, these are also the energy densities for the family $\epsilon = 1$ and for other regions for certain values of γ.

4.3.4 Kink variety for a model with two vacua (Case 3)

The remaining configuration of values of n_1 and n_2 that produces a potential (4.10) with two minima is $n_1 = \frac{1}{2}$ and $n_2 = 1$. Even if the number of minima is the same as in Case 2, their distribution on the torus and the kink variety will be different. This corresponds to Case 3, which shall be now studied. In particular, this choice

of n_i produces a potential

$$V_{\frac{1}{2},1}(\theta,\varphi) = \frac{1}{2}\left[\frac{m_1^2}{4r^2}\,\cos^2\frac{\theta}{2} + \frac{m_2^2}{(R+r\sin\theta)^2}\,\cos^2\varphi\right], \tag{4.72}$$

which can be derived from the following four superpotentials, one for each value combination of $\epsilon_i = \pm 1$

$$W_{\frac{1}{2},1}(\theta,\varphi) = (-1)^{\epsilon_1}\, m_1\, \sin\frac{\theta}{2} + (-1)^{\epsilon_2}\, m_2\, \sin\varphi\,. \tag{4.73}$$

Once again, the fact that these superpotentials are not periodic on the torus allows the existence of BPS non-topological kinks. However, since the two minima are aligned in the poloidal direction

$$\mathcal{M}_{\frac{1}{2},1} = \left\{ v^1 = \left(\pi, \frac{\pi}{2}\right)\ ,\ v^2 = \left(\pi, \frac{3\pi}{2}\right)\right\},$$

as it is shown in Figure 4.16, the singular non-topological kinks in this model will be poloidal and not toroidal. On the other hand, in this case only translations $\varphi \to \varphi+\pi$ will allow us to identify solutions from different superpotentials. This splits the torus into two equivalent regions again. Notice, however, that these regions are different from those of Case 2. In each of these two regions two singular topological kinks, two singular non-topological kinks and two families of non-topological kinks are found:

- **Singular Φ_K-kinks**: General expression (4.46) for toroidal orbits provides now topological singular kinks because of the new alignment of the minima

$$\Phi_K^{(k_1,k_2)}(x) = \left((2k_1+1)\pi\ ,\ (k_2+1)\pi + \ \mathrm{Gd}\left[(-1)^{k_2+\epsilon_2+1}\,\frac{m_2\bar{x}}{R^2}\right]\right). \tag{4.74}$$

  Indeed, this expression describes singular topological kinks and their antikinks, which asymptotically connect minima v^1 and v^2, see Figure 4.16. Notice that depending on k_1 and k_2 the expression above describes different singular kinks in the $\theta-\varphi-$plane, but on the torus only $[k_2]$ distinguishes between different kinks. In fact, the multiplicity of energy density profiles for Φ_K-kinks of previous models disappears since only one profile emerges

$$\varepsilon\left(\Phi_K(x)\right) = \frac{m_2^2}{R^2}\,\mathrm{sech}^2\left(\frac{m_2\bar{x}}{R^2}\right), \qquad E[\Phi_K] = 2m_2 \tag{4.75}$$

  and these solutions describe only one type of extended particle.

- **Singular Θ_K-kinks**: Poloidal singular solutions (4.49) now read

$$\Theta_K^{(k_1k_2)}(x) = \left(2\,(k_1+1)\pi + 2\ \mathrm{Gd}\left[(-1)^{k_1+k_2+1}\frac{m\bar{x}}{2r}\right]\ ,\ \frac{(2k_2+1)}{2}\pi\right),$$

  describing a pair of non-topological kinks and their antikinks. This is, these poloidal solutions asymptotically reach at both infinities v^1 or v^2 depending on the value of k_2, see Figure 4.16. While k_1 labels different kinks in the $\theta-\varphi-$plane, on the torus it will describe the same kink. As stated before, the energy density and total energy of these kinks is independent of k_i

$$\varepsilon\left(\Theta_K(x)\right) = \frac{m_1^2}{4r^2}\,\mathrm{sech}^2\left(\frac{m_1\bar{x}}{4r^2}\right), \qquad E[\Theta_K] = 2m_1\,.$$

  As a result, only one type of singular brochoson will be present in this model.

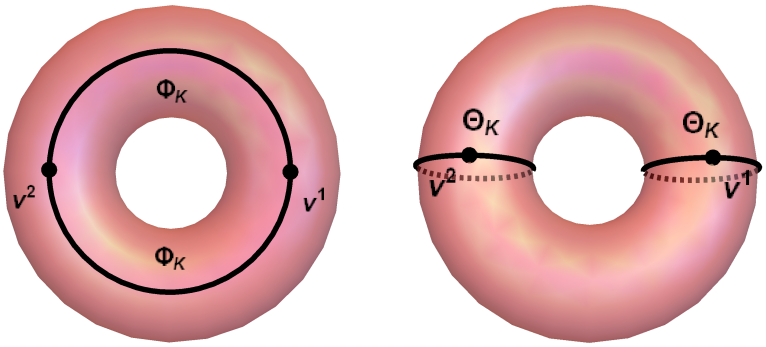

Figure 4.16: Φ_K and Θ_K-kink orbits are represented on the torus, where dotted lines represent kinks on the back side. See how these singular kinks combined split the torus into two regions related by symmetries of the potential.

- **Families of kinks**: The new value of n_1 makes the expression for the new parameter $\xi(x)$ more complicated, but it is still analytically available. Instead of showing this expression, as in the previous cases, the two families $\epsilon = 0, 1$ on the torus are displayed by presenting the orbit equation

$$\sin\varphi = \tanh\left[\gamma + (-1)^{\epsilon}\,\frac{2m_2 r^2}{m_1} f(\theta)\right], \tag{4.76}$$

where the parameter $\gamma \in (-\infty, \infty)$ is an integration constant and the function f is defined as follows

$$f(\theta) = \frac{2\log\left(\left|1 + \frac{2}{\cot\left(\frac{\theta}{4}\right)-1}\right|\right)}{R^2} + \frac{(2r-3R)\tan^{-1}\left(\frac{2r\left(\tan\left(\frac{\theta}{4}\right)+1\right)\sqrt{\frac{R}{r}-1}}{2r\left(\tan\left(\frac{\theta}{4}\right)+1\right)-R\sec^2\left(\frac{\theta}{4}\right)}\right)}{rR^2\left(\frac{R}{r}-1\right)^{3/2}}$$
$$- \frac{2r\left(r\sin\left(\frac{\theta}{2}\right)+R\cos\left(\frac{\theta}{2}\right)\right)}{R\left(r^2-R^2\right)\left(r\sin(\theta)+R\right)} + \frac{\sqrt{r}(2r+3R)\tanh^{-1}\left(\frac{\sqrt{r}\left(\cos\left(\frac{\theta}{2}\right)-\sin\left(\frac{\theta}{2}\right)\right)}{\sqrt{r+R}}\right)}{R^2(r+R)^{3/2}}.$$

Solutions of this orbit equation connect v^1 and v^2, see Figure 4.17.

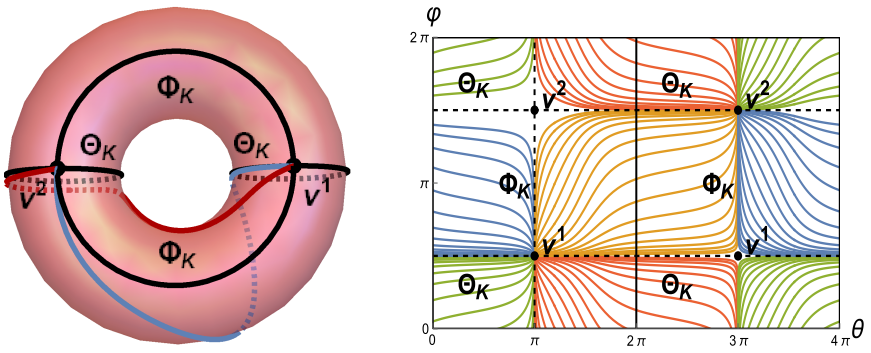

Figure 4.17: Family $\Sigma_K^{(k_1,k_2,0)}(x;\gamma)$ connects minima v^1 and v^2 on the torus and in the $\theta-\varphi-$plane. The two solutions depicted on the torus correspond to two solutions $\Sigma_K^{(0,0,0)}(x;\gamma)$ in the $\theta-\varphi-$plane for $\gamma = -2$ (red) and $\gamma = 2$ (blue).

Exactly as before, members of these solutions shall be denoted as $\Sigma_K^{(k_1,k_2,\epsilon)}(x;\gamma)$, where each family member is labelled by the parameter γ. In this case, once more, neither of the following symmetries between superpotentials

$$(\theta,\varphi)\to(\theta,\varphi+(2l+1)\pi)\ ,\qquad (\theta,\varphi)\to(\theta,2\pi l-\varphi)\ , \tag{4.77}$$

for $l\in\mathbb{Z}$, change the topological cluster of the solutions. Similarly to previous cases, these transformations generate a change in the orbit equation which can be absorbed by $\epsilon\to\epsilon+1$ and $\bar{\gamma}=-\gamma$

$$\sin\varphi=\tanh\left[\bar{\gamma}+(-1)^{\epsilon+1}\,\frac{2m_2r^2}{m_1}f(\theta)\right]\ . \tag{4.78}$$

This orbit equation corresponds to members of the other family $\epsilon+1$ labelled with parameter $\bar{\gamma}$, which identify members $\Sigma_K^{(k_1,k_2,0)}(x;\gamma)=\Sigma_K^{(k_1,k_2+1,1)}(x;-\gamma)$. This implies that also in this case only one family exists in each region of the torus. Once more, two copies of the same torus have been represented in the $\theta-\varphi-$plane so that both related solutions can be seen.

Limits of the orbit equation are similar to those of previous models. Considering that $\lim_{\theta\to\pm\pi}f(\theta)=\pm\infty$, it is easy to prove that, a Φ_K-kink and a Θ_K-kink on one hand and a Θ_K and a Φ_K-kink on the other, are recovered as limits for the family $\epsilon=0$ for $\gamma\to-\infty$ and $\gamma\to\infty$ respectively in the region labelled by $k_1=k_2=0$. Symmetries relating these families immediately provide the limits for the other family, which only swaps the positions of the left and right Θ_K-kink. As would be expected, only two types of extended particles appear in the limits of these families

$$\lim_{\gamma\to-\infty}\Sigma_K^{(0,0,0)}(x;\gamma)\equiv\Phi_K(x)\cup\Theta_K(x)\,,\qquad \lim_{\gamma\to\infty}\Sigma_K^{(0,0,0)}(x;\gamma)\equiv\Theta_K(x)\cup\Phi_K(x)\,, \tag{4.79}$$

$$\lim_{\gamma\to-\infty}\Sigma_K^{(0,0,1)}(x;\gamma)\equiv\Phi_K(x)\cup\Theta_K(x)\,,\qquad \lim_{\gamma\to\infty}\Sigma_K^{(0,0,1)}(x;\gamma)\equiv\Theta_K(x)\cup\Phi_K(x)\,, \tag{4.80}$$

which can be observed in Figure 4.18. Finally, the absence of intermediate conjugate points along the kink orbits proves their stability.

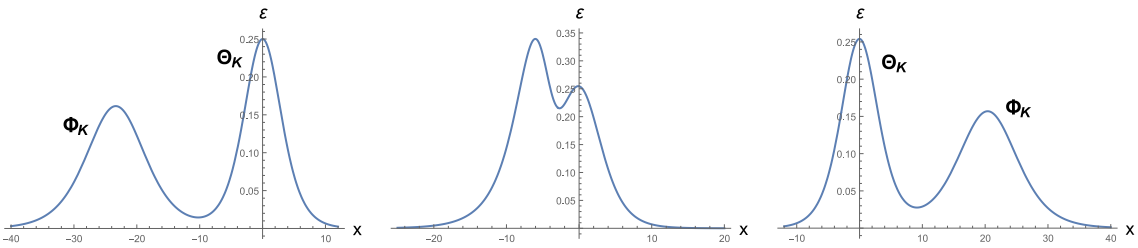

Figure 4.18: Energy densities for three members of the family $\Sigma_K^{(0,0,0)}(x;\gamma)$ given by $\gamma=-3$, $\gamma=0$ and $\gamma=5$ respectively. Values of parameters $(R,r,m_1,m_2)=(2.5,1,1,1)$ have been used. Notice how combinations of singular kinks are obtained as limits. Since orbits of both families $\epsilon=\pm1$ and in different regions are related by symmetries, these are also the energy densities for the family $\epsilon=1$ and for other regions for certain values of γ.

4.3.5 Kink variety for a model with one vacuum point

The number of vacua of these Sigma models $|4n_1n_2|$ is minimised when the values $n_1 = n_2 = \frac{1}{2}$ are taken to the potential (4.10) and is equal to 1. This is precisely the scenario in Case 4, where this choice of n_i leads to a model with only one minimum. As has been advanced, this forces any emerging kink in this model to be non-topological, among which brochosons are expected to be identified. In particular, these conditions produce a potential of the form

$$V_{\frac{1}{2},\frac{1}{2}}(\theta,\varphi) = \frac{1}{8}\left[\frac{m_1^2}{r^2}\cos^2\frac{\theta}{2} + \frac{m_2^2}{(R+r\sin\theta)^2}\cos^2\frac{\varphi}{2}\right], \tag{4.81}$$

which can be derived in this last case from these four superpotentials

$$W_{\frac{1}{2},\frac{1}{2}}(\theta,\varphi) = (-1)^{\epsilon_1} m_1 \sin\frac{\theta}{2} + (-1)^{\epsilon_2} m_2 \sin\frac{\varphi}{2}. \tag{4.82}$$

Observe that in this model the superpotentials are non-periodic on the torus in both angles. This situation, forbidden in the first family of potentials in this chapter, will enable the existence of non-topological BPS kinks in both directions. As intended, the set $\mathcal{M}$ contains now only a vacuum point

$$\mathcal{M}_{\frac{1}{2},\frac{1}{2}} = \left\{v^1 = (\pi,\pi)\right\},$$

as it can be observed in Figure 4.19. Notice that every symmetry in previous models that related solutions from different superpotentials on the torus disappear in this case. Indeed, these become translations of 2π in both angles. The kink variety in the torus will include two singular non-topological kinks and a family of non-topological kinks. Indeed, the existence of only one vacuum point forces every kink to be non-topological. A thorough description of these kinks is as follows:

- **Singular Φ_K-kinks**: Naturally, since there exists only one vacuum point on the torus, no more than one kink of this type can be found

$$\Phi_K^{(k_1,k_2)}(x) = \left((2k_1+1)\pi\ ,\ 2(k_2+1)\pi + 2\ \mathrm{Gd}\left[(-1)^{\epsilon_2+1}\frac{m_2\overline{x}}{4R^2}\right]\right), \tag{4.83}$$

  see Figure 4.19. Once again, singular kinks with different k_i in the $\theta-\varphi-$plane will represent the same kink on the torus. Its energy density and total energy are of the form

$$\varepsilon\left(\Phi_K(x)\right) = \frac{m_2^2}{4R^2}\,\mathrm{sech}^2\left(\frac{m_2\bar{x}}{4R^2}\right), \qquad E[\Phi_K] = 2m_2\,.$$

- **Singular Θ_K-kinks**: For the same reason as in the case of $\Phi-$kinks, only one type of $\Theta-$kink can emerge in this model

$$\Theta_K^{(k_1,k_2)}(x) = \left(2\,(k_1+1)\,\pi + 2\ \mathrm{Gd}\left[(-1)^{k_1+\epsilon_1+1}\frac{m_1\overline{x}}{4r^2}\right]\ ,\ (2k_2+1)\pi\right),$$

  where k_1 and k_2 will affect the position in the $\theta-\varphi-$plane but not on the torus, see Figure 4.19. The energy density and total energy of these kinks are

$$\varepsilon\left(\Theta_K(x)\right) = \frac{m_1^2}{4r^2}\,\mathrm{sech}^2\left(\frac{m_1\bar{x}}{4r^2}\right), \qquad E[\Theta_K] = 2m_1\,.$$

  Notice that in this case only one Θ_K-kink and only one Φ_K-kink are found. Both are brochosons, as they revolve around the torus in one direction each.

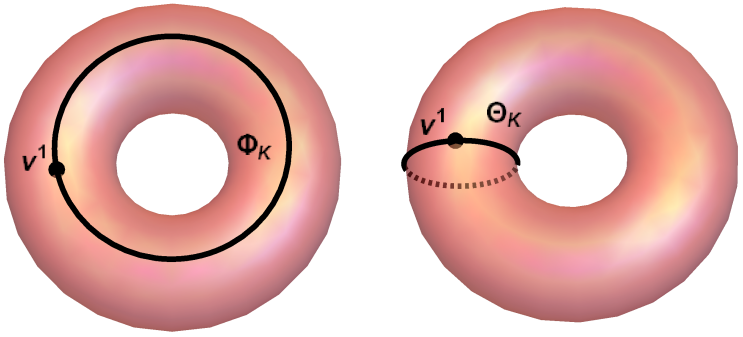

Figure 4.19: Φ_K and Θ_K-kink orbits are represented on the torus, where dotted lines represent the part of the Θ_K-kink orbit on the back side.

- **Families of kinks**: The reparametrisation $\xi(x)$ is identical to that of Case 3, but once again the orbit equation will be presented instead

$$\sin\frac{\varphi}{2}=\tanh\left[\gamma+(-1)^{\epsilon}\,\frac{m_2r^2}{2m_1}f(\theta)\right]\,, \tag{4.84}$$

where the parameter $\gamma\in(-\infty,\infty)$ is again an integration constant and f is the function defined in last section. Let us denote once more solutions of these families on the torus as $\Sigma_K^{(k_1,k_2,\epsilon)}(x;\gamma)$ with parameter γ. The relation between families from previous models persists and plotting one of the families in the $\theta-\varphi-$plane is enough to identify all these non-topological kinks. These two families $\epsilon=0,1$ are still related by one of the transformations

$$(\theta,\varphi)\to(\theta,\varphi+(2l+1)\pi)\,,\qquad(\theta,\varphi)\to(\theta,4\pi l-\varphi)\,, \tag{4.85}$$

for $l\in\mathbb{Z}$, producing the same identification of members $\Sigma_K^{(k_1,k_2,0)}(x;\gamma)=\Sigma_K^{(k_1,k_2+1,1)}(x;-\gamma)$. Indeed, these shifts produce a change in the orbit equation that can be absorbed by swapping the family $\epsilon\to\epsilon+1$ and redefining the parameter $\bar\gamma=-\gamma$:

$$\sin\frac{\varphi}{2}=\tanh\left[\bar\gamma+(-1)^{\epsilon+1}\,\frac{m_2r^2}{m_1}f(\theta)\right]\,.$$

This implies that both values $\epsilon=0,1$ produce the same orbits on the torus, which revolve around the toroidal direction, see Figure 4.20. Both $\epsilon=0,1$ lead to the same family of non-topological kinks. On the other hand, it is obvious that these transformations cannot change the topological cluster of solutions, as only one exists. By construction, only non-topological kinks are allowed to exist in this model, solutions leave the minimum to return to it. However, within this topological cluster three different topological sectors contain kinks. Let us denote as $(\omega_\theta,\omega_\varphi)$ the winding numbers around the poloidal and toroidal directions. Singular kinks revolve once around one of the directions, that is, the Θ_K-kink has $(|\omega_\theta|,|\omega_\varphi|)=(1,0)$ while the Φ_K-kink has $(|\omega_\theta|,|\omega_\varphi|)=(0,1)$. Here the absolute value is necessary given that a kink and its anti-kink will describe the same orbit. However, unlike these singular kinks, members of the family of kinks revolve simultaneously around

both directions $(|\omega_\theta|, |\omega_\varphi|) = (1, 1)$. Therefore, kinks in this family belong to a third topological sector, even if they belong to the same topological cluster.

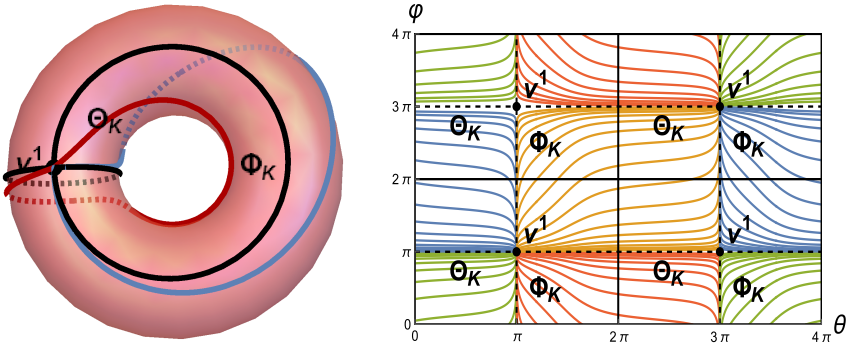

Figure 4.20: Family $\Sigma_K^{(k_1,k_2,0)}(x;\gamma)$ connects minimum v^1 with itself on the torus and in the $\theta - \varphi-$plane. The two solutions depicted on the torus correspond to two solutions $\Sigma_K^{(0,0,0)}(x;\gamma)$ in the $\theta - \varphi-$plane for $\gamma = -2$ (red) and $\gamma = 2$ (blue).

Following an identical procedure as in the previous sections, the same formal limits for both families as in the previous model are retrieved. These limits represent a combination of a Θ_K-kink and a Φ_K-kink. However, in this case all these are non-topological

$$\lim_{\gamma\to-\infty} \Sigma_K^{(0,0,0)}(x;\gamma) \equiv \Phi_K(x) \cup \Theta_K(x)\,, \qquad \lim_{\gamma\to\infty} \Sigma_K^{(0,0,0)}(x;\gamma) \equiv \Theta_K(x) \cup \Phi_K(x)\,. \tag{4.86}$$

Of course, these conjunctions of kinks are congruent with the energy sum rules (4.53) as it is perceivable in Figure 4.21. Note that in this last case, not only two different singular brochosons arise in the same theory, but also members of the family of kinks are a combination of these two. Indeed, these singular brochosons are found at arbitrary separation distance as limits of the kink family.

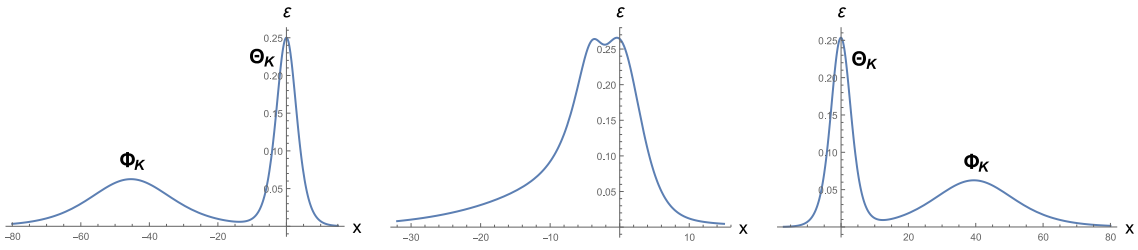

Figure 4.21: Energy densities for three members of the family $\Sigma_K^{(0,0,0)}(x;\gamma)$ given by $\gamma = -10$, $\gamma = 0$ and $\gamma = 10$ respectively. Values of parameters $(R, r, m_1, m_2) = (2, 1, 1, 1)$ have been used. Notice how combinations of singular kinks are obtained as limits.

Lastly, it is worth highlighting that all the solutions that arise in this model, all of them brochosons, lack intermediate conjugate points. This fact makes the members of this family stable from the perspective of Morse Theory.

4.4 Further comments

In this chapter two families of Sigma models on the torus $\mathbb{S}^1 \times \mathbb{S}^1$ have been constructed and their kink variety analysed for some representative cases. The main motivation behind the choice of the torus as target manifold is the fact that this is a non-simply connected manifold. This implies that, unlike in simply connected spaces, different classes of homotopy of curves and loops arise. In particular, the notion of brochoson emerges naturally on the torus, as an infinite number of homotopical classes of loops that cannot decay into vacuum appear. Indeed, the fundamental group of the torus is $\pi_1(\mathbb{S}^1 \times \mathbb{S}^1) = \mathbb{Z} \times \mathbb{Z}$. This implies that homotopy classes of curves and loops will be labelled by the winding number around both poloidal and toroidal directions. In this sense, an infinite number of classes of topological kinks and brochosons could arise on the torus. In light of the impossibility to characterise the topological sector of a kink only by the initial and final points on the torus, the notion of topological cluster has been introduced, grouping an infinite number of topological sectors that share initial and final points in the same topological cluster. In this manner, the notion of topological sector is extended.

Two rich families of potentials with different number of vacua distributed on the torus has been presented. These models exhibit, on one hand, singular kinks asymptotically connecting vacua and, on the other, families of kinks replicated in the $|4n_1n_2|$ regions delimited by precisely these singular kinks. Notice that there is not a one-to-one correspondence between potentials and number of vacua. Indeed, different combinations of n_1 and n_2 will correspond to the same number of vacua $|4n_1n_2|$ in both families of Sigma models. In light of this multiplicity of potentials, only a few representative cases will be presented for each family of Sigma models.

For the first family of potentials, three cases have been chosen for different values of n_1 and n_2, which in turn determine the number of vacua in the model as well as their position on the torus. Models with eight, four and two vacua have been considered. While the explicit expressions for the field profiles of the singular kinks are available, those of the families are not. However, the orbit equation for these families can be integrated as it has been shown in the cases described above.

The spectral analysis of the second order small kink fluctuation operator for every singular kink in our cases reveals their linear stability. On the other hand, the absence of points along the orbits of families of kinks where the flow is undefined makes these families also linearly stable. All the kinks found in the first two cases, singular kinks and members of the families, are topological. However, in Case 3 non-topological kinks are also found. Indeed, half of the singular kinks and all the families of kinks are non-topological in this last case. This represents another example where the topology of the target space prevents non-topological kinks from decaying to the vacuum due to the non-contractibility of these loops.

The identification of these brochosons on the torus has only been possible for the case with two vacua. As mentioned before, no further reduction of the number of vacua can be made, as the periodicity of the potential would be lost otherwise. Unfortunately, this excludes models with only one vacuum point, where every kink on the torus would be forced to be non-topological. This leads us to propose a second family of potentials on the torus, hoping that this situation can be obtained.

The second family of potentials for Sigma models on the torus $(\mathbb{S}^1 \times \mathbb{S}^1)$, presented in the second part of this chapter, is constructed from a family of separable

superpotentials such that a model with only one vacuum point can be found. The fact that the superpotential is separable has a direct consequence. There exist two non-equivalent superpotentials that minimise the static energy. This allows two different one-parameter families of kinks to emerge, except for cases with two or one vacua where only one arises. Moreover, the superpotentials with which the Bogomol'nyi arrangement can be performed have the same minimum level of energy. This implies in turn that the stability of these kinks is ensured given the smoothness of the superpotential. Nevertheless, given the existence of families of kinks, two zero modes would be expected to appear in the spectral analysis of the Hessian operator for these solutions.

The kink variety of models that belong to this second family of Sigma models with four, two and only one minima is thoroughly studied. A different number of singular kinks, those with either θ or φ constant, are obtained in each model. Their energies can be modulated by parameters m_1 and m_2, instead of just the parameter m in the first part of the chapter. While the energy density profiles of all singular Θ_K-kinks are indistinguishable in every model, $|n_1|$ and $|n_1|+1$ types of energy density profiles appear in each model for Φ_K-kinks when n_1 is even and odd respectively. In particular, three types of singular kinks are obtained in the first two cases while only two in the last two. These extra profiles appear as a result of the asymmetry by construction between toroidal and poloidal coordinates. Indeed, exterior and interior Φ_K-kinks in the first two cases, unlike Θ_K-kinks, describe curves with different length. When only one toroidal singular kink can appear, as is the case with Cases 3 and 4, these extra profiles disappear.

Apart from these singular kinks, one-parameter families of kinks are found in each model, whose energies are simultaneously modulated by both m_1 and m_2. A similar scenario was found for the first family of models, where the energy was modulated by the parameter m. In fact, the energy of all members of all families of kinks in both scenarios comply with rules of sum with respect the energies of the singular kinks. Indeed, different limit members of these families coincide with combinations of singular kinks. It is worth noting that in the second part of the chapter the explicit field profiles of the members of the families of kinks can be analytically derived. This allows us in turn to find the energy density profile of not only the singular kinks, but also any member of the families of kinks, where limits of the families can be clearly identified as combinations of singular kinks.

On the other hand, it is worth highlighting that even if in the first family of models the different regions where the kink variety is replicated is divided by the symmetries of the potential, in the second one it is a combination of these and the symmetries that relate solutions of the Bogomol'nyi equations for the four different superpotentials. This identification of solutions from different superpotentials affects both to singular and members of the families. However, only in the first case with four minima these transformations change the topological cluster of the solution.

In particular, for the second family of models, only topological kinks are found in the model of four minima (Case 1), four singular kinks and two families of kinks replicated in the four regions of the torus. This was expected given that the superpotential is periodic on the torus in this case. However, models with two or one minima do admit non-topological kinks since the superpotential is not periodic on the torus. In Cases 2 and 3 with two minima topological and non-topological kinks coexist. Two topological and two non-topological kinks and one family of topological

kinks are found in both regions of the torus. In Case 4, with only one minimum and one region, all kinks are forced to be non-topological. Two non-topological singular kinks and one family of non-topological kinks are identified. Interestingly, all the non-topological kinks that have been identified in these models are brochosons, as no non-topological kink is contractible to a point. Lastly, it is of note that in all these models kinks revolve at most once around each poloidal and toroidal directions. It would be interesting to explore different models where this scarcity of topological sectors is averted.

Chapter 5

Deformation methods for non-linear Sigma models

In last chapters several kinks have been identified in non-linear Sigma models on Riemannian manifolds. This was possible due to the form of the considered potentials, which allows the Bogomol'nyi arrangement. Given a coordinate chart on a target manifold, when an appropriately selected form of the superpotential is employed, it becomes possible to construct models with interesting analytical solutions. An alternative method for constructing models with available analytical solutions involves the transformation of a known solution, leading to another model for which the transformed solution is a solution. For example, Bäcklund transformations in the early 1970s were employed by Zakharov and Mikhailov for this purpose while preserving the integrability properties. Another example is the methods of deformation developed by Bazeia et al. during the decade of the 2000s [3–5, 7, 21, 32, 34–39, 50, 53, 55], for which a plethora of applications in physics have been found. This procedure focuses on manipulating Bogomol'nyi equations to derive other first order differential equations that correspond to the Bogomol'nyi equations of other field theories.

In this chapter, the procedure of deformation of Bazeia et al. will be generalised by presenting a new formalism of deformation. While reproducing the particular framework of Bazeia et al., it will extend its application to non-linear Sigma models on Riemannian manifolds. In particular, the procedure of deforming a given kink will be comprised of three steps. First, a kink profile of the original model will be manipulated to express it in terms of a parametrised curve on the target manifold. This will allow us to construct what shall be referred to as a kink diagram. Secondly, from this curve another parametrised curve in another target manifold will be constructed. Points of the orbit of both the original and deformed curve will be related by a map between these Riemannian manifolds and a possible reparametrisation in the new curve will be included. This will define a deformation diagram, which will transform a kink diagram into another diagram. Lastly, in order to make the resulting diagram a kink diagram, it must correspond to that of an actual kink of a Sigma model. In particular, deformations between models whose potentials admit the Bogomol'nyi arrangement will be considered. This will lead to a compatibility condition between the original and deformed superpotentials.

This method will be first illustrated by presenting simple examples, showing how this formalism contains deformations for Euclidean spaces that are equivalent to those of Bazeia et al. Moreover, deformations between different Riemannian

manifolds will be considered. Specifically, deformations between Sigma models on the plane, sphere and torus will be sought. Finally, the possibility of deformations between non-linear Sigma models with target manifolds of different dimensions is explored.

5.1 Kink diagrams

Kinks are finite-energy solutions of field theories whose energy density profiles travel at constant velocity and without losing their form. This type of solutions is sought by imposing the ansatz $\phi^i(\gamma(x-vt))$ for a velocity v on each kink profile $i = 1,\dots,\dim M$, where M denotes the target manifold of the Sigma model. Equivalently, static solutions can be sought, as a boost will set such a solution it into motion. Notice that field profiles of this type $\phi^i(\gamma(x-vt))$ send to the same real number every point in the line defined by $x-vt=c$ for a constant $c\in\mathbb{R}$. In other words, the field $\phi:\mathbb{R}^{1,1}\to M$ will assign to all points that belong to the line $x-vt=c$ in Minkowski space $\mathbb{R}^{1,1}$ the same point in M, see Figure 5.1.

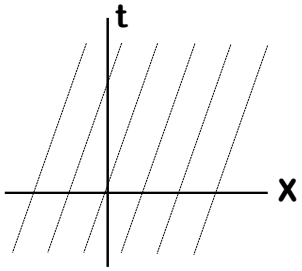

Figure 5.1: Different values of the velocity v define lines of different slopes with same value of the field $\phi^i(\gamma(x-vt))$.

Therefore, it suffices to specify for only one point in each line the point of M that is being mapped to. In this sense, a perpendicular line to this collection of parallel lines can be drawn and used as representative where ϕ is applied. Clearly, when $v=0$ these lines are vertical and the spatial line can act as representative. Of course, this is encoded in the mechanical analogy seen in previous chapters. Indeed, this ansatz is transformed into the static condition when a particular boost is applied.

As previously indicated, the first step in this formalism of deformation is to express the field $\phi:\mathbb{R}^{1,1}\to M$ of the chosen kink in terms of a curve $s:\mathbb{R}\to M$ on M. The use of the ansatz allows us to work with the representative line instead of all Minkowski space $\mathbb{R}^{1,1}$. Therefore, this line can be used to parametrise curves on M. Moreover, an intermediate transformation can be performed in this line. In summary, a kink $(\phi^1(\gamma(x-vt)),\dots,\phi^m(\gamma(x-vt)))$ with $m=\dim M$ of a Sigma model on M will be decomposed into the following three maps:

- **Ansatz condition**: Kinks must be of the form $\phi(\gamma(x-vt))$ by construction. Accordingly, let us introduce the following map

$$\begin{array}{rccc}\varphi_v: & \mathbb{R}^{1,1} & \longrightarrow & \mathbb{R} \\ & (t,x) & \longmapsto & \varphi=\gamma(x-vt)\end{array}$$

  where $\gamma=\frac{1}{\sqrt{1-v^2}}$.

- **Reparametrisation**: For the sake of convenience, let us introduce an intermediate reparametrisation

$$\begin{array}{rccc} T_c\colon & \mathbb{R} & \longrightarrow & \mathbb{R} \\ & \varphi & \longmapsto & T = T_c(\varphi) \end{array}$$

  which must be admissible or piecewisely admissible. Note that when this map is the identity $T_c = Id_{\mathbb{R}}$ the unaltered chosen representative line in the Minkowski space is employed to parametrise the curve.

- **Curve on** M: Let us denote as $s : \mathbb{R} \to M$ a differentiable curve on the Riemannian manifold (M, g), which is the target manifold of the non-linear Sigma model.

This is, given a kink $\phi : \mathbb{R}^{1,1} \to M$ of a Sigma model on a Riemannian manifold (M, g), a *kink diagram* will be any commutative diagram of the form

$$\begin{array}{ccc} \mathbb{R}^{1,1} & \xrightarrow{\phi} & M \\ {\scriptstyle \varphi_v}\downarrow & & \uparrow{\scriptstyle s} \\ \mathbb{R} & \xrightarrow{T_c} & \mathbb{R} \end{array} \tag{5.1}$$

that is, in which $\phi = s \circ T_c \circ \varphi_v$. Taking coordinates on a chart $(U_M, \{\lambda^i_M\})$, the field profiles will satisfy

$$\phi^i(\gamma(x(p) - vt(p))) = \lambda^i_M \circ (s \circ T_c \circ \varphi_v)(p) \equiv s^i \circ T_c \circ \varphi_v(p)\,,$$

where $p \in \mathbb{R}^{1,1}$ and s^i denote the components of the curve s in the chosen coordinates. Notice that this decomposition is not unique. Let us see an example to illustrate this kink decomposition.

Kink diagrams of a kink of the ϕ^4-model

Let us consider the simplest case in which kinks can be obtained, which is the ϕ^4-model. In particular, let us consider a potential of the form

$$V = \frac{1}{2}\left(1 - \phi^2\right)^2\,,$$

for which the static solution $\phi(x) = \tanh(x - x_0)$ with $x_0 \in \mathbb{R}$ can be found as a particular case of the solutions derived in Chapter 1. Since in this example a time-independent kink has been chosen, the ansatz encoded in the map $\varphi = \varphi_0(t, x) = x$ corresponds to static solutions. Therefore, the spatial axis will parametrise curves. The following pairs of maps define three possible kink diagrams for this kink

- $T = T_c(\varphi) \equiv \varphi = x \qquad \text{and} \qquad s(T) \equiv \tanh(T - x_0)\,,$
- $T = T_c(\varphi) \equiv 2\varphi = 2x \quad \text{and} \qquad s(T) \equiv \tanh\left(\frac{T}{2} - x_0\right)\,,$
- $T = T_c(\varphi) \equiv \varphi^3 = x^3 \quad \text{and} \qquad s(T) \equiv \tanh\left(T^{\frac{1}{3}} - x_0\right)\,,$

as in all this cases the kink profile is recovered $\phi(x) = s(T_c(x)) = \tanh(x - x_0)$. Notice that even though only three kink diagrams have been presented, an infinite number of decompositions of kinks can be found.

5.2 Deformations between Riemannian target manifolds

The main idea behind this formalism of deformation is to transform a kink diagram into another so that the latter corresponds to a kink of another Sigma model. In order to achieve this, from the original curve a new curve will be generated on the target manifold of the new Sigma model. This will be accomplished by sending points of the original curve to the new target manifold by a map $F : M \to N$ between Riemannian manifolds (M, g) and (N, h). This map F, which will define the orbit of the deformed new curve, will receive the name of *distortion*. In the process, an admissible or piecewisely admissible reparametrisation $r : \mathbb{R} \to \mathbb{R}$ will be introduced. Thus, the new curve $\tilde{s} : \mathbb{R} \to N$ on N will be related to the original one $s : \mathbb{R} \to M$ as follows

$$\begin{array}{ccc} M & \xrightarrow{F} & N \\ \uparrow{\scriptstyle s} & & \uparrow{\scriptstyle \tilde{s}} \\ \mathbb{R} & \xrightarrow{r} & \mathbb{R} \end{array} \tag{5.2}$$

By definition of Riemannian manifold, in general the distortion F will require the use of charts on both manifolds M and N. Let us then consider two charts $(U_M, \{\lambda_M^i\})$ and $(U_N, \{\lambda_N^i\})$ on (M, g) and (N, h) respectively. This allows us to map points in one manifold to points in the other by identifying coordinates in both charts. Indeed, the identification by means of the differentiable map

$$F_c : \lambda_M(U_M) \subseteq \mathbb{R}^{dimM} \to F_c(\lambda_M(U_M)) \subseteq \mathbb{R}^{dimN}$$

closes the diagram

$$\begin{array}{ccc} U_M & \xrightarrow{\lambda_M} & \lambda_M(U_M) \subseteq \mathbb{R}^{dimM} \\ \downarrow{\scriptstyle F} & & \downarrow{\scriptstyle F_c} \\ U_N & \xleftarrow[\lambda_N^{-1}]{} & F_c(\lambda_M(U_M)) \subseteq \mathbb{R}^{dimN} \end{array}$$

where $F_c(\lambda_M(U_M)) \subseteq \lambda_N(U_N)$. This is, the image of F_c must be well-defined as coordinates on the chart $(U_N, \{\lambda_N^i\})$. Furthermore, for the sake of convenience, F_c will be defined so that each F_c^i with $i = 1, \ldots, \dim N$ is invertible or piecewisely invertible. Thus, the distortion is defined in terms of this map F_c between vector spaces

$$F = \lambda_N^{-1} \circ F_c \circ \lambda_M \, .$$

In this formalism Sigma models that admit the Bogomol'nyi arrangement will be deformed into others that also admit the Bogomol'nyi arrangement. Since Bogomol'nyi equations describe a gradient system, the behaviour of the tangent vector fields to the deformed curve will be essential. Moreover, the same parametrisation of the deformed curve $\tilde{s}$ will be employed for its tangent vector field. These two maps, F and r, completely define the transference of the parametrised curve $s : \mathbb{R} \to M$ to the other manifold $\tilde{s} : \mathbb{R} \to N$ and its new parametrisation. Let us denote

as $\tilde{T} = r(T)$ the parameter of the deformed curve $\tilde{s}$. By construction (5.2), the following identity holds by the commutativity of the diagram

$$\tilde{s}(\tilde{T}) = F(s(T))\,.$$

This implies that the vector field tangent to the transferred curve can be written, by making use of the chain rule, as follows

$$\frac{d\tilde{s}(\tilde{T})}{d\tilde{T}} = \frac{dT}{d\tilde{T}}\left(\frac{\partial F_c^1(\phi)}{d\phi^j}\bigg|_{s(T)}\frac{ds^j(T)}{dT},\ldots,\frac{\partial F_c^{dimN}(\phi)}{d\phi^j}\bigg|_{s(T)}\frac{ds^j(T)}{dT}\right), \tag{5.3}$$

where Einstein summation convention has been employed for $j = 1,\ldots,\dim M$.

It is worth noting that other orientations of arrows for the distortion and the reparametrisation could have been chosen in (5.2). When these arrows are invertible, the expressions written above can be recovered by considering the inverse of these maps. An interesting scenario appears when the orientation of any of these arrows is different from those represented above and only piecewise inverses exists. This will give rise to a multiplicity of deformed curves as we shall see later on.

Lastly, notice that the dimension of the target manifolds M and N are allowed to be different in general. Although deformations between Riemannian manifolds with different dimensions will be studied in this chapter, let us restrict for now to cases where these dimensions coincide.

5.2.1 Deformation diagrams

The above defined distortion and reparametrisation determine completely the transference of parametrised curves between two Riemannian manifolds. However, the new parametrised curve must be integrated in a kink diagram, so that it can correspond to a kink of a new Sigma model. Let a kink diagram (5.1) correspond to the kink $\phi(\gamma(x-vt))$ of a Sigma model on the Riemannian manifold (M,g). This kink diagram can be extended (5.2) by a distortion F and a reparametrisation r so that another diagram of the same form can be found as follows

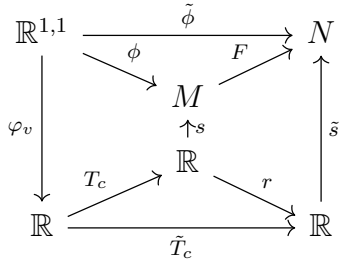

(5.4)

This is, a new reparametrtisation $\tilde{T}_c$, a new curve $\tilde{s}$ on N and a new orbit $\tilde{\phi}$ can be related to the original ones as follows

$$\tilde{\phi} = F\circ\phi\,,\qquad \tilde{T}_c = r\circ T_c\,,\qquad \tilde{s} = F\circ s\circ r^{-1}\,. \tag{5.5}$$

If this new diagram corresponds to a kink diagram, that is, if $\tilde{\phi}(\gamma(x-vt))$ is a kink of another non-linear Sigma model on the Riemannian manifold (N,h), then we shall say that the diagram above is a *deformation diagram*. Accordingly, we shall say that the new Sigma model on (N,h) is a deformation of the original model on (M,g). It

is important to highlight that an infinite number of models can be constructed from one single model as seed. In fact, each chosen kink of the original model may lead to a different deformed Sigma model in certain cases. On the other hand, notice that the reference frame of the deformed kink will be that of the original kink by construction. In particular, when a static kink is deformed, a new static kink will be obtained. In this static scenario, $\tilde{T}_c$ is just a reparametrisation of the spatial axis.

Note that to obtain the curve $\tilde{s}$ and its reparametrisation $\tilde{T}_c$, both the reparametrisation r and an inverse r^{-1} are required. Since the inverse of the reparametrisation r may be defined piecewisely, multiple parametrisations $\tilde{T}_c$ may emerge. Similarly, if the distortion is defined reversing the direction of the arrow of reference, multiple piecewise inverses F_α^{-1} may appear when the inverse is piecewisely defined. Therefore, multiple orbits $\tilde{\phi}_\alpha = \phi \circ F_\alpha^{-1}$ may also emerge. Consequently, the directions with which the arrows of the distortion and the reparamentrisation are defined are crucial in certain scenarios. The choice of direction of arrows for the distortion and reparametrisation of the diagram (5.4) will be taken as reference. We will say that a distortion or a reparametrisation is of type A if the arrow is defined in the same direction as in the reference diagram. Otherwise, we shall say it is of type B. Note that when deformations with both type B distortions and type B reparametrisation are considered, the deformation diagram can be inverted retrieving the original form

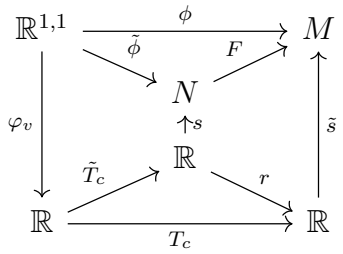

On the other hand, consecutive deformations can be performed. If both distortions and both reparametrisations share type, then arrows can be directly combined. If these do not coincide for distortions or for reparametrisations, then maps must be inverted until another deformation of the same type is obtained. Note that when in these cases piecewise inverses exist, multiple deformation diagram emerge. Let us assume that either both types coincide or the corresponding rearranged deformation diagram is being considered. Let us consider a kink $\phi(\gamma(x-vt))$ and a kink diagram for this kink. Moreover, let $(F_1 : M \to N, r_1)$ and $(F_2 : N \to Q, r_2)$ be two deformations of type (A, A) for Riemannian manifolds M, N and Q. The combination of both deformations diagrams can be written as follows

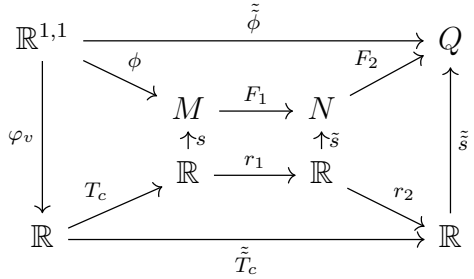

(5.6)

including a new reparametrisation $\tilde{\tilde{T}}_c$, a new curve $\tilde{\tilde{s}}$ and a new orbit $\tilde{\tilde{\phi}}$. Therefore, this diagram can be written as one deformation diagram of the form (5.4) by defining

the composition of distortions $F_3 = F_2 \circ F_1$ and that of reparametrisations $r_3 = r_2 \circ r_1$

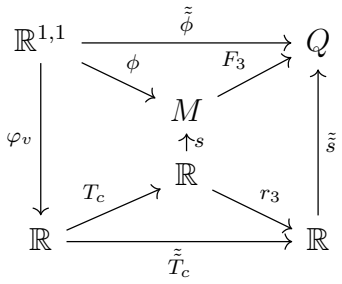

This is, similar relations as before are retrieved for the new orbit, the new reparametrisation and the new curve

$$\tilde{\tilde{\phi}} = F_3 \circ \phi, \qquad \tilde{\tilde{T}}_c = T_c \circ r_3, \qquad \tilde{\tilde{s}} = F_3 \circ s \circ r_3^{-1} .$$

This process has been shown for compositions of deformations of type (A, A). A similar result is obtained when both deformations are of types (A, B), (B, A) and (B, B). However, as has been stated, when their types are different, in order to combine these diagrams, arrows must be inverted. This implies that in cases where piecewise inverses arise, multiple deformation diagrams will emerge as combinations of the two original ones.

5.2.2 Compatibility conditions for deformations

Deformation diagrams have been introduced in last section so that new diagrams can be derived from a kink diagram. However, the objective is to extend it so that the new diagrams are kink diagrams. This is, so that these correspond to kink-like solutions of a new Sigma model. In this section conditions for such deformations between original and deformed models are derived.

As has been shown, the distortion F and the reparametrisation r introduced in the deformation diagrams (5.4) create a relation between the orbits of the original and deformed parametrised curves

$$\tilde{s}^i(\tilde{T}) = F_c^i(s(T)) \,, \tag{5.7}$$

for $i = 1, \ldots, \dim N$. Given that reparametrisations r are defined as invertible or piecewise invertible and therefore $r^{-1} \circ r = Id_{\mathbb{R}}$, the parameter $\tilde{T}$ can be employed to parametrise the original curve s in the above equation

$$\tilde{s}^i(\tilde{T}) = F_c^i(s(r^{-1}(\tilde{T}))) \,.$$

One possibility for constructing a new Sigma model for which this parametrised curve corresponds to a kink, is to employ the chain's rule and the relation between curves (5.7) to relate the original set of second order field equations on the Riemannian manifolds (M, g) to those on the new target Riemannian manifold (N, h)

$$\frac{d^2 s^i}{dT^2} + \Gamma^i_{jk}\left[s(T)\right] \frac{ds^j}{dT} \frac{ds^k}{dT} = g^{ik}\left[s(T)\right] \frac{\partial V}{\partial \phi^k}\left[s(T)\right] \,,$$
$$\frac{d^2 \tilde{s}^i}{d\tilde{T}^2} + \tilde{\Gamma}^i_{jk}\left[\tilde{s}(\tilde{T})\right] \frac{d\tilde{s}^j}{d\tilde{T}} \frac{d\tilde{s}^k}{d\tilde{T}} = h^{ik}\left[\tilde{s}(\tilde{T})\right] \frac{\partial \tilde{V}}{\partial \tilde{s}^k}\left[\tilde{s}(\tilde{T})\right] \,,$$

where indices k, j are summed, $\tilde{\Gamma}^i_{jk}$ are the Christoffel symbols in the chosen coordinates on a chart on N and V and $\tilde{V}$ are the original and deformed potential function respectively. When a potential function $\tilde{V}$ on N can be obtained by integrating these equations a new Sigma model is constructed. Although this establishes a compatibility condition to obtain a solution in the second Sigma model, special care has to be taken when choosing the distortion and reparametrisation. Indeed, our aim is obtaining a kink, not a general solution. Now, the integration of $\tilde{V}$ from these equations presents a formidable complexity, prompting the exploration of an alternative compatibility condition.

Instead of considering the general second order field equations, let us restrict the type of potential functions that are being considered in both the original and deformed Sigma models. In particular, let us consider only those for which the Bogomol'nyi arrangement can be performed. This implies that two superpotentials W and $\tilde{W}$ can be constructed so that parametrised curves s and $\tilde{s}$ satisfy respectively

$$\frac{ds}{dT} = (-1)^{\epsilon_1}\text{grad}_g W\,, \qquad \frac{d\tilde{s}}{d\tilde{T}} = (-1)^{\epsilon_2}\text{grad}_h \tilde{W}\,, \tag{5.8}$$

with $\epsilon_i = 0, 1$ and where gradients are defined on the Riemannian manifolds M and N respectively. Notice that the vector field tangent to the new curve has been fixed by the distortion and the reparametrisation (5.3). Let us write this expression for one coordinate

$$\frac{d\tilde{s}^i(\tilde{T})}{d\tilde{T}} = \frac{dT}{d\tilde{T}}\,\frac{\partial F^i_c(\phi)}{\partial \phi^j}\bigg|_{s(T)}\,\frac{ds^j(T)}{dT}\,, \tag{5.9}$$

where the index $j = 1, \ldots, dim M$ is summed. Even though deformations of type (A, A) have been considered to derive these equations, analogous expressions can be easily derive for the rest of cases. Now, when the Bogomol'nyi equations for both Sigma models are introduced in equation (5.9), the following compatibility condition between curves is obtained

$$\text{grad}_h \tilde{W}\left[\tilde{s}(\tilde{T})\right] = (-1)^{\epsilon}\frac{dT}{d\tilde{T}}\,\frac{\partial F_c(\phi)}{\partial \phi^j}\bigg|_{s(T)}\left[\text{grad}_g W\right]^j\left[s(T)\right]\,, \tag{5.10}$$

where $\epsilon = \epsilon_1 - \epsilon_2$. Note that these equations define relations between parameters T and $\tilde{T}$. In order to construct the new superpotential $\tilde{W}(\tilde{\phi})$, these parameters must be expressed in terms of fields $\tilde{\phi}^1, \ldots, \tilde{\phi}^{\text{dim}N}$. Finding these dependences $T = T(\tilde{\phi})$ and $\phi = \phi(\tilde{\phi})$ is possible as both distortions F and reparametrisations r are defined as invertible or piecewisely invertible. In particular, from the distortion diagram follows natural choices for the parameters $T = T(\tilde{\phi})$ and $\tilde{T} = \tilde{T}(\tilde{\phi})$. Indeed, the following options appear

$$T = s_i^{-1}(F^{-1}(\tilde{\phi}))\,, \qquad \tilde{T} = \tilde{s}_j^{-1}(\tilde{\phi})\,,$$

for components of curves s_i and $\tilde{s}_j$ with $i = 1, \ldots, \text{dim}M$ and $j = 1, \ldots, \text{dim}N$. Notice that multiple dependencies arise as any of the coordinates i, j can me employed. Furthermore, these can be mixed so that a more complicated dependence appear in the compatibility condition. Let us see an example.

- **Example of different parameter substitutions**: Let us consider a kink in a field theory with target space $\mathbb{R}^2$ given by

$$(\phi^1(T), \phi^2(T)) = (\tanh(T), \tanh(T))\,,$$

with $T=\gamma(x-vt)$ and an associated curve for the kink diagram $(s^1(T),s^1(T))=(\tanh(T),\tanh(T))$. Let us consider now a deformation given by a simple distortion $\tilde{\phi}^i=F_c^i(\phi)\equiv 2\phi^i$ and a reparametrisation $\tilde{T}=r(T)=T^{\frac{1}{3}}$. This gives rise to the following deformed configuration

$$(\tilde{\phi}^1(\tilde{T}),\tilde{\phi}^2(\tilde{T}))=(2\tanh(\tilde{T}^3),2\tanh(\tilde{T}^3))\,.$$

The following are three of the infinite number of possibilities for the parameter T:

- $T(\tilde{\phi}^1)=\arctan\frac{\tilde{\phi}^1}{2}$
- $T(\tilde{\phi}^2)=\arctan\frac{\tilde{\phi}^2}{2}$
- $T(\tilde{\phi}^1,\tilde{\phi}^2)=a\arctan\frac{\tilde{\phi}^1}{2}+(1-a)\arctan\frac{\tilde{\phi}^2}{2}$ for any $a\in[0,1]$

while the following are three possibilities for the deformed parameter $\tilde{T}$:

- $\tilde{T}(\tilde{\phi}^1)=\left(\arctan\frac{\tilde{\phi}^1}{2}\right)^{\frac{1}{3}}$
- $\tilde{T}(\tilde{\phi}^2)=\left(\arctan\frac{\tilde{\phi}^2}{2}\right)^{\frac{1}{3}}$
- $\tilde{T}(\tilde{\phi}^1,\tilde{\phi}^2)=a\left(\arctan\frac{\tilde{\phi}^1}{2}\right)^{\frac{1}{3}}+(1-a)\left(\arctan\frac{\tilde{\phi}^2}{2}\right)^{\frac{1}{3}}$ for any $a\in[0,1]$

The dependencies for these parameters can be chosen so that the compatibility equations are decoupled, leading to an additive separable superpotential. More complicated forms for the parameter may give rise to more interesting superpotentials. However, the dependencies must be taken cautiously, since the cross derivative condition to integrate the superpotential may not hold.

When the above compatibility condition between curves is expressed in terms of the new fields $\tilde{\phi}^j$, condition (5.10) produces a set of first order differential equations for the new superpotential

$$\mathrm{grad}_h\tilde{W}\left[\tilde{\phi}\right]=(-1)^{\epsilon}\frac{dT}{d\tilde{T}}\left[\tilde{\phi}\right]\frac{\partial F_c(\phi)}{\partial\phi^j}\left[\tilde{\phi}\right]\left[\mathrm{grad}_g W\right]^j\left[\tilde{\phi}\right]\,. \tag{5.11}$$

It is worth noting that this compatibility condition is imposed on the superpotential instead of directly on the potentials. In addition, if the explicit form of the kink is employed to obtain equation (5.11), the deformed model will only admit this particular deformed kink. Hence, in these scenario this mechanism of deformation will be seed-dependent. This can be avoided in certain cases as we shall see. Now, once a solution $\tilde{W}$ of these equations is obtained, the potential $\tilde{V}$ of the deformed Sigma model can be constructed

$$\tilde{V}(\tilde{\phi})=\frac{1}{2}h\left(\mathrm{grad}_h\tilde{W},\mathrm{grad}_h\tilde{W}\right)\,. \tag{5.12}$$

The Sigma model on the new Riemannian manifold (N,h) given by this potential function will support $\tilde{s}=F\circ s\circ r^{-1}$ with parameter $\tilde{T}$ on N as a solution curve. Therefore, configuration $\tilde{\phi}(p)=\tilde{s}(\tilde{T}(p))$ for $p\in\mathbb{R}^{1,1}$ will be a kink of this Sigma

model. Furthermore, by construction this solution is analytically available as it is related to that of the original model as

$$\tilde{\phi}(p) = F(s(T(p))) = F(s(r^{-1}(\tilde{T}(p)))) \,.$$

In summary, this procedure deforms kinks into kinks as the energy of the deformed configuration is finite. Indeed, the asymptotic conditions are guaranteed by the fact that Bogomol'nyi equations is a gradient system (5.8). Lastly, even if only the case with $(A, A)-$type deformations has been presented, the procedure for other types are similar. Let us now examine some simple examples of deformations through pure distortions and pure reparametrisations.

5.3 Deformations by pure distortions

As demonstrated in last section, deformations can be accomplished via several approaches. In this section deformations without reparametrisation, i.e. $r = Id_{\mathbb{R}}$, will be explored. This is, pure distortions will be considered. Let us first consider deformations where the distortions are of type A. The deformation diagram of a deformation of this type is of the following form

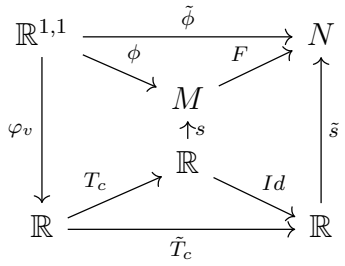

As a particular case of the general procedure described in last section, the compatibility condition (5.11) reads for pure distortions of type A as

$$\left(\text{grad } \tilde{W}\right)^i = \frac{\partial F_c^i}{\partial \phi^j} \left(\text{grad } W\right)^j \,. \tag{5.13}$$

where Einstein summation convention is employed for the index $j = 1, \ldots, \dim M$. Every superpotential $\tilde{W}$ solution of these compatibility equations defines by equation (5.12) a potential, which in this case reads in coordinates as

$$\tilde{V}(\tilde{\phi}) = \frac{1}{2}\left(h_{mn} g^{la} g^{pb} \frac{\partial F_c^m}{\partial \phi^l} \frac{\partial F_c^n}{\partial \phi^p}\right)\left[\tilde{\phi}\right] \frac{\partial W}{\partial \phi^a}\left[\tilde{\phi}\right] \frac{\partial W}{\partial \phi^a}\left[\tilde{\phi}\right] \tag{5.14}$$

$$\equiv \frac{1}{2} G^{ab}[\tilde{\phi}] \, \frac{\partial W}{\partial \phi^a}\left[\tilde{\phi}\right] \frac{\partial W}{\partial \phi^a}\left[\tilde{\phi}\right] \,, \tag{5.15}$$

where again indices are summed. Notice that when the deformation is distortionless, that is $M = N$, $F_c = Id_{\mathbb{R}^{dim M}}$ and the same charts are used, then $\tilde{\phi} = \phi$, $G^{ab}[\tilde{\phi}] = g^{ab}[\phi] = h^{ab}[\phi]$ and the original potential is recovered $\tilde{V}(\tilde{\phi}) = V(\phi)$ as it was expected. On the other hand, when distortions of type B are considered, an analogue condition can be derived. The arrow of F is in the reverse direction

compared to that of case A. This is, the deformation diagram is of the form

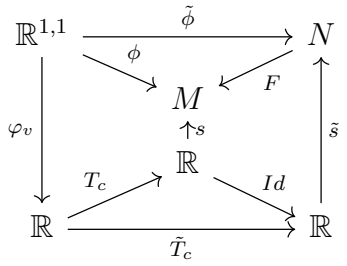

While this deformation diagram is equivalent to that of case A when F is invertible, when piecewise inverses appear this procedure of transference may fragment the original curve in the process. Indeed, in these cases the deformed curve may be transformed into different curves $\tilde{s} = F^{-1} \circ s$. If this relation is written as $F \circ \tilde{s} = s$ and the derivative respect to the deformed parameter is taken, a similar procedure leads to the analogue compatibility condition

$$\frac{\partial F^i}{\partial \tilde{\phi}^j} \left(grad\, \tilde{W} \right)^j = (grad\, W)^i \,, \qquad i = 1, \ldots, \dim N \,, \tag{5.16}$$

where once more the index j is summed $j = 1, \ldots, \dim N$. Superpotentials that are solutions of these equation will define Sigma models (5.12) for which the curve $\tilde{s} = F^{-1} \circ s$ is a kink. Lastly, it should be noted that the form of the kink which is being deformed does not intervene in the process. The deformed model is completely determined by the distortion and therefore every kink will be transferred to the new Sigma model. Let us see simple examples of each type to illustrate this procedure of pure distortion deformations.

5.3.1 Pure distortion of type A of the ϕ^4-model

Let us deform one the simplest models in which kinks can be identified, specifically, the ϕ^4-model with a single field. In particular, let us consider first a pure distortion of type A. The potential of the ϕ^4-model, which is usually written as follows

$$V = \frac{1}{2} \sum_i^n (\phi_i^2 - 1)^2 \,,$$

admits the superpotential $W = \phi - \frac{\phi^3}{3}$. Let us deform the kink that corresponds to the curve $s(T) = \tanh T$ with $T_c = Id_{\mathbb{R}}$. That is, the kink that corresponds to the kink diagram

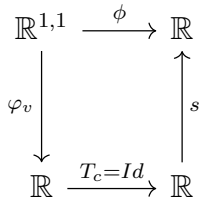

As anticipated, this kink will be deformed without introducing any reparametrisation i.e. $r = Id_{\mathbb{R}}$ and with a distortion of type A. This leads to the following deformation

diagram

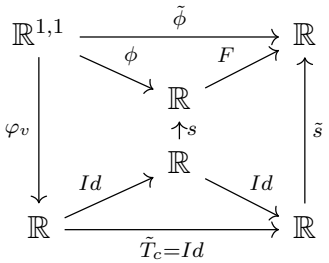

For the sake of simplicity, let us also consider a distortion of the form $\tilde{\phi} = F_c(\phi) \equiv \phi^3$. The compatibility condition for this particular case (5.13) produces an ordinary first order differential equation for the deformed superpotential

$$\frac{d\tilde{W}}{d\tilde{\phi}} = \pm \frac{dF_c(\phi)}{d\phi} \frac{dW(\phi)}{d\phi} = \pm 3\ \phi^2(1-\phi^2) = \pm 3\ \tilde{\phi}^{2/3}\left(1-\tilde{\phi}^{2/3}\right)\,,$$

which can be easily integrated, resulting in non-polynomial superpotential. Therefore, this superpotential $\tilde{W}$ exists and a Sigma model with non-polynomial potential function can be constructed

$$\tilde{V}(\tilde{\phi}) = \frac{9}{2}\left(\sqrt[3]{\tilde{\phi}^2}-1\right)^2 \sqrt[3]{\tilde{\phi}^4}\,.$$

Notice that this potential function, unlike the original one, presents an extra vacuum point at the origin $\tilde{\phi} = 0$, see Figure 5.2.

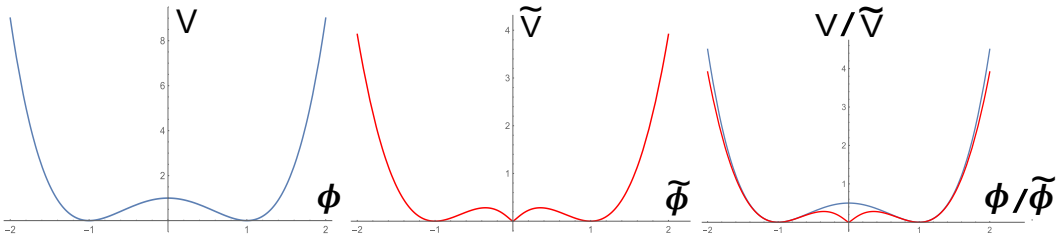

Figure 5.2: Comparison between the original potential function and the deformed one. It is worth highlighting how a new vacuum point emerges in the origin.

However, the deformed kink, which is a solution of this Sigma model

$$\tilde{\phi}(\tilde{T}) = F_c(\phi(T(\tilde{T}))) = \tanh^3 \tilde{T}\,,$$

asymptotically connects the vacua located at $\tilde{\phi} = \pm 1$, crossing an intermediate vacuum point without stopping, see Figure 5.3. This is due to the fact that, while this new potential is C^1-differentiable at the origin, it is not C^2. On the other hand, because of the choice of distortion, the energy of the deformed kink is less energetic than the original

$$E[\tilde{\phi}] = \frac{36}{35} < \frac{4}{3} = E[\phi]\,.$$

Lastly, even though this particular deformed model is new, this type of deformed models where the potential is non-polynomial has also been studied by Bazeia et al [37].

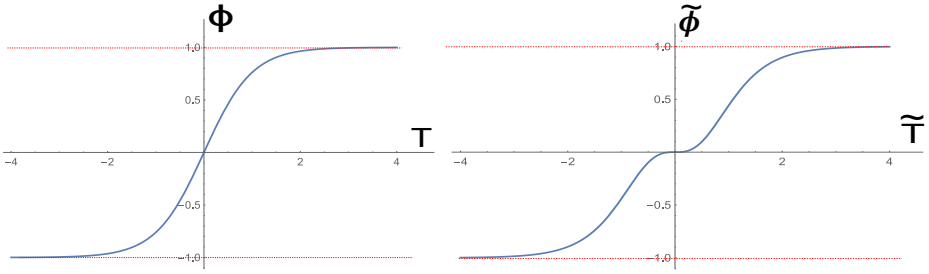

Figure 5.3: Original and deformed profiles respectively. Notice how the derivative of the deformed profile vanishes at the origin, but instead of remaining at that point it continues to the next vacuum point.

5.3.2 Pure distortion of type B of the ϕ^4-model

In last section an example of deformation via a pure distortion of type A was presented. In this section an example for the remaining case where the distortion is type B is shown. For convenience, let us apply this procedure by pure distortion type B once again to the ϕ^4-model, in particular to the kink $\phi(T) = \tanh T$. This implies, by definition, that the arrow of the distortion will be directed in the opposite direction in the deformation diagram

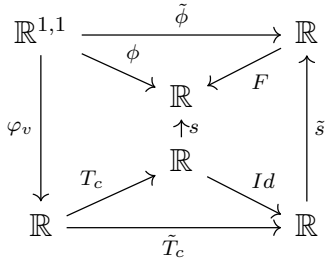

Moreover, in order to split the deformed curve into pieces, a distortion with piecewise inverses will be imposed. In particular, the function $\phi = F_c(\tilde{\phi}) \equiv \tilde{\phi}^2 - 1$ will be chosen. Indeed, two piecewise inverses appear $\tilde{\phi} = \pm\sqrt{1+\phi}$. Thus, two deformed curves will be generated in the transference instead of just one

$$\tilde{s}(T) = F^{-1}(s(T)) = \pm\sqrt{1+\tanh T}\,.$$

Notice that these two configurations connect asymptotically $\tilde{\phi} = 0$ to the value $\tilde{\phi} = -\sqrt{2}$ or the value $\tilde{\phi} = \sqrt{2}$, see Figure 5.4.

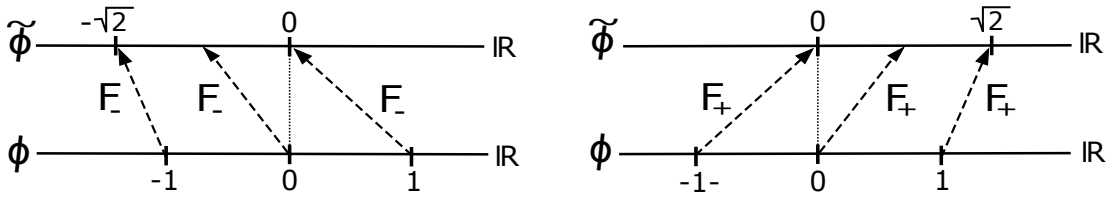

Figure 5.4: The orbit of the original kink is split into two orbits in the transference to the new Sigma model due to the existence of piecewise inverses of the distortion.

There are two approaches for performing this deformation. One as an $A-$type distortion, involving one of the piecewise inverses (5.13), and the other as a $B-$type

distortion (5.16). Both approaches result in the same superpotential

$$\frac{d\tilde{W}}{d\tilde{\phi}} = \pm\frac{1}{2}\tilde{\phi}\left(2-\tilde{\phi}^2\right) \qquad \Rightarrow \qquad \tilde{W} = \frac{\tilde{\phi}^2}{8}\left(4-\tilde{\phi}^2\right),$$

where the equivalent negative superpotential could have been also considered and where the irrelevant constant of integration has been set to zero. The fact that both the asymptotic limits of the field profile and the form of the superpotential are now different, implies that the energy of the deformed kink may differ from that of the original. In fact, computing its energy from the difference of superpotential at both asymptotic limits, it becomes apparent that the deformed kinks are less energetic than the original

$$E[\tilde{\phi}] = \frac{1}{2} < \frac{4}{3} = E[\phi]\,.$$

Of course, the energy of these kinks can be modulated by introducing a parameter in the distortion as can be easily checked. Now, this deformed superpotential leads to the potential function

$$\tilde{V}(\tilde{\phi}) = \frac{1}{8}\sum_{i=1}^{n}\tilde{\phi}^2\left(2-\tilde{\phi}^2\right)^2,$$

which corresponds to a ϕ^6-model where an extra vacuum has emerged at the origin, see Figure 5.5. Indeed, this was expected as the new kink orbits tend asymptotically to zero at one of the ends.

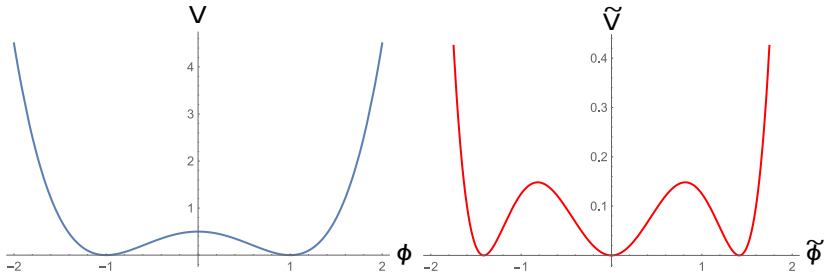

Figure 5.5: Original ϕ^4-model potential and deformed potential. An extra vacuum point appears in the origin in this new potential, which corresponds to that of a ϕ^6-model.

Even though the form of the potential is similar to that of the previous section, the deformed kinks of this model do not cross any vacua. The reason behind this difference in behaviour is the fact that in this case the deformed potential is C^∞. It is worth noting that this procedure can be easily generalised considering distortions with an arbitrary number of piecewise inverses. This would split kink orbits into more pieces, creating more vacua and therefore more topological sectors. Lastly, it should be stressed that this formalism is able to reproduce the deformations introduced by Bazeia et al [37], where deformations of this type are considered.

5.3.3 Deformation of families of kinks

When the explicit field profiles of a kink in a Sigma model are not available, integrating the orbit equations provides valuable insights into the behaviour of solutions.

In this section, an alternative method for deformations through pure distortion is introduced. Specifically, a new orbit equation is derived from the original by a distortion of type B. This is, instead of employing a particular kink as seed for the deformation, a whole family of kinks will be deformed into families of kinks of a new Sigma model. Let us consider a Sigma model on a Riemannian manifold (M, g) and a family of kinks given by the orbit equation $O_M(\phi^1, \ldots, \phi^m) = C$, where C is a constant that distinguishes between members of this family. Let us consider then a pure distortion as a deformation into a new Riemannian manifold (N, h). The upper part of the deformation diagram will contain the information about the transformations of orbits of curves

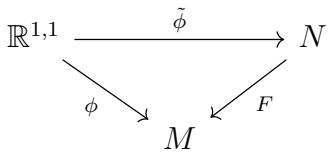

This is, the relation between points in both manifolds can be written as $\phi = F(\tilde{\phi})$. Substituting this relation into the orbit equation on M allows us to transfer to N all members of this family of curves

$$O_N(\tilde{\phi}^1, \ldots, \tilde{\phi}^{dimN}) \equiv O_M(\phi^1(\tilde{\phi}), \ldots, \phi^{dimM}(\tilde{\phi})) = C\,. \tag{5.17}$$

On one hand, the distortion F must be defined so that members of this new family of curves on (N, h) have a kink-like behaviour. On the other, in order to obtain kinks, a Sigma model on (N, h) must be constructed so that the orbit flow equation provides solutions that can be identified with (5.17). If this field theory can be found, then the complete deformation diagram can be constructed

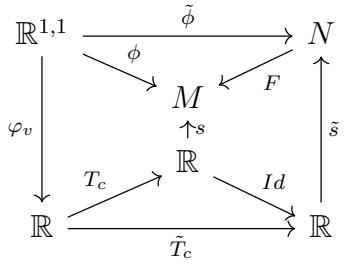

and the kink profile of each member will have the dependence $\tilde{\phi}(\tilde{T})$. Taking derivatives respect to this parameter $\tilde{T}$ in the new orbit equation O_N the following condition is derived

$$\frac{dO_N}{d\tilde{T}} = \frac{\partial O_N}{\partial \tilde{\phi}^i}\frac{d\tilde{\phi}^i}{d\tilde{T}} = 0\,,$$

where Einstein summation convention is employed. Furthermore, let us restrict to Sigma models where the Bogomol'nyi arrangement can be performed. Thus, Bogomol'nyi equations enables us to transform the above condition into a first order differential equation in partial derivatives for the superpotential $\tilde{W}$

$$\sum_{i,j} \frac{\partial O_N}{\partial \tilde{\phi}^i} h^{ij} \frac{\partial \tilde{W}}{\partial \tilde{\phi}^j} = 0\,. \tag{5.18}$$

Once more, if a superpotential $\tilde{W}$ is found so that the equation above holds, then the distortion of the original orbit $\tilde{\phi} = F^{-1} \circ \phi$ is a solution of the Sigma model on (N, h) with potential function

$$\tilde{V} = \frac{1}{2} h(grad\ \tilde{W}, grad\ \tilde{W}) \,.$$

Example of deformation of a family of kinks

Let us illustrate this type of deformation with an example where a model on the plane is deformed into another model also on the plane. In particular, the double ϕ^4-model given by the following potential

$$V(\phi^1, \phi^2) = \frac{1}{2}\left(1 - \phi_1^2\right)^2 + \frac{1}{2}\left(1 - \phi_2^2\right)^2$$

will be deformed. This potential admits a Bogomol'nyi arrangement as has been previously shown. From Bogomol'nyi equations the orbit flow equation is obtained

$$\frac{d\phi^1}{d\phi^2} = \frac{1 - \phi_1^2}{1 - \phi_1^2} \,,$$

which produces an orbit equation of the form

$$O_M(\phi^1, \phi^2) \equiv \operatorname{arctanh} \phi^1 - \operatorname{arctanh} \phi^2 = \gamma \,,$$

where $\gamma \in \mathbb{R}$ is a constant of integration that labels every member of the family of kinks. Let us consider now a distortion of type B given by $\phi_i = F_i(\phi_1, \phi_2) \equiv \tilde{\phi}_i^2$ for $i = 1, 2$. This gives rise to the following orbit equation on the plane

$$O_N(\tilde{\phi}_1, \tilde{\phi}_2) \equiv \operatorname{arctanh} \tilde{\phi}_1^2 - \operatorname{arctanh} \tilde{\phi}_2^2 = \gamma \,,$$

whose orbits have been depicted and compared to those of the original model in Figure 5.6. Notice that the deformed orbits are related to the original ones by relation $\tilde{\phi}_i = F_i^{-1}(\phi) = \pm\sqrt{|\phi_i|}$. Consequently, since for this distortion of type B piecewise inverses appear, these transferred curves are split in the new model.

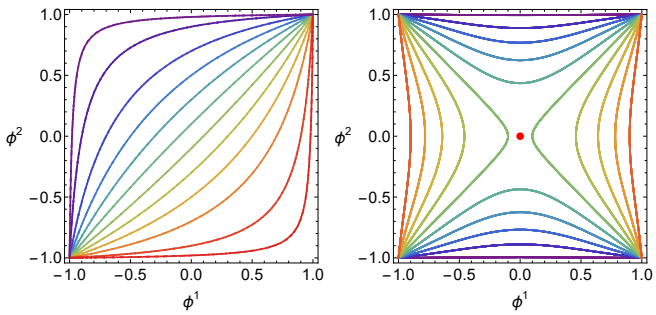

Figure 5.6: Orbits for the original family of kinks of the double ϕ^4-model and orbits for the deformed model on the plane. Notice that the deformed curves avoid the origin, now a singularity of the deformed potential.

This set of deformed solutions will be comprised of kinks if these are indeed solutions of a Sigma model on the plane. The equation that defines the superpotential of such model (5.18) reads in this case

$$\frac{2\tilde{\phi}_1}{1 - \tilde{\phi}_1^4}\frac{\partial \tilde{W}}{\partial \tilde{\phi}_1} - \frac{2\tilde{\phi}_2}{1 - \tilde{\phi}_2^4}\frac{\partial \tilde{W}}{\partial \tilde{\phi}_2} = 0 \,.$$

The simplest solution of these equations consists in the following superpotential

$$\tilde{W}(\tilde{\phi}_1, \tilde{\phi}_2) = \frac{1}{4}\left(\tilde{\phi}_1^4 + \tilde{\phi}_2^4 - \log \tilde{\phi}_1^4 \tilde{\phi}_2^4\right) ,$$

which leads to a potential function with a singularity in the origin and the same four vacua that were present in the original model

$$\tilde{V}(\tilde{\phi}_1, \tilde{\phi}_2) = \frac{1}{2}\left(\frac{1-\tilde{\phi}_1^4}{\tilde{\phi}_1}\right)^2 + \frac{1}{2}\left(\frac{1-\tilde{\phi}_2^4}{\tilde{\phi}_2}\right)^2 .$$

This emerging singularity "repels" solutions from the origin, completely altering the behaviour of the transferred kinks. It is worth highlighting the fact that this potential is independent of the parameter γ. While it is not difficult to find this scenario where it depends on γ, each parameter γ would define a particular potential that support a particular kink. Therefore, this situation must be avoided if the aim is to obtain a whole family of kinks.

5.4 Deformations by pure reparametrisations

The previous sections have primarily focused on examining straightforward examples of deformations achieved through pure distortions. In contrast, this section will delve into the remaining unexplored degree of freedom, i.e. the reparametrization. A distortionless deformation diagram of a kink diagram for a reparametrisation of type A takes the form

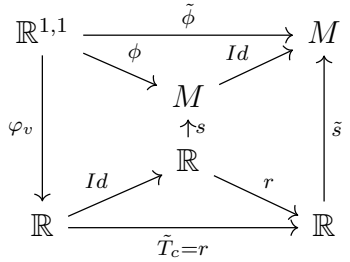

where M is the Riemannian target manifold of a Sigma model. Notice that this implies that the orbits of the transferred kinks will be identical to the original ones $\tilde{\phi} = \phi$. Now, the first order compatibility equation (5.11) without any distortion reads

$$grad_g\ \tilde{W} = (-1)^{\epsilon}\frac{dT}{d\tilde{T}}\ grad_g\ W\,.$$

One could impose a reparametrisation r so that the equation above can be transformed into an equation in terms of the deformed fields

$$\tilde{T}(\tilde{\phi}^1, \ldots, \tilde{\phi}^M) = r(s^{-1}(\tilde{\phi}))\,.$$

In general, this would lead to models that only support as inherited solution the deformed kink $\tilde{\phi}(\tilde{T})$ that the equation above defines. This is, this mechanism of deformation would be seed-dependent in general. Alternatively, instead of defining directly the reparametrisation r, for the sake of convenience let an auxiliary function $f : \mathcal{U}_M \subseteq M \to \mathbb{R}$ on M contain such information. In particular, since the image of the original curve $s(T)$ for any value of the parameter T is a point on M, the

evaluation of the function f at this point will be defined as the slope of the inverse of the reparamentrisation, this is

$$\frac{dT}{d\tilde{T}} \equiv f(\phi)|_{s(T)} \qquad \Rightarrow \qquad \tilde{T} = r(T) = \tilde{T}_0 + \int \frac{dT}{f(s(T))}\,.$$

The presence of zeroes in this function f will imply that the transference of curves will be performed piecewisely $\tilde{s} = s \circ r^{-1}$. The existence of plateaux in the above derivative expression will give rise to different topological sectors as we shall see. By definition, this reparametrisation can be written as a function of the coordinates ϕ on the manifold M

$$\frac{dT}{d\tilde{T}} \equiv f(s(T)) = f(\phi)\,. \tag{5.19}$$

which, due to the absence of distortion $\phi = \tilde{\phi}$, allows us to write the compatibility equation in terms of the deformed fields

$$grad_g\ \tilde{W} = \pm f(\tilde{\phi})\ \ (grad_g\ W)\,[\tilde{\phi}]\,. \tag{5.20}$$

When a solution superpotential $\tilde{W}$ can be found, the potential function can be constructed as follows

$$\tilde{V}(\tilde{\phi}) = \frac{1}{2} g\left(grad_g\ \tilde{W}, grad_g\ \tilde{W}\right) = f^2(\tilde{\phi})\ V(\tilde{\phi})\,,$$

where the square of the auxiliary function f appears as a global factor. This implies that zeroes of this function create new vacua in the deformed model, which will be asymptotically connected by kinks. Indeed, this global factor also appears in the new Bogomol'nyi equations

$$\frac{d\tilde{\phi}^i}{d\tilde{T}} = \pm f(\tilde{\phi}) g^{ij} \frac{\partial \tilde{W}}{\partial \tilde{\phi}^j}\,.$$

This alternative where the reparametrisation r is not directly defined is particularly useful for three reasons. The first one is that a proper choice of this function f can simplify the compatibility condition. Secondly, it also allows us to design the extra field profiles that shall emerge in the deformed model. Thirdly, the use of the auxiliary function avoids the need of introducing the particular form of the kink which is being deformed. Consequently, when this function is employed, the same deformed model is obtained regardless of the kink that is used as seed. Lastly, it must be stressed that this auxiliary function f that arises in this formalism of deformations by pure reparametrisations is equivalent to the deformation function employed by Bazeia et al, see for instance [32]. Let us see a simple example to illustrate this type of deformations.

5.4.1 Pure reparametrisation of type A of the ϕ^4-model

In order to exemplify this method of deformation, let us apply it to the ϕ^4-model. Similarly to previous cases, Bogomol'nyi decomposition generates a superpotential

$$V = \frac{1}{2}(1-\phi^2)^2 \qquad \Rightarrow \qquad \frac{dW}{d\phi} = \pm(1-\phi^2)\,,$$

from which solutions immediately follows. In particular, the kink that will be deformed is the one corresponding to the curve $s(T) = \tanh T$ and kink diagram

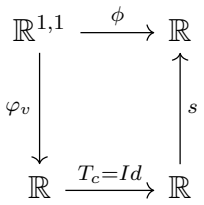

A distortionless deformation, i.e. $F = Id_{\mathbb{R}}$, with reparametrisation of type A will transform this kink diagram into another diagram as follows

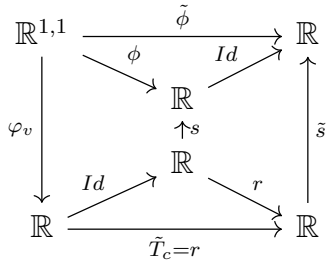

Let us choose a simple function $f(\phi)$ so that the compatibility equation can be analytically integrated. In fact, two functions will be considered simultaneously $f(\phi) = \pm\phi^2$, which will give rise to two different reparametrisations $r_\pm$

$$\frac{dT}{d\tilde{T}} = \pm\phi^2 = \pm\tanh^2(T) \qquad \Rightarrow \qquad \tilde{T} = \tilde{T}_0 \pm (T - \coth(T)) = r_\pm(T)\,.$$

Regardless of the sign introduced in the function f , the new parameter $\tilde{T}$ tends to infinity or minus infinity when it approaches the value $T = 0$, see Figure 5.7.

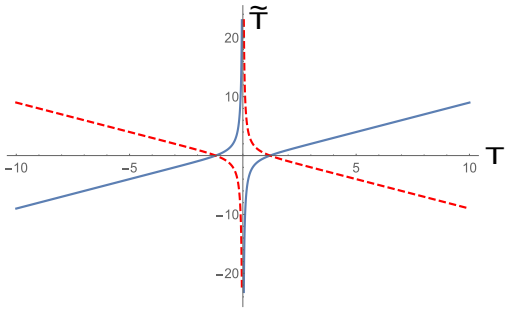

Figure 5.7: The reparametrisation $\tilde{T}(T)$ presents a singularity at $T = 0$. Inverting this function will result in two piecewise inverses, which split the deformed curve into two disjoint pieces. The reparametrisation with positive sign r_+ has been depicted in blue while the red dashed ones correspond to the negative sign r_-.

This implies that instead of reaching the image point $s(0)$, it will tend to it asymptotically at both sides of this singularity. As a consequence, two piecewise inverses of $r_\pm$ will appear and therefore two transferred curves will emerge

$$\tilde{s}(\tilde{T}) = s(r_\pm^{-1}(\tilde{T}))\,,$$

one for each sign in f. The image of one kink and its antikink correspond to $s((-\infty, 0]))$ while the image of the other kink and its antikink correspond to $s((0, \infty]))$.

On the other hand, the definition of the function $f(\phi)$ fixes the form of the new superpotential $\tilde{W}$. Indeed, the compatibility condition (5.20) demands the form of the superpotential

$$\frac{d\tilde{W}}{d\tilde{\phi}} = \tilde{\phi}^2 \frac{dW}{d\phi}[\phi(\tilde{\phi})] = \tilde{\phi}^2(1-\tilde{\phi}^2) \qquad \Rightarrow \qquad \tilde{W}(\tilde{\phi}) = \frac{\tilde{\phi}^3}{3} - \frac{\tilde{\phi}^5}{5}\,.$$

This superpotential, in turn, defines the potential function of the deformed model

$$\tilde{V}(\tilde{\phi}) = \frac{1}{2}\left(\frac{d\tilde{W}}{d\tilde{\phi}}\right)^2 = \frac{1}{2}\tilde{\phi}^4(1-\tilde{\phi}^2)^2\,,$$

which by construction includes a new zero at the origin, see Figure 5.8. This was expected, as the deformed curves tend asymptotically to the origin at one end, which is now a vacuum point in the deformed model.

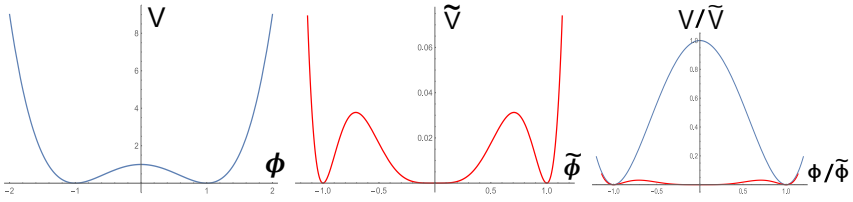

Figure 5.8: Potentials of the original and deformed models. In the process of deformation an extra vacuum point appears at the origin. Lastly, these two are simultaneously shown to compare their relative heights.

Note also that the height of the peaks of the deformed potential are considerably lower that those of the original model. However, these heights can be modulated by introducing a global parameter in the function f. On the other hand, since the new superpotential is different from the unaltered one, the energy of these new kinks must be calculated. Similarly to previous cases, the deformed kinks are less energetic

$$E[\tilde{\phi}] = \frac{4}{15} < \frac{4}{3} = E[\phi]\,.$$

However, introducing a modulating parameter in f would allow to control their energy as well. It is worth noticing that only one extra vacuum point has been introduced into the deformed potential in this section. Similarly to the case of pure distortions, this procedure can be generalised to include a higher number of vacua. Indeed, this can be easily accomplished by defining a function $f(\phi)$ with more zeroes.

Finally, it is worth noting that this deformed potential could also have been derived through pure distortion. If both superpotentials, the original and the deformed one, are introduced in the compatibility condition for pure distortions the following equation is obtained

$$\frac{d\tilde{\phi}}{d\phi}\frac{1}{(1-\tilde{\phi}^2)\tilde{\phi}^2} = \frac{1}{(1-\phi^2)} \qquad \Rightarrow \qquad \operatorname{arctanh}\,\tilde{\phi} - \frac{1}{\tilde{\phi}} = \pm \operatorname{arctanh}\,\phi\,.$$

Therefore, this deformation can also be performed by a pure distortion of type B given by the relation of coordinates

$$\phi = F_c(\tilde{\phi}) = \pm \tanh\left[C + \operatorname{arctanh}\,\tilde{\phi} - \frac{1}{\tilde{\phi}}\right].$$

Interestingly, this distortion presents a discontinuity at $\tilde{\phi} = 0$ but limits of the derivative from the left and from the right coincide at this point, see Figure 5.9. Fortunately, not the distortion $F_c(\tilde{\phi})$ but the square of its derivative $\left(F_c'(\tilde{\phi})\right)^2$ appears in the compatibility condition (5.13) and in the potential function (5.14). As a result, the deformed potential can also be found by this method and a new vacuum point appears when this derivative vanishes, that is, at the origin $\tilde{\phi} = 0$.

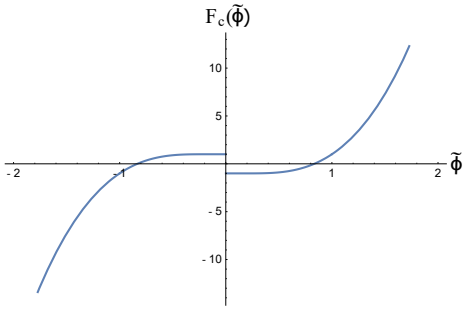

Figure 5.9: Distortion of type B equivalent to the deformation through reparametrisation shown in this section. Even though this function is discontinuous at the origin, the limit of its derivative from the left and from the right coincide.

5.5 Deformation from the plane to the sphere

Thus far, the target manifolds of both the original Sigma model and the deformed one were Euclidean spaces. In this section we shall go a step further and find examples of deformations that involve non-Euclidean Riemannian target manifolds. This, by definition of manifold, will require the choice of charts on each target manifold. As advanced, the first case that shall be considered is the deformation of Sigma models in the Euclidean plane into others in the two-dimensional sphere $\mathbb{S}^2$.

Let ϕ be a kink in a Sigma model in the plane and $s : \mathbb{R} \to \mathbb{R}^2$ be the curve employed for constructing its kink diagram. The deformation procedure to the sphere $\mathbb{S}^2$ that shall be employed in this section will involve both a distortion and a reparametrisation. This is, the deformation diagram will be of the form

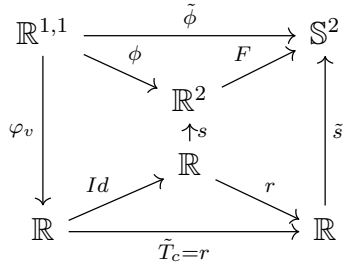

where for convenience both the distortion and reparametrisation have been chosen of type A. Cartesian coordinates $(\mathbb{R}^2, \{\phi^i\})$ with $i = 1, 2$ will be chosen for the plane, while stereographic coordinates $(U_{\mathbb{S}^2}, \{\psi^j\}))$ with $j = 1, 2$ will be employed for the sphere. In particular, the stereographic projection $P : U_{\mathbb{S}^2} = \mathbb{S}^2 - \{N\} \to \mathbb{R}^2$ from the north pole $N \equiv (0, 0, 1)$ onto the plane $Z = 0$ will be used, see Figure 5.10.

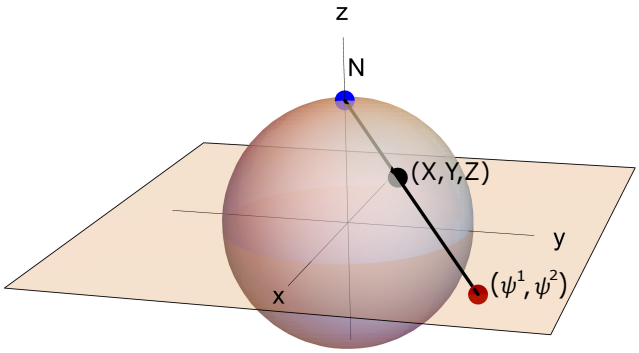

Figure 5.10: Stereographic projection that maps every point in $\mathbb{S}^2 - N$ to the plane.

This stereographic projection relates the coordinates on the sphere inherited by the ambient space $(\mathbb{R}^3, \{X, Y, Z\})$ to the new ones $P(X, Y, Z) = (\psi^1, \psi^2)$ as follows

$$\psi^1 = \frac{X}{1-Z}\,, \quad \psi^2 = \frac{Y}{1-Z}\,.$$

Conversely, these coordinates in the stereographic plane determine the coordinates of the sphere in the ambient space

$$(X, Y, Z) = \left(\frac{2\psi_1}{1+\psi_1^2+\psi_2^2}, \frac{2\psi_2}{1+\psi_1^2+\psi_2^2}, \frac{-1+\psi_1^2+\psi_2^2}{1+\psi_1^2+\psi_2^2}\right)\,.$$

In these coordinates the metric tensor is conformal to the Euclidean plane

$$g = \frac{4}{(1+\psi_1^2+\psi_2^2)^2}(d\psi^1 \otimes d\psi^1 + d\psi^2 \otimes d\psi^2)\,.$$

Notice that the global factor tends to zero as we approach infinities and reaches its maximum in this plane at the point that corresponds to the south pole, which in these coordinates is the origin $(\psi^1, \psi^2) = (0, 0)$. Given that the metric tensor is conformal to a plane, a global factor appears in the compatibility condition

$$g^{ii}\frac{\partial \tilde{W}}{\partial \psi^i} = \pm \frac{dT}{d\tilde{T}}\frac{\partial F_c^i(\phi)}{\partial \phi^j}\frac{\partial W(\phi)}{\partial \phi^j} \quad \Rightarrow \quad \frac{\partial \tilde{W}}{\partial \psi^i} = \pm \frac{4}{(1+\psi_1^2+\psi_2^2)^2}\frac{dT}{d\tilde{T}}\frac{\partial F_c^i(\phi)}{\partial \phi^j}\frac{\partial W(\phi)}{\partial \phi^j}\,.$$

While trying to integrate this equation to obtain a deformed superpotential $\tilde{W}$ is exceedingly challenging in general, it can be simplified significantly for certain choices of the reparametrisation. Pursuing the elimination of the global factor in the compatibility condition, the reparametrisation is defined using the components of the dual metric tensor as follows

$$\frac{dT}{d\tilde{T}} \equiv g^{ii}(F(s(T))) = \frac{(1+F_c^1(s(T))^2+F_c^2(s(T))^2)^2}{4}\,,$$

where the distortion F has been included. Note that $f(\phi) = g^{ii}(F(\phi))$ corresponds to the function (5.19). Thus, the integration of this equation defines the reparametrisation of the deformed kink

$$\tilde{T} = \tilde{T}_0 + \int \frac{4}{(1+F_c^1(s(T))^2+F_c^2(s(T))^2)^2} dT\,. \tag{5.21}$$

Similarly to the previous case, by construction this reparametrisation can be expressed as a function of the stereographic coordinates on the sphere

$$\frac{dT}{d\tilde{T}} = \frac{(1+F_c^1(\phi)^2+F_c^2(\phi)^2)^2}{4} = \frac{(1+\psi_1^2+\psi_2^2)^2}{4}\,. \tag{5.22}$$

The substitution of this factor greatly simplifies the compatibility equation, which now reads

$$\frac{\partial \tilde{W}}{\partial \psi^i} = \pm \frac{\partial F_c^i(\phi)}{\partial \phi^j}\,[\psi]\,\frac{\partial W(\phi)}{\partial \phi^j}\,[\psi] \qquad i=1,2\,.$$

If a superpotential that satisfies these two equations is found, then a potential for a Sigma model on the sphere can be constructed

$$\tilde{V} = \frac{(1+\psi_1^2+\psi_2^2)^2}{8}\sum_{i,j=1}^{2}\left(\frac{\partial F_c^i(\phi)}{\partial \phi^j}\,[\psi]\,\frac{\partial W(\phi)}{\partial \phi^j}\,[\psi]\right)^2\,, \tag{5.23}$$

so that the curve $\tilde{s} = F \circ s \circ r^{-1}$ is a solution. Once again, by this definition of reparametrisation, the potential of the deformed model will not depend on the kink that has been chosen as seed. However, by equation (5.22) the parametrisation of each kink will. Notice that if the distortion is just a global dilation, this is, it relates the coordinates of both charts as $\psi^i = F^i(\phi) \equiv a\,\phi^i$ with $a > 0$, then the superpotential reads

$$\tilde{W}(\psi) = a^2\; W\left(\frac{\psi}{a}\right) \tag{5.24}$$

and the potential function can be written in terms of the original potential in the plane as

$$\tilde{V} = a^2\frac{(1+\psi_1^2+\psi_2^2)^2}{8}V\left(\frac{\psi}{a}\right)\,. \tag{5.25}$$

The introduction of this parameter of the dilation a has another implication, as the energy of the deformed kinks will be modulated by its square a^2. Indeed, the asymptotic limits of the curves $\tilde{s}(\tilde{T})/a$ and $s(T)$ will be identical by the definition of distortion. Consequently, the energy of the deformed kinks will be controlled by this parameter a

$$\begin{aligned} E[\psi] &= \left|\lim_{\tilde{T}\to\infty}\tilde{W}(\tilde{s}(\tilde{T})) - \lim_{\tilde{T}\to-\infty}\tilde{W}(\tilde{s}(\tilde{T}))\right| \\ &= a^2\left|\lim_{\tilde{T}\to\infty} W\left(\frac{\tilde{s}(\tilde{T})}{a}\right) - \lim_{\tilde{T}\to-\infty} W\left(\frac{\tilde{s}(\tilde{T})}{a}\right)\right| \\ &= a^2\left|\lim_{T\to\infty} W(s(T)) - \lim_{T\to-\infty} W(s(T))\right| = a^2\; E[\phi]\,, \end{aligned} \tag{5.26}$$

which is higher than the original for $a > 1$ and lower for $0 < a < 1$. In particular when the deformation is distortionless, i.e. $a = 1$, the deformed potential is the original one multiplied by a non-vanishing global factor

$$\tilde{V} = \frac{(1+\psi_1^2+\psi_2^2)^2}{8}V\left(\psi\right)\,, \tag{5.27}$$

and the energies are identical $E[\phi] = E[\psi]$. In sum, in order to construct particular Sigma models on the sphere, on one hand the reparametrisation will be defined so

that it "absorbs" the curvature of the sphere. Indeed, the choice (5.22) leads to the same compatibility condition than the one that arises in a plane. On the other hand, the distortion will be chosen as a dilation, so that the energy of the deformed kinks can be rescaled. Let us apply this procedure of deformation into the sphere to two models in the plane, the ϕ^4-model and the sine-Gordon model.

5.5.1 Deformation of the double ϕ^4-model

Let us take as seed of this type of deformation to the sphere a kink of the double ϕ^4-model in the plane as first example. This model admits a superpotential that in Cartesian coordinates reads

$$W(\phi^1,\phi^2)=\alpha\left(\phi_1-\frac{\phi_1^3}{3}\right)+\beta\left(\phi_2-\frac{\phi_2^3}{3}\right),$$

where two parameters $\alpha,\beta\in\mathbb{R}$ have been introduced to modulate the energy of the emerging kinks. This superpotential leads in turn to a potential function of the form

$$V(\phi^1,\phi^2)=\frac{\alpha^2}{2}\left(1-\phi_1^2\right)^2+\frac{\beta^2}{2}\left(1-\phi_2^2\right)^2,$$

whose peaks are also modulated by the values of the parameters α,β. Since the vacuum manifold $\mathcal{M}$ of the ϕ^4-model is comprised by two points, four vacua will emerge in the double ϕ^4-model as combinations of values $\phi^1=\pm1$ and $\phi^2=\pm1$

$$\mathcal{M} \;=\; \{v^1=(1,1);v^2=(1,-1);v^3=(-1,1);v^4=(-1,-1)\}.$$

These vacua will be asymptotically linked by kinks, which shall be found as solutions of Bogomol'nyi equations

$$\frac{d\phi_1}{dT}=\pm\alpha\left(1-\phi_1^2\right),\qquad \frac{d\phi_2}{dT}=\pm\beta\left(1-\phi_2^2\right).$$

The kink variety of this model presents a total of four singular kinks and antikinks. These can be easily identified by Rajaraman's trial orbit method and are given by the explicit expressions

$$\phi_A=((-1)^{\epsilon_1}\tanh(x-x_0),(-1)^{\epsilon_2}),\qquad E[\phi_A]=\frac{4}{3}|\alpha|,$$
$$\phi_B=((-1)^{\epsilon_1},(-1)^{\epsilon_2}\tanh(x-x_0)),\qquad E[\phi_B]=\frac{4}{3}|\beta|,$$

where $\epsilon_1,\epsilon_2=0,1$ and static solutions have been considered for simplicity. Note that the energy of each type of singular kink is modulated by a different parameter. Now, the orbits of these kinks correspond to segments with constant coordinate ϕ^2 and ϕ^1 respectively, see Figure 5.11. In addition to the singular kinks described above, two families of kinks appear as general solutions of Bogomol'nyi equations

$$\phi_C=((-1)^{\epsilon_1}\tanh(x-x_1),(-1)^{\epsilon_2}\tanh(x-x_2)),\quad E[\phi_C]=\frac{4}{3}\left(|\alpha|+|\beta|\right), \tag{5.28}$$

where parameters x_1 and x_2 will distinguish between members with different orbits and ϵ_1 and ϵ_2 will distinguish between the two families. Notice that the following energy sum rule emerges

$$E[\phi_C]=E[\phi_A]+E[\phi_B].$$

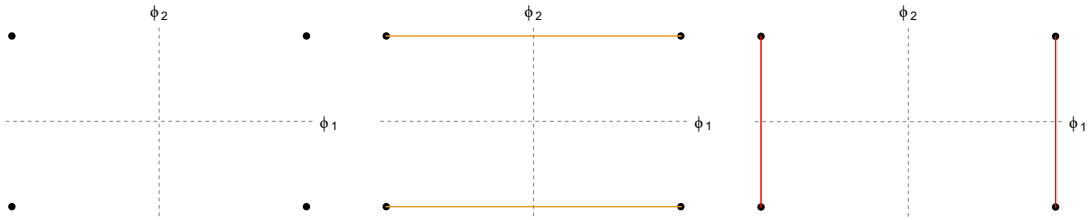

Figure 5.11: Set of vacua and singular kinks A and B for the double ϕ^4-model in the plane. While the orbits of the singular ϕ_A kinks describe two horizontal segments, those for singular ϕ_B kinks are vertical.

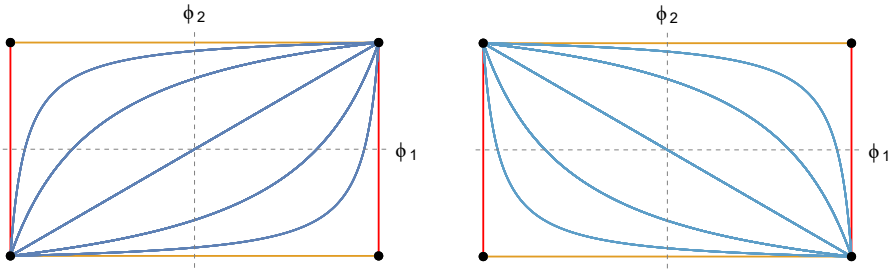

Figure 5.12: Two different families of kinks ϕ_C emerge as general solutions of Bogomol'nyi equations. Note that the topological sector of each family is different. Indeed, they asymptotically connect different vacua.

This is consistent with the fact that limits of these families of kinks coincide with combinations of singular kinks, see figure 5.12. Let us apply now to this model the formalism of deformation described in last section. This is, let us consider a reparametrisation that simplifies the compatibility equation and a distortion that consists in a dilation. This produces the superpotential

$$\tilde{W}(\psi_1,\psi_2) = a^2\alpha\left(\frac{\psi_1}{a} - \frac{\psi_1^3}{3a^3}\right) + a^2\beta\left(\frac{\psi_2}{a} - \frac{\psi_2^3}{3a^3}\right),$$

which is globally rescaled by the parameter a of the dilation. This, subsequently, defines the potential of the deformed Sigma model on the sphere

$$\tilde{V}(\psi^1,\psi^2) = a^2\frac{(1+\psi_1^2+\psi_2^2)^2}{8}\left[\alpha^2\left(1-\frac{\psi_1^2}{a^2}\right)^2 + \beta^2\left(1-\frac{\psi_2^2}{a^2}\right)^2\right],$$

which is modulated not only by the original parameters α and β, but also by the dilation parameter a. Notice that the emerging global factor adds no extra vacua to the model since it presents no zeroes. Moreover, as advanced, the manner in which the reparametrisation has been defined leads to the same deformed model regardless of the kink in the plane that it is being considered as seed. However, each deformed curve will have its own parametrisation since equation (5.21) depends on the trajectory. Even if the explicit solution of the deformed kinks is not analytically obtained, the orbits can be calculated by the distortion $\psi = F\circ\phi$, as can be seen in Figures 5.13 and 5.14. This is

$$\psi_A = a\phi_A\,, \qquad \psi_B = a\phi_B\,, \qquad \psi_C = a\phi_C\,.$$

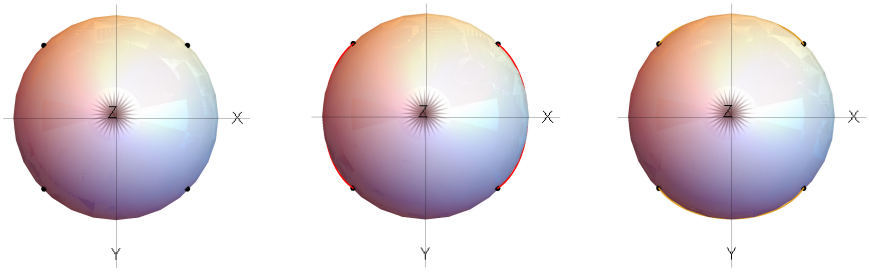

Figure 5.13: Vacua and singular kinks of type A and B of the double ϕ^4-model transferred to the sphere. Note that every kink remains in its topological sector.

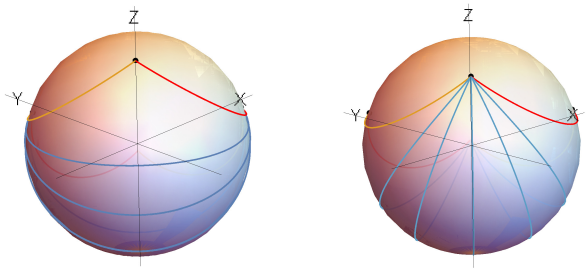

Figure 5.14: The two families of kinks that correspond to solution C are transferred to the sphere. Each family is comprised by topological kinks with different topological sector.

Finally, as demonstrated (5.26), the energy of the deformed kinks will be controlled by the parameter of the distortion a. In particular, the energy of the transferred singular kinks and any member of the transferred families of kinks on the sphere will be given by

$$E[\psi_A] = \frac{4a^2}{3}|\alpha|\,, \qquad E[\psi_B] = \frac{4a^2}{3}|\beta|\,, \qquad E[\psi_C] = \frac{4a^2}{3}\left(|\alpha| + |\beta|\right)\,.$$

5.5.2 Deformation of the double sine-Gordon

As an additional example, let us examine the deformation to the sphere of the double sine-Gordon model in the plane. Since the kink variety of this model is richer than that of the double ϕ^4-model, the kink variety that shall be obtained in the sphere is expected to be richer as well. This model can be constructed from the superpotential

$$W(\phi^1, \phi^2) = \frac{\alpha}{\pi}\sin\left(\pi\phi_1\right) + \frac{\beta}{\pi}\sin\left(\pi\phi_2\right)\,,$$

where once more two parameters $\alpha, \beta \in \mathbb{R}$ have been introduced to modulate the energy of the arising kinks. This leads to a potential function of the form

$$V(\phi^1, \phi^2) = \frac{\alpha^2}{2}\cos^2\left(\pi\phi_1\right) + \frac{\beta^2}{2}\cos^2\left(\pi\phi_2\right)\,.$$

Unlike in the ϕ^4-model, the set of vacua $\mathcal{M}$ of this model consists of an infinite two-dimensional lattice of points periodically distributed in the plane

$$\mathcal{M} \;=\; \left\{v^{n_1 n_2} = \left(\tfrac{2n_1+1}{2}, \tfrac{2n_2+1}{2}\right)/n_1, n_2 \in \mathbb{Z}\right\}\,,$$

which will be asymptotically connected by solutions of Bogomol'nyi equations for this potential. Solutions of these equations can be written in terms of the Gudermannian function. Let us define the auxiliary function

$$q_i(x) = (n_i + 1) + \frac{1}{\pi}\mathrm{Gd}\left[(-1)^{\epsilon_i}\pi\alpha_i(x - x_{0,i})\right] ,$$

for $i = 1, 2$, $\epsilon_i = 0, 1$ and $\alpha_1 = \alpha$ and $\alpha_2 = \beta$. On one hand, an infinite number of singular kinks with constant $\phi_2(x)$ or with constant $\phi_1(x)$ can be found. Their field profiles are respectively

$$\phi_A = \left(q_1(x), \frac{2n_2 + 1}{2}\pi\right) , \qquad E[\phi_A] = 2|\alpha| \quad \forall n_1, n_2 , \tag{5.29}$$

$$\phi_B = \left(\frac{2n_1 + 1}{2}\pi, q_2(x)\right) , \qquad E[\phi_B] = 2|\beta| \quad \forall n_1, n_2 , \tag{5.30}$$

where all possible values of n_1 and n_2 generate all singular kinks, periodically replicated in the plane. The orbits of these singular kinks correspond then to horizontal and vertical segments joining vacua asymptotically, see Figure 5.15. Notice that their energy are modulated again by these parameters α or β. Moreover, given the "additive separability" of the superpotential, not one but two families of topological kinks can be found in the plane

$$\phi_C = (q_1(x), q_2(x)) , \qquad E[\phi_C] = 2\left(|\alpha| + |\beta|\right) \quad \forall n_1, n_2,$$

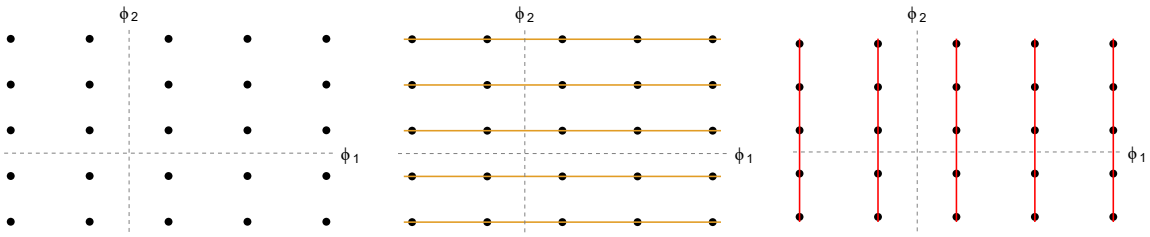

Figure 5.15: Set of vacua and singular kinks A and B for the double sine-Gordon model in the plane. While the orbits of the singular ϕ_A kinks describe horizontal segments, those for singular ϕ_B kinks are vertical.

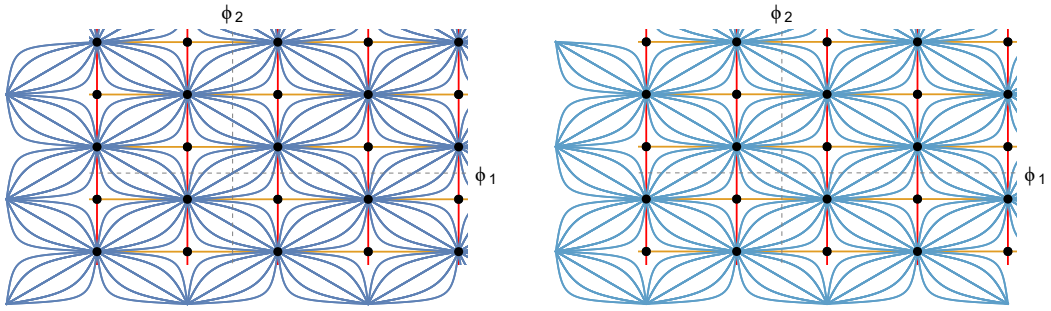

Figure 5.16: Two different families of kinks ϕ_C emerge as general solutions of Bogomol'nyi equations. Note that the topological sector of each family is different. Indeed, they asymptotically connect different vacua.

Indeed, different combinations of values of $\epsilon_1 = 0, 1$ and $\epsilon_2 = 0, 1$ will generate these two families. Note that limits of these families, also replicated in the whole plane, coincide with combinations of singular kinks, see Figure 5.16. This was expected given the energy sum rule

$$E[\phi_C] = E[\phi_A] + E[\phi_B] \,.$$

Following the same procedure as in the previous section, this model will be deformed with reparametrisation (5.21) and a dilation as distortion, i.e. $\psi^i = a\phi^i$ for $i = 1, 2$. This produces a superpotential on the sphere in stereographic coordinates

$$\tilde{W}(\psi_1, \psi_2) = \frac{\alpha a^2}{\pi} \sin\left(\pi \frac{\psi_1}{a}\right) + \frac{\beta a^2}{\pi} \sin\left(\pi \frac{\psi_2}{a}\right),$$

for which a potential function for a Sigma model on the sphere $\mathbb{S}^2$ is constructed

$$\tilde{V}(\psi^1, \psi^2) = a^2 \frac{(1 + \psi_1^2 + \psi_2^2)^2}{4} \left(\frac{\alpha^2}{2} \cos^2\left(\pi \frac{\psi_1}{a}\right) + \frac{\beta^2}{2} \cos^2\left(\pi \frac{\psi_2}{a}\right)\right),$$

once more modulated by the dilation parameter a. The energy of these kinks will also depend on this parameter, which affects the energy of all these deformed kinks equally

$$E[\psi_A] = 2a^2|\alpha| \,, \qquad E[\psi_B] = 2a^2|\beta| \,, \qquad E[\psi_C] = 2a^2 \left(|\alpha| + |\beta|\right) .$$

The proposed distortion defines the transference of the infinite number of kink orbits that emerge in the double sine-Gordon model to the sphere, where a Sigma model that admit the deformed orbits as solutions has been constructed. This includes, on one hand, the original singular kinks, which are translated to the sphere by the stereographic projection, see Figure 5.17.

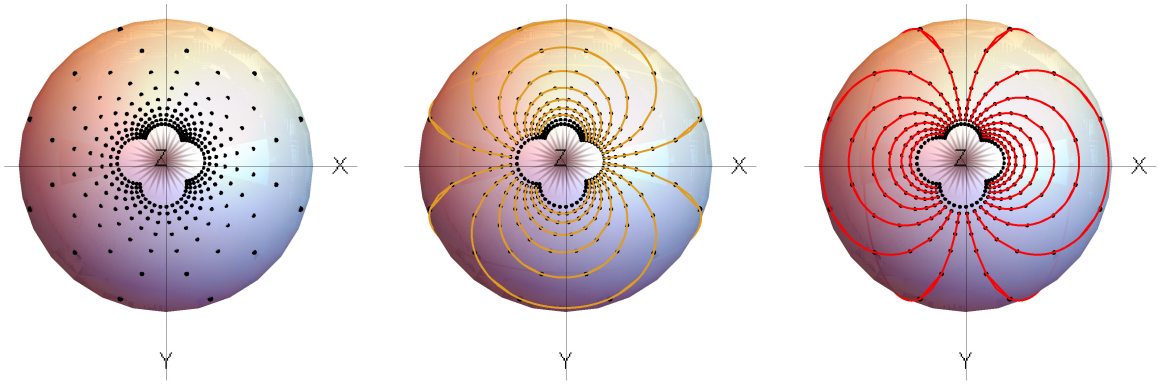

Figure 5.17: Vacua and singular kinks of type A and B of the double sine-Gordon model are transferred to the sphere $\mathbb{S}^2$ via the stereograhic projection. The repeating pattern of the lattice in the plane is transformed into a pattern that approaches but never reaches the north pole due to the compactification.

On the other hand, the two families of kinks replicated in the plane are also sent to the sphere, where they are also replicated, see Figure 5.18. Once again, this method allows us to "hide" the effect of the curvature of the sphere in the reparametrisation and to modulate the energy of the deformed kinks. Similarly to

the deformation in the previous section, no extra vacua are added to the vacuum manifold given the form of the arising global factor in the potential. Lastly, even if this deformation has been performed for every possible kink as seed, the explicit profile of each deformed kink will employ a different parametrisation (5.21). Unfortunately, the equation for these reparametrisations cannot be integrated analytically in general. However, the distortion allows us to find their orbits $\psi = F \circ \phi$.

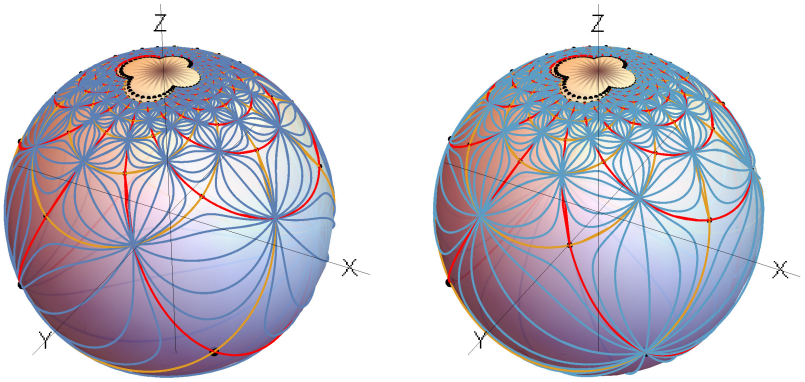

Figure 5.18: The two different families of kinks that correspond to solution C in the sine-Gordon model are transferred to the sphere $\mathbb{S}^2$ via the stereograhic projection. The repeating pattern of the lattice in the plane is transformed into a pattern that approaches but never reaches the north pole due to the compactification.

5.6 Deformation between conformally flat manifolds

The deformation between the plane and the sphere $\mathbb{S}^2$ described in the previous section exploits the fact that a coordinate chart that makes the sphere conformally flat can be found. Indeed, the sphere $\mathbb{S}^2$ is conformally flat in stereographic coordinates, as the metric tensor is that of the plane with a multiplying non-negative global factor. This allows us to define a reparametrisation that simplifies the compatibility condition and obtain that of a plane. In this section deformations between other conformally flat Riemmanian manifolds will be explored. First, the procedure to deform a model in the plane to the torus will be described. Then, the possibility of deformations between the sphere and the torus will be investigated.

5.6.1 Deformations from the plane to the torus

The objective of this section is to find a coordinate chart on the torus that allows us to simplify the compatibility condition, similarly to the case of the deformation between the plane and the sphere. This is, a coordinate chart on the torus $(\mathbb{S}^1 \times \mathbb{S}^1, g)$ for which the metric tensor is conformally flat will be sought. If such a coordinate chart exists, then kinks defined on the Euclidean plane can be sent to the torus, where a Sigma model that supports them as solutions can be sought. Of course, the reverse direction of deformation is also possible. Now, let us first consider the

following toroidal coordinates

$$\begin{aligned} \phi^1(\theta,\varphi) &= (R + r\sin\theta)\cos\varphi\,, \\ \phi^2(\theta,\varphi) &= r\cos\theta\,, \\ \phi^3(\theta,\varphi) &= (R + r\sin\theta)\sin\varphi\,, \end{aligned} \tag{5.31}$$

with poloidal $\theta \in [0, 2\pi)$ and toroidal $\varphi \in [0, 2\pi)$ coordinates and where R and r are the major and minor radii of the torus $R > r > 0$. In these coordinates the metric tensor is clearly non-conformally flat

$$g = r^2 d\theta \otimes d\theta + (R + r\sin\theta)^2 d\varphi \otimes d\varphi\,.$$

However, a change of coordinates $(\theta, \varphi) \to (\alpha, \beta)$ can be sought so that it is conformally flat. Imposing that in the new coordinate system the metric tensor is a non-negative global factor times the metric tensor of the Euclidean plane, the following condition is derived

$$\pm r\frac{d\theta}{d\alpha} = (R + r\sin\theta)\frac{d\varphi}{d\beta}\,.$$

When separable solutions are sought, a simple solution can be found, which is given by the following change of coordinates $f(\theta, \varphi) = (\alpha, \beta)$

$$\alpha = \arctan\left(\frac{r + R\tan(\frac{\theta}{2})}{\sqrt{R^2 - r^2}}\right) \qquad \beta = \frac{\sqrt{R^2 - r^2}}{2r}\varphi\,, \tag{5.32}$$

where the positive sign has been considered in the second equation for convenience. Notice that these new coordinates are defined in $\alpha \in (-\frac{\pi}{2}, \frac{\pi}{2})$ and $\beta \in (0, \frac{\sqrt{R^2-r^2}}{r}\pi)$. For completeness, let us write the inverses

$$\theta = 2\arctan\left(\frac{-r + \sqrt{R^2 - r^2}\tan(\alpha)}{R}\right)\,, \qquad \varphi = \frac{2r}{\sqrt{R^2 - r^2}}\beta\,.$$

Indeed, these transformation of coordinates leads to a conformally flat metric tensor which can be written as

$$g_c = \left(\frac{2rR\sqrt{R^2 - r^2}}{R^2 + r^2\cos(2\alpha) - r\sqrt{R^2 - r^2}\sin(2\alpha)}\right)^2 (d\alpha \otimes d\alpha + d\beta \otimes d\beta)\,.$$

Let us write for the sake of convenience $\Delta(\alpha) \equiv g_c^{11} = g_c^{22}$. In this scenario a similar procedure to that of the deformation to the sphere will be followed. Let us consider a kink in the plane given by $(\phi^1(T), \phi^2(T))$. Let us also consider a similar deformation diagram in this case, which will be of the form

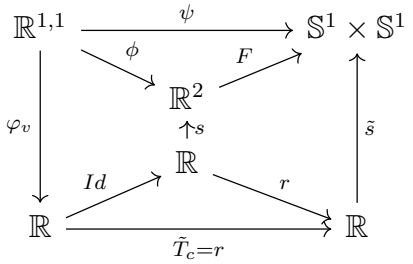

Now, given that the metric tensor is diagonal and all its components in the diagonal are identical, the compatibility equation can be written as

$$\frac{1}{\Delta(\alpha)}\frac{\partial \tilde{W}}{\partial \psi^i} = \pm \frac{dT}{d\tilde{T}}\frac{\partial F_c^i(\phi)}{\partial \phi^j}\frac{\partial W(\phi)}{\partial \phi^j}\,,$$

for $i = 1, 2$ and where (ϕ^1, ϕ^2) are the Cartesian coordinates on the plane and $(\psi^1, \psi^2) \equiv (\alpha, \beta)$. This enables us to define the reparametrisation so that it absorbs the global factor $\Delta(\alpha)$ arising in the metric tensor

$$\frac{dT}{d\tilde{T}} \equiv \frac{1}{\Delta(\alpha(\theta(\phi^1(T), \phi^2(T))))}\,,$$

where the coordinate α is written in terms of θ via (5.32) and this coordinate is in turn written in terms of the Cartesian coordinates in the plane via equations (5.31). This leads to the same compatibility condition that one would obtain in the plane with no reparametrisation

$$\frac{\partial \tilde{W}}{\partial \psi^i} = \pm \frac{\partial F_c^i(\phi)}{\partial \phi^j}\frac{\partial W(\phi)}{\partial \phi^j}\,,$$

and therefore a potential that supports these deformed kinks can be constructed on the torus

$$\tilde{V} = \frac{1}{2\Delta(\alpha)}\sum_{i,j=1}^{2}\left(\frac{\partial F_c^i(\phi)}{\partial \phi^j}[\psi]\frac{\partial W(\phi)}{\partial \phi^j}[\psi]\right)^2\,.$$

Notice that if the distortion is a dilation, then the same relation as in the case of the sphere appears between the energies of the original and deformed kinks

$$E[\psi] = a^2 E[\phi]\,.$$

Once again, the parametrisation of every deformed kink will depend on the kink profile of the original kink. Lastly, once more the explicit profile will not be analytically available in general, but the orbits of the deformed kinks in the torus can be easily found $\tilde{s} = F \circ s \circ r^{-1}$. See Figure 5.19 for an example where solutions of the double ϕ^4-model of the previous section are sent to the torus without distortions.

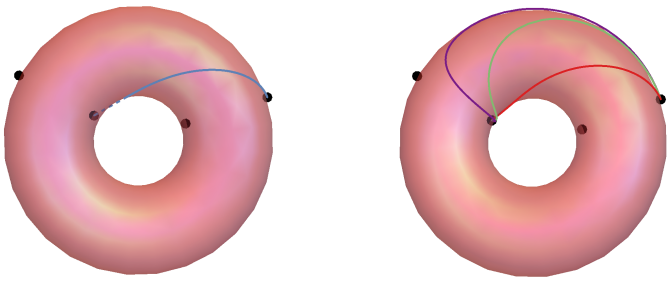

Figure 5.19: Vacua and kinks for the double ϕ^4-model in the plane transferred to the torus with no distortion.

See also Figure 5.20 for another example where solutions of the double ϕ^4-model of the previous section are sent to the torus, now employing a distortion. In particular, the used distortion for this second case is given by

$$(\alpha,\beta)=(F_c^1(\phi),F_c^2(\phi))\equiv\left(\frac{\pi}{3}+\frac{\pi}{4}\phi^1,\frac{\sqrt{R^2-r^2}}{2r}+2\phi^2\right).$$

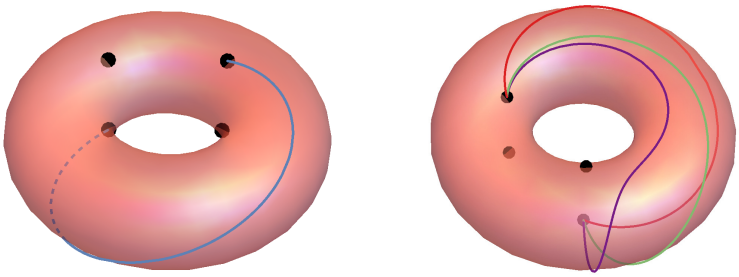

Figure 5.20: Vacua and kinks for the double ϕ^4-model in the plane transferred to the torus with distortion.

5.6.2 Deformations from the sphere to the torus

In the previous sections deformations between the plane and the sphere and between the plane and the torus have been investigated. The primary factor that allowed the construction of the deformed Sigma models is that a coordinate system in which these manifolds were conformally flat was found. Since both the sphere and the torus are conformally flat in those coordinates, it is only natural that deformations between these two manifolds may also be found. Indeed, these two manifolds are conformal in those coordinates and therefore a similar trick to that employed in previous sections should be available.

For instance, a solution $(\phi^1(T),\phi^2(T))$ in stereographic coordinates on the sphere $(\mathbb{S}^2,g)$ can be sent to the torus $(\mathbb{S}^1\times\mathbb{S}^1,\tilde{g})$ when the coordinates defined in last section $(\psi^1,\psi^2)=(\alpha,\beta)$ are chosen on the torus. Let us consider the following deformation diagram

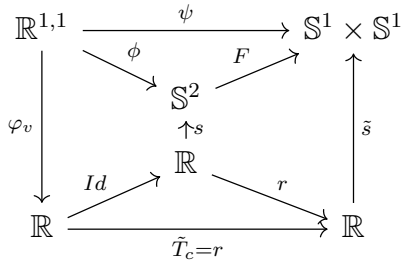

From this diagram a similar compatibility condition can be derived. However, in this case both manifolds are non-Euclidean. Consequently, this equation (5.11) will involve components of both metric tensors

$$\tilde{g}^{ii}\frac{\partial\tilde{W}}{\partial\psi^i}=\pm\frac{dT}{d\tilde{T}}\frac{\partial F_c^i(\phi)}{\partial\phi^j}g^{jj}\frac{\partial W(\phi)}{\partial\phi^j}.$$

Fortunately, since coordinates have been chosen so that both metric tensors are conformally flat, a global factor can be absorbed by the reparametrisation. In particular, this occurs when the reparametrisation is defined as follows

$$\frac{dT}{d\tilde{T}} \equiv \frac{\tilde{g}^{ii}(F(\phi(T)))}{g^{ii}(\phi(T))} \equiv \Delta(\phi(T))\,.$$

Indeed, this reparametrisation transforms the compatibility equation into that of a plane as in previous cases

$$\frac{\partial \tilde{W}}{\partial \psi^i} = \pm \frac{\partial F_c^i(\phi)}{\partial \phi^j}\,[\psi]\,\frac{\partial W(\phi)}{\partial \phi^j}\,[\psi]\ ,$$

giving rise to a potential that admits the deformed kinks $\tilde{s}(\tilde{T}) = F(s(r^{-1}(\tilde{T})))$, which is of the form

$$\tilde{V}(\psi) = \frac{1}{2\Delta(\psi)} \sum_{i,j=1}^{2} \left(\frac{\partial F_c^i(\phi)}{\partial \phi^j}\,[\psi]\,\frac{\partial W(\phi)}{\partial \phi^j}\,[\psi] \right)^2 .$$

Examples of this deformation can be observed in the figures of the sphere and the torus for the double ϕ^4-model, as the same kinks in the plane were sent to both spaces. In fact, this can be seen as a composite deformation (5.6), where the parametrisation encodes the information about the change of curvature in the target manifold. In conclusion, deformations between the Euclidean plane, the sphere and the torus have been constructed. However, it is worth highlighting that this procedure could be generalised to other scenarios. For instance, conformal Riemannian manifolds can be considered, where a distortion can be conveniently defined to further simplify the compatibility condition.

5.7 Deformation between manifolds of different dimension

In this chapter only deformations between Riemannian manifolds with the same dimension have been studied. In this section we go beyond this limitation as we delve into deformations between Riemannian manifolds with different dimension. In order to illustrate this new scenario, only deformations through pure distortions of type A will be considered, even though multiples examples for the rest of the cases could be found. The type of deformation under consideration will be a pure distortion between Riemannian manifolds (M, g) and (N, g), summarised in the following deformation diagram

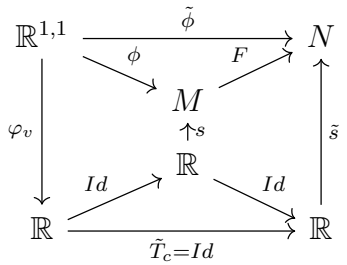

This is, relations $\tilde{\phi} = F \circ \phi$ and $\tilde{s} = F \circ s$ must hold. Two examples of this type of deformations will be shown. The first one will be deforming a Sigma model on a circumference $\mathbb{S}^1$ into another on the sphere $\mathbb{S}^2$. In the last example the deformation will consist in a radial projection from $\mathbb{R}^3$ to the sphere $\mathbb{S}^2$.

5.7.1 Deformation from the circumference to the sphere

In this first example, kinks on the circumference will be sent to the sphere. Thus, the first step is to choose coordinate charts on both manifolds. Let us take a chart on the circumference $(U_{\mathbb{S}}, \Omega)$ with angular coordinate $\Omega \in (0, 2\pi)$, for which the metric tensor will be defined as

$$g = r^2 d\Omega \otimes d\Omega \,,$$

where r denotes the radius of the circumference. Let us construct a Sigma model making use of this chart on $\mathbb{S}^1$. Specifically, let us define the following superpotential

$$W(\Omega) = \sin \Omega \,,$$

which corresponds to a sine-Gordon model on the circumference, as the potential function is of the form

$$V(\Omega) = \frac{1}{2} \cos^2 \Omega \,.$$

This model presents two vacua $v^1 = \frac{\pi}{2}$ and $v^2 = \frac{3\pi}{2}$, which will be asymptotically linked by solutions of Bogomol'nyi equations

$$\Omega(T) = \pm \mathrm{Gd}\left[\frac{T - T_0}{r^2}\right] \,,$$

where Gd denotes the Gudermannian function, see Figure 5.21.

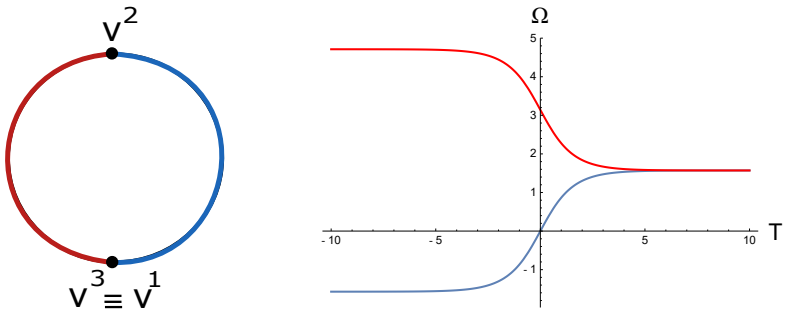

Figure 5.21: Solutions for this Sigma model on $\mathbb{S}^1$ with two vacua, where two types of topological kinks emerge.

Let us now deform this model with these solutions into another Sigma model on the sphere $\mathbb{S}^2$. For this purpose, a coordinate chart must be chosen on the sphere. In particular, the chart on the sphere $(U_{\mathbb{S}^2}, \{\theta, \varphi\})$ with radius R and with the usual spherical coordinates

$$\begin{aligned} x &= R \sin\theta \cos\varphi \,, \\ y &= R \sin\theta \sin\varphi \,, \\ z &= R \cos\theta \,, \end{aligned}$$

will be taken, where x, y, z are the Cartesian coordinates in the ambient space $\mathbb{R}^3$ and $\theta \in (0, \pi)$ and $\varphi \in (0, 2\pi)$. When this model is deformed, the distortion must be defined so that its image must be interpretable as spherical coordinates on the sphere and therefore it must be contained within the rectangle $D = (0, \pi) \times (0, 2\pi) \subset \mathbb{R}^2$. In order to ensure this for all solutions of the proposed model that shall be deformed, the distortion F will be defined so that all points in the circumference $(0, 2\pi) \equiv I$ will be sent inside this rectangle

$$\begin{array}{ccc} \mathbb{S}^1 & \xrightarrow{\quad F \quad} & \mathbb{S}^2 \\ \Big\downarrow{\scriptstyle \lambda_{\mathbb{S}^1}} & & \Big\uparrow{\scriptstyle \lambda^{-1}_{\mathbb{S}^2}} \\ I & \xrightarrow{F_c} & (F_1(I), F_2(I)) \subset D \end{array}$$

by means of two functions F_1 and F_2 which must satisfy respectively $F_1(I) \subset [0, \pi]$ and $F_2(I) \subset [0, 2\pi]$. With these two functions the compatibility condition (5.11) reads

$$\frac{1}{R^2}\frac{\partial \tilde{W}}{\partial \theta} = \pm \frac{1}{r^2} F_1'(\Omega) W'(\Omega)\,, \qquad \frac{1}{R^2 \sin^2\theta}\frac{\partial \tilde{W}}{\partial \varphi} = \pm \frac{1}{r^2} F_2'(\Omega) W'(\Omega)\,.$$

In order to further simplify these differential equations, let us assume that both functions that define the distortion, i.e. F_1 and F_2, are not independent but are related as follows

$$F_2'(\Omega) = \frac{H(\Omega)}{\sin^2 F_1(\Omega)}\,. \tag{5.33}$$

This forces us to define $F_1(\Omega)$ so that it does not vanish at any point of its domain. This condition (5.33), since functions F_1 and F_2 are analytically invertible or piecewisely invertible, allows us to construct an additively separable superpotential $\tilde{W} = \tilde{W}_1(\theta) + \tilde{W}_2(\varphi)$ as follows

$$\frac{d\tilde{W}_1}{d\theta} = \pm \frac{R^2}{r^2} F_1'(\Omega(\theta)) W'(\Omega(\theta))\,, \tag{5.34}$$

$$\frac{d\tilde{W}_2}{d\varphi} = \pm \frac{R^2}{r^2} H(\Omega(\varphi)) W'(\Omega(\varphi))\,. \tag{5.35}$$

Lastly, any superpotential solution of these equations defines a potential for a Sigma model on the sphere

$$\tilde{V}(\theta, \varphi) = \frac{R^4}{2r^4}\left[\left(F_1'(\Omega(\theta))\ \cos(\Omega(\theta))\right)^2 + \frac{1}{R^2 \sin^2\theta}\left(H(\Omega(\varphi))\ \cos(\Omega(\varphi))\right)^2 \right]\,,$$

for which any deformed curve $\tilde{s} = F \circ s$ is a solution. This procedure of transference is well-defined as long as the imposed function $F_1(\Omega)$ avoids the values 0 and π and produces in equation (5.33) a function $F_2(\Omega)$ which can be interpreted as an angle $\varphi = F_2(\Omega) \in (0, 2\pi)$. It is also worth noticing that the function $H(\Omega)$ introduces an infinite number of possible deformations. Let us now see in detail a particular example of this type of distortion.

Distortion $\theta = F_1(\Omega) \equiv \alpha\ \Omega + \frac{\pi}{4}$

This distortion is "centred" at $\theta = \frac{\pi}{2}$ and cannot reach either 0 or π when $0 < \alpha < \frac{1}{4}$. For the sake of simplicity let us also assume $H(\Omega) = \beta$ with $\beta \in \mathbb{R}$. This produces, after solving equation (5.33), a distortion that satisfies all requirements

$$\theta(\Omega) = \alpha\Omega + \frac{\pi}{2}\,, \qquad \varphi(\Omega) = \varphi_0 + \frac{\beta}{\alpha}\tan\left(\alpha\Omega\right),$$

where $\varphi_0 \in \mathbb{R}$ and β must be carefully chosen to guarantee that the deformed curve lies within the rectangle D. The inverse of these functions can be analytically derived

$$\Omega(\theta) = \frac{1}{\alpha}\left(\theta - \frac{\pi}{2}\right), \qquad \Omega(\varphi) = \frac{1}{\alpha}\arctan\left(\frac{\alpha(\varphi-\varphi_0)}{\beta}\right)$$

and therefore the reduced compatibility equations (5.34) and (5.35) for additively separable superpotentials reads

$$\frac{d\tilde{W}_1}{d\theta} = \pm\alpha\frac{R^2}{r^2}\cos(\Omega(\theta))\,, \qquad \frac{d\tilde{W}_2}{d\varphi} = \pm\beta\frac{R^2}{r^2}\cos(\Omega(\varphi))\,.$$

The explicit expression for the superpotential cannot be obtained in general since the second equation cannot be integrated in general. However, it exists and it is modulated by both parameters α and β. This implies that the energy of the deformed kinks will also be modulated by these parameters. Notice that by definition both α and β are bounded and thus so is the energy of the new kinks on the sphere. Lastly, the potential will be of the form

$$\tilde{V}(\theta,\varphi) = \frac{R^4}{2r^4}\left[\alpha^2\ \cos^2\left(\Omega(\theta)\right) + \frac{\beta^2}{R^2\sin^2\theta}\ \cos^2(\Omega(\varphi))\right].$$

Notice that this potential presents a singularity at $\theta = 0, \pi$. However, all deformed kinks will elude this singularity by the definition of the distortion F. In fact, this potential has four vacua, since two vacua are produced for each angular coordinate on the sphere

$$\begin{aligned}
\tilde{v}^{11} &= (F_c^1(v^1), F_c^1(v^1)) = \left((\alpha+1)\frac{\pi}{2}, \varphi_0 + \frac{\beta}{\alpha}\tan\left(\frac{\pi\alpha}{2}\right)\right),\\
\tilde{v}^{12} &= (F_c^1(v^1), F_c^1(v^2)) = \left((\alpha+1)\frac{\pi}{2}, \varphi_0 + \frac{\beta}{\alpha}\tan\left(\frac{3\pi\alpha}{2}\right)\right),\\
\tilde{v}^{21} &= (F_c^1(v^2), F_c^1(v^1)) = \left((3\alpha+1)\frac{\pi}{2}, \varphi_0 + \frac{\beta}{\alpha}\tan\left(\frac{\pi\alpha}{2}\right)\right),\\
\tilde{v}^{22} &= (F_c^1(v^2), F_c^1(v^2)) = \left((3\alpha+1)\frac{\pi}{2}, \varphi_0 + \frac{\beta}{\alpha}\tan\left(\frac{3\pi\alpha}{2}\right)\right).
\end{aligned}$$

Exactly as in previous cases, the orbits of the deformed kinks for this new potential on the sphere can be immediately found by applying the distortion to the original solutions, see Figure 5.22.

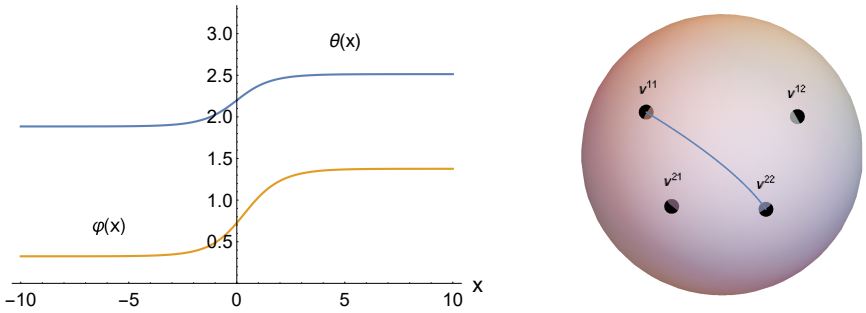

Figure 5.22: A representative solution of the sine-Gordon model in the region $\Omega \in (0, 2\pi)$ in the circumference transferred to the sphere.

5.7.2 Deformation via projection from $\mathbb{R}^3$ to $\mathbb{S}^2$

Let us now study a case where a Sigma model is deformed into another with a target manifold of lower dimension. In particular, the distortion will be defined so that the Euclidean space $\mathbb{R}^3$ is radially projected to a sphere $\mathbb{S}^2$ of radius R. More specifically, the model that will be deformed is the triple ϕ^4-model, which is given by a potential function written in Cartesian coordinates x, y, z as

$$V = \frac{1}{2}(1-x^2)^2 + \frac{1}{2}(1-y^2)^2 + \frac{1}{2}(1-z^2)^2 \,.$$

Let us choose a particular kink as seed of this deformation, which corresponds to a vertical segment in $\mathbb{R}^3$

$$(x, y, z) = (1, 1, \tanh(T - T_0)) \,.$$

On the sphere, the same chart in spherical coordinates used in the previous section will be employed. For the sake of simplicity, let the deformation be a pure distortion. Once coordinates are fixed, the distortion is determined by the map F_c that relates the coordinates in both charts

$$\begin{array}{ccc} \mathbb{R}^3 & \xrightarrow{\quad F \quad} & \mathbb{S}^2 \\ \Big\downarrow{\scriptstyle \lambda_{\mathbb{S}^1}} & & \Big\uparrow{\scriptstyle \lambda^{-1}_{\mathbb{S}^2}} \\ \mathbb{R}^3 & \xrightarrow{F_c} & (F_c^1(\mathbb{R}^3), F_c^2(\mathbb{R}^3)) \subseteq \mathbb{R}^2 \end{array}$$

Once again, the image of these functions F_c^1 and F_c^2 must be interpretable as spherical coordinates. In particular, as has been advanced, we will define the distortion as the radial projection

$$\begin{array}{rccc} F_c\colon & \mathbb{R}^3 & \longrightarrow & D \subset \mathbb{R}^2 \\ & (r, \theta, \varphi) & \longmapsto & (\theta, \varphi) \end{array}$$

given by the following functions F_c^1 and F_c^2

$$(\theta, \varphi) = (F_c^1(x, y, z), F^2(x, y, z)) = \left(\arccos\left(\frac{z}{\sqrt{x^2+y^2+z^2}} \right), \varphi_0 + \arctan\left(\frac{y}{x}\right) \right) ,$$

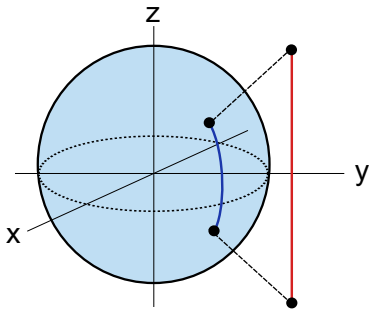

Figure 5.23: Radial projection from R^3 to the sphere $\mathbb{S}^2$ for the kink employed as a seed, whose orbit describes a vertical segment.

where the constant $\varphi_0 \in \mathbb{R}$ is a shift in the coordinate φ, see Figure 5.23. It is worth noticing that the distortion is not defined on the whole space $\mathbb{R}^3$, as the origin must be excluded. Indeed, this projection is not defined for this point. This radial projection allows us to express the deformed curve in spherical coordinates on the sphere as

$$(\theta(T), \varphi(T)) = \left(\arccos\left(\frac{\tanh(T - T_0)}{\sqrt{2 + \tanh^2(T - T_0)}} \right), \pi \right) ,$$

where $\varphi_0 = \frac{3\pi}{4}$ has been fixed for convenience. Notice that by construction the variable θ is not allowed to reach the north and south poles, since these will correspond to singularities as we shall see. With these conditions the compatibility conditions read

$$\begin{aligned} \frac{\partial \tilde{W}}{\partial \theta} &= \pm R^2 \left(\frac{(x+y)z}{\sqrt{x^2+y^2}(x^2+y^2+z^2)} + \frac{\sqrt{x^2+y^2}}{x^2+y^2+z^2}(1-z^2) \right) [\theta, \varphi] , \\ \frac{\partial \tilde{W}}{\partial \varphi} &= \pm R^2 \sin^2\theta \left(\frac{x(1-y^2) + y(1-x^2)}{x^2+y^2} \right) [\theta, \varphi] , \end{aligned} \tag{5.36}$$

where x, y, z must be written in terms of the angles on the sphere θ and φ. This compatibility condition cannot hold in these coordinates, and therefore a seed-independent deformation cannot be found. However, the explicit form of the seed kink can be introduced in equation (5.10) to obtain a Sigma model that supports this kink in particular

$$\begin{aligned} \left. \frac{\partial \tilde{W}}{\partial \theta} \right|_{\tilde{s}(T)} &= \pm \frac{2\sqrt{2}R^2}{1 + 3\cosh(2(T - T_0))} = \pm \frac{R^2}{4\sqrt{2}} \left(1 - 3\cos 2\theta(T)\right) , \\ \left. \frac{\partial \tilde{W}}{\partial \varphi} \right|_{\tilde{s}(T)} &= 0 \equiv (\varphi(T) - \pi) , \end{aligned} \tag{5.37}$$

where in the second equation the simplest function in φ that satisfies that condition has been chosen. Nevertheless, an infinite number of possibilities could have been chosen for this function. Therefore, the following representative of additively separable superpotentials

$$\tilde{W}(\theta, \varphi) = \frac{R^2}{4\sqrt{2}}(\theta - 3\sin\theta) + \frac{1}{2}(\varphi - \pi)^2$$

is obtained. This leads to a potential function that supports the deformed curve

$$V = \frac{R^4}{64}\left(1 - 3\cos\theta\right)^2 + \frac{1}{2R^2\sin^2\theta}\left(\varphi - \pi\right)^2 \ .$$

It should be stressed that even if two singularities are present in this potential, by construction the deformed kink will never reach these singularities. In conclusion, this represents an example of deformation of a Sigma model into another with a target manifold of lower dimension. Furthermore, this also represents an example of a seed-dependent deformation, as depending of the kink employed for deformation the form of the potential of the model shall be different.

5.8 Further comments

In this chapter the formalism of deformation of Bazeia et al. has been generalised for non-linear Sigma models, also allowing seed-dependent deformations. The first step consists in constructing the kink diagram of a kink of the original Sigma model, replacing the solution by a parametrised curve on the target manifold. Then, the distortion and the reparametrisation define the transference of this parametrised curve to a new Riemannian manifold, where another Sigma model is constructed so that the configuration that corresponds to this deformed curve is a kink. To ensure that a superpotential for this deformed model can be constructed, two types of compatibility equations are derived. The deformed model for the first one (5.10) depends in general on the kink which is being deformed as the explicit substitutions $T(\phi)$ may be used. On the other hand, the other compatibility condition is entirely written in terms of the new coordinates (5.11). This produces the same model for every kink used as seed when the reparametrisation is the identity or when it is defined making use of the auxiliary function on the original target manifold (5.19). For instance, pure distortions produce deformed superpotentials that are independent of the kink that has been chosen to be deformed. Lastly, the potential of the deformed non-linear Sigma model is constructed from the deformed superpotential.

Examples of deformations via pure distortions and pure reparametrisation have been displayed to illustrate this procedure. In particular, these techniques have been applied to the ϕ^4-model, where different types of deformations give rise to different deformed models. It is worth highlighting that when the distortion or the reparametrisation are piecewisely invertible, depending on the orientation of their arrows, multiple deformed kinks may emerge. Notice that deformations via pure distortions between Sigma models with Euclidean target spaces are equivalent to the methods of deformation of Bazeia et al.

Generalising to Riemannian target manifolds, a procedure to deform Sigma models on the plane to obtain Sigma models on the sphere $\mathbb{S}^2$ is described and employed for two examples. Namely, the double ϕ^4-model and the double sine-Gordon model. Unlike in previous sections, this deformation involves both a parametrisation and a distortion. The parametrisation allows us to simplify the compatibility equations when stereographic coordinates are taken on the sphere. Indeed, in these coordinates the sphere is conformally flat and a reparametrisation can cancel out the extra global term that the metric tensor creates. Hence, the curvature of the sphere is "absorbed" in the reparametrisation, resulting in the compatibility equation for a plane. It is worth mentioning that the explicit profiles of the deformed kinks are

not analytically available since the reparametrisation equation cannot be integrated in general. However, the orbits of these kinks can be derived by the distortion. Furthermore, the parametrisation of each deformed curve will be different, as the reparametrisation has been defined so that it varies according to the trajectory of the original kink. In other words, each deformed kink will have associated a different mechanical local time. On the other hand, the distortion, defined as a dilation, enables us to modulate the energy of solutions. The parameter a of this modulation also controls the proximity of solutions to the south pole, which is represented in the stereographic plane by the origin. Notice that instead of a global dilation, asymmetrical dilations could have been considered, so that the energy of each kink may be affected differently. Furthermore, more elaborate distortions could lead to even more interesting kink varieties, even though these have not been explored here.

This mechanism of simplifying the compatibility condition by employing coordinates that make a Riemannian manifold conformally flat can be reproduced for other Riemannian manifolds. In fact, analogous coordinates have been found on the torus, allowing deformations between the torus and the plane. This also allows this type of deformations between the torus and the sphere, as it can be seen as composite deformation. In this last case, the reparametrisation absorbs the change in curvature, leading again to the compatibility condition for a plane.

Lastly, deformations between Sigma models with target manifolds of different dimensions are constructed. Specifically, two scenarios of pure distortions are studied. In the first one a sine-Gordon model on the circumference is deformed into a Sigma model on the sphere $\mathbb{S}^2$. In the other scenario, the distortion is defined as the radial projection of $\mathbb{R}^3$ to the sphere $\mathbb{S}^2$. In the first one the compatibility equations can be analytically solved for every kink, allowing for seed-independent deformations. In contrast, in the second deformation, the constructed model will only admit as a solution the deformation of the kink used as seed, which is a singular kink in the deformed model.

Chapter 6

Other deformation techniques

In Chapter 5 the methods of deformation of Bazeia et al. have been generalised to Sigma models on Riemannian manifolds. This extension implies that the versatility of Bazeia's deformation techniques for constructing new models in various fields of physics is now also present in the context of Sigma models. In this chapter, three other types of deformation techniques will be developed. The first one will be based on the deformation formalism described in last chapter. However, this one will consist in cutting kink orbits in different ways, so that Sigma models that admit these trims as kinks are constructed. Secondly, the inverse process will be investigated. Kinks of different Sigma models will be piecewisely combined to form a kink of a new Sigma model. The gluing conditions for this procedure will be derived. Lastly, from two non-linear Sigma models, a new non-linear Sigma model will be constructed on the Cartesian product of the original target manifolds. Employing this new target manifold will allow us to couple different Sigma models, entangling their dynamics. Furthermore, this method will be adapted to produce similar Sigma models on the sphere. These new methods will contribute to the existing corpus of deformation methods, thereby expanding the range of accessible models through deformations.

6.1 Trims of kinks

In last chapter the formalism of deformation of a kink was based on transferring its whole orbit to the target manifold of a new Sigma model. Under certain conditions, piecewise inverses of distortions and reparametrisations caused the deformed kink to split, thereby cutting these original kinks into different pieces. In this section, another technique for cutting kink orbits will be explored, which will receive the name of *trimming* of kinks. The main idea is to cut the orbit of a kink and construct a Sigma model which admits as a solution a part of the trimmed orbit. Notice that this implies that the points where the kinks are cut become vacua of the new field theory. Let us describe this procedure in detail, which shall also employ the notion of kink diagram introduced in Chapter 5. Let us consider a kink ϕ, solution of a Sigma model on a Riemannian manifold M, such that when it is decomposed by the

kink diagram

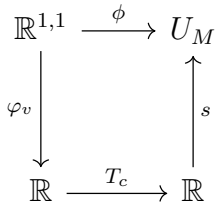

the curve s has analytical inverse or piecewise inverses. In order to cut a part of its orbit, instead of applying the curve s to the whole real numbers $\mathbb{R}$, the *trim* will be defined as the image of s when applied to an interval $I \subset \mathbb{R}$, see Figure 6.1.

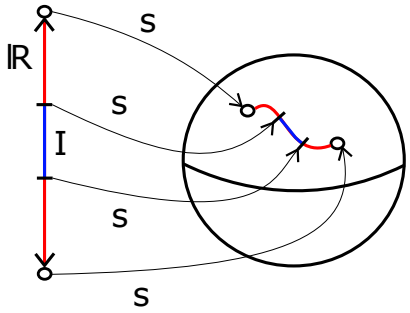

Figure 6.1: A trim of a kink is obtained in the picture by cutting the original kink orbit at two points. This procedure replaces the whole image of the curve by the image of the curve s restricted to the interval $I \subset \mathbb{R}$.

Thus, the curve is restricted to the interval $I \subset \mathbb{R}$. For compact intervals $I = [a, b]$ with $a, b \in \mathbb{R}$ the kink orbit will be trimmed at both ends. If, on the contrary, the interval is of the form $I = [a, \infty)$ or $I = (\infty, b]$, then the kink orbit will be trimmed on one side only. This interval can be defined by means of an auxiliary differentiable function $q : \mathbb{R} \to I \subset \mathbb{R}$ with analytical inverse or piecewise analytical inverse, which shall be referred to as *trimming function*. Furthermore, let us include in the process a distortion between two manifolds M and N. This will enable us to send the truncated orbit to other manifolds, introducing additional degrees of freedom that can be exploited. A trim where $M = N$ will receive the name of proper trim while the case where $M \neq N$ will receive the name of improper trim. Now, once a trimming function and a distortion have been chosen, a kink diagram can be deformed to construct a trimming diagram as follows

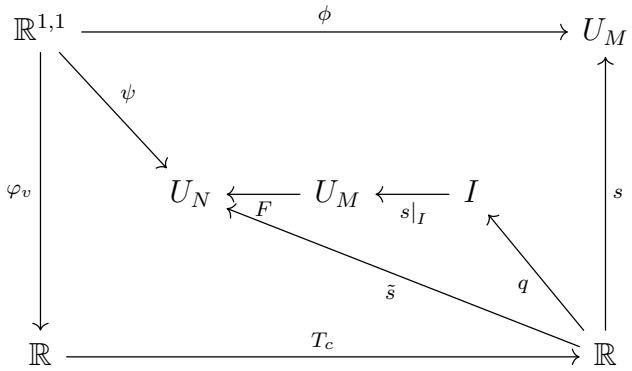

where $s|_I$ is the restriction of the curve s to the interval I and a new map ψ has been introduced. Defining the maps $\tilde{s}$ and ψ by the commutativity of the diagram

$$\tilde{s} = F \circ s|_I \circ q\,, \qquad \psi = \tilde{s} \circ T_c \circ \varphi_v\,,$$

the lower triangle in the trimming diagram defines a new kink diagram

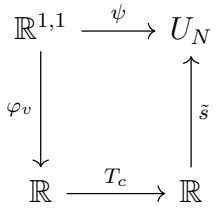

which leads to the configuration $\psi = F \circ s|_I \circ q \circ T_c \circ \varphi_v$. Therefore, a Sigma model on (N, h) will be sought so that the field configuration corresponding to the diagram above

$$\psi(p) = F(\, s|_I \,(q\,[\gamma(x(p) - vt(p))]))\,,$$

for each point in the Minkowski space $p \in \mathbb{R}^{1,1}$, is a kink. For static configurations this expression reads

$$\psi(p) = F(\, s|_I \,(q(x(p))))\,.$$

Note that no reparametrisation is introduced, both curves s and $\tilde{s}$ share the same parametrisation T. Now, if this new configuration corresponds to a kink of a Sigma model on a Riemannian manifold (N, h), it must be a solution of its field equations. Once again, let us restrict to Sigma models where the Bogomol'nyi arrangement can be performed. In this context, a superpotential for a Sigma model that supports the trimmed curve $\tilde{s}$ can be found if Bogomolo'nyi equations hold

$$\frac{d\tilde{s}^j(T)}{dT} = \pm \left[h^{ij} \frac{\partial \tilde{W}}{\partial \tilde{\phi}^i} \right]_{\tilde{s}(T)}\,, \tag{6.1}$$

where $j = 1, \ldots, \dim N$ and Einstein summation convention is employed. In order to obtain a superpotential $\tilde{W}$ that satisfies the equation above, the dependence on T must be transformed into a dependence on the coordinates $\tilde{\phi}^i$ on N. Since by definition the distortion F, the trimming function q and the original curve s are analytically invertible or piecewisely invertible, the trimmed curve $\tilde{s}$ is also analytically invertible or piecewisely invertible

$$\tilde{T}(\tilde{\phi}) = \tilde{s}^{-1}(\tilde{\phi}) = q^{-1}\left(s^{-1}\big|_I \left(F^{-1}(\tilde{\phi}) \right) \right)\,.$$

This implies that equation (6.1) can be expressed entirely in terms of the coordinates $\tilde{\phi}^i$ on N

$$\frac{d\tilde{s}^j}{dT}\left[T(\tilde{\phi}) \right] = \pm\, h^{ij}\left(\tilde{\phi} \right) \frac{\partial \tilde{W}}{\partial \tilde{\phi}^i}\,. \tag{6.2}$$

Accordingly, if a superpotential $\tilde{W}$ solution of the above equations can be found, then a potential for a Sigma model on (N, h) that admits the trim as solution can be constructed

$$\tilde{V}(\tilde{\phi}) = \frac{1}{2} h\left(\mathrm{grad}_h\, \tilde{W}, \mathrm{grad}_h\, \tilde{W} \right)\,.$$

Notice that the functions $T(\tilde{\phi}^i)$ may not be well-defined beyond an open set that contains the trimmed curve Im $\tilde{s}$. Therefore, special care must be taken when specifying the region where the deformed potential is defined. Nevertheless, the emerging potentials can be glued to others so that these new field theories are

defined beyond these limits. Even if this will be the main focus later on in this chapter, let us focus now on the trimming procedure. Lastly, in this section only compact intervals I will be considered. Consequently, the procedure of trimming a curve has, apart from those coming from the distortion, two degrees of freedom. Indeed, the interval I can always be defined by specifying the interval centre T_0 and its width $\lambda > 0$. In next sections different trims are considered. More specifically, proper and improper trims of a ϕ^4-model will be explored.

6.1.1 Proper trims of a ϕ^4-model

In this section proper trims of a kink of the ϕ^4-model are performed. The simplicity of this model will help us to illustrate the inner workings of this procedure. Specifically, the kink $\phi(T) = \tanh T$ with kink diagram

$$\begin{array}{ccc} \mathbb{R}^{1,1} & \xrightarrow{\phi} & \mathbb{R} \\ {\scriptstyle \varphi_v}\downarrow & & \uparrow{\scriptstyle s} \\ \mathbb{R} & \xrightarrow{Id} & \mathbb{R} \end{array}$$

and curve $s(T) = \tanh T$ will be trimmed. When a distortionless proper trim of a kink is performed, the orbit of the new curve is smaller than the original by the definition of trim. Nevertheless, should a distortion be introduced, this situation can be altered. The distortion in proper trims can be defined so that the trimmed orbit is larger or smaller. In this case, we shall consider distortions for which at least one of the ends of the new kink orbit coincide with one of the original ones. In pursuit of this goal, the following two sets of families of trims A and B will be proposed by choosing a dilation as distortion

$$\tilde{s}_A(T) = \frac{s(q(T))}{\lim\limits_{T\to-\infty} s(q(T))}\,, \qquad \tilde{s}_B(T) = \frac{s(q(T))}{\lim\limits_{T\to\infty} s(q(T))}\,. \tag{6.3}$$

Notice that for these families of curves $\tilde{s}_A$ and $\tilde{s}_B$, the trim has been defined to exclusively depend on the trimming function q. For simplicity, only the following two candidates will be considered in this section

$$q_1(T) = T_0 + \lambda \tanh T\,, \qquad q_2(T) = T_0 + \lambda \arctan T\,,$$

which depend in turn on the width λ and the trim centre T_0. Hence, each of these functions are in fact a family of trims, since the centre T_0 and the width λ are yet to be fixed. It is worth noticing that when both limits $T \to \pm\infty$ of the composition of a curve s and a trimming function q coincide

$$\lim_{T\to-\infty} s^i(q(T)) = \lim_{T\to\infty} s^i(q(T))\,,$$

both sets of families of trims $\tilde{s}_A$ and $\tilde{s}_B$ coincide. This will not be the case in general, and it is not the case here as $s(T) = \tanh T$. However, in this particular case, when $T_0 = 0$ both s and q exhibit antisymmetry in their arguments and the image of $\tilde{s}_A$ is exactly that of $\tilde{s}_B$, but run in reverse direction. In fact, their images are identical to

the image of the original curve $\mathrm{Im}\, s = (-1, 1)$. This is, the trim is rescaled so that the image is the same than the original $F(s|_I\,(q(\mathbb{R}))) = s(\mathbb{R})$, see Figure 6.2. As we shall see, this procedure generates variations of the original kink while conserving its topological sector. Finally, to elevate these trims to the status of kinks of a new Sigma model, a potential $\tilde{W}$ that satisfies equation (6.2) must be analytically found. Since the form of the superpotential will depend on the chosen trimming function, let us analyse both q_1 and q_2 separately. For convenience, since T_0 will not vanish in general, only one of these families of trims will be chosen. Let us consider the family of curves $\tilde{s}_B$, for which only the second end of the original orbit will be fixed in general. Notice, however, that the case with $\tilde{s}_A$ is formally identical.

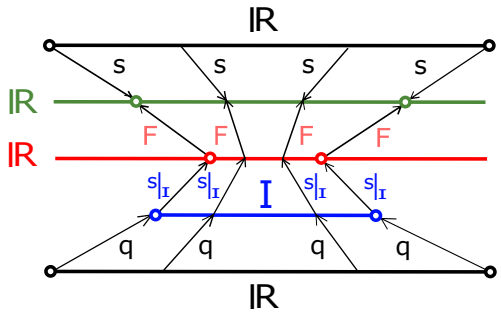

Figure 6.2: The value of the parameter $T_0 = 0$ is chosen to make the orbit of the proper trim identical to that of the original curve s.

Family of trimming functions $q_1(T) = T_0 + \lambda \tanh(T)$

When this family of trimming functions is employed in this trimming formalism to the kink $s(T) = \tanh T$ with the above defined distortion F, it produces the following family of curves

$$\tilde{s}_B(T) = \frac{\tanh\left(T_0 + \lambda \tanh(T)\right)}{\tanh\left(T_0 + \lambda\right)}\,.$$

This family of curves does not contain the original curve and all members share a pivotal point shifted by the parameter T_0, see Figure 6.3. Note that the combination of parameters for which $\lambda + T_0 = 0$ is forbidden by construction. Now, this family of curves admits a family of superpotentials, from which the following family of potential functions can be constructed

$$\tilde{V}(\tilde{\phi}) = \frac{\lambda^2 \coth^2\left(T_0 + \lambda\right)}{2}\left(\frac{\left(T_0 - \mathrm{arctanh}\left[\tilde{\phi}\tanh\left(T_0 + \lambda\right)\right]\right)^2}{\lambda^2} - 1\right)^2 \times \left(\tilde{\phi}^2 \tanh^2(T_0 + \lambda) - 1\right)^2 .$$

This family does not contain the original potential function, but it tends to it at the limit $\lambda \to 0$ when $T_0 = 0$, that is when the width tends to zero and the curve is antisymmetric. On the other hand, it becomes unboundedly high as λ approaches infinity. Note that when $T_0 \neq 0$ the peak of the potential in the region where the trim is defined gets larger as $\lambda \to \infty$. On the other hand, when $T_0 = 0$ both ends

are fixed at the same points as the original curve, but as T_0 moves away from zero the first vacuum point is moved a quantity that also depends on the width λ, see Figure 6.3. Lastly, in the limit $T_0 \to \infty$ the curve approaches a constant solution as it reaches the vacuum point on the right. In conclusion, this procedure constructs a family of Sigma models for which each member of the family of trims is a solution of a member of the constructed family of potential functions. This also means that new vacua are formed so that trims can tend asymptotically to them. It is worth noting as well that these potentials are only defined in a region that completely restricts to the image of the curve when $\lambda \to \infty$. If one wants to further extend the domain of the potential function of the Sigma model, this potential must be glued to another one. This procedure will be covered later on in future sections. Lastly, the energy of each particular trim can be numerically computed by integrating the energy density profile. However, the representation of the peaks in the potential reveals that the energy augments as λ increases. Also, since the original model is retrieved when $T_0 = 0$ and $\lambda \to 0$, in this limit the energy of the original model is recovered.

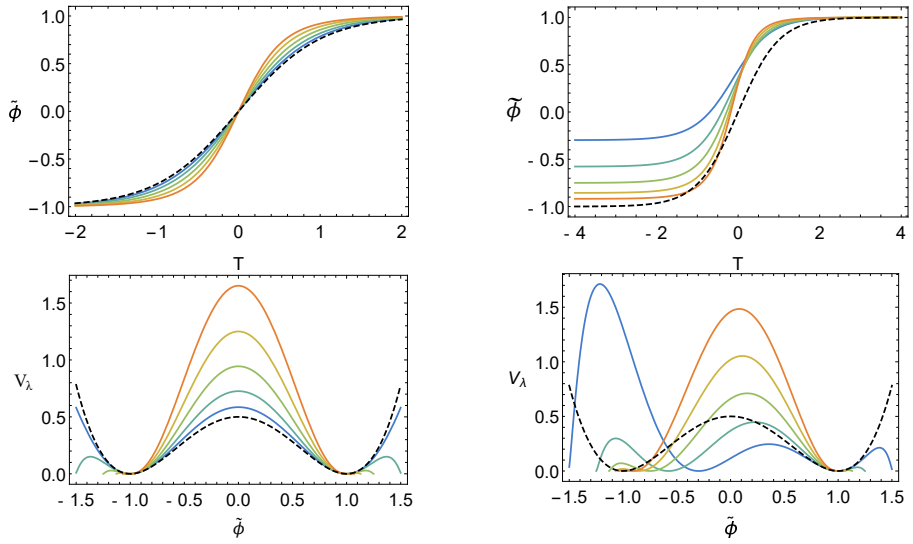

Figure 6.3: Trimmed curves (up) and respective potential functions (down) for q_1 and for the values of width $\lambda = 0.5, 0.8, 1.1, 1.4, 1.7$ respectively. The cases with $T_0 = 0$ and $T_0 = 0.3$ have been depicted on the left and on the right respectively. The reference case of the ϕ^4-model has been represented with a dashed black line.

Family of trimming functions $q_1(T) = T_0 + \lambda \arctan(T)$

If the same procedure is applied employing the other family of trimming functions q_2, the family of trims that are obtained by trimming the ϕ^4-model reads

$$\tilde{s}_B(T) = \frac{\tanh\left(T_0 + \lambda \arctan(T)\right)}{\tanh\left(T_0 + \frac{\lambda\pi}{2}\right)},$$

where once more by construction a particular relation between the width and the trim centre is forbidden $T_0 + \frac{\lambda\pi}{2} \neq 0$. Even if these curves look similar to those for q_1 and have the same properties, see Figure 6.4, in this case the arising family of

potential function reads differently

$$\tilde{V}(\tilde{\phi}) = \frac{\lambda^2 \coth^2\left(T_0 + \frac{\pi\lambda}{2}\right)}{2} \cos^4\left(\frac{T_0 - \operatorname{arctanh}\left[\tilde{\phi}\tanh\left(T_0 + \frac{\pi\lambda}{2}\right)\right]}{\lambda}\right) \times$$
$$\operatorname{sech}^4\left(\frac{T_0 - \lambda\left(T_0 - \operatorname{arctanh}\left[\tilde{\phi}\tanh\left(T_0 + \frac{\pi\lambda}{2}\right)\right]\right)}{\lambda}\right) .$$

In fact, limits of this family of functions are different from those for the case with q_1. In this case, the ϕ^4-model's potential cannot be recovered in the limit $\lambda \to 0$ for any value of T_0. Instead, the peak of this potential gets arbitrarily smaller as λ approaches zero, see Figure 6.4. This also implies that, unlike in the first case with trimming function q_1, the energy of these trims is also allowed to be lower than that of the original kink of the ϕ^4-model.

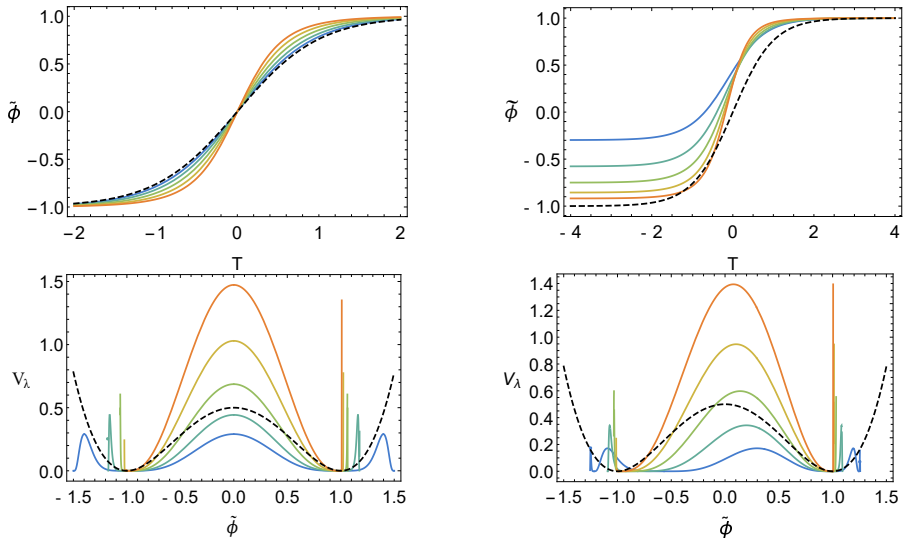

Figure 6.4: Trimmed curves (up) and respective potential functions (down) for q_2 and for the values of width $\lambda = 0.5, 0.8, 1.1, 1.4, 1.7$ respectively. The cases with $T_0 = 0$ and $T_0 = 0.3$ have been depicted on the left and on the right respectively. The reference case of the ϕ^4-model has been represented with a dashed black line.

Thus, employing the trimming procedure once more, a whole family of trims of a kink of the ϕ^4-model has been promoted to a family of kinks, which are solutions of a family of Sigma models with the family of potentials described above. In this method, depending on the location of the trim centre and its width different models are obtained. It is important to emphasise that in order to extend the definition of these potentials beyond the orbit of these trims, these potentials may need to be glued to others. In this case with only one field there exists only one function $T(\tilde{\phi})$. However, when considering target manifolds with more dimensions, more than one of these functions $T(\tilde{\phi}^i)$ will appear. This complicates the process of gluing potentials. Lastly, in this section only proper trims have been considered. This motivates next section, where improper trims are sought, sending the ϕ^4-model's trims to other Riemannian manifolds. In particular, improper trims sent to the two-dimensional sphere $\mathbb{S}^2$ and torus $\mathbb{S}^1 \times \mathbb{S}^1$ will be sought.

6.1.2 Improper trims of a ϕ^4-model

Let us now apply the trimming procedure to a kink of the double ϕ^4-model, so that instead of leaving the cut orbit in $\mathbb{R}^2$, it is transferred to another manifold where it is a kink of a Sigma model. This is, let us proceed by performing improper trims of this model. Among all solutions of the double ϕ^4-model in Cartesian coordinates, the kink $(\phi^1, \phi^2) = (\tanh T, \tanh T)$ will be chosen to be trimmed. For this solution, the following kink diagram with curve $s(T) = (s^1(T), s^2(T)) = (\tanh T, \tanh T)$ is constructed

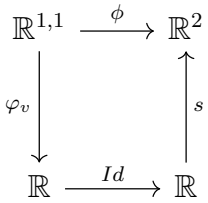

Notice that the orbit of this kink is a diagonal segment in $\mathbb{R}^2$, see Figure 6.5.

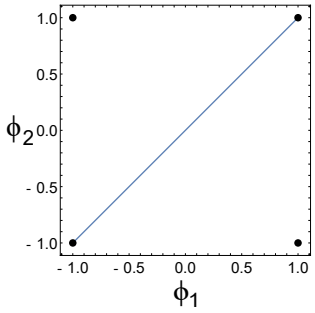

Figure 6.5: The orbit of the chosen kink of the double ϕ^4-model corresponds to a diagonal segment in $\mathbb{R}^2$. The four vacua of this theory are represented by black points.

In this case, the distortion must send points in the plane $\mathbb{R}^2$ to points in another manifold. Let us consider the sphere $(\mathbb{S}^2, \{\theta, \varphi\})$ in spherical coordinates and the torus $(\mathbb{S}^1 \times \mathbb{S}^1, \{\theta, \varphi\})$ in toroidal coordinates simultaneously. This implies that the new target manifold is for both cases $N = \mathbb{S}^2$ and $N = \mathbb{S}^1 \times \mathbb{S}^1$. This leads to the following trimming diagram

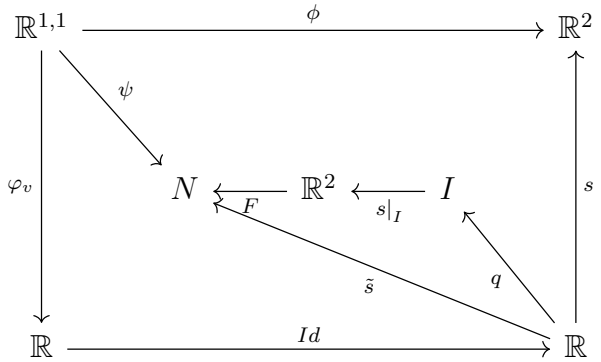

Since all these variables are angular variables, distortions to both manifolds can be considered simultaneously $(\theta, \varphi) = (F_c^1(\phi), F_c^2(\phi))$ so that all sent points for these curves are interpretable as angular variables in both manifolds $F_c(s(T)) \in (0, \pi) \times (0, 2\pi)$. Note that by performing both distortions simultaneously only half of the torus is being targeted. Now, the trim of this kink will be defined similarly

as in the proper trim case, making use of a dilation as distortion and the trimming function of the form q_1 for both components. That is, the angular coordinates for the trim will have in both manifolds the form

$$\theta_B(T) = F_c^1(s(T)) = \frac{\tanh\left(T_0 + \lambda_1 \tanh(T)\right)}{\tanh\left(T_0 + \lambda_1\right)}\,,$$

$$\varphi_B(T) = F_c^1(s(T)) = \frac{\tanh\left(T_0 + \lambda_2 \tanh(T)\right)}{\tanh\left(T_0 + \lambda_2\right)}\,,$$

where the B denotes that the right end of the orbit is fixed. The width of the trim in each component, λ_1 and λ_2, will be allowed to vary independently. The coordinates produced by the distortion (θ, φ) are interpreted in the cases of the sphere and the torus differently. In order to make these coordinates lie within the rectangle $[0, \pi] \times [0, 2\pi)$, the following condition on the trim centre and width will be imposed in each component

$$\begin{aligned} \pi > T_0 + \lambda_1 > T_0 - \lambda_1 > 0\,, \\ \pi > T_0 + \lambda_2 > T_0 - \lambda_2 > 0\,. \end{aligned}$$

Notice that a different trimming centre T_0 could have been employed in each component. However, to illustrate this method more clearly, let us consider the case where the trim centre T_0 is identical in both components. Bogomol'nyi equations (6.2) for the deformed orbit in the sphere can be transformed into two ordinary differential equations when additively separable superpotentials $\tilde{W} = \tilde{W}_1(\phi) + \tilde{W}_2(\varphi)$ are sought

$$\frac{d\tilde{W}_1}{d\theta} = \pm R^2 \frac{d\theta_B}{dT}\left[T(\theta)\right]\,, \qquad \frac{d\tilde{W}_2}{d\varphi} = \pm R^2 \sin^2\theta_B[T(\varphi)] \frac{d\varphi_B}{dT}[T(\varphi)]\,,$$

where $R > 0$ is the radius of the sphere. Solutions of these equations, $\tilde{W}_1$ and $\tilde{W}_2$, define the superpotential $\tilde{W}$ on the sphere. In the case of the torus, Bogomol'nyi equations read

$$\frac{d\tilde{W}_1}{d\theta} = \pm r^2 \frac{d\theta_B}{dT}\left[T(\theta)\right]\,, \qquad \frac{d\tilde{W}_2}{d\varphi} = \pm (R + r\sin\theta_B[T(\varphi)])^2 \frac{d\varphi_B}{dT}[T(\varphi)]\,,$$

where R and r are the major and minor radius of the torus $R > r > 0$. The family of potential functions for the case of the sphere reads

$$\begin{aligned} \tilde{V}_{\mathbb{S}^2}(\theta, \varphi) = {} & \frac{\lambda_1^2 \coth^2(T_0 + \lambda_1)}{2R^2} \left(\frac{\left(T_0 - \operatorname{arctanh}[\theta \tanh(T_0 + \lambda_1)]\right)^2}{\lambda_1^2} - 1 \right)^2 \\ & \times \left(\theta^2 \tanh^2(T_0 + \lambda_1) - 1\right)^2 + \frac{\lambda_2^2 \coth^2(T_0 + \lambda)}{2R^2 \sin^2\theta} \left(\varphi^2 \tanh^2(T_0 + \lambda_2) - 1\right)^2 \\ & \times \left(\frac{\left(T_0 - \operatorname{arctanh}[\varphi \tanh(T_0 + \lambda_2)]\right)^2}{\lambda_2^2} - 1 \right)^2\,, \end{aligned}$$

while for the case of the torus is almost identical except for the factor that depends

on the metric

$$\tilde{V}_{\mathbb{S}^1\times\mathbb{S}^1}(\theta,\varphi) = \frac{\lambda_1^2\coth^2(T_0+\lambda_1)}{2R^2}\left(\frac{(T_0-\operatorname{arctanh}[\theta\tanh(T_0+\lambda_1)])^2}{\lambda_1^2}-1\right)^2$$
$$\times\left(\theta^2\tanh^2(T_0+\lambda_1)-1\right)^2+\frac{\lambda_2^2\coth^2(T_0+\lambda_2)}{2R^2\sin^2\theta}\left(\varphi^2\tanh^2(T_0+\lambda_2)-1\right)^2$$
$$\times\left(\frac{(T_0-\operatorname{arctanh}[\varphi\tanh(T_0+\lambda_2)])^2}{\lambda_2^2}-1\right)^2.$$

For cases where the same width is chosen to perform the trim in both components, the orbits of the family of trims resemble those of the trims in the plane. Only one orbit appears when $\lambda_1=\lambda_2=\lambda$ for any width λ. However, even if the orbit in $\mathbb{R}^2$ is a straight segment, the improper trim will lead to different orbits when the widths λ_1 and λ_2 are different. The effect of altering the difference of widths can be seen in Figure 6.6, where orbits of different trims in both the sphere and the torus are depicted.

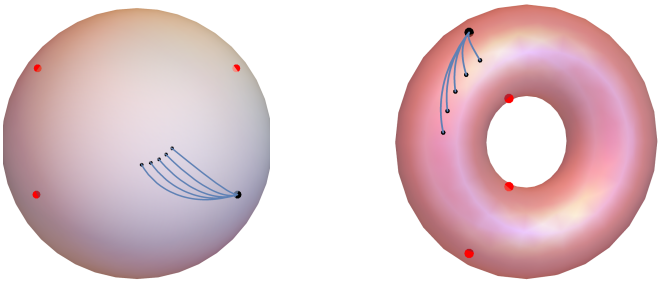

Figure 6.6: Improper trims of a kink of the double ϕ^4-model transferred to the sphere and torus. Each curve joins the sent vacuum point to a new one, which is created on the sphere and torus at the cutting point. The three red points represent the disappeared vacua of the original ϕ^4-model sent to the sphere and torus. Values $T_0=1$, $\lambda_1=0.7$ and $\lambda_2=0.1,0.3,0.5,0.7,0.9$ have been employed.

In conclusion, this formalism of trims can also be employed to construct Sigma models on other Riemannian manifolds. Even though the original kink orbit is fixed, the trim centre T_0 and its widths λ_i are still free to generate different deformed kink orbits. Furthermore, the inclusion of a distortion allows us to modulate the size of the orbits of proper trims, making them equal-sized or even larger than the original. It also allows us to consider cases where the trim is mapped to another Riemannian manifold. On the other hand, non-topological kinks can be transformed into topological kinks by means of a proper trim.

Lastly, notice that even if this procedure is based on the deformation formalism introduced in last chapter, it goes a step further. Indeed, the seed-dependent deformations described in this section cut the original kink orbit, instead of sending the whole orbit to the new manifold. Hence, this procedure serves as a new example of deformation method.

6.2 Hybridisation and extention of kinks

In last section, kink orbits are cut and sent to new Riemmanian manifolds, where Sigma models that admit these trims as solutions are constructed. It is only natural to consider the inverse process, that is, combining different kinks to construct another kink of another Sigma model. This is precisely the aim of this section, the piecewise construction of potentials of Sigma models that admit piecewise curves as solutions. These piecewise curves will receive the name of *hybrids* and the process of construction shall be referred to as *hybridisation*.

First of all, conditions for gluing kinks will be derived, which as we shall see, will frequently involve the use of interpolations. Then, a method for hybridisation is applied to simple kinks, so that points where these can be properly glued are sought. Lastly, different methods of extensions of kinks are discussed and examples found in $\mathbb{R}^n$ and other Riemannian manifolds. Notice that while the information to trim a kink, once the trimming function is fixed, is just the two points where the cutting occurs, extensions can be performed in an infinite number of ways. The gluing of curves must be at least C^2 at the junction where they are glued. However, the potentials must be at least C^1 not only at the junction of curves, but also in a neighbourhood that contains such a curve. Therefore, extra information must be added in general to perform the gluing of potentials. This will require us to employ distinct strategies to successfully extend curves and potentials.

6.2.1 Gluing of curves and potentials

The first problem that must be addressed when combining kinks is whether two kinks that are piecewisely combined allow the corresponding potentials to be piecewisely combined. That is, whether a potential of a Sigma model can be defined on a region that contains the piecewise curve so that this curve is a solution of such Sigma model. Let $s_1, s_2 \in C^2(\mathbb{R}, M)$ be two curves on a Riemannian manifold (M, g) that correspond to two kinks of two Sigma models on M such that they intersect $s_1(T_0) = s_2(T_0)$ at the point given by the parameter value T_0. Moreover, let us assume that also the first and second derivatives of these curves at T_0 coincide. Then, let us construct the combined curve as follows

$$s(T) = \begin{cases} s_1(T) & \text{if } T \leq T_0 \\ s_2(T) & \text{if } T_0 < T \end{cases}$$

which is C^2 at the junction by definition. The objective is not only to combine these curves, but also the corresponding potentials V_1 and V_2

$$V(\phi) = \begin{cases} V_1 & \text{if } \phi \in \text{Region } A \\ V_2 & \text{if } \phi \in \text{Region } B \end{cases}$$

finding regions A and B in the chart on M so that they can merge differentiably. This is, the potential must be well-defined not only at the junction of curves, but also along the junction of regions A and B where the individual curves are defined, see for example Figure 6.7. Notice that for field theories with only one field, the boundary between regions A and B is just a point. However, as the dimension of the target manifold augments, so does the dimension of the boundary between A and B, increasing the complexity of the gluing process.

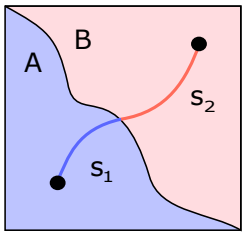

Figure 6.7: The potentials for the separate curves must be properly glued even outside the junction of curves. In this particular example where a two-dimensional target space has been considered, the junction is a curve in $\mathbb{R}^2$.

For the sake of convenience, let us first search for the condition under which this piecewise potential function is continuous and differentiable at the junction of curves. This is, at the point where these curves intersect $s_1(T_0) = s_2(T_0)$.

- **Continuity at the junction**: Let us assume that these potentials, both the one defined on the region A and that defined on region B, admit a superpotential. This implies that these can be written as follows

$$V_1(\phi) = \frac{1}{2} g\left(\text{grad } W_1, \text{grad } W_1\right) , \qquad V_2(\phi) = \frac{1}{2} g\left(\text{grad } W_2, \text{grad } W_2\right) ,$$

and that solutions of Bogomol'nyi equations are kink-type solutions

$$\frac{ds_1^a}{dT} = \pm g^{ma} \frac{\partial W_1}{\partial \phi^m} , \qquad \frac{ds_2^a}{dT} = \pm g^{na} \frac{\partial W_2}{\partial \phi^n} .$$

Curves must be C^2 and consequently the gluing must also be C^1, that is

$$s_1(T_0) = s_2(T_0) , \qquad \left.\frac{ds_1}{dT}\right|_{T_0} = \left.\frac{ds_2}{dT}\right|_{T_0} .$$

Then, if one of these potentials is evaluated at the junction T_0, using Bogomol'nyi equations the evaluation of the other potential at that same point is obtained

$$V_1(s_1(T_0)) = \frac{1}{2} g\left(grad\ W_1|_{s_1(T_0)} , grad\ W|_{s_1(T_0)}\right) = \frac{g_{ab}(s_1(T_0))}{2} \left.\frac{ds_1^a}{dT}\right|_{T_0} \left.\frac{ds_1^b}{dT}\right|_{T_0}$$

$$= \frac{g_{ab}(s_2(T_0))}{2} \left.\frac{ds_2^a}{dT}\right|_{T_0} \left.\frac{ds_2^b}{dT}\right|_{T_0} = V_2(s_2(T_0)) .$$

This implies that the continuity of piecewise potentials along C^2-piecewise curves for potentials constructed from a superpotential is guaranteed $V_1(s_1(T_0)) = V_2(s_2(T_0))$.

- **Differentiability at the junction**: The second order differential equations corresponding to the two original Sigma models on a Riemannian manifold M read

$$\frac{d^2 s_1^i}{dT^2} + \Gamma^i_{jk} \frac{ds_1^j}{dT} \frac{ds_1^k}{dT} = g^{ik} \left.\frac{\partial V_1}{\partial \phi^k}\right|_{s(T)} ,$$

$$\frac{d^2 s_2^i}{dT^2} + \Gamma^i_{jk} \frac{ds_2^j}{dT} \frac{ds_2^k}{dT} = g^{ik} \left.\frac{\partial V_2}{\partial \phi^k}\right|_{s(T)} .$$

These equations allow us to isolate the derivatives of both potential functions along the curves s_1 and s_2 respectively

$$\left.\frac{\partial V_1}{\partial \phi^a}\right|_{s_1(T)} = g_{ai}(s_1(T))\left(\frac{d^2 s_1^i}{dT^2} + \Gamma^i_{jk}(s_1(T))\frac{ds_1^j}{dT}\frac{ds_1^k}{dT}\right),$$
$$\left.\frac{\partial V}{\partial \phi^a}\right|_{s_2(T)} = g_{ai}(s_2(T))\left(\frac{d^2 s_2^i}{dT^2} + \Gamma^i_{jk}(s_2(T))\frac{ds_2^j}{dT}\frac{ds_2^k}{dT}\right).$$

Notice that in these equations not only do the first derivatives of the curves $\frac{ds_1^j}{dT}$ and $\frac{ds_2^j}{dT}$ appear, but also the second derivatives $\frac{d^2 s_1^j}{dT^2}$ and $\frac{d^2 s_2^j}{dT^2}$. Since the piecewise curve is by construction C^2

$$s_1(T_0) = s_2(T_0)\,, \qquad \left.\frac{ds_1}{dT}\right|_{T_0} = \left.\frac{ds_2}{dT}\right|_{T_0}, \qquad \left.\frac{d^2 s_1}{dT^2}\right|_{T_0} = \left.\frac{d^2 s_2}{dT^2}\right|_{T_0},$$

then the derivatives of both potentials can be related as follows

$$\left.\frac{\partial V_1}{\partial \phi^a}\right|_{s_1(T_0)} = g_{ai}(s_1(T_0))\left(\left.\frac{d^2 s_1^i}{dT^2}\right|_{T_0} + \Gamma^i_{jk}(s_1(T_0))\left.\frac{ds_1^j}{dT}\right|_{T_0}\left.\frac{ds_1^k}{dT}\right|_{T_0}\right)$$
$$= g_{ai}(s_2(T_0))\left(\left.\frac{d^2 s_2^i}{dT^2}\right|_{T_0} + \Gamma^i_{jk}(s_2(T_0))\left.\frac{ds_2^j}{dT}\right|_{T_0}\left.\frac{ds_2^k}{dT}\right|_{T_0}\right) = \left.\frac{\partial V_2}{\partial \phi^a}\right|_{s_2(T)}.$$

Consequently, since curves s_1 and s_2 share the same tangent vector and the same curvature at the junction, the piecewise potential function is C^1 at the junction.

In summary, since the gluing of curves s_1 and s_2 is C^2, then the potential functions can be C^1-glued at the junction of curves. When only one field is present, the potential function is automatically well-defined since the boundary between regions A and B is just the junction of curves. However, when Sigma models with multiple fields are considered, the gluing must be performed at least in a neighbourhood of the junction. In order to make this potential function well-defined, it will be defined not just on the curve but at least in a strip that contains it. Let us consider the two dimensional case, even if higher-dimensional cases can be treated similarly. In order to be able to extend the potential into a strip, two extra regions, C and D, are added in the chart between regions A and B. These regions combined will form a strip, see Figure 6.8.

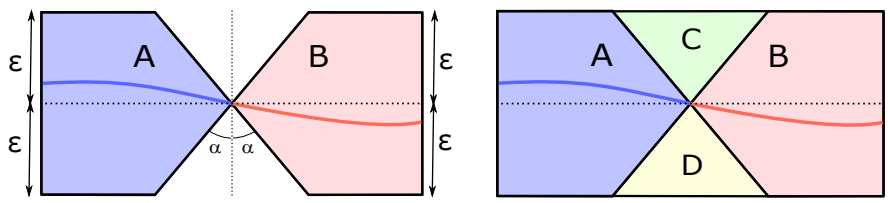

Figure 6.8: Two regions are introduced between regions A and B so that there is room for interpolation of potentials. Parameters ε and α are chosen in each case so that curves s_1 and s_2 are confined to regions A and B respectively.

The width of the strip $\epsilon > 0$ and the angle $\alpha > 0$ are introduced to ensure that both curves s_1 and s_2 are contained in their respective regions A and B. In general, the orientation of the strip will be different from that of the Figure 6.8. However, coordinates can be rotated until such orientation is obtained to simplify the expressions. Let us denote the rotated "Cartesian" coordinates ϕ^1 and ϕ^2. Let us introduce in the region C, which is the upper triangle, new coordinates h and t as follows

$$\phi^1 = h \sin\alpha\,(2t-1)\,, \qquad \phi^2 = h\cos\alpha\,,$$

with $t \in [0,1]$ and $h \in [0, \frac{\epsilon}{\cos\alpha}]$. These coordinates correspond to the lateral length of the triangle h and a variable t that describes positions on the horizontal segments between regions A and B, see Figure 6.9.

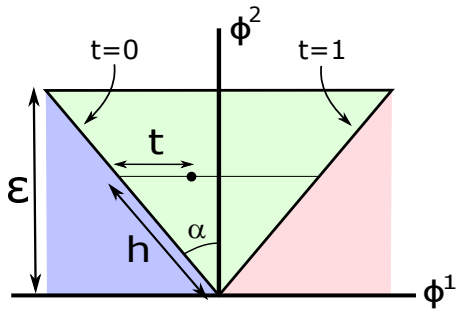

Figure 6.9: A new coordinate system is introduced in region C so that an interpolation of potential functions can be performed. While h controls the location of the horizontal segment, t indicates the position on this segment.

Note that $t = 1$, which defines points related as $\phi^1 = \phi^2 \tan\alpha$, describes points of the boundary between C and B while $t = 0$, which defines points related as $\phi^1 = -\phi^2 \tan\alpha$, describes points of the boundary between A and C. On the other hand, similar coordinates can be defined in region D, but the procedure is identical and therefore it is omitted here. These coordinates in C can be inverted

$$t = \frac{1}{2}\left(1 + \frac{\phi^1}{\phi^2}\cot\alpha\right)\,, \qquad h = \frac{\phi^2}{\cos\alpha}\,.$$

Making use of the coordinate $t(\phi)$ expressed in terms of the original Cartesian coordinates, an interpolation of the potentials defined on A and that on B can be constructed in C as follows

$$V_C(\phi) = (1 - t(\phi))\; V_1(\phi) + t(\phi)\; V_2(\phi)\,,$$

However, while the values are correctly interpolated, derivatives are not

$$\frac{\partial V_C(\phi)}{\partial \phi^i} = (1 - t(\phi))\; \frac{\partial V_1(\phi)}{\partial \phi^i} + t(\phi)\; \frac{\partial V_2(\phi)}{\partial \phi^i} + (V_2(\phi) - V_1(\phi))\frac{\partial t(\phi)}{\partial \phi^i}\,,$$

since functions $\frac{\partial t(\phi)}{\partial \phi^i}$ with $i = 1, 2$ do not vanish when $t = 0$ and $t = 1$. As a consequence, the following change of coordinate in the horizontal segments is performed

$$\tilde{t}(t) = \frac{1}{4}\left(2 - 3(2t-1) + (2t-1)^3\right)\,,$$

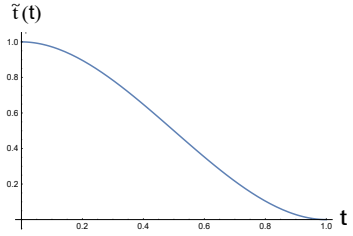

Figure 6.10: Representation of the change of coordinate $t \to \tilde{t}$ in the horizontal segments. Notice that these variables are run in inverse directions, when one is zero the other is one and viceversa.

see Figure 6.10. This new coordinate $\tilde{t}$ instead of running from zero to one will run from 1 to zero. This implies that now $\tilde{t} = 1$ corresponds to the boundary with A and $\tilde{t} = 0$ to the boundary with B. This new coordinate, which can be written in terms of ϕ^1 and ϕ^2 as

$$\tilde{t}(\phi^1, \phi^2) = \frac{1}{4}\left(2 - 3\frac{\phi^1}{\phi^2}\cot\alpha + \left(\frac{\phi^1}{\phi^2}\cot\alpha\right)^3\right) ,$$

apart from having the values for the two boundaries swapped, has vanishing partial derivatives $\frac{\partial\tilde{t}(\phi)}{\partial\phi^i} = 0$ when $\phi^1 = \phi^2 \tan\alpha$ and $\phi^1 = -\phi^2 \tan\alpha$. This is, in the boundaries of C with both A and B. This allows us to interpolate simultaneously in C the potentials and their partial derivatives from Region A to Region B swapping the interpolation terms as follows

$$V_C(\phi) = \tilde{t}(\phi)\ V_1(\phi) + (1 - \tilde{t}(\phi))\ V_2(\phi)\,.$$

Indeed, given the form of this interpolation, the potentials and their partial derivatives for $i = 1, 2$ are recovered in the boundaries of C

$$V_C(\phi)|_{\tilde{t}=1} = V_1(\phi)\,, \qquad V_C(\phi)|_{\tilde{t}=0} = V_2(\phi)\ ,$$
$$\left.\frac{\partial V_C(\phi)}{\partial\phi^i}\right|_{\tilde{t}=1} = \frac{\partial V_1(\phi)}{\partial\phi^i}\,, \qquad \left.\frac{\partial V_C(\phi)}{\partial\phi^i}\right|_{\tilde{t}=0} = \frac{\partial V_2(\phi)}{\partial\phi^i}\,.$$

We conclude then that it is enough to define the gluing of curves as C^2 to be able to construct a piecewise potential on a strip that contains the piecewise curve. It is worth noticing that this procedure can be iteratively employed to piecewisely combine multiple curves, see Figure 6.11. On the other hand, when two curves cannot be directly C^2-glued, an interpolation will be necessary. This possibility will be explored in next section.

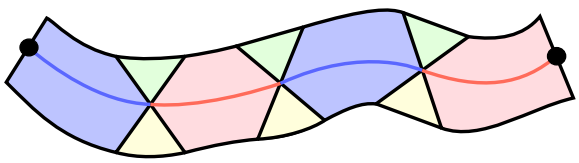

Figure 6.11: A chain of piecewise curves is constructed when the gluing procedure is iteratively employed, leading to a strip where the different potential functions are interpolated.

6.2.2 Cubic and quartic polynomial interpolations

When the curves corresponding to two kinks cannot be directly C^2-glued, an additional step must be included to construct the hybrid Sigma model. An intermediate curve can be introduced between the two original curves to ensure that they satisfy the C^2-gluing condition with this newly added curve. That is, an interpolation curve can be considered to facilitate this type of gluing. According to the results from the previous section, for the formation of the strip that contains the piecewise curve, the potential function in each portion of the piecewise curve must be analytically available. This implies that if an interpolation curve must be added, a potential function for which it is solution must be analytically available. Regardless of whether the potential can be derived from a superpotential, the evaluation of the potential along an interpolation curve $c(T)$ can be written as follows

$$V(c(T)) = \frac{1}{2} g_{ab}(c(T)) \frac{dc^a}{dT} \frac{dc^b}{dT} \,, \tag{6.4}$$

which does not have singularities if g_{ab} does not include them. If the interpolation curve $c(T)$ is analytically invertible $T(\phi^i)$ for $i = 1, \ldots, \dim M$, then from the expression above potential functions that admit that interpolation curve $c(T)$ as solution can be constructed $V(c(T(\phi)))$. The substitution of these functions $T(\phi^i)$ can be performed such that the potential is separable. In this scenario a superpotential function can always be constructed. Therefore, if the gluing of curves is C^2, the continuity and differentiability conditions for the potential at the junctions with interpolation curves are also satisfied. Notice that while in the case of just one field this potential is unique

$$V(\phi) = \frac{1}{2} \left(\frac{dc}{dT} \left[T(\phi) \right] \right)^2 \,, \tag{6.5}$$

when more than one are present an infinite number of combination arise. Given this multiplicity of potentials, the substitutions $T(\phi^i)$ must be therefore performed in the most convenient manner. In particular, polynomial interpolation functions will be specially useful. In fact, polynomials of degree three and four will be considered in this chapter. Frequently, polynomials with lower degree than three do not have enough degrees of freedom to successfully interpolate curves. On the other hand, for degrees higher than four the analytical inverse is not available anymore. Since the inverse of third-degree polynomials is considerably simpler than that of degree four, polynomial interpolation functions of degree three for each component $i = 1, \ldots, \dim M$

$$c_i(T) = \alpha_i (T - T_0)^3 + \beta_i (T - T_0)^2 + \gamma_i (T - T_0) + \delta$$

with free parameters $\alpha, \beta, \gamma, \delta \in \mathbb{R}$ will be chosen when possible. In certain situations, as we shall see, third-degree polynomials will not suffice. In this scenarios a polynomial interpolation function of degree four for each component

$$c_i(T) = \alpha_i (T - T_0)^4 + \beta_i (T - T_0)^3 + \gamma_i (T - T_0)^2 + \delta (T - T_0) + \epsilon$$

with free parameters $\alpha, \beta, \gamma, \delta, \epsilon \in \mathbb{R}$ will be considered. It is of note that other interpolation techniques can be applied, but the simplicity of the inverse function must be prioritised. The next step in the process of constructing hybrid kinks is to analyse the energy of the resulting hybrid. Indeed, the energy of kinks must be finite.

6.2.3 Energy of a hybrid

A Hybrid is a piecewise curve that is a solution of a Sigma model with a C^1 piecewise potential function. As such, the hybrid has associated an energy, obtained by integrating and summing the contribution to the energy of every part. When interpolations are employed to link different pieces, the energy of the combined curve will depend on the interpolation that has been chosen. Indeed, the constructed potential function defined on the region of the interpolation curve (6.4) depends on the form of the curve. If we denote as $s(T)$ the hybrid curve and $V(s(T))$ the combined potential function on the curve, then the energy density can be written as

$$\varepsilon(T) = \frac{1}{2} g_{ab}(s(T)) \frac{ds^a}{dT} \frac{ds^b}{dT} + V[s(T)] = g_{ab}(s(T)) \frac{ds^a}{dT} \frac{ds^b}{dT} \,,$$

and then the energy is obtained by integrating this function along the whole real line

$$E\,[s] = \int_{-\infty}^{\infty} \varepsilon(T)\; dT \,.$$

The energy density is by construction piecewisely defined and therefore we can express the energy as the sum of the contributions of all the curves that form the hybrid. For a hybrid with m pieces of kinks and $m-1$ interpolations between them, the energy can be written as the sum of $2m-1$ contributions

$$E\,[s] = \int_{-\infty}^{T_1} \varepsilon_1 \; dT + \int_{T_1}^{T_2} \varepsilon_2 \; dT + \cdots + \int_{T_{2m-2}}^{T_{2m-1}} \varepsilon_{2m-1} \; dT \,, \tag{6.6}$$

where parameters $(T_1, \ldots, T_{2m-1})$ define the locations of the junctions of the gluings. The interpolation curves that are being considered are C^∞, as only polynomial interpolations are being employed. This implies that unless a curve crosses a singularity of the metric, the contribution to the energy of an interpolation curve $c_i(T)$ will always be finite

$$E\,[c_i] = \int_{T_{i,0}}^{T_{i,f}} \varepsilon(c_i(T))\; dT = \int_{T_{i,0}}^{T_{i,f}} g_{ab}(c_i(T)) \frac{dc_i^a}{dT} \frac{dc_i^b}{dT} \; dT < \infty \,,$$

since this function is defined on a compact $(T_{i,a}, T_{i,b}) \subset \mathbb{R}$. On the other hand, the contributions to the energy of the cut kinks must be smaller than those of the whole kinks

$$\int_{T_{i,a}}^{T_{i,b}} \varepsilon_{kink_i} < \int_{-\infty}^{\infty} \varepsilon_{kink_i} = E_{kink_i} < \infty$$

and therefore they are also finite. Finally, this implies that the total energy (6.6) of the hybrid is finite

$$E[s] < \sum_{i=1}^{n} E_{kink_i} + \sum_{j=1}^{m} E_{interpolation_j} < \infty \,.$$

Consequently, since the energy of the hybrid is finite, the hybrid is indeed a kink of the Sigma model on the Riemannian manifold M with the constructed piecewise potential function. Lastly, notice that the combined curve has been constructed from fragments of kinks. If this is not the case, the contribution to the energy of all the involved pieces must be calculated and the finiteness of the energy checked.

6.2.4 Hybridisation of models with one field

In order to exemplify this procedure of hybridisation, let us first restrict to field theories with only one field. Curves corresponding to kinks must be combined in a manner such that the gluings are C^2. As a consequence, the junctions where the original curves are combined to produce the piecewise curve s, must be carefully chosen so that this condition holds. Let us consider two scenarios, one where two curves s_1 and s_2 are directly merged and another that involves a polynomial interpolation of degree three between these curves.

1. **No interpolation**: When the gluing is directly performed, the condition that the piecewise curve must be C^2 can be written as

$$\begin{aligned} f_1(T) &\equiv s_1(T) - s_2(T) = 0\,, \\ f_2(T) &\equiv s_1'(T) - s_2'(T) = 0\,, \\ f_3(T) &\equiv s_1''(T) - s_2''(T) = 0\,, \end{aligned}$$

   where these three auxiliary functions f_1, f_2 and f_3 have been defined. An intersection at T_0 of the graphs of these three functions where they all vanish

$$f_1(T_0) = f_2(T_0) = f_3(T_0) = 0\,,$$

   implies the possibility of C^2-gluing these two curves at the value of the parameter T_0. On the other hand, the absence of this intersection prevents the implementation of this type of C^2-gluings. In these cases an interpolation will be necessary.

2. **Polynomial interpolation of degree three**: When an interpolation is involved, instead of just a junction at T_0, two values of the parameter of curves T_1 and T_2 will represent the position of such junctions. Different values of T_1 and T_2 define different hybrid curves $s : \mathbb{R} \to \mathbb{R}$ of s_1 and s_2, as the interpolation curve c is introduced between different points

$$s(T) = \begin{cases} s_1(T) & \text{if } T \leq T_1 \\ c(T) & \text{if } T_1 \leq T \leq T_2 \\ s_2(T) & \text{if } T \geq T_2 \end{cases}$$

   These cutting points T_1 and T_2 are free to vary as long as the order $T_2 \geq T_1$ is maintained. Note that the case $T_2 \leq T_1$ corresponds to permuting the order in which curves s_1 and s_2 appear. This is, therefore, a whole family of hybrid curves that depends on parameters T_1 and T_2. In this section, only polynomial interpolations of degree three will be considered

$$c(T) = a_0 + a_1(T - T_1) + a_2(T - T_1)^2 + a_3(T - T_1)^3\,,$$

   where $a_0, a_1, a_2, a_3 \in \mathbb{R}$, since this degree will be enough for the examples that shall be shown. Notice that a shift in T have been performed so that $a_0 = s_1(T_1)$. Now, the two cutting values of the parameters $T_1, T_2 \in \mathbb{R}$ must be found so that the C^2 gluing conditions hold

$$\begin{aligned} s_1(T_1) &= c(T_1), & c(T_2) &= s_2(T_2), \\ s_1'(T_1) &= c'(T_1), & c'(T_2) &= s_2'(T_2), \\ s_1''(T_1) &= c''(T_1), & c''(T_2) &= s_2''(T_2). \end{aligned}$$

This set of six equations can be reduced to the following two conditions when $T_1 \neq T_2$

$$F_1(T_1, T_2) = 0\,, \qquad F_2(T_1, T_2) = 0\,,$$

this is, when the interpolation step is not skipped. These functions are defined as

$$\begin{aligned} F_1(T_1,T_2) =& s_1''(T_1)(T_2-T_1)^2 - (T_2-T_1)\left[s_2'(T_2) - s_1'(T_1)\right] \\ &+ 3\left[s_2(T_2) - s_1(T_1) - s_1'(T_1)(T_2-T_1) - \frac{1}{2}s_1''(T_1)(T_2-T_1)^2\right], \\ F_2(T_1,T_2) =& s_2(T_2) - s_1(T_1) - s_1'(T_1)(T_2-T_1) - \frac{1}{2}s_1''(T_1)(T_2-T_1)^2 \\ &- \frac{(T_2-T_1)^2}{6}\left[s_2''(T_2) - s_1''(T_1)\right]. \end{aligned}$$

Solutions (T_1, T_2) of these two equations not only determine the two cutting points in s_1 and s_2, but also the interpolation function

$$\begin{aligned} c(T) =& s_1(T_1) + s_1'(T_1)(T-T_1) + \frac{1}{2}s_1(T_1)(T-T_1)^2 \\ &+ \frac{s_2(T_2) - s_1(T_1) - s_1'(T_1)(T_2-T_1) - \frac{1}{2}s_1''(T_1)(T_2-T_1)^2}{(T_2-T_1)^3}(T-T_1)^3\,. \end{aligned}$$

Notice that solving analytically these two equations, i.e. $F_i(T_1, T_2) = 0$ for $i = 1, 2$, will not be possible in general and numerical methods may be necessary.

Once this hybridisation procedure has been described, let us apply it to merge different simple kinks to illustrate this method. In particular, different solutions of the ϕ^4-model and other models will be combined.

Hybridisation between $\tanh T$ and $\tanh T/2$

When this formalism is applied to two solutions of the ϕ^4-model given by $s_1(T) = \tanh T$ and $s_2(T) = \tanh T/2$, equations must be solved numerically. If the previously defined auxiliary functions f_1, f_2 and f_3 are simultaneously plotted, it becomes clear that direct gluings are not possible in this case, see Figure 6.12.

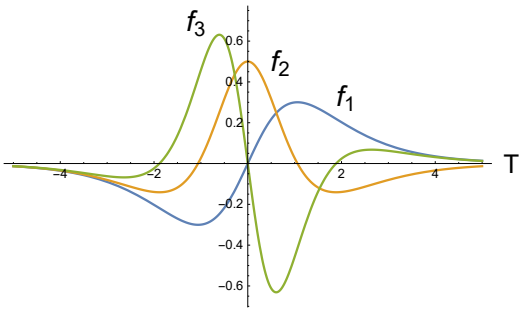

Figure 6.12: Since no simultaneous intersection of the three graphs exist, an interpolation is needed to construct the hybrid kink.

When interpolations of degree three are considered, the C^2-gluing requirement leads us to conditions $F_1(T_1, T_2) = 0$ and $F_2(T_1, T_2) = 0$. See Figure 6.13 for the

simultaneous contourplot of $F_1(T_1, T_2) = 0$ and $F_2(T_1, T_2) = 0$. Each point in the contourplot of each function $F_i = 0$ is a pair of parameters (T_1, T_2) for which the corresponding equation holds. Intersections of both contourplot curves, surrounded in Figure 6.13 by a red circumference, will provide us with pairs (T_1, T_2) that satisfy both equations simultaneously. These intersections occur for the chosen kinks at pairs

$$(T_1, T_2) = (0, 0)\,, \quad (T_1, T_2) = (-5.08845, -1.0996)\,, \quad (T_1, T_2) = (5.08845, 1.0996)\,.$$

Even though three solutions appear, one of them corresponds to swapping the order in which these kinks are combined. Only solutions that satisfy $T_2 \geq T_1$ will be considered. On the other hand, notice that in the derivation of these equations $T_2 \neq T_1$ is imposed for the interpolated case. Hence, the first solution $(0, 0)$ must be discarded. Finally, the correspoding interpolation of curves and potentials can be observed for the remaining solution in Figure 6.13. Even if the energy of the hybrid has not been explicitly calculated, it can be obtained numerically by integrating the piecewise energy density.

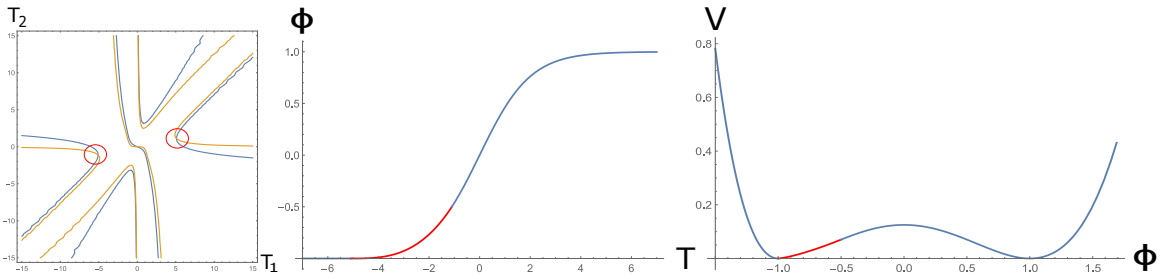

Figure 6.13: On the left the simultaneous contourplot of both equations $F_i = 0$ are shown. Two non-vanishing pairs (T_1, T_2) for which both equations are simultaneously satisfied and $T_2 \geq T_1$ appear as solutions. In the centre the piecewise curve has been plotted and on the right the piecewise potential is displayed.

Hybridisation between $\tanh T$ and $\tanh\left(T - \frac{1}{2}\right)$

If the same procedure is applied to kinks of the same ϕ^4-model given by $s_1(T) = \tanh T$ and $s_2(T) = \tanh\left(T - \frac{1}{2}\right)$, the impossibility of direct hybridisation becomes apparent once more, see Figure 6.14.

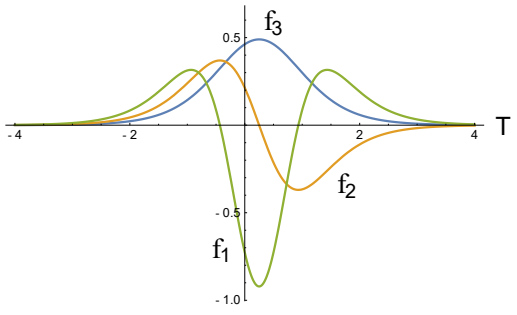

Figure 6.14: Since no simultaneous intersection of the three graphs exists, an interpolation is needed to construct the hybrid kink.

Indeed, no simultaneous intersection of the three graphs arises. On the other hand, a numerical solution of equations $F_1(T_1, T_2) = F_2(T_1, T_2) = 0$ with $T_2 > T_1$ is found at $(T_1, T_2) = (-1.15002, 1.65003)$. Therefore, these solutions can only be hybridised by means of an interpolation, see Figure 6.15. Once more, the symmetrical hibridisation appears as solution, even though it has been omitted. Lastly, once again the energy of the hybrid can be obtained numerically by integrating the piecewise energy density.

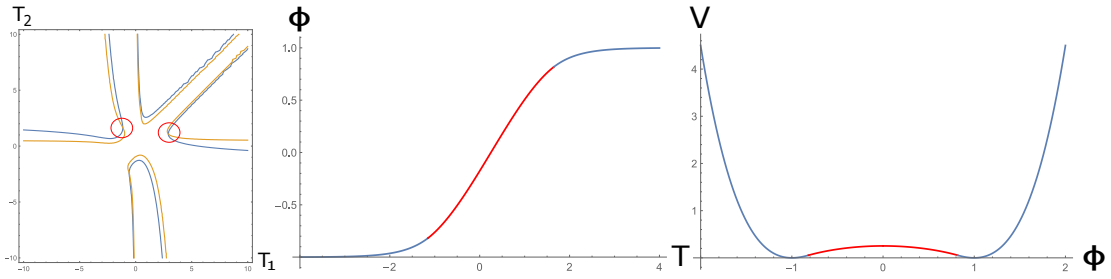

Figure 6.15: On the left the simultaneous contourplot of both equations $F_i = 0$ are shown. Only one pair (T_1, T_2) for which both equations are simultaneously satisfied and $T_2 > T_1$ appears as solution. In the centre the piecewise curve has been plotted and on the right the piecewise potential is displayed.

Hybridisation between $\tanh T$ and $\arctan T$

In this last case, instead of combining different kinks of the same field theory, kinks of different models are merged. In particular, let us apply the same procedure to a kink of the ϕ^4-model $s_1(T) = \tanh T$ and another curve $s_2(T) = \arctan T$, for which a potential must be constructed. These curves have been selected because they exhibit similar behaviour, even though they approach different values at infinities. First, in order to construct the hybrid, cutting points for which interpolation is not needed are sought by simultaneously plotting f_1, f_2 and f_3. In contrast to previous examples, for these curves, s_1 and s_2, the direct hydridisation can be performed for the value $T = 0$. Indeed, the graphs of these three functions intersect at the origin $f_1(0) = f_2(0) = f_3(0) = 0$, see Figure 6.16.

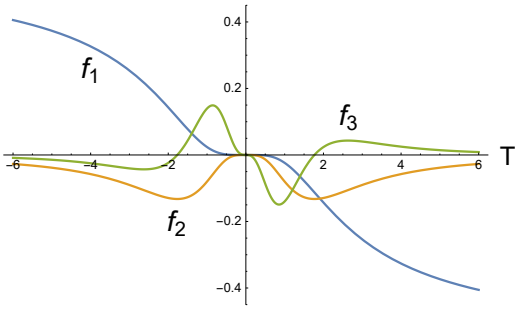

Figure 6.16: Simultaneous intersection of the three graphs exists at $T = 0$ and therefore no interpolation is needed to construct the hybrid kink.

Moreover, interpolation curves of degree three can be inserted in between to see whether other types of hybrid can be constructed. If the same procedure as before is followed, no pair of parameters (T_1, T_2) that satisfies $T_1 \neq T_2$ is found, see Figure

6.17. Therefore, in this case whether the hybrid is constructed without interpolation, merging at the origin $\phi = 0$, or more general interpolations must be considered. For simplicity let us maintain the direct hybridisation.

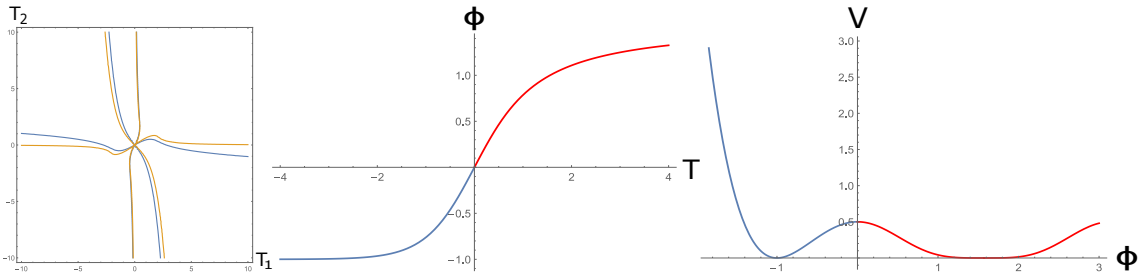

Figure 6.17: On the left the simultaneous contourplot of both equations $F_i = 0$ are shown. No pair (T_1, T_2) for which both equations $F_1(T_1, T_2) = F_2(T_1, T_2) = 0$ are simultaneously satisfied and $T_2 > T_1$ appears as solution. In the centre the piecewise curve with no interpolation has been plotted and on the right the piecewise potential is displayed.

On the other hand, the potentials must also be interpolated. Thus, let us construct the potential of a Sigma model for which s_2 is a kink. This can be easily accomplished

$$V(\phi) = \frac{1}{2}\left(\frac{ds_2(T)}{dT}\right)^2 [T(\phi)] = \frac{1}{2}\cos^4\phi\,,$$

for which the original kink $s_2(T) = \arctan T$ has an energy of $E_2 = \frac{\pi}{2}$. Given that both curves have been cut at the origin, the energy of this hybrid kink is the average of the energies of the two original kinks

$$E = \frac{E_1 + E_2}{2} = \frac{\pi}{4} + \frac{2}{3}\,.$$

Notice that the direct gluing procedure has been possible in this case because these curves are joined at the origin, where the original curves reach the maximum of their respective potentials functions. In this section, hybridisation of kinks of fields theories with only one field has been explicitly shown. When this procedure is applied to cases with more fields, where the dimension of the internal space is higher, the potential must be extended to a strip. This situation will be discussed in next sections.

6.2.5 Extentions of kinks

Thus far, our efforts have been focusing on combining different kinks so that the result is another kink. This is, the objective was to construct hybrid kinks. In this section another interesting scenario is explored. Instead of hybridising two kinks, kinks will be extended to create particular forms of orbits, constructing a Sigma model for which the extended curve is a kink. This leads to an infinite number of possibilities to perform this procedure. However, in all these the conditions derived in last sections must be satisfied. First, the gluing of curves must be C^2. Secondly, the potential must be defined in each region and not only along the curve. Lastly, the contribution to the energy of the extension must be finite. This last requirement forces the orbit of the extended kink to converge to a point of the target manifold at the new end. This point in the target manifold M will be a vacuum point of the

new Sigma model. Let us assume that $s_1(T)$ is a curve that corresponds to a kink of a Sigma model. The extension $s(T)$ of this curve $s_1(T)$ by a second curve $s_2(T)$ will be, once a chart $(U_M, \{\lambda^i_M\})$ on M is chosen, a piecewise curve

$$s(T) = \begin{cases} s_1(T) & \text{if } T \leq T_0 \\ c(T) & \text{if } T_0 < T \leq T_1 \\ s_2(T) & \text{if } T_1 < T \end{cases}$$

where a polynomial interpolation curve $c(T)$ has been introduced with gluings at values of the parameter T_0 and T_1. The main mechanism that shall be employed to force s_2 to converge in the limit $T \to \infty$ is the introduction of a function that behaves similarly to trimming functions $q : \mathbb{R} \to I \subset \mathbb{R}$. Let us illustrate this for the simplest case of extension, which is field theories with only one field. In this scenario this function $q(T)$ can be employed to force s_2 to converge at a point as follows

$$s(T) = \begin{cases} s_1(T) & \text{if } T \leq T_0 \\ c(T) & \text{if } T_0 < T \leq T_1 \\ s_2(T) = a + b\ q(T) & \text{if } T_1 < T \end{cases}$$

where $a, b \in \mathbb{R}$ will modulate the location of the new vacuum point. This technique can be trivially generalised to describe curves in a chart on a Riemannian manifold. For instance, it suffices to consider $a, b \in \mathbb{R}^{\dim M}$. Notice that when the dimension of the target manifold is greater than one, even if the tangent vector to s_2 can be modulated with the parameter that accompanies the function $q(T)$, its orbit will correspond to a segment in the chart. Since the curvature of s_2 vanishes, the interpolation $c(T)$ will be needed in general to ensure the C^2-gluing. Indeed, the curvature of both curves at the junction must coincide.

Alternatively, an extension making use of geodesics can be performed. Instead of extending the curve by a segment in the chart, a geodesic that crosses the junction can be used. Indeed, the theorem of existence and uniqueness of geodesics guarantees that there exists one and only one geodesic passing through a given point with a given tangent vector. Since the curvature of the geodesic at the junction may be different from that of the original curve, an interpolation function will also be needed in general

$$s(T) = \begin{cases} s_1(T) & \text{if } T \leq T_0 \\ c(T) & \text{if } T_0 \leq T \leq T_1 \\ s_2(T) = \text{geo}_{c(T_1), \frac{dc}{dT}(T_1)}(q(T)) & \text{if } T_1 < T \end{cases}$$

where $\text{geo}_{c(T_1), \frac{dc}{dT}(T_1)}(q(T))$ denotes the geodesic that passes through point $c(T_1)$ with tangent vector $\frac{dc}{dT}(T_1)$. It is worth noticing that when the target manifold is Euclidean both methods of extension coincide.

If a C^2 extension is performed so that a potential function can be found on a strip that contains $s_2(T)$ and its contribution to the energy is finite

$$E\left[s_2\right] = \int_{T_1}^{\infty} \epsilon(T)\ dT < \infty\,,$$

then the extended kink will have been constructed. In next sections this procedure of extensions will be applied to two different cases. First, we shall search for an extension of a kink of the ϕ^4-model as illustration. Then, non-topological kinks will be constructed in the plane and in the torus using this procedure.

6.2.6 Examples of extensions of kinks

In this section the extension formalism will be applied in three different scenarios. In the first one a kink of the ϕ^4-model will be extended and the form of the piecewise potential obtained. In the second part of this section, a non-topological kink in $\mathbb{R}^2$ is constructed by conveniently extending a kink of the double ϕ^4-model. Lastly, an example of extension is performed in the torus.

Extensions of a kink of the ϕ^4-model

Let us first consider the ϕ^4-model with one field given by the potential function

$$V(\phi) = \frac{1}{2}\left(1 - \frac{\phi^2}{\beta^2}\right)^2 ,$$

where $\beta \in \mathbb{R}$ controls the position of the two emerging vacua $\phi_v = \pm\beta$. Let us choose the kink of this model given by $s_1(T) = \beta \tanh T$. In order to extend it, the curve must be cut first at some point, which will correspond to the value of the parameter T_0. Moreover, the extension $s(T)$ of this curve s_1 will be performed including an interpolation c as follows

$$s_{comp}(T) = \begin{cases} s_1(T) = \beta \tanh T & \text{if } T \leq T_0 \\ c(T) = \phi_0 + A(T-T_0) + B(T-T_0)^2 + C(T-T_0)^3 & \text{if } T_0 < T \leq T_1 \\ s_2(T) = \phi_1 + \alpha \tanh\left(T - T_1\right) & \text{if } T_1 < T \end{cases}$$

where the auxiliary function has been chosen as $q(T) = \tanh\left(T - T_1\right)$ and the values of the parameters $\phi_0, \phi_1, A, B, C, \alpha \in \mathbb{R}$ must be such that the gluings are C^2. This condition leads to the following values for the parameters

$$\begin{aligned} &\phi_0 = \beta \tanh T_0, \qquad A = \beta\ \mathrm{sech} T_0, \qquad B = -\beta\ \mathrm{sech}^2 T_0 \tanh T_0\,, \\ &C = \frac{\beta}{3(T_1 - T_0)}\ \mathrm{sech}^2 T_0 \tanh T_0\,, \qquad \alpha = A + 2B(T_1 - T_0) + 3C(T_1 - T_0)^2\,, \\ &\phi_1 = \phi_0 + A(T_1 - T_0) + 2B(T_1 - T_0)^2 + C(T_1 - T_0)^3\,. \end{aligned}$$

This solution for the coefficients depends exclusively on the parameter β of the original ϕ^4-model and the parameters T_0 and T_1 that control where the curves are cut. As a consequence, regardless of the points where these curves are cut, an extension is possible. This is, a whole family of extensions is obtained. In fact, because of the form of the extended curve, variables T_0 and T_1 corresponds to points $s_1(T_0) = \phi_0$ and $s_2(T_1) = \phi_1$ and the piecewise potential can be written as follows

$$V_{comp}(\phi) = \begin{cases} \frac{1}{2}\left(1 - \frac{\phi^2}{\beta^2}\right)^2 & \text{if } \phi \leq \phi_0 \\ V_c & \text{if } \phi_0 \leq \phi \leq \phi_1 \\ \frac{1}{2}\left(1 - \frac{(\phi-\phi_1)^2}{\alpha^2}\right)^2 & \text{if } \phi \geq \phi_1 \end{cases}$$

where V_c is the potential function that corresponds to the cubic interpolation function (6.5), see Figure 6.18. It should be highlighted that the potential function of this extension is that of a ϕ^4-model. Indeed, the auxiliary function $q(T) = \tanh\left(T - T_1\right)$ plays the role of the profile of a kink of the ϕ^4-model. Notice, however, that the form of the extended potential for other models will be more complicated in general.

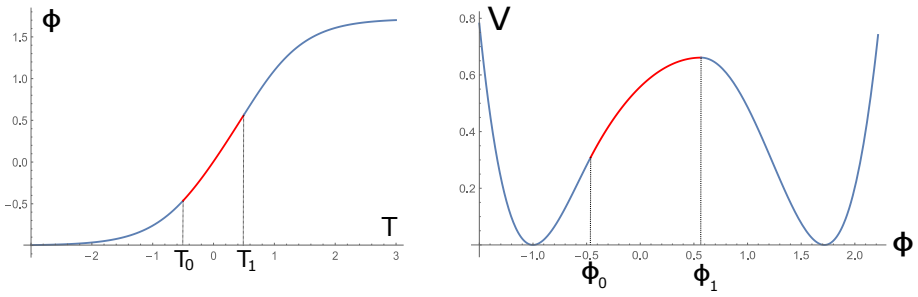

Figure 6.18: Profile of the extended kink on the left and the corresponding extended potential on the right for the values $T_1 = -T_0 = \frac{1}{2}$.

Construction of non-topological kinks in $\mathbb{R}^2$

Since this formalism allows us to extend kink orbits, in particular an orbit in $\mathbb{R}^2$ can be extended in such a way that it tends at infinity to the same point it departs from at minus infinity. This is the aim of this section, the piecewise construction of non-topological kinks in $\mathbb{R}^2$. In order to construct this piecewise non-topological kink, two singular kinks of the double ϕ^4-model that share one asymptotic vacuum point will be interpolated. Moreover, an intermediate circumference will be introduced to facilitate the interpolation. The interpolation between the original kinks and the circumference will be performed by polynomials of degree four for each component. This implies that the expression of the potential for these interpolation curves will be considerably more complicated. However, as we shall see, degree three would not suffice.

Once the curve of the non-topological kink is constructed, potential functions must be found on all regions that contain the piecewise curve. On one hand, the double ϕ^4-model provides us with a potential for the region where the kinks of the ends are defined. On the other, potentials (6.4) can be constructed for the regions of polynomial interpolation of degree four. Finally, a potential function must be found for the region where the involved part of the circumference is defined. It is worth highlighting that, as has been proven before, since the ends of the hybrid correspond to kinks, the energy will be finite. This construction corresponds to a non-topological kink indeed.

Let us denote as s_1 and s_3 the two kinks of the ϕ^4-models that shall be interpolated, which as stated, must share an asymptotic limit. Let us also denote as s_2 the included fragment of the circumference, whose centre will be located at (K_1, K_2) with $K_1, K_2 \in \mathbb{R}$. Finally, let us denote as c_1 and c_2 the interpolations between s_1 and s_2 and between s_2 and s_3 respectively. With these elements the hybrid curve is constructed by means of the following four gluings at values of the parameter of the hybrid curve $T = T_0, T_1, T_2, T_3$

$$s(T) = \begin{cases} s_1(T) = (\epsilon_1 + \epsilon_1 \tanh T, 0) & \text{if } T \leq T_0 \\ c_1(T) & \text{if } T_0 < T \leq T_1 \\ s_2(T) = (K_1 + r\cos(T - T_1 + \theta), K_2 + r\sin(T - T_1 + \theta)) & \text{if } T_1 < T < T_2 \\ c_2(T) & \text{if } T_2 < T \leq T_3 \\ s_3(T) = (0, \epsilon_2 - \epsilon_2 \tanh(T - T_3)) & \text{if } T_3 < T \end{cases}$$

where parameters $\epsilon, \epsilon_2 \in \mathbb{R}$, the radius of the circumference $r > 0$ and a phase $\theta \in [0, 2\pi)$ are introduced to modulate the orbits, see Figure 6.19.

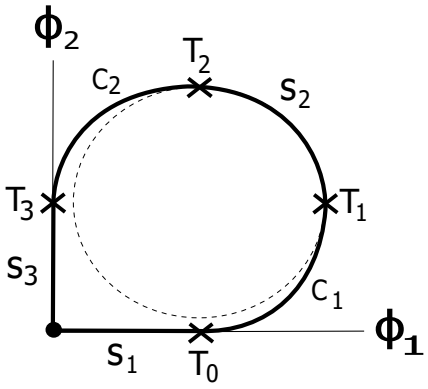

Figure 6.19: Pictorial representation of the hybrid curve in construction, closed by consecutive gluings at T_0,T_1,T_2 and T_3 of two kinks s_1 and s_3 of the double ϕ^4-model, a circumference s_2 and two interpolation quartic polynomials c_1 and c_2.

Given that the target space is $\mathbb{R}^2$, the C^2 requirement produces 24 equations, two for each of the following conditions

$$\begin{aligned}
&s_1(T_0) = c_1(T_0), \qquad s_1'(T_0) = c_1'(T_0), \qquad s_1''(T_0) = c_1''(T_0)\,,\\
&c_1(T_1) = s_2(T_1), \qquad c_1'(T_1) = s_2'(T_1), \qquad c_1''(T_1) = s_2''(T_1)\,,\\
&s_2(T_2) = c_2(T_2), \qquad s_2'(T_2) = c_2'(T_2), \qquad s_2''(T_2) = c_2''(T_2)\,,\\
&c_2(T_3) = s_3(T_3), \qquad c_2'(T_3) = s_3'(T_3), \qquad c_2''(T_3) = s_3''(T_3)\,.
\end{aligned}$$

On the other hand, these equations involve a total of 30 variables and therefore 6 degrees of freedom will be present. Among all possibilities, the location of the gluings T_0 , T_1 , T_2 and T_3, the radius r and the phase θ of the circumference will be chosen as free variables. Now, even though this system of equations can be solved, due to the lengths of the explicit expressions, these will be omitted. Instead, particular solutions are shown in Figure 6.20 for different values of r and T_0.

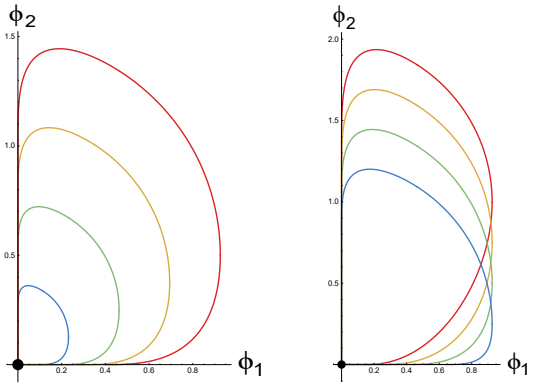

Figure 6.20: Constructed closed hybrid kink orbits in $\mathbb{R}^2$ for $T_0 = -1$ and different values of the radius $r = 0.25, 0.5, 0.75, 1$ on the left and for $r = 1$ and values $T_0 = -2, -1.5, -1, -0.5$ on the right. The rest of the values have been fixed at $(T_1, T_2, T_3, \theta) = (0, 1, 2, 0)$.

Therefore, families of these closed hybrid kink orbits have been constructed. The final step is to be able to obtain a potential function for each separate curve s_1, s_2 and s_3. In the case of the quartic interpolation functions, as has been shown, the existence of the potential is already guaranteed. Let us explore the rest of cases.

- **Segments s_1 and s_3**: By construction, these curves are pieces of solutions of a double ϕ^4-model on the plane. Since the potential of this model can be written in terms of a superpotential W, the particular form of the potential can be easily derived from the derivatives of these curves. The derivative along these segments s_1 and s_3

$$\frac{ds_1}{dT} = (\epsilon \operatorname{sech}^2 T, 0)\,, \quad \frac{ds_3}{dT} = (0, -\epsilon_2 \operatorname{sech}^2 T)\,,$$

corresponding to values of the parameter $T \leq T_0$ and $T > T_3$ respectively, can be expressed in terms of fields ϕ^1 and ϕ^2 respectively as follows

$$\begin{aligned}
\frac{ds_1}{dT} &= \left(\epsilon_1\left(1 - \frac{(\phi_1-\epsilon_1)^2}{\epsilon_1^2}\right), 0\right)\Big|_{s_1(T)} \equiv \pm\left(\frac{\partial W}{\partial\phi^1}, \frac{\partial W}{\partial\phi^2}\right)\Big|_{s_1(T)}\,,\\
\frac{ds_3}{dT} &= \left(0, \epsilon_2\left(\frac{(\phi_2-\epsilon_2)^2}{\epsilon_2^2} - 1\right)\right)\Big|_{s_3(T)} \equiv \pm\left(\frac{\partial W}{\partial\phi^1}, \frac{\partial W}{\partial\phi^2}\right)\Big|_{s_3(T)}\,,
\end{aligned}$$

which corresponds to the Bogomol'nyi equations of a ϕ^4-model with potential function

$$V_{1,3} = \frac{1}{2\epsilon_1^2}\left(\epsilon_1^2 - (\phi_1-\epsilon_1)^2\right)^2 + \frac{1}{2\epsilon_2^2}\left(\epsilon_2^2 - (\phi_2-\epsilon_2)^2\right)^2\,.$$

Thus, both curves are solutions of a Sigma model on the plane with this potential. It is worth noting that among the four vacua of this potential

$$\mathcal{M} = \{(0,0), (0,2\epsilon_2), (2\epsilon_1, 0), (\epsilon_1, \epsilon_2)\}\,,$$

only that located at $(0,0)$ will be in the region where this potential will be defined. This is the vacuum point of the non-topological kink in construction.

- **Circumference s_2**: The derivative of the curve s_2 that describes the circumference with $T_1 < T < T_2$ can be written as

$$\frac{ds_2}{dT} = (-r\sin\tilde{T}, r\cos\tilde{T}) = \left(-\sqrt{r^2-(\phi_1-K_1)^2}, \sqrt{r^2-(\phi_2-K_2)^2}\right)\Big|_{s_2(T)}\,,$$

where $\tilde{T} = T - T_1 + \theta$. Hence, a potential that admits this solution can be constructed in the region given by $\phi_1 \in (K_1-r, K_1+r)$ and $\phi_2 \in (K_2-r, K_2+r)$ as

$$V_{circ} = \frac{1}{2}\left(\frac{ds_2^1}{dT}\right)^2 + \frac{1}{2}\left(\frac{ds_2^2}{dT}\right)^2 = r^2 - \frac{(\phi_1-K_1)^2 + (\phi_2-K_2)^2}{2}\,.$$

Clearly, this region contains the circumference. In particular, the value of the potential remains constant along the curve $V_{circ}(s_2(T)) = \frac{r^2}{2}$. Notice that this potential can be extended to a strip that surrounds the circumference. However, the width of the strip must be defined so that the continuum of vacua of this potential is avoided.

Therefore, since the curve has been C^2-glued and the potential functions exist in all the regions of a strip surrounding each individual curve s_1, c_1, s_2, c_2, s_3, as has been proven, a piecewise C^1 potential function can be defined in this strip surrounding the hybrid kink, see Figure 6.21.

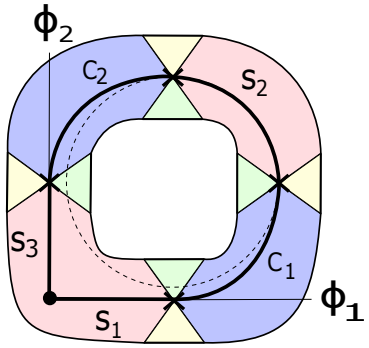

Figure 6.21: Once a potential is constructed on each region of the strip surrounding each curve, an interpolation between the potentials can be performed. This creates a closed strip that contains the non-topological hybrid kink.

Finally, it is worth noting that if the potential function is differentiably extended throughout the entire interior of the loop, then this kink would be able to decay into vacuum because of the elastic forces. However, if in this extension of the potential a singularity is introduced, then as has been shown in Chapters 1, 3 and 4, the decay into vacuum would be forbidden by the topology of the target manifold. Indeed, these would be brochosons, as these loops would not be able to be contracted to a point, see Figure 6.22.

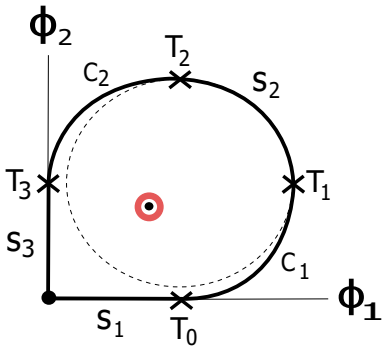

Figure 6.22: If a singularity, depicted in red, is introduced into the potential defined in the interior region, then the constructed non-topological kink cannot decay into vacuum.

Kink extensions in other Riemannian manifolds

As has been described, the gluing of curves must be C^2 in the chart where coordinates are defined. However, the same interpolation that is performed in a chart can be conducted in an infinite number of other manifolds. Indeed, the equations for the C^2-requirement will be identical. For instance, the previously constructed non-topological kinks can be taken to the torus in toroidal coordinates (θ, φ). The potentials, however, will be different. The fact that the form of the metric tensor on the torus is different has two direct consequences. First, the components of the metric tensor will appear explicitly in the construction of the potential. Secondly, in order to construct additively separable superpotentials, the explicit form of each curve must be imposed. This leads to the emergence of extra terms in the potential

on each region

$$V_{1,3} = \frac{r^2}{2\epsilon_1^2}\left(\epsilon_1^2 - (\theta-\epsilon_1)^2\right)^2 + \frac{R^4}{2\epsilon_2^2(R+r\sin\theta)^2}\left(\epsilon_2^2-(\varphi-\epsilon_2)^2\right)^2 ,$$
$$V_{circ} = \frac{|R_c^2-(\theta-K_1)^2|}{2}r^2 + \frac{|R_c^2-(\varphi-K_2)^2|}{2(R+r\sin\theta)^2}\left(R+r\sin\left(f(\varphi)\right)\right)^4 ,$$

where R and r are the major and minor radii of the torus, the radius of the circumference has been denoted as R_c and the auxiliary function $f(\varphi)$ has been defined as

$$f(\varphi) = K_1 \pm \sqrt{R_c^2-(\varphi-K_2)^2}\,.$$

Similarly, the potential for the polynomial interpolation curves can be obtained (6.4). See in Figure 6.23 the previously shown non-topological hybrid kink orbits on the plane transferred to the torus. Notice that all these potentials must be defined in a subset of the chart so that the potential is unaffected by the non-periodicity in the torus. Indeed, they are only defined in a strip that contains the non-topological hybrid kink. In summary, it is important to note that this extension procedure and this non-topological hybrid kink construction can be applied to any Riemannian manifold, where every hybrid kink defines different potentials.

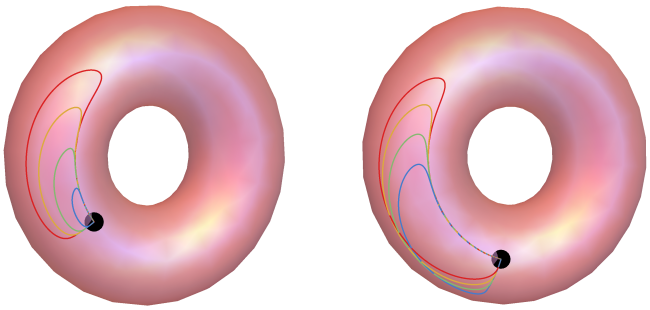

Figure 6.23: Piecewisely constructed non-topological kinks on the torus when the interpolated coordinates are interpreted as toroidal coordinates. Members of these families for different values of radius R_c of the circumference and different values of T_0 are shown on the left and right respectively.

6.3 Composite Sigma models

In this section, a new mechanism for generating Sigma models by leveraging existing ones is presented. Moreover, this will be accomplished in a manner that allows the new Sigma model to inherit certain solutions from the original models. Given two Sigma models on manifolds M_1 and M_2 respectively, the main idea is to construct another Sigma model on the product manifold $M_1 \times M_2$, coupling their dynamics in the process. First, the product manifold is endowed with a Riemannian manifold structure and the Levi-civita connection. This can be easily achieved as it well-known in the literature, see for example [58, 111]. Then, the general framework of Sigma models on this product of manifolds will be presented. The isolated dynamics of the original Sigma models will be entangled by defining a superpotential on the product manifold which is not additively separable. Finally, particular examples of

these "composite Sigma models" will be shown to illustrate this procedure. Specifically, ϕ^4-models and sine-Gordon models will be combined to produce generalised double and triple ϕ^4-models and sine-Gordon models. Lastly, composite Sigma models will be constructed on the sphere.

6.3.1 Product of two Riemannian manifolds

As has been advanced, the objective is to construct Sigma models on the product of the target manifolds of two other Sigma models. In order to be able to accomplish this, this product manifold must be equipped with the Riemannian manifold structure and the Levi-Civita connection. In this section, this process, well-known in the literature [58, 111], is summarised. Let (M_1, g_1, ∇^1) and (M_2, g_2, ∇^2) be two Riemannian manifolds equipped with metric tensors g_1 and g_2 and their respective Levi-Civita connections ∇^1 and ∇^2. In order to endow the product manifold $M_1 \times M_2$ with these structures, let us first define the projections $\pi_1 : M_1 \times M_2 \to M_1$ and $\pi_1 : M_1 \times M_2 \to M_1$ and the following immersions

$$\begin{aligned} i_1^q : M_1 &\longrightarrow M_1 \times M_2 \\ p &\longmapsto (p, q) \end{aligned} \qquad\qquad \begin{aligned} i_2^p : M_2 &\longrightarrow M_1 \times M_2 \\ q &\longmapsto (p, q) \end{aligned}$$

From these definitions, both the Riemannian metric and the Levi-Civita connection can be constructed on $M_1 \times M_2$ by sending vector fields defined on $T(M_1 \times M_2)$ to the tangent bundle of each manifold TM_1 and TM_2. Indeed, there, the original Riemannian metric tensors and Levi-Civita connections can be employed. In particular, the following two results can be proven

1. The metric tensor defined on $M_1 \times M_2$ given by

$$g \equiv \pi_1^* g_1 + \pi_2^* g_2 \,,$$

   is a Riemannian metric, where π_i^* denotes the pullback of the projection π_i.

2. The connection defined as follows

$$\nabla_X Y(p, q) \equiv di_1^q \left[\nabla^1_{d\pi_1(X)} d\pi_1(Y)\right] + di_1^q \left[\nabla^1_{d\pi_1(X)} d\pi_1(Y)\right]$$

   is the Levi-Civita connection, where $d\pi_i$, di_1^q y di_2^p are the tangent maps of the maps π_i, i_1^q and i_2^p respectively.

Thus, the manifold $(M_1 \times M_2, g, \nabla)$ is a Riemannian manifold endowed with the Levi-Civita connection. This will allow us to define what shall be referred to as composite Sigma models. Now, let us fix the notation for the coordinates on the chart of each manifold. For $i = 1, \ldots, m_1$ and $j = 1, \ldots, m_2$ with $m_i = dim M_i$:

- On the product manifold $M_1 \times M_2$ the following notation for the coordinates on the chart will be employed

$$\left\{U_{M_1 \times M_2}, \left(\left\{\phi^i\right\}, \left\{\psi^j\right\}\right)\right\} \,.$$

- On the original manifold M_1 notation $\{U_{M_1}, \{\Phi^i\}\}$ will be used for its coordinates.

- On the original manifold M_2 notation $\{U_{M_2}, \{\Psi^i\}\}$ will be employed.

Now, using the notation introduced above, by the definition of pullback, $\pi_i^* g_i$ acting on elements of the base can be written as follows

$$\pi_1^*(\partial\Phi^a \otimes \partial\Phi^b) = \frac{\partial\Phi^a}{\partial\phi^l}\frac{\partial\Phi^b}{\partial\phi^k}\, d\phi^l \otimes d\phi^k\,,$$

where Einstein summation convention is employed. In order to simplify future calculations, the projections π_i will be chosen so that coordinates on the original manifolds are related to those of the product manifold as

$$\Phi^i = [\pi_1(\phi)]^i \equiv \phi^i\,, \qquad \Psi^i = [\pi_2(\phi)]^i \equiv \psi^i\,. \tag{6.7}$$

Lastly, this construction leads to two blocks in the associated matrix of the metric tensor, where one block will contain coordinates on M_1 while the other contains coordinates on M_2. This also implies that each term g^{ab} cannot mix coordinates on M_1 and M_2 and therefore Christoffel symbols

$$\Gamma^i_{kl} = \frac{1}{2}g^{ij}\left(\frac{\partial g_{jk}}{\partial x^l} + \frac{\partial g_{jl}}{\partial x^k} - \frac{\partial g_{kl}}{\partial x^j}\right)$$

can be split into two disjoint sets of non-vanishing Christoffel symbols, one for the coordinates on M_1 denoted as $\Gamma^i_{1,kl}(\phi)$ for $i = 1, \ldots, m_1$ and another for those on M_2 denoted as $\Gamma^i_{2,kl}(\psi)$ for $i = m_1+1, \ldots, m_1+m_2$. Indeed, this was expected given the definition above of the Levi-Civita connection, where coordinates on $M_1 \times M_2$ are separated into two different terms.

6.3.2 Sigma models on a product manifold

Since the product manifold is endowed with a Riemannian metric and the Levi-Civita connection, Sigma models can be constructed on it. Given a configuration $\Omega : \mathbb{R}^{1,1} \to M_1 \times M_2$, the action of a Sigma model can be written in terms of the pull-back of the metric tensor g on $M_1 \times M_2$

$$S[\Omega] = \int_{\mathbb{R}^{1,1}} \left[\frac{1}{2}\, Tr(\Omega^* g) - V(\Omega)\right] dx\, dt\,.$$

In coordinates this action can be decomposed into one term identical to that of the original Sigma model on M_1, another identical to that on M_2 and a potential function V that intertwines the dynamics of the two submanifolds by coupling coordinates

$$S[\Omega] = \int_{\mathbb{R}^{1,1}} \left[\frac{1}{2}\, \eta^{\alpha\beta} g_{1,ij}\frac{d\phi^i}{dx^\alpha}\frac{d\phi^j}{dx^\beta} + \frac{1}{2}\, \eta^{\alpha\beta} g_{2,ij}\frac{d\psi^i}{dx^\alpha}\frac{d\psi^j}{dx^\beta} - V(\phi,\psi)\right] dxdt\,.$$

This intertwinedness in the potential can also be observed in the field equations, which can also be split in two sets, one for all coordinates corresponding to M_1 and another for those of M_2

$$-\frac{\partial^2\phi^i}{\partial t^2} + \frac{\partial^2\phi^i}{\partial x^2} - \Gamma^i_{1,ab}\left[\frac{\partial\phi^a}{\partial t}\frac{\partial\phi^b}{\partial t} - \frac{\partial\phi^a}{\partial x}\frac{\partial\phi^b}{\partial x}\right] = g_1^{ji}\frac{\partial V}{\partial\phi^j}\,, \quad i = 1, \ldots, m_1\,,$$
$$-\frac{\partial^2\psi^i}{\partial t^2} + \frac{\partial^2\psi^i}{\partial x^2} - \Gamma^i_{2,ab}\left[\frac{\partial\psi^a}{\partial t}\frac{\partial\psi^b}{\partial t} - \frac{\partial\psi^a}{\partial x}\frac{\partial\psi^b}{\partial x}\right] = g_2^{ji}\frac{\partial V}{\partial\psi^j}\,,\ i = m_1+1, \ldots, m_1+m_2\,,$$

where as mentioned $\Gamma^i_{1,ab}$ and $\Gamma^j_{2,ab}$ are the respective Christoffel symbols on M_1 and M_2. Clearly, this Sigma model on $M_1 \times M_2$ couples the original Sigma models on M_1 and on M_2. Notice that if the potential can be decomposed as $V(\phi, \psi) = V_1(\phi) + V_2(\psi)$, then equations are decoupled and the isolation of the two original Sigma models is recovered. This procedure allows us then to combine two Sigma models to obtain a more general one. Now, these models will be extended so that solutions of the original isolated Sigma models on each submanifold M_i are maintained. In particular, this extension will be performed so that when a vacuum solution of one of the original Sigma model is fixed at the corresponding submanifold M_i, all solutions of the original Sigma model in the other submanifold are retrieved. This can be accomplished by two different approaches.

- **Extending the potential**: Let $V_1 : M_1 \to \mathbb{R}$ and $V_2 : M_2 \to \mathbb{R}$ be the potential functions of the original Sigma models on M_1 and M_2 respectively. In order to extend these potentials, a potential function $V : M_1 \times M_2 \to \mathbb{R}$ can be defined on the product manifold $M_1 \times M_2$ such that it satisfies

$$\left.\frac{\partial V}{\partial \phi^i}\right|_{\psi_v} = \frac{\partial V_1}{\partial \phi^i}\,, \qquad \left.\frac{\partial V}{\partial \psi^j}\right|_{\phi_v} = \frac{\partial V_2}{\partial \psi^j}\,,$$

  where ϕ_v and ψ_v denote the vacuum solutions of the original Sigma models on M_1 and M_2 respectively. This can be accomplished by defining a potential of the form

$$V(\phi, \psi) = V_1(\phi) + V_2(\psi) + f(\phi, \psi)\; V_1(\phi)\; V_2(\psi)\,,$$

  where a non-negative auxiliary function $f : M_1 \times M_2 \to \mathbb{R}$ that does not remove any zero of any potential V_i has been introduced. Notice that this implies that when any vacuum solution of an original Sigma model is chosen for a submanifold M_i, the original field equations for the other Sigma model on the other submanifold are retrieved. While this is a valid extension, the general solutions of these equations will not be analytically available in general. Instead, one could restrict to potentials that admit the Bogomol'nyi arrangement. This leads in general to differential equations that are simpler to solve.

- **Extending the superpotential**: Another method to achieve this extension is considering potentials for which the Bogomol'nyi arrangement can be performed. Indeed, if the original Sigma models admit superpotentials $W_1 : M_1 \to \mathbb{R}$ and $W_2 : M_2 \to \mathbb{R}$, then superpotentials can be defined on the product manifold $W : M_1 \times M_2 \to \mathbb{R}$

$$W(\phi, \psi) = W_A(\phi) + W_B(\psi) + K\; W_A(\phi)\; W_B(\psi)\,, \tag{6.8}$$

  where $K \in \mathbb{R}$, for which Bogomol'nyi equations read

$$\frac{d\phi^i}{dT} = \pm\,[1 + KW_B]\;\; g_1^{ia}\frac{\partial W_A}{\partial \phi^a}\,, \qquad \frac{d\psi^j}{dT} = \pm\,[1 + KW_A]\;\; g_2^{jb}\frac{\partial W_B}{\partial \psi^b}\,. \tag{6.9}$$

  It is worth noticing that the decoupled case is recovered when the value $K = 0$ is considered. On the other hand, vacuum solutions of one of the original Sigma model make one of these equations trivially hold, while the other equation

corresponds to that of the other original model up to a reparametrisation by a constant. To see this, let us consider for instance the vacuum solution $\phi = \phi_v$. When one of these points is fixed on M_1, the first equation holds and the second one reads

$$\frac{d\psi^j}{d\tilde{T}} = \pm\, g_2^{jb}\frac{\partial W_B}{\partial \psi^b}\,,$$

where a reparametrisation by a constant $\tilde{T} = [1 + KW_A(\phi_v)]\, T$ has been performed. Notice that this reparametrising factor may vanish for certain value of K, which leads to losing the corresponding original solution for that value. Even if the parametrisation of Bogomol'nyi equations has been altered slightly, orbits of solutions restricted to M_2 are identical to those of the original Sigma model. Indeed, the orbit flow equations for each submanifold are identical to the original ones

$$\frac{d\phi^i}{d\phi^j} = \frac{g_1^{ia}\frac{\partial W_A}{\partial \phi^a}}{g_1^{jb}\frac{\partial W_A}{\partial \phi^b}}\,, \qquad \frac{d\psi^i}{d\psi^j} = \frac{g_2^{ia}\frac{\partial W_B}{\partial \psi^a}}{g_2^{jb}\frac{\partial W_B}{\partial \psi^b}}\,.$$

However, it is important to note that solving the orbit flow equations that mix coordinates on M_1 and M_2 will be highly complex in general

$$\frac{1 + KW_A}{g_1^{ia}\frac{\partial W_A}{\partial \phi^a}} d\phi^i = \frac{1 + KW_B}{g_2^{jb}\frac{\partial W_B}{\partial \psi^b}} d\psi^j\,.$$

Lastly, this newly defined superpotential defines the potential function on the product manifold $V : M_1 \times M_2 \to \mathbb{R}$

$$V = (1 + KW_B(\psi))^2\; V_1(\phi) + (1 + KW_A(\psi))^2\; V_2(\psi)\,, \tag{6.10}$$

which not only inherits the vacua from the submanifolds, but also potentially engenders new ones. As it is only natural, the case with $K = 0$ recovers the decoupled case $V(\phi, \psi) = V_1(\phi) + V_2(\psi)$.

This last method of extension, based on the superpotential, will be applied to five cases as examples. The first two will combine two simple models with one field each to form composite Sigma models on $\mathbb{R}^2$. The third and the forth will generate models in $\mathbb{R}^3$. Finally, a Sigma model on the sphere with this type of extended superpotential is presented.

6.3.3 Composite Sigma models on $\mathbb{R} \times \mathbb{R}$

In order to illustrate this method, let us consider first the simplest case, where composite Sigma models will be constructed on $\mathbb{R}^2$. In this section two examples will be displayed. In the first one two ϕ^4-models will be combined to form a composite Sigma model on $\mathbb{R}^2$, generalising the double ϕ^4-model. Then, as example of merging of different models, a ϕ^4-model will be mixed with a sine-Gordon model. These generalisations of models will allow us to identify more interesting kink varieties.

Composite double ϕ^4

As first example, let us consider two ϕ^4-models for which the following superpotentials $W_A, W_B : \mathbb{R} \to \mathbb{R}$ have been chosen

$$W_A(\phi) = \phi - \frac{\phi^3}{3}\,, \qquad W_B(\psi) = \psi - \frac{\psi^3}{3}\,.$$

Following the procedure described in last section, a composite Sigma model on the plane $\mathbb{R} \times \mathbb{R} = \mathbb{R}^2$ will be constructed via the superpotential method (6.8)

$$W = W_A + W_B + K\, W_A\, W_B\,,$$

where the parameter K of the extension modulates the coupling. This superpotential, in turn, produces by equation (6.10) a potential function $V : \mathbb{R}^2 \to \mathbb{R}$ for each value of K

$$V(\phi, \psi; K) = \frac{1}{2}\left[1 + K\left(\psi - \frac{\psi^3}{3}\right)\right]^2 (1-\phi^2)^2 + \frac{1}{2}\left[1 + K\left(\phi - \frac{\phi^3}{3}\right)\right]^2 (1-\psi^2)^2\,.$$

Combinations of the vacua of the original models generate four vacua in this model. However, extra vacua emerge as other factors in the potential generate more zeroes (p_i, p_j), where p_i is any real solution of the equation

$$1 + K\left(p - \frac{p^3}{3}\right) = 0\,.$$

Only one real solution of this equation is found when $|K| < \frac{3}{2}$, two when $|K| = \frac{3}{2}$ and three when $|K| > \frac{3}{2}$. Consequently, the vacuum manifold is comprised of a different number of vacua depending on the value of K

$$\mathcal{M}_K = \{(-1,-1), (-1,1), (1,-1), (1,1), (p_i, p_j)\}\ .$$

In particular, one extra vacuum point appears in the potential when $|K| < \frac{3}{2}$, three when $|K| = \frac{3}{2}$ and nine when $|K| > \frac{3}{2}$. This is, cases with non-vanishing K lead to a total of 5, 8 and 13 vacua respectively, see Figure 6.25. Now, this superpotential produces the following pair of Bogomol'nyi equations

$$\frac{d\phi}{dT} = \pm\left[1 + K\left(\psi - \frac{\psi^3}{3}\right)\right]\ (\phi^2 - 1)\,, \qquad \frac{d\psi}{dT} = \pm\left[1 + K\left(\phi - \frac{\phi^3}{3}\right)\right]\ (\psi^2 - 1)\,,$$

which cannot be directly integrated. However, singular kinks can be sought when the trial orbits $\phi = \pm 1$ or $\psi = \pm 1$ are imposed. Indeed, each of these conditions leads by a reparametrisation to a singular solution of the ϕ^4-model

$$\frac{d\phi}{d\tilde{T}} = \pm\ (\phi^2 - 1) \qquad \text{or} \qquad \frac{d\psi}{d\tilde{T}} = \pm\ (\psi^2 - 1)\,.$$

except for the case when $|K| = \frac{3}{2}$, where certain singular kinks are forbidden. Indeed, Bogomolnyi's equations hold trivially when $\phi = -\mathrm{sg}(K)$ or $\psi = -\mathrm{sg}(K)$, where $\mathrm{sg}(K)$ denotes the sign of the constant K. Now, even if Bogomol'nyi equations cannot be directly integrated, the orbit flow equation can, which reads

$$\left|\frac{1-\phi}{1-\psi}\right|^{2K+3} \left|\frac{1+\phi}{1+\psi}\right|^{2K-3} = C\, e^{K(\phi^2 - \psi^2)}\,, \tag{6.11}$$

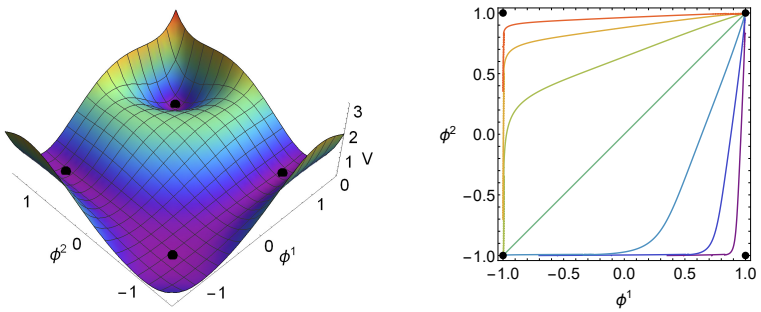

Figure 6.24: The potential function in the square enclosed by the original four vacua and a contourplot of the orbits of the solution for different values of the constant C.

where $C > 0$ is a constant that distinguishes between members of the arising family of kinks. Let us first consider the case with $K = 1$, for which the behaviour in the central area $\phi, \psi \in (-1, 1)$ resembles that of the ϕ^4-model since no extra vacua is present in this area, see Figure 6.24. Instead of two families that asymptotically join diagonally aligned vacua as it occurs in the conventional double ϕ^4-model, only a family of kinks is obtained. Indeed, this model is not separable. Moreover, their trajectories are asymmetric because of the form of the potential as it approaches the vacuum point $(1, 1)$. Notice also that limits of the constant $C \to \infty$ and $C \to 0$ correspond to the different singular kinks that can be derived from Bogomol'nyi equations.

When $|K| = 1$, unlike in the standard double ϕ^4-model, outside the central region there exists also another vacuum point that is asymptotically connected by a kink to the vacuum point located at $(1, 1)$, see Figure 6.25. When $|K| = \frac{3}{2}$ more vacua and more kinks linking them appear. Notice that since kink's orbits cannot intersect because of the Picard-Lindelöf theorem, two of the singular kinks of the standard ϕ^4-model are forbidden in this case. This was expected for this value of K, as these solutions are lost in Bogomol'nyi equations. Lastly, for $|K| > \frac{3}{2}$ these lost singular kinks are again recovered and more vacua and kinks appear. On the other hand, some of these solutions go to infinity. Even if these must be discarded, their existence will be discussed in a future section.

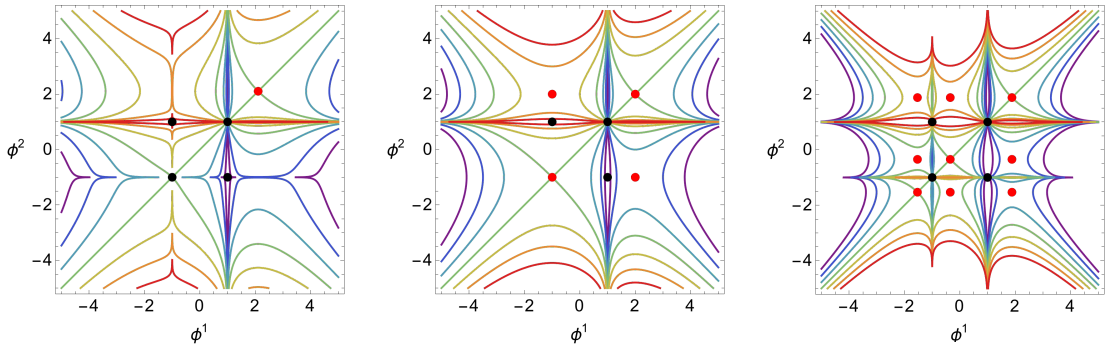

Figure 6.25: Contourplot of the orbits of the emerging family of solutions for different values of the constant C for $K = 1$, $K = \frac{3}{2}$ and $K = 3$ respectively. The four central vacua are represented in black while the extra ones are depicted in red.

In conclusion, this method allows in this case the construction of a whole family of models on the product manifold, one per each value of K. The standard double

ϕ^4-model is recovered when $K=0$, but it is successfully generalised for other values of K. As a result of the introduction of these higher-order coupling terms, richer kink varieties emerge.

Composite of a sine-Gordon model and a ϕ^4-model

Let us combine now a ϕ^4-model with a different model in this case, which is the sine-Gordon model. In particular, let us choose a superpotential for each of these models as follows

$$W_1 = \phi - \frac{\phi^3}{3}\,, \qquad W_2 = \sin\psi\,.$$

The potential on the product manifold $\mathbb{R}^2$ is derived in the same manner as before (6.10), including the parameter K that modulates the coupling

$$V(\phi,\psi) = \frac{1}{2}\left[1+K\,\sin\psi\right]^2\,\left(1-\phi^2\right)^2 + \frac{1}{2}\left[1+K\left(\phi-\frac{\phi^3}{3}\right)\right]^2\cos^2\psi\,.$$

Members of this family of potential functions have when $K\neq 0$ an infinite number of vacua, which can be labelled as

$$\mathcal{M} = \left\{\left(1,\frac{\pi}{2}+n_1\pi\right),\left(-1,\frac{\pi}{2}+n_2\pi\right),\left(p_i,2\pi n_3\,\arcsin\left(\frac{-1}{K}\right)\right)\right\}\,,$$

with integers $n_1,n_2,n_3\in\mathbb{Z}$ and where p_i is any real solution of the equation

$$1+K\sin p = 0\,. \tag{6.12}$$

This implies that the number of vacua will also depend on the value of K, see Figure 6.26.

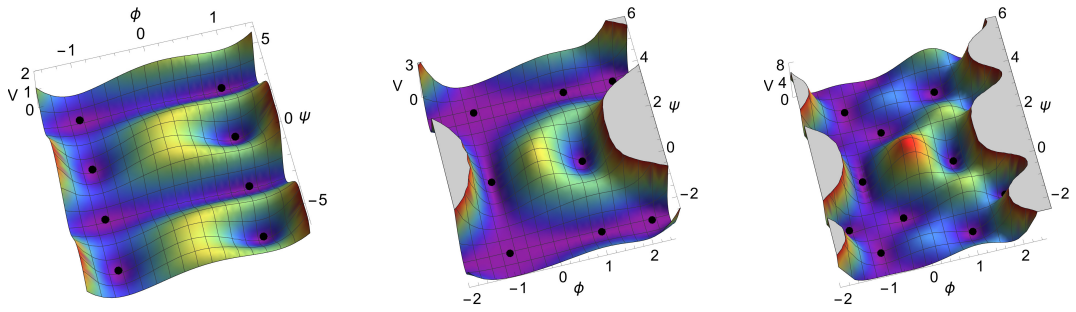

Figure 6.26: Potential function depicted in the central regions for values $K=0.5,1,3$ respectively. The vacua in these regions have been represented as black dots.

Notice that unlike in the previous model, when $|K|<1$ no extra vacuum point emerges. Indeed, equation (6.12) does not admit any real solution. On the other hand, once again Bogomol'nyi equations

$$\frac{d\phi}{dT} = \pm\left[1+K\sin\psi\right]\,\left(\phi^2-1\right), \qquad \frac{d\psi}{dT} = \pm\left[1+K\left(\phi-\frac{\phi^3}{3}\right)\right]\,\cos\psi\,,$$

cannot be directly integrated, but the orbit equation can

$$\frac{|1+\phi|^{3-2K}}{|1-\phi|^{3+2K}\,|\cos\psi|^{6K}} = C\,e^{-K\phi^2}e^{6\,\mathrm{arctanh}[\sin\psi]}\,,$$

where the constant $C > 0$ distinguishes between members of this family of solutions, see Figure 6.27. In this case, limits $C \to 0$ and $C \to \infty$ correspond to an infinite number of singular kinks, for which one of the coordinates will be constant. Once more, solutions that go to infinity must be discarded, as these do not correspond to kinks.

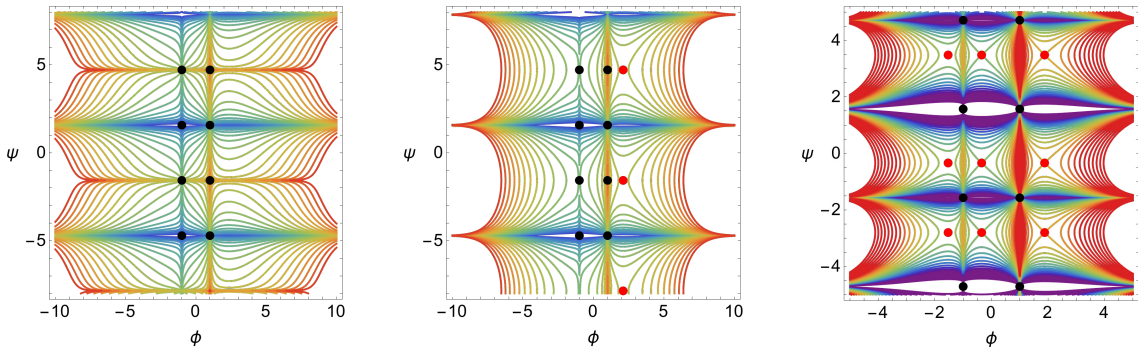

Figure 6.27: Contourplot of the orbits of the arising family of solutions for different values of the constant C. Inherited vacua have been represented by black dots, while the extra vacua have been depicted in red.

6.3.4 Composite triple ϕ^4- model

In the previous two examples two Sigma models with only one field were combined to construct another Sigma model in $\mathbb{R}^2$. In this section a step further will be taken. A model in Cartesian coordinates in the Euclidean space $\mathbb{R}^3$ will be constructed by combining a double ϕ^4-model with a ϕ^4-model. This is, the following superpotential $W : \mathbb{R}^3 \to \mathbb{R}$ will be considered

$$W = W_A(\phi_1, \phi_2) + W_B(\phi_3) + K\, W_A(\phi_1, \phi_2)\, W_B(\phi_3)\,,$$

where $K \in \mathbb{R}$ and the superpotentials of the original models are those of the following ϕ^4-models

$$W_A = \phi_1 - \frac{\phi_1^3}{3} + \phi_2 - \frac{\phi_2^3}{3}\,, \qquad W_B = \phi_3 - \frac{\phi_3^3}{3}\,.$$

This superpotential produces a potential function that generalises that of a standard triple ϕ^4-model

$$\begin{aligned} V =& \frac{1}{2}\left[1 + K\left(\phi_3 - \frac{\phi_3^3}{3}\right)\right]^2 \left[\left(1-\phi_1^2\right)^2 + \left(1-\phi_2^2\right)^2\right] \\ &+ \frac{1}{2}\left[1 + K\left(\phi_1 - \frac{\phi_1^3}{3} + \phi_2 - \frac{\phi_2^3}{3}\right)\right]^2 \left(1-\phi_3^2\right)^2\,. \end{aligned}$$

The Cartesian product of the vacua of the original models results in the presence of eight vacuum points in this potential. In fact, these vacua form a cube with the following vertices

$$\mathcal{M} = \{v_{\epsilon_1,\epsilon_2,\epsilon_3} = ((-1)^{\epsilon_1}, (-1)^{\epsilon_2}, (-1)^{\epsilon_3})\}\,,$$

with $\epsilon_1, \epsilon_2, \epsilon_3 = 0, 1$. Moreover, a continuum of vacua appears, whose location is controlled by the parameter K. Specifically, the distribution of points of this continuum of vacua is given by the following two equations

$$1+K\left(\phi_1-\frac{\phi_1^3}{3}+\phi_2-\frac{\phi_2^3}{3}\right)=0\,,$$
$$1+K\left(\phi_3-\frac{\phi_3^3}{3}\right)=0\,.$$

It is worth noting that condition $|K|<\frac{3}{2}$ leads to a scenario where the continuum of vacua is contained in a plane outside the mentioned cube, see Figure 6.28. When $|K|=\frac{3}{2}$ another continuum appears in a plane that contains the bottom face of the cube, e.g. $\phi_3=-1$. When this critical value of $|K|$ is surpassed, this last plane is split into two parallel planes with the same continuum of vacua. While two of these three planes will never intersect with the cube, the one that emerges in the bottom face of the cube when $|K|=\frac{3}{2}$ will be approaching the centre of the cube $\phi_3=0$ as $|K|\to\infty$. Conversely, the other two planes will tend to values $\phi_3=\pm\sqrt{3}$ as $|K|\to\infty$. Lastly, notice that when the parameter K vanishes, the standard triple ϕ^4-model is recovered and the vacuum manifold is again discrete.

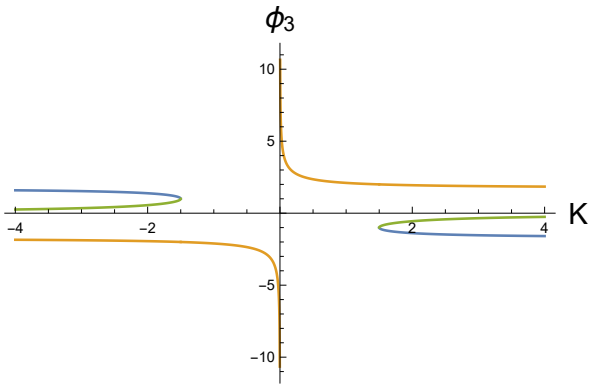

Figure 6.28: Non-vanishing values of K such that $|K|<\frac{3}{2}$ implies the existence of only one plane containing a continuum of vacua, which is placed outside the cube. When $|K|=\frac{3}{2}$ another one appears tangently crossing the bottom face of the cube. When $|K|>\frac{3}{2}$ this last plane is split into two parallel planes.

Two scenarios will be considered to illustrate the change in the kink variety. One where no vacuum point is inside the cube $|K|<\frac{3}{2}$ and another where a continuum of vacua crosses the cube $|K|>\frac{3}{2}$, see Figure 6.29.

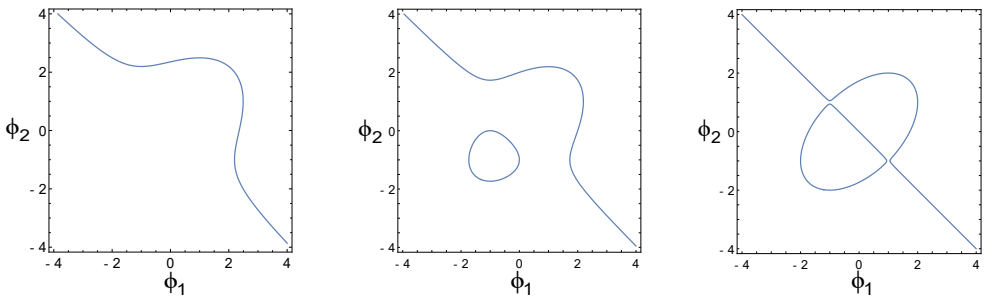

Figure 6.29: Distribution of the points in the continuum of vacua in each of these planes for the values $K=0.5,\frac{3}{2},300$. When $|K|=\frac{3}{2}$ a new continuum of vacua is created, which tends to merge with the other one as $|K|\to\infty$.

The location of points that belong to the vacuum manifold is controlled by the parameter K. When the value of $|K|$ is sufficiently large to allow a continuum of vacua to pass through the cube, the presence of these vacua significantly affects the behaviour of the arising family of kinks. This can be observed in Bogomol'nyi equations (6.9) in the dependence on K, which read for this composite triple ϕ^4-model as

$$\begin{aligned}
\frac{d\phi_1}{dT} &= \pm\left[1+K\left(\phi_3-\frac{\phi_3^3}{3}\right)\right](1-\phi_1^2)\,,\\
\frac{d\phi_2}{dT} &= \pm\left[1+K\left(\phi_3-\frac{\phi_3^3}{3}\right)\right](1-\phi_2^2)\,,\\
\frac{d\phi_3}{dT} &= \pm\left[1+K\left(\phi_1-\frac{\phi_1^3}{3}+\phi_2-\frac{\phi_2^3}{3}\right)\right](1-\phi_3^2)\,.
\end{aligned}$$

These equations cannot be directly integrated, as this new model is clearly non-separable. Nevertheless, the orbits of the emerging kinks will be identified in two scenarios with different parameter K. In each scenario solutions will be classified according to the number of fields that remain constant:

1. **Vaccuum solutions**: Configurations for which all fields ϕ_1,ϕ_2,ϕ_3 are fixed correspond, as mentioned, to the set of discrete vacua $v_{\epsilon_1,\epsilon_2,\epsilon_3}$ located at vertices of the cube or those points that belong to a continuum of vacua.

2. **Solutions as edges of the cube:** When two fields are fixed at constant values $\phi_i=(-1)^{\epsilon_i}$ and $\phi_j=(-1)^{\epsilon_j}$ with $i\neq j$, different singular kinks appear. Bogomol'nyi equations are then reduced to the differential equation of a ϕ^4-model for the remaining coordinate ϕ_l, which can be simultaneously shown for all coordinates as
$$\frac{d\phi_l}{d\tilde{T}_l}=\pm(1-\phi_l^2)\,,$$
where the following reparametrisations $\tilde{T}_l$ has been performed
$$\begin{aligned}
\tilde{T}_1 &= \left(1+(-1)^{\epsilon_3}\frac{2K}{3}\right)T\,,\\
\tilde{T}_2 &= \left(1+(-1)^{\epsilon_3}\frac{2K}{3}\right)T\,,\\
\tilde{T}_3 &= \left(1+(-1)^{\epsilon_1+\epsilon_2}\frac{2K}{3}\right)T\,.
\end{aligned}$$
Notice that some of these reparametrisations are not allowed when $|K|=\frac{3}{2}$. Therefore, eight singular kinks emerge as edges of the cube with vacua $v_{\epsilon_1,\epsilon_2,\epsilon_3}$ as vertices when $|K|\neq\frac{3}{2}$, see Figure 6.30. Similarly to previous examples, for these critical values of the parameter $|K|=\frac{3}{2}$ half of these singular kinks disappear.

3. **Families on the faces of the cube:** When only one field is fixed, depending on which one has been chosen different families of kinks appear. These families are generated by the orbit flow equations, which are immediately derived from Bogomol'nyi equations:

- If the first coordinate is constant $\phi_1 = (-1)^{\epsilon_1}$, two orbit equations are produced, one for each face of the cube where this coordinate is constant

$$\frac{d\phi_2}{d\phi_3} = \frac{1 + K\left(\phi_3 - \frac{\phi_3^3}{3}\right)}{1 + K\left((-1)^{\epsilon_1}\frac{2}{3} + \phi_2 - \frac{\phi_2^3}{3}\right)} \frac{1-\phi_2^2}{1-\phi_3^2}.$$

- When the second coordinate is fixed $\phi_2 = (-1)^{\epsilon_2}$, the same two orbit equations are obtained but replacing ϕ_2 by ϕ_1

$$\frac{d\phi_2}{d\phi_3} = \frac{1 + K\left(\phi_3 - \frac{\phi_3^3}{3}\right)}{1 + K\left((-1)^{\epsilon_2}\frac{2}{3} + \phi_1 - \frac{\phi_1^3}{3}\right)} \frac{1-\phi_1^2}{1-\phi_3^2}.$$

- Lastly, when it is the third coordinate that is constant $\phi_3 = (-1)^{\epsilon_3}$, a simpler orbit equation is obtained because of the common factor in Bogomol'nyi equations

$$\frac{d\phi_1}{d\phi_2} = \frac{1-\phi_1^2}{1-\phi_2^2},$$

whose solutions are confined to $\phi_1, \phi_2 \in (-1, 1)$ as can be seen in the explicit solution, written in terms of a constant of integration C

$$\phi_1 = \tanh\left[C + \operatorname{arctanh}\phi_2\right]. \tag{6.13}$$

The orbit equations of the first two cases can also be integrated to obtain implicit orbit equations, but given their length these will be omitted. Nevertheless, several members of these families can be found depicted in Figure 6.30.

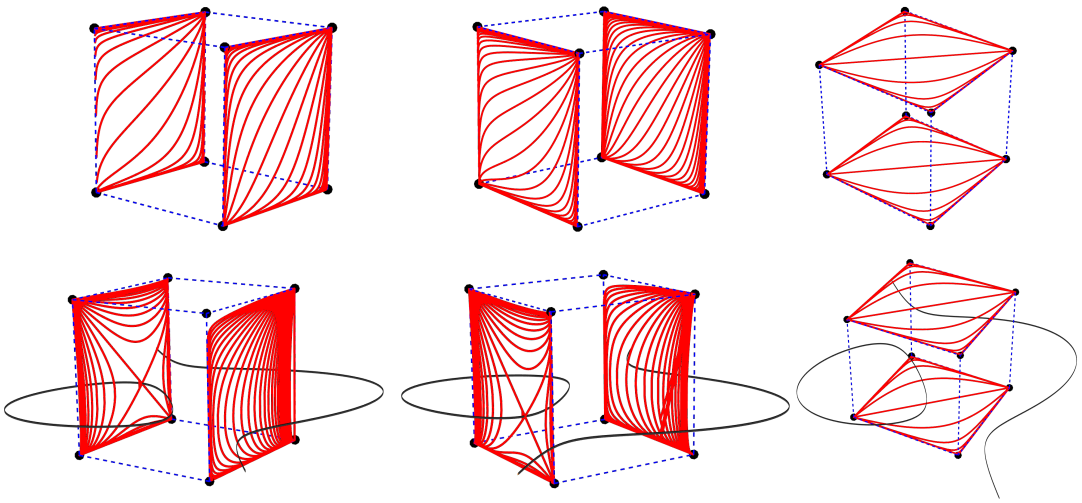

Figure 6.30: Different orbit equations give rise to families of kinks in different faces of the cube. Cases with $K = 0.5$ (up) and with $K = 3$ (down) have been represented for different values of the integration constants. The presence of the continuum of vacua inside the cube changes radically the behaviour of kinks. Certain kinks asymptotically connect vacua located at vertices of the cube with the new vacua in the faces of the cube.

It is worth mentioning that the value of K changes completely the dynamics of these kinks. Indeed, the presence of vacua in each face of the cube forces kinks to change their trajectory or even tend to this new vacua.

4. **Families in the interior of the cube**: When none of these fields are fixed, Bogomol'nyi equations produce two orbit equations that must be satisfied simultaneously. The chosen two orbit flow equations will be the following

$$\begin{aligned}\frac{d\phi_1}{d\phi_2} =& \frac{1-\phi_1^2}{1-\phi_2^2}\,,\\ \frac{d\phi_2}{d\phi_3} =& \frac{1+K\left(\phi_3-\frac{\phi_3^3}{3}\right)}{1+K\left(\phi_1-\frac{\phi_1^3}{3}+\phi_2-\frac{\phi_2^3}{3}\right)}\frac{1-\phi_1^2}{1-\phi_3^2}\,.\end{aligned}$$

Solutions of these equations are two-parameter families of curves in $\mathbb{R}^3$. The first equation, as has been described above, can be easily integrated resulting in condition (6.13), which relates both coordinates $\phi_1(\phi_2)$. Once more, because of the form of this equation, the dynamic of these coordinates must be contained within the rectangle $\phi_1, \phi_2 \in (-1, 1)$. This explicit orbit equation can be introduced in the second equation above to obtain a separable differential equation

$$\frac{d\phi_2}{d\phi_3} = \frac{1+K\left(\phi_3-\frac{\phi_3^3}{3}\right)}{1+K\left(\phi_1(\phi_2)-\frac{\phi_1^3(\phi_2)}{3}+\phi_2-\frac{\phi_2^3}{3}\right)}\frac{1-\phi_1^2}{1-\phi_3^2}\,.$$

Once again, given the length of the expressions, the resulting implicit orbit equation that relates ϕ_2 to ϕ_3 will be omitted. However, several orbits are depicted in Figure 6.31, where the effect of the parameter K can be observed again.

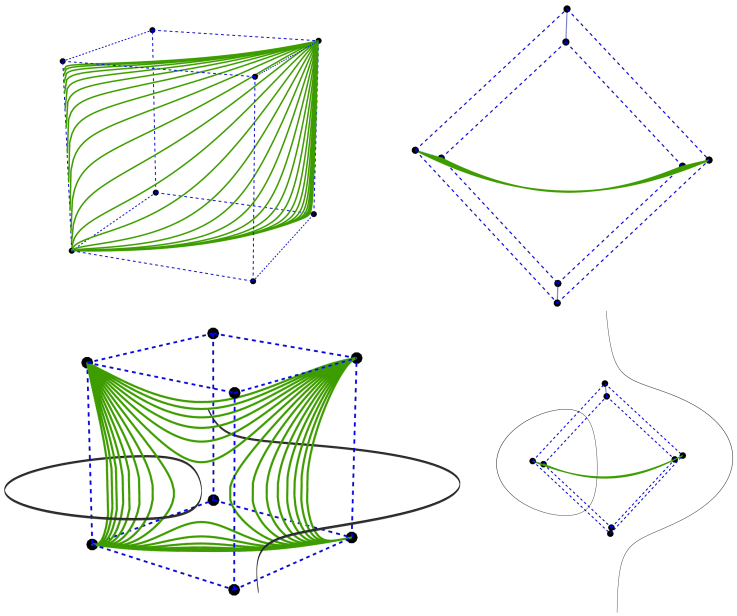

Figure 6.31: Different orbit equations give rise to families of kinks in the interior of the cube. Cases with $K = 0.5$ (up) and with $K = 3$ (down) have been represented for $C = 0.5$ and for different values of the other integration constant that arises. On one hand, the presence of the continuous vacuum inside the cube changes radically the behaviour of kinks. On the other, an infinite number of solutions connect the discrete vacua with points of the continuum of vacua inside the cube.

Values of this parameter $|K| > \frac{3}{2}$ modify entirely the dynamics of the kinks inside the cube. On the other hand, apart from the constant of integration that selects the member of the family of kinks shown in Figure 6.31, the other integration constant C will determine the proximity of these solutions to the faces of the cube. Indeed, limits of this constant $C \to \pm\infty$ and the other one will coincide with combinations of kinks that belong to families of kinks in the faces of the cube. This is again consistent with the usual energy sum rules that appear, as the energy of these solutions depends exclusively on the evaluation of the superpotential at the final and initial points of the kink.

Hence, by this procedure a generalisation of the triple ϕ^4-model has been constructed, which is not separable when $K \neq 0$ and it recovers the original model when $K = 0$. It should be noted that while the potential function of the original ϕ^4-model is of degree four in each field, this generalised model includes coupling inhomogeneous terms of degree $4, 5, 6, 7, 8$ and 10. On the other hand, this parameter K allows to introduce subtle changes in the triple ϕ^4-model trajectories when $|K| < \frac{3}{2}$. However, the dynamics is completely modified for values $|K| > \frac{3}{2}$, which describes a whole new scenario.

Lastly, the emergence of continua of vacua in this composite model is caused by the fact that the superpotential of the ϕ^4-model is not positive semidefinite. However, if a model with positive semidefinite superpotential is chosen, then the vacuum manifold of the composite model will be entirely discrete for $K \geq 0$ if the vacuum manifolds of the original models are also discrete. This is precisely the objective of next section.

6.3.5 Composite triple sine-Gordon model

As an example of composite Sigma model with more than two fields where the vacuum manifold is always discrete, sine-Gordon models will be combined. Unlike the superpotential for a ϕ^4- model, the superpotential of the sine-Gordon can be chosen to be positive semidefinite $W(\phi) = 1 - \cos\phi$. The present procedure allows then to construct a model in the Euclidean space $\mathbb{R}^3$ with a positive semidefinite superpotential

$$W = W_A(\phi_1, \phi_2) + W_B(\phi_3) + K\, W_A(\phi_1, \phi_2)\, W_B(\phi_3)\,,$$

when the parameter is defined as non-negative $K \geq 0$ as both original superpotentials W_A and W_B are defined as positive semidefinite

$$W_A = 2 - \sin\phi_1 - \sin\phi_2\,, \qquad W_B = 1 - \sin\phi_3\,.$$

This implies that the potential function, constructed from this superpotential W, presents as vacua only the Cartesian product of the vacua of the original models, with no continuum of vacua emerging

$$\begin{aligned} V =& \frac{1}{2}\left[1 + K\ (1 - \sin\phi_3)\right]^2 \left[\cos^2\phi_1 + \cos^2\phi_2\right] \\ &+ \frac{1}{2}\left[1 + K\ (2 - \sin\phi_1 - \sin\phi_2)\right]^2 \cos^2\phi_3\,. \end{aligned}$$

Once again, the case with $K = 0$ recovers the original triple sine-Gordon model. In this case, the vacuum manifold is independent of the value of the parameter

K. Since both original sine-Gordon models present an infinite number of vacua, an infinite number of vacua will appear in the composite Sigma model

$$\mathcal{M} = \left\{ v_{n_1,n_2,n_3} = \left(\frac{\pi}{2} + n_1\pi, \frac{\pi}{2} + n_2\pi, \frac{\pi}{2} + n_3\pi \right) \right\} ,$$

for integers n_1, n_2 and n_3. Thus, an infinite number of cube-shaped regions where kinks are expected to arise emerge in $\mathbb{R}^3$. On the other hand, the coupling between fields in the potential produce again non-separable Bogomol'nyi equations

$$\begin{aligned}
\frac{d\phi_1}{dT} &= \mp \left[1 + K\ (1 - \cos\phi_3)\right] \cos\phi_1 \,, \\
\frac{d\phi_2}{dT} &= \mp \left[1 + K\ (1 - \cos\phi_3)\right] \cos\phi_2 \,, \\
\frac{d\phi_3}{dT} &= \mp \left[1 + K\ (2 - \cos\phi_1 - \cos\phi_2)\right] \cos\phi_3 \,.
\end{aligned}$$

Information about solutions of these equations can be obtained by imposing trial orbits and from the integration of the orbit flow equations. Similarly to the model described in the previous section, sine-Gordon solutions appear as edges of the cube when two fields are fixed. Moreover, families that lie on faces of the cube are obtained when two fields are constant. Let us focus here on the orbits of the general solution with no constant fields. The chosen orbit equations will be of the form

$$\begin{aligned}
\frac{d\phi_1}{d\phi_2} &= \frac{\cos\phi_1}{\cos\phi_2} \,, \\
\frac{d\phi_2}{d\phi_3} &= \frac{1 + K\,(1 - \cos\phi_3)}{1 + K\,(2 - \cos\phi_1 - \cos\phi_2)} \frac{\cos\phi_2}{\cos\phi_3} \,.
\end{aligned}$$

The first equation can be easily integrated, which by simplicity will be solved for the central cube $\phi_1, \phi_2, \phi_3 \in (-\frac{\pi}{2}, \frac{\pi}{2})$

$$\phi_1 = \mathrm{Gd}\ \left[C + \mathrm{Gd}^{-1}\ [\phi_2] \right] \,, \tag{6.14}$$

where Gd denotes the Gudermannian function and C is an integration constant. Making use of equation (6.14), the second orbit equation becomes separable

$$\frac{d\phi_2}{d\phi_3} = \frac{1 + K\,(1 - \cos\phi_3)}{1 + K\left(2 - \mathrm{sech}\left[C + \mathrm{Gd}^{-1}\ [\phi_2] \right] - \cos\phi_2\right)} \frac{\cos\phi_2}{\cos\phi_3} \,.$$

This equation can be integrated and the resulting solution can be written as follows

$$\left| \frac{\cos\frac{\phi_2}{2} - \sin\frac{\phi_2}{2}}{\cos\frac{\phi_2}{2} + \sin\frac{\phi_2}{2}} \right|^{2K+1} \left| \frac{\cos\frac{\phi_3}{2} + \sin\frac{\phi_3}{2}}{\cos\frac{\phi_3}{2} - \sin\frac{\phi_3}{2}} \right|^{K+1} = \gamma\, e^{-KF(\phi_2,\phi_3;C)} \tag{6.15}$$

where $\gamma \in (0, \infty)$ is a constant originated in the integration and $F(\phi_2, \phi_3; C)$ is a function defined as follows

$$F(\phi_2, \phi_3; C) = \phi_2 - \phi_3 + 2\arctan\left[2\csc\phi_2 \sin\frac{\phi_2}{2} \left(\cosh C \sin\frac{\phi_2}{2} + \cos\frac{\phi_2}{2} \sinh C \right) \right] .$$

The first thing it must be highlighted is that when $K = 0$ the orbit equations are considerably simplified as expected. Indeed, the orbits of the separable triple sine-Gordon model must be recovered. As the constant K increases in value, trajectories

are affected more strongly by the new higher-order terms, see Figure 6.32. All the depicted solutions share the same value of C, creating a surface inside the cube. All possible values of this constant C will produce surfaces that fill the interior of the cube. On the other hand, energy sum rules are expected to appear. Also, limit members of these families of kinks for both parameters of the families, C and γ, must coincide with combinations of different singular kinks that belong to families of kinks on the faces of the cube.

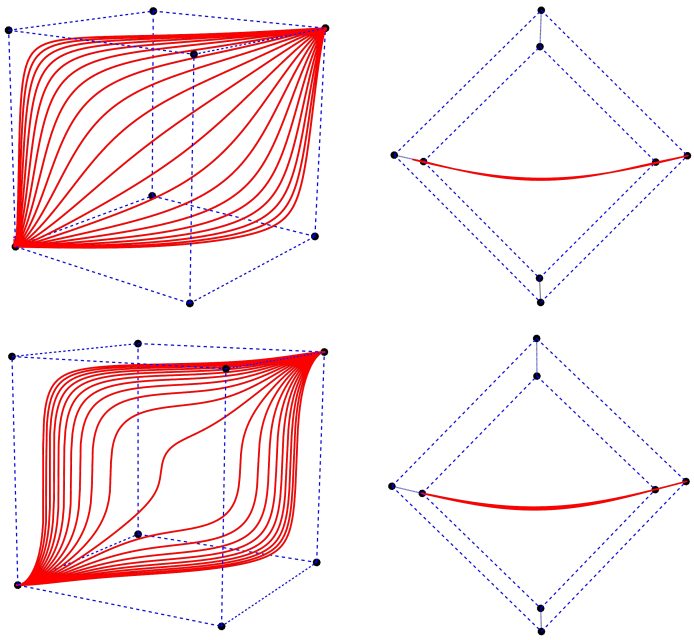

Figure 6.32: Orbits of different members of the families of kinks with common parameter $C = 0.5$ when $K = 0.5$ (up) and when $K = 100$ (down). As the value of the parameter K increases, kink orbits present more curvature around the centre of the cube.

Note that these solutions have been derived for the central cube $\phi_1, \phi_2, \phi_3 \in (-\frac{\pi}{2}, \frac{\pi}{2})$, but similar results can be found for any other cube in $\mathbb{R}^3$. Therefore, this model represents a generalisation of the triple sine-Gordon, with a significantly richer kink variety. Lastly, even though this procedure has been applied only to Euclidean spaces, a Sigma model with this type of higher-order coupling can be constructed on general Riemannian manifolds. The particular case where this is achieved for the sphere will be shown in the next section.

6.3.6 A model on the sphere with extended superpotential

Let us construct in this section a Sigma model on the sphere $\mathbb{S}^2$ from a superpotential of the form (6.8). This is, a superpotential that include higher-order coupling terms modulated by a parameter K. Notice that this procedure is different from that of previous sections, as the sphere has not been constructed as the product of other two Riemannian manifolds. In particular, stereographic coordinates will be employed on the sphere, since in these coordinates the sphere is conformally flat. This implies that orbits in the stereographic plane will be the same as those of the case where $\mathbb{R}^2$ is taken as target manifold. This fact has already been shown in Chapter 5, where deformations between the plane and the sphere were considered. Therefore, this fact allows us to automatically transfer any kink of any Sigma model on the plane into

the sphere $\mathbb{S}^2$. Let us then denote stereographic coordinates as $(U_{\mathbb{S}^2}, \{\psi_1, \psi_2\})$ and construct a superpotential on this chart given by

$$W = W_A(\psi_1) + W_B(\psi_2) + K\, W_A(\psi_1)\, W_B(\psi_2)\,,$$

where $K \in \mathbb{R}$ and $W_A, W_B : \mathbb{R} \to \mathbb{R}$ are superpotentials of two field theories with one field. Bogomol'nyi equations read as those for the plane but with a common global factor that emerges from the metric

$$\begin{aligned}
\frac{d\psi_1}{dT} &= \pm\left[1 + KW_B(\psi_2)\right] \frac{\left(1+\psi_1^2+\psi_2^2\right)^2}{4} \frac{dW_A}{d\phi_1}\,,\\
\frac{d\psi_2}{dT} &= \pm\left[1 + KW_A(\psi_1)\right] \frac{\left(1+\psi_1^2+\psi_2^2\right)^2}{4} \frac{dW_B}{d\psi_2}\,.
\end{aligned}$$

Therefore, this factor disappears in the orbit flow equation, which reads

$$\frac{d\psi_1}{d\psi_2} = \frac{1 + KW_B(\psi_2)}{1 + KW_A(\psi_1)} \frac{W_A'(\psi_1)}{W_B'(\psi_2)}\,.$$

As a particular example to illustrate this procedure, let us consider two superpotentials corresponding to ϕ^4-models

$$W_A(\psi_1) = \psi_1 - \frac{\psi_1^3}{3}\,, \qquad W_B(\psi_2) = \psi_2 - \frac{\psi_2^3}{3}\,.$$

This leads to the same orbit equation that was obtained for the plane (6.11), but in this case the variables are coordinates in the stereographic plane. These kink orbits are depicted on the sphere in Figure 6.33 for the similar values of parameter $K = \frac{1}{2}, \frac{3}{2}, 3$ that were employed in the case of the plane. Notice that orbits that tend to infinity on the plane asymptotically connect vacua now. This is, the kink variety on the sphere is notably richer than the analogue kink variety in the plane. Notice that the same procedure can be applied, for instance, to the previously described composite double sine-Gordon, which would lead to an infinite number of vacua and kinks on the sphere.

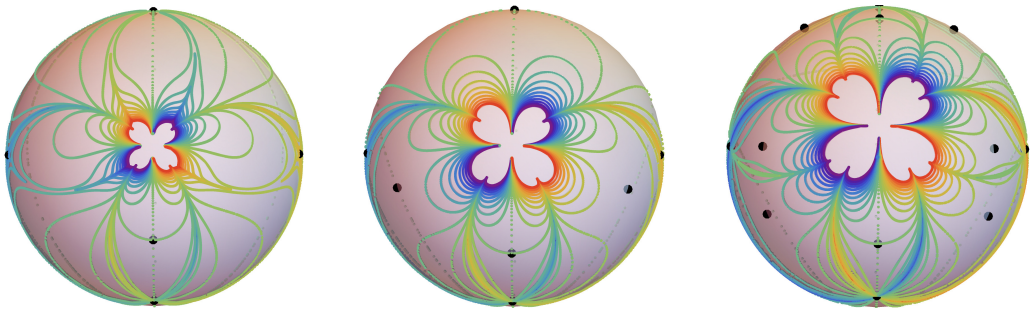

Figure 6.33: Orbits of the generalised double ϕ^4-model on the sphere for parameter values $K = \frac{1}{2}, \frac{3}{2}, 3$. Trajectories that go to infinity on the plane are connected at the north pole in the case of the sphere.

Lastly, it is important to note that this procedure can be employed considering other Riemannian manifolds as target manifolds. Indeed, other Sigma models on other Riemannian manifolds can be constructed making use of these extended superpotentials.

6.4 Further comments

In this chapter new methods of deformations that allow us to identify new kinks in the deformed Sigma models have been constructed. On one hand, the trimming procedure allows us to cut kink orbits to form new Sigma models for which the cut orbit is a solution. Different widths, trim centers and trimming functions allow variability in the type of orbits that can be obtained via trimming. Moreover, including a distortion, the image of these deformed curves can be further controlled, which can be even taken to other manifolds to construct Sigma models on them. It must be stressed, though, that this procedure is seed-dependent. This is, the constructed potential will not admit families of trims as solutions, but only a particular trimmed orbit. Accordingly, a family of potentials must be constructed to support a family of trims.

Secondly, a formalism for hybridisation and extension of kinks is described. In order to find a Sigma model that supports a piecewise curve as a kink, three condition must hold. The gluing of curves must be C^2, the potential must be found analytically in all regions that contain the piecewise curve and the contribution of each part to the energy must be finite. These conditions allows the construction of hybrid kinks, for which the piecewise potentials can be extended to a strip that contains the hybrid. It has also been proven that this is also true even when certain types of polynomial interpolations are involved. Making use of this formalism, several piecewise kinks have been constructed, including ϕ^4-model's extensions and the construction of non-topological kinks in $\mathbb{R}^2$ and in the torus.

Lastly, a formalism to construct Sigma models on the Cartesian product of the target manifolds of another two Sigma models is presented. Moreover, the superpotential is defined in such a manner that it enables us to couple the dynamics of these originally isolated Sigma models. In particular, new models that generalise the double ϕ^4-model or a combination of a ϕ^4-model with a sine-Gordon model are constructed in $\mathbb{R}^2$. Similarly, an extended triple ϕ^4-model and an extended triple sine-Gordon are constructed in $\mathbb{R}^3$. These generalise their respective standard models, introducing higher-order terms and enriching their kink variety. Lastly, a Sigma model is constructed on the sphere $\mathbb{S}^2$ employing a similar extended superpotential.

Conclusions

In this thesis, an examination of various aspects of kinks in non-linear Sigma models and methods of deformations has been conducted. In this final chapter, the key conclusions drawn from this exploration will be summarised.

- The Bogomol'nyi arrangement facilitates the analytical identification of kinks in non-linear Sigma models. Depending on whether the potential is Hamilton-Jacobi separable, Bogomol'nyi equations may lead to one or more families of kinks. In particular, in the cases that have been studied where the target manifolds are two-dimensional, one or two families emerge. On the other hand, this procedure allows us to design the vacuum manifold of the non-linear Sigma model. For example, Sigma models with a rich kink variety on the two-dimensional sphere with homogeneous quartic potential are constructed, presenting six vacua symmetrically distributed on the sphere. This designability of the vacuum manifold increases the opportunities for finding physical applications. In a similar vein, Sigma models with different distributions and number of vacua on the torus can be constructed. In fact, a Sigma model on the torus with only one vacuum point has been constructed, forcing all the emerging kinks to be non-topological. The complexity of the analysis of linear stability under small perturbations increases considerably for non-Euclidean target manifolds.

- The existence of stable non-topological kinks that cannot decay into vacuum has been proven. The term brochoson has been coined for these non-topological kinks, whose decay into vacuum is forbidden due to the homotopy properties of the target space. A method for constructing Sigma models that admit brochosons has been introduced, which is based on two conditions. First, the Sigma model must be constructed making use of a superpotential which is non-periodic in the chart in at least one angular coordinate. Secondly, the target space must be non-simply connected to allow the existence of different homotopy classes of loops. If the original target space is simply connected, potential functions with singularities can force the appearance of these homotopy classes. For example, one and two vacua are the minimum number of vacua that must be present in the Euclidean plane and the two-dimensional sphere respectively to allow brochosons to arise. On the other hand, brochosons are allowed to arise on the torus, as it is non-simply connected. This scenario has motivated the definition of topological clusters, as collections of topological sectors that share the same orbit's ends.

- A mechanism for continuous geometrical constriction of kinks has been introduced, generalising the work of Bazeia et al. The target space of a field theory has been extended, continuously altering the geometry of this extended space in a very particular manner. When kinks of the new field theory, defined in the extended space, are projected to the original target space, the resulting curves correspond to variations of the kinks of the original field theory, asymptotically connecting the same vacua as the original ones. The presence of a parameter that controls the intensity of the constriction extends the versatility of this mechanism in physics. Furthermore, this new mechanism allows us to introduce asymmetry in the kink and energy density profiles in a continuous manner.

- A formalism that generalises the methods of deformation of Bazeia et al. has been developed. On one hand, this new formalism allows us to analytically obtain kinks in non-linear Sigma models from other non-linear Sigma models. On the other, it also enables seed-dependent deformations, giving rise to different Sigma models depending on the kink that is being deformed. Additionally, in deformations that involve conformally flat Riemannian manifolds, a reparametrisation can be introduced to "absorb" or correct the change in curvature between these target manifolds. This allows us to simplify the orbit flow equations.

- Three other deformation techniques have been developed. First, based on the formalism of deformation, new non-linear Sigma models can be constructed from trims of kink orbits. This procedure is seed-dependent by construction, which implies that different trimming methods will result in different non-linear Sigma models. On the other hand, kinks can also be glued forming hybrids, ensuring the gluing of potentials of the corresponding non-linear Sigma models. For instance, non-topological kinks can be piecewisely constructed. Lastly, Sigma models can be combined to create others where the dynamics of the original models are intertwined. Kinks of the original Sigma models can be preserved in the composite Sigma model by extending the superpotential appropriately. This leads to the presence of higher-order terms in the potential and to richer kink varieties.

Appendix A

Modified Pöschl-Teller potential

The analysis of the linear stability of solutions involves the study of spectral equations. Although an analytical approach is not always available, spectral equations where this is possible will frequently emerge for the types of solutions that are being analysed in this thesis. Two important types of solutions fall into this category. The first one corresponds to the spectral equations that arise for vacuum solutions, whose simplicity makes their analysis straightforward. The second type is commonly associated with spectral problems arising for modified Pöschl-Teller potentials

$$\frac{d^2\psi}{dz^2} + \left[\epsilon - v\cosh 2\mu - v\sinh 2\mu \tanh z + v\cosh^2\mu \ \mathrm{sech}^2 z\right] = 0\,.$$

This corresponds to a Legendre equation [105] with real constants v and μ, where ϵ denotes the rescalated eigenvalue. Although the expressions for the eigenfunctions read complicated, the discrete spectrum can be written when $\epsilon < ve^{-2\mu}$ as follows

$$\epsilon_n = v\cosh 2\mu - \left[\sqrt{v\cosh^2\mu + \frac{1}{4}} - \left(n+\frac{1}{2}\right)\right]^2 - \frac{v^2\sinh^2 2\mu}{\delta^2(\mu,v)}\,,$$

where the auxiliary function $\delta(\mu, v)$ has been defined as

$$\delta(\mu,v) = \sqrt{v\cosh^2\mu + \frac{1}{4}} - \frac{1}{2} - \sqrt{\frac{1}{2}v\sinh 2\mu}$$

and n is a non-negative integer whose upper limit is determined by the values of parameters v and μ

$$n = 0, 1, 2, \cdots < \delta(\mu, v)\,.$$

In particular, when $\mu = 0$ this spectral equation becomes considerably simpler

$$\frac{d^2\psi}{dz^2} + \left[\epsilon - v + v\ \mathrm{sech}^2 z\right] = 0\,, \tag{A.1}$$

and the discrete spectrum is also simplified

$$\epsilon_n = v - \left[\sqrt{v+\frac{1}{4}} - \left(n+\frac{1}{2}\right)\right]^2\,, \tag{A.2}$$

where now $n = 0, 1, \cdots < \sqrt{v+\frac{1}{4}} - \frac{1}{2}$. Moreover, a continuous spectrum arises at $\epsilon = v$. Notice, however, that it is the discrete spectrum that will encode the information regarding the stability of solutions.

Appendix B

Newton's equation on Riemannian manifolds

In this section, a summary of the geometrical approach described in [71] to derive Newton's equations on Riemannian manifolds is presented. Let us consider an $m-$dimensional Riemannian Manifold (M, g) with Riemannian metric tensor g and the Levi-Civita connection on it. Once a chart $(U_M, \{\lambda^i_M\})$ with $i = 1, \ldots, m = \dim M$ is chosen on M, a curve c on M can be written locally as

$$\begin{array}{rccl} c\colon & \mathbb{R} & \longrightarrow & U_M \subseteq M \\ & x & \longmapsto & c(x) = (c^1(x), \ldots, c^m(x))\,, \end{array}$$

where x parametrises such a curve. Let us restrict to natural Lagrangians, that is, to Lagrangians of the form

$$L(c, \dot{c}) = \frac{1}{2} g(\dot{c}, \dot{c}) - U(c(x))\,,$$

where $U : M \to \mathbb{R}$ is the mechanical potential function and $\dot{c} \in \mathfrak{X}(M)$ is the vector field tangent to the curve. For the sake of convenience, this vector field will be written in coordinates as follows

$$\dot{c}(x) = \frac{\partial c^i(x)}{\partial \phi^i} \frac{\partial}{\partial \phi^i} \qquad i = 1, \ldots, m\,,$$

where the elements of the basis of a tangent space are denoted as $\{\frac{\partial}{\partial \phi^i}\}$. For natural Lagrangians the action of a mechanical system is of the form

$$S\,[c] = \int_{-\infty}^{\infty} L(c, \dot{c})\; dx = \int_{-\infty}^{\infty} \left[\frac{1}{2} g(\dot{c}, \dot{c}) - U(c(x))\right]\; dx\,. \tag{B.1}$$

Curves c that extremise this functional will be regarded as solutions of this mechanical system. Now, in order to find such trajectories, let us consider a one-parameter family of variations of curves with parameter ξ. In particular, let us define a proper variation $\varphi(x, \xi)$ of a reference curve $c(x)$ as any differentiable map

$$\begin{array}{rccl} \varphi\colon & \mathbb{R} \times (-\epsilon, \epsilon) & \longrightarrow & M \\ & (x, \xi) & \longmapsto & \varphi(x, \xi)\,, \end{array}$$

such that the original case is recovered when $\varphi(x,0) = c(0)$, ϵ is a positive real number which is small enough to make the curve be well-defined and for which the ends are fixed

$$\lim_{x\to-\infty} \varphi(x,\xi) = \lim_{x\to-\infty} c(x) \qquad \forall \xi \in (-\epsilon,\epsilon)\,, \tag{B.2}$$

$$\lim_{x\to\infty} \varphi(x,\xi) = \lim_{x\to\infty} c(x) \qquad \forall \xi \in (-\epsilon,\epsilon)\,. \tag{B.3}$$

See Figure B.1 for a pictorial example of a proper variation in a Riemannian manifold. It is important to emphasise that these are small proper variations in general. Indeed, they have been defined for small values of ϵ to force variations to be well-defined.

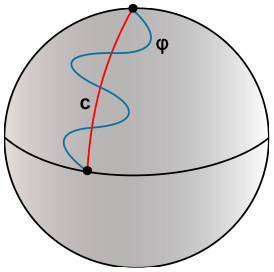

Figure B.1: Pictorial example of proper variation φ of a reference curve c in the sphere $\mathbb{S}^2$. Notice that by construction the original curve must be included in the family of variations.

In turn, any proper variation $\varphi(x,\xi)$ defines a surface in M generated by two different vector fields, the vector field tangent to the variation and the vector field that contains the information regarding how members of the family of variations transform into others

$$\dot{\varphi}(x,\xi) = \frac{\partial \varphi^i(x,\xi)}{\partial x}\frac{\partial}{\partial \phi^i}\,, \quad \psi(x,\xi) = \frac{\partial \varphi^i(x,\xi)}{\partial \xi}\frac{\partial}{\partial \phi^i}\,.$$

In order to alleviate notation let us write $\dot{c}(x) \equiv \dot{c}(x,0)$ and $\psi(x) \equiv \psi(x,0)$ for the unaltered case $\xi = 0$. Since by definition $\varphi(x,0) = c(x)$, the identification $\dot{\varphi}(x,0) = \dot{c}(x)$ is also made. Let us assume that the reference curve $c(x)$ is a solution, that is, it extremises the action (B.1). If a proper variation φ of such a curve is considered, then the action for this family of curves

$$S\left[\varphi\right] = \int_{-\infty}^{\infty} \left[\frac{1}{2} g(\dot{\varphi},\dot{\varphi}) - U(\varphi(x))\right] dx \tag{B.4}$$

is now a function of the parameter ξ, for which the extremal case is obtained when $\xi = 0$. This implies that if c is indeed a solution, then the following condition must hold

$$\left.\frac{\partial S\left[\varphi\right]}{\partial \xi}\right|_{\xi=0} = 0\,.$$

Let us start by deriving an expression for the derivative $\frac{\partial S[\varphi]}{\partial \xi}$. Limits of integration do not depend on the parameter of the variation ξ. This allows us to introduce the derivative inside the integral, leading to the following expression for this derivative

$$\frac{\partial S\left[\varphi\right]}{\partial \xi} = \int_{-\infty}^{\infty} \left[\frac{1}{2}\frac{\partial}{\partial \xi} g(\dot{\varphi},\dot{\varphi}) - \frac{\partial U(\varphi(x))}{\partial \xi}\right] dx\,. \tag{B.5}$$

The following four properties shall be necessary to express the integrand of the action above in a more convenient manner:

1. From the fact that the Levi-Civita connection is compatible with the metric and that Riemannian metric tensors are symmetric, the following relation follows
$$\frac{\partial}{\partial\xi} g\left(\dot{\varphi},\dot{\varphi}\right) = 2g\left(\frac{D\dot{\varphi}}{\partial\xi},\dot{\varphi}\right),$$
where the covariant derivative along ψ has been denoted as $\frac{D}{\partial\xi} \equiv \nabla_{\psi}$.

2. The Levi-Civita connection is torsionless, which implies that, given the commutativity of elements of the basis $\left[\frac{\partial}{\partial x},\frac{\partial}{\partial\xi}\right] = 0$, the following condition is satisfied
$$\frac{D\dot{\varphi}}{\partial\xi} = \frac{D\psi}{\partial x}\,.$$
In fact, this result is employed in the usual derivation of the Euler-Lagrange equations, where the derivative of the variation is equaled to the variation of the derivative.

3. The definition of the gradient grad U of a differentiable function $U : M \to \mathbb{R}$ defined on a Riemannian manifold (M, g) enables us to express the potential term as the metric tensor acting on the vector fields:
$$g\left(\text{grad } U, \psi(x,\xi)\right) = \psi(x,\xi)U(\varphi(x,\xi)) = \frac{\partial U(x,\xi)}{\partial\xi}\,.$$

4. The property of compatibility of the connection with the metric can be written as
$$g\left(\frac{D\psi}{\partial x},\dot{\varphi}\right) = \frac{\partial}{\partial x}g(\psi,\dot{\varphi}) - g\left(\psi,\frac{D\dot{\varphi}}{\partial x}\right),$$
which allows us to derive a rule of "integration by parts" by taking into consideration the asymptotic conditions (B.2). Indeed, these conditions make the terms evaluated at infinities vanish and we obtain
$$\begin{aligned}\int_{-\infty}^{\infty} g\left(\frac{D\psi}{\partial x},\dot{\varphi}\right)\,dx &= \int_{-\infty}^{\infty}\frac{\partial}{\partial x}g(\psi,\dot{\varphi})\,dx - \int_{-\infty}^{\infty} g\left(\psi,\frac{D\dot{\varphi}}{\partial x}\right)\,dx \\ &= -\int_{-\infty}^{\infty} g\left(\psi,\frac{D\dot{\varphi}}{\partial x}\right)\,dx\,.\end{aligned}$$

These identities allow us to write the derivative of the action with respect to the parameter of the variation ξ when the reference curve is recovered $\xi = 0$ for any proper variation as
$$\frac{dS}{d\xi}\left[\varphi\right]\Big|_{\xi=0} = -\int_{-\infty}^{\infty} g\left(\frac{D\dot{c}}{\partial x} + \text{grad } U,\psi\right)\,dx = 0\,.$$

The fundamental theorem of variational calculus can be applied here. Let us denote as Φ^i the terms that accompany the coordinates of the variation V^i, so that the above condition can be written as
$$\int_{-\infty}^{\infty}\sum_{i=1}^{m}\Phi^i\psi^i\,dx = 0\,. \tag{B.6}$$

By construction, since the metric tensor components g_{ij} are continuous, the functions Φ^i must also be continuous. Since this must be true for all proper variations, it is also true in particular when all its components except for an arbitrary component ψ^j vanish. For the sake of the argument, let us consider this type of variations. Condition (B.6) for this type of variation has the form

$$\int_{-\infty}^{\infty} \Phi^j \psi^j \, dx = 0 \, .$$

Let us assume that Φ^j does not vanish everywhere. If this is true, since these functions are continuous, then an interval $I \subset \mathbb{R}$ where this function does not vanish can be found. If ψ^j is chosen to be zero outside this interval and only zero in the boundary of I, then this integral cannot be zero and a contradiction is found. Therefore, Φ^j must vanish everywhere. Since this is done for an arbitrary component j, it is true for all of them. We conclude then that the following equation must hold for any solution

$$\frac{D\dot{c}}{\partial x} + \text{grad } U = 0 \, . \tag{B.7}$$

These equations can be written in coordinates producing m second order differential equations

$$\frac{d^2 c^i}{dx^2} + \Gamma^i_{jk} \frac{dc^j}{dx} \frac{dc^k}{dx} = -g^{ik} \frac{\partial U}{\partial c^k} \, , \tag{B.8}$$

which is the usual form of Newton equations on a Riemannian manifold. Notice that the equations of motion of a free particle moving on this Riemannian manifold, this is, when the potential term vanishes $U = 0$, correspond to the geodesics on this manifold. Specifically, when $\mathbb{R}^n$ with Cartesian coordinates is chosen as target space, the familiar equations are recovered

$$\frac{d^2 c^i}{dt^2} = -\frac{\partial U}{\partial c^i} \, .$$

Lastly, it is worth highlighting that while Newton equations provide solutions for the mechanical system, the stability of such solutions requires further study. In fact, variations of such solutions may transform solutions into other solutions. Although this analysis is of no direct interest in field theory, it equips us with the tools that shall be employed in field theory. This serves as the motivation for Appendix C.

Appendix C

Linear stability in mechanics

Even though the primary objective of this thesis is to study kinks in field theory, the analysis of linear stability under small perturbations in classical mechanics will serve us as a guide for a similar study in field theory. This section will provide a summary of the results described in [71] related to this particular direction. Solutions must be extremal configurations of the action, as it has been discussed in Appendix B. This implies that the derivative of the action S with respect to the parameter of the variation must vanish for any solution. However, the information regarding whether solutions are maxima, minima or saddle points escapes this first derivative. Indeed, the stability of solutions hides behind the behaviour of the second derivative with respect the parameter of the variation. Equation (B.5) can be written, by making use of the property of compatibility of the connection with the metric and the torsionless property, as follows

$$\frac{\partial S\left[\varphi\right]}{\partial \xi} = \int_{-\infty}^{\infty} \left[\frac{1}{2}\, g\left(\frac{D\psi}{\partial x}, \dot{\varphi}\right) - g\left(\text{grad } U, \psi\right)\right] \, dx \,.$$

Since it is the second derivative which is being sought, this equation will be differentiated again with respect to the parameter of the variation ξ. This leads to

$$\frac{\partial^2 S\left[\varphi\right]}{\partial \xi^2} = \int_{-\infty}^{\infty} \left[\frac{1}{2}\, \frac{\partial}{\partial \xi} g\left(\frac{D\psi}{\partial x}, \dot{\varphi}\right) - \frac{\partial}{\partial \xi} g\left(\text{grad } U, \psi\right)\right] \, dx \,.$$

This expression can be further manipulated taking into consideration the following two properties of the Riemann curvature tensor:

1. The Riemmanian curvature tensor measures the commutativity of covariant derivatives
$$\frac{D}{\partial \xi}\frac{D\psi}{\partial t} - \frac{D}{\partial t}\frac{D\psi}{\partial \xi} = R(\dot{c}, \psi)\psi \,.$$

2. Properties of the Riemannian curvature tensor can be employed to show that the following anticommutativity property holds
$$g\left(R(\dot{c}, \psi)\psi, \dot{c}\right) = -g\left(R(\dot{c}, \psi)\dot{c}, \psi\right) \,.$$

These two properties, in conjunction with the connection's compatibility with the metric and the fact that proper variations vanish at infinities, enable us to write the

second derivative of the action as

$$\frac{d^2S}{d\xi^2}[\varphi]\Big|_{\xi=0} = \int_{-\infty}^{\infty} g\left(-\frac{D^2\psi}{\partial x^2} - R(\dot{c},\psi)\dot{c} - \nabla_{\psi}\text{grad } U, \psi\right) dx \qquad \text{(C.1)}$$
$$\equiv \int_{-\infty}^{\infty} g\left(\mathcal{H}(\psi),\psi\right) dx\,,$$

which has already been evaluated at solution c by taking $\xi = 0$. Note that the operator $\mathcal{H}$, which receives the name of Hessian operator in the literature, has been introduced to simplify notation. Therefore, the linear stability under small perturbations will depend on the spectrum of the Hessian operator $\mathcal{H}$. Among all proper variations of a solution, the small linear ones $\varphi(x,\xi) = c_K(x) + \xi\,\psi(x)$ which are solutions of Newton equations to the first order in the parameter of the variation ξ, will encapsulate its leading evolution. When this condition is imposed in Newton equations (B.8), these leading variations are defined by the following equations for the variation field $\psi(x)$

$$\partial_x^2\psi^a + 2\Gamma^a_{ij}\partial_x\psi^i\frac{dc^j_K}{dx} + \frac{\partial\Gamma^a_{ij}}{\partial c^m}\Big|_{c_K}\frac{dc^i_K}{dx}\frac{dc^j_K}{dx}\psi^m$$
$$= g^{ma}(c_K)\,\frac{\partial U}{\partial c^m\partial c^n}\Big|_{c_K}\psi^n + \frac{\partial U}{\partial c^m}\Big|_{c_K}\frac{\partial g^{ma}}{\partial c^n}\Big|_{c_K}\psi^n\,.$$

These equations can be written more concisely by identifying terms as $\mathcal{H}(\psi) = 0$. This implies that the second derivative of the mechanical action (C.1) for a solution when this type of variations are considered must vanish

$$\frac{d^2S}{d\xi^2}[\varphi]\Big|_{\xi=0} = 0\,.$$

Indeed, these modify solutions transforming them into other solutions to the first order in ξ. This result is generalised to the context of field theory in Chapter 2, where the introduction of time will lead to significant changes. Lastly, it is worth noting that in the simplest case, which is the Euclidean space in Cartesian coordinates, the familiar Hessian operator form is recovered for the component a

$$[\mathcal{H}(\psi)]_a = \frac{d^2\psi^a}{dx^2} + \psi^a\,\frac{\partial^2 U}{\partial\varphi^b\partial\varphi^a}\Big|_c\,.$$

Appendix D

Riemannian geometry of the Torus

Several well-known results in Riemannian geometry related to the torus are required throughout Chapter 4. For the sake of completeness, these and others are compiled in this section. The notation is adapted to the chosen parametrisation of the torus in Chapter 4, in which the torus is embedded in the Euclidean space $\mathbb{R}^3$. This is, the following equations are considered

$$\begin{aligned}\phi^1(\theta,\varphi) &= (R + r\sin\theta)\cos\varphi\,,\\ \phi^2(\theta,\varphi) &= r\cos\theta\,,\\ \phi^3(\theta,\varphi) &= (R + r\sin\theta)\sin\varphi\,,\end{aligned}$$

where $\theta \in [0, 2\pi)$ and $\varphi \in [0, 2\pi)$. As expected, these coordinates make the following constraint identically hold

$$\left(R - \sqrt{\phi_1^2 + \phi_3^2}\right)^2 + \phi_2^2 - r^2 = 0\,,$$

which is the constraint that defines the points of a torus of radii R and r with $R > r > 0$. This embedding makes the torus inherit a metric tensor from the Euclidean metric in $\mathbb{R}^3$, which can be written as

$$\begin{aligned}ds^2 = &\left(d\phi^1 \otimes d\phi^1 + d\phi^2 \otimes d\phi^2 + d\phi^3 \otimes d\phi^3\right)\big|_{\mathbb{S}^1\times\mathbb{S}^1}\\ =&r^2 d\theta\otimes d\theta + (R+\sin\theta)^2 d\varphi\otimes d\varphi = g_{11}\, d\theta\otimes d\theta + g_{22}\, d\varphi\otimes d\varphi\,.\end{aligned}$$

On the other hand, given that the Levi-Civita connection is being considered, this metric tensor gives rise to the following Christoffel symbols

$$\begin{aligned}&\Gamma^k_{ij} = \frac{1}{2}g^{kl}\left(\frac{\partial g_{il}}{\partial u^j} + \frac{\partial g_{lj}}{\partial u^i} - \frac{g_{ij}}{\partial u^l}\right) \quad , \quad i,j,k,\cdots = 1,2 \quad , \quad u^1 = \theta\ ,\ u^2 = \varphi\,,\\ &\Gamma^1_{22} = -\frac{1}{r}\cos\theta(R + r\sin\theta), \quad \Gamma^2_{12} = \Gamma^2_{21} = \frac{r\cos\theta}{R + r\sin\theta}\,,\\ &\Gamma^1_{11} = \Gamma^1_{12} = \Gamma^1_{21} = \Gamma^2_{11} = \Gamma^2_{22} = 0\,,\end{aligned}$$

where Einstein summation convention over repeated indices have been employed, and g^{ij} denotes, as usual, the components of the dual metric tensor. The Riemann tensor, in the case of surfaces, can be written in terms of the Gaussian curvature as

follows

$$
\begin{aligned}
&R_{ijkl} = K\left(g_{ik}g_{jl} - g_{il}g_{jk}\right)\,,\\
&R_{1111} = R_{1112} = R_{1121} = R_{1122} = R_{1211} = R_{1222} = 0\,,\\
&R_{2111} = R_{2122} = R_{2211} = R_{2212} = R_{2221} = R_{2222} = 0,\\
&R_{1212} = -R_{1221} = \frac{1}{r}\sin\theta(R + r\sin\theta)\,, \quad -R_{2112} = R_{2121} = \frac{r\sin\theta}{R + r\sin\theta}\,.
\end{aligned}
$$

Finally, the Ricci tensor components and the scalar curvature can be written as

$$
\begin{aligned}
&R_{ij} = R^{l}_{ilj} = Kg_{ij}\,, \qquad R = g^{ij}R_{ij} = g^{11}R_{11} + g^{22}R_{22}\,,\\
&R_{12} = R_{21} = 0\,, \quad R_{11} = \sin\theta\left(\frac{R}{r} + \sin\theta\right)\,, \quad R_{22} = \frac{\sin\theta}{\frac{R}{r} + \sin\theta}\,,\\
&R = 2K = 2\frac{\sin\theta}{r(R + r\sin\theta)}\,.
\end{aligned}
$$

Bibliography

[1] M.J. Ablowitz, P.A. Clarkson, *Solitons, non-linear evolution equations and inverse scattering*, Cambridge Univ. Press, Cambridge, 1991.

[2] M.J. Ablowitz , J.T. Cole, *Nonlinear optical waveguide lattices: Asymptotic analysis, solitons, and topological insulators*, Physica D **440** (2022) 133440.

[3] V.I. Afonso, D. Bazeia, M.A. Gonzalez Leon, L. Losano, J. Mateos Guilarte, *Orbit-based deformation procedure for two-field models*, Phys. Rev. D **76** (2007) 025010.

[4] V.I. Afonso, D. Bazeia, M.A. Gonzalez Leon, L. Losano, J. Mateos Guilarte, *Constructing networks of defects with scalar fields*, Phys. Lett. B **662** (2008) 75.

[5] V.I. Afonso, D. Bazeia, M.A. Gonzalez Leon, L. Losano, J. Mateos Guilarte, *Construction of topological defect networks with complex scalar fields*, Nucl. Phys. B **810** (2009) 427.

[6] G.P. Agrawall, *Nonlinear Fiber Optics*, Academic Press, San Diego, 1995.

[7] C.A. Almeida, D. Bazeia, L. Losano, J.M.C. Malbouisson, *New results for deformed defects*, Phys. Rev. D **69** (2004) 067702.

[8] A. Alonso Izquierdo, M.A. Gonzalez Leon, J. Mateos Guilarte, *Kink manifolds in (1+1)-dimensional scalar field theory*, J. Phys. A: Math. Gen. **31** (1998) 209-229.

[9] A. Alonso Izquierdo, M.A. Gonzalez Leon, J. Mateos Guilarte, *Kink from dynamical systems: domain walls in a deformed O(N) linear sigma model*, Nonlinearity **13** (2000) 1137-1169.

[10] A. Alonso Izquierdo, M.A. Gonzalez Leon, J. Mateos Guilarte, *Stability of kink defects in a deformed O(3) linear sigma model*, Nonlinearity **15** (2002) 1097-1125.

[11] A. Alonso Izquierdo, M.A. Gonzalez Leon, J. Mateos Guilarte, M. de la Torre Mayado, *Adiabatic motion of two-component BPS kinks*, Phys. Rev. D **66** (2002) 105022.

[12] A. Alonso Izquierdo, M. A. González León, J. Mateos Guilarte, *Kink variety in systems of two coupled scalar fields in two space-time dimensions*, Phys. Rev. D **65** (2002) 085012.

[13] A. Alonso Izquierdo, J.C. Bueno Sánchez, M.A. Gonzalez Leon, M. de la Torre Mayado, *Kink manifolds in a three-component scalar field theory*, J. Phys. A: Math. Gen. **37** (2004) 3607-3626.

[14] A. Alonso Izquierdo, M.A. Gonzalez Leon, J. Mateos Guilarte, M. de la Torre Mayado, *Jacobi metric and Morse Theory of Dynamical Systems*, Publ. R. Soc. Mat. Esp. **6** (2004) 81-91.

[15] A. Alonso Izquierdo, M.A. Gonzalez Leon, J. Mateos Guilarte, *Changing shapes: adiabatic dynamics of composite solitary waves*, Physica D **200** (2005) 220-241.

[16] A. Alonso-Izquierdo, J. Mateos Guilarte, *One-dimensional solitary waves in singular deformations of $SO(2)$ invariant two-component scalar field theory models*, Nonlinearity **20** (2007) 2691-2719.

[17] A. Alonso-Izquierdo, M.A. González León, J. Mateos Guilarte, *Kinks in a non-linear massive sigma model*, Phys. Rev. Lett. **101** (2008) 131602.

[18] A. Alonso-Izquierdo, M.A. González León, J. Mateos Guilarte, *BPS and non-BPS kinks in a massive non-linear S^2-sigma model*, Phys. Rev. D **79** (2009) 125003.

[19] A. Alonso Izquierdo, M.A. González León, J. Mateos Guilarte, and M. J. Senosiain, *On the semiclassical mass of S^2-kinks*, J. Phys. A: Math. Theor. **42** (2009) 385403.

[20] A. Alonso-Izquierdo, M.A. Gonzalez Leon, J. Mateos Guilarte, M. de la Torre Mayado, *On domain walls in a Ginzburg-Landau non-linear $\mathbb{S}^2$-sigma model*, JHEP **8** (2010) 111.

[21] A. Alonso-Izquierdo, D. Bazeia, L. Losano, J. Mateos Guilarte, *New models for two real scalar fields and their kinklike solutions*, Advances in High Energy Physics (2013) 183295.

[22] A. Alonso-Izquierdo, A.J. Balseyro Sebastián, M.A. González León, *Domain walls in a non-linear $\mathbb{S}^2-$sigma model with homogeneous quartic polynomial potential*, JHEP **11** (2018) 23.

[23] A. Alonso-Izquierdo, M.A. Gonzalez Leon, J. Martín Vaquero, M.de la Torre Mayado, *Kink scattering in a generalized Wess-Zumino model*, Commun. Nonlinear Sci. and Numer. Simul. **103** (2021) 106011.

[24] A. Alonso-Izquierdo, *Kink dynamics in the MSTB model*, Phys. Scr. **94** (2019) 085302.

[25] A. Alonso-Izquierdo, *Non-topological kink scattering in a two-component scalar field theory model*, Commun. Nonlinear Sci. Numer. Simul. **85** (2020) 105251.

[26] A. Alonso-Izquierdo, A.J. Balseyro Sebastian, J. Mateos Guilarte, M.A. Gonzalez Leon, *Kinks in massive non-linear $\mathbb{S}^1 \times \mathbb{S}^1-$Sigma models*, Phys. D **440** (2022) 1-12.

[27] A. Alonso-Izquierdo, A.J. Balseyro Sebastian, M.A. Gonzalez Leon, *Topological and non-topological kink families in non-linear $\mathbb{S}^1 \times \mathbb{S}^1-$Sigma models*, Commun. Nonlinear Sci. Numer. Simul. **126** (2023) 107503.

[28] M. Arai, M. Naganuma, M. Nitta, and N. Sakai, *Manifest supersymmetry for BPS walls in $\mathcal{N} = 2$ non-linear sigma model*, Nucl. Phys. B **652** (2002) 35-71.

[29] V.I. Arnold, *Mathematical Methods of Classical Mechanics*, Graduate Texts in Mathematics. Vol. 60, 1983.

[30] A.J. Balseyro Sebastian, D. Bazeia and M.A. Marques, *Mechanism to induce geometric constriction on kinks and domain walls*, EPL **141** (2022) 34003.

[31] D. Bazeia and E. Ventura, *Topological twistons in crystalline polyethylene*, Chem. Phys. Lett. **303** (1999) 341.

[32] D. Bazeia, L. Losano, J.M.C. Malbouisson, *Deformed defects*, Phys. Rev. D **66** (2002) 101701(R).

[33] D. Bazeia, W. Freire, L. Losano, R.F. Ribeiro, *Topological defects and the trial orbit method*, Phy. Lett. A **17** (2002) 1945.

[34] D. Bazeia, M.A. Gonzalez Leon, L. Losano, J. Mateos Guilarte, *Deformed defects for scalar fields with polynomial interactions*, Phys. Rev. D **73** (2006) 105008.

[35] D. Bazeia and L. Losano, *Deformed defects with applications to braneworlds*, Phys. Rev. D **73** (2006) 025016.

[36] D. Bazeia, M.A. Gonzalez Leon, L. Losano, J. Mateos Guilarte, *New scalar field models and their defect solutions*, EPL **93** (2011) 21001.

[37] D. Bazeia, M.A. Gonzalez Leon, L. Losano, J. Mateos Guilarte, J.R.L. Santos, *Construction of new scalar field models from the standard ϕ^4 theory*, Phys. Scr. **87** (2013) 045101.

[38] D. Bazeia, R. Casana, M.M. Ferreira, E. da Hora and L. Losano, *Deformed self-dual magnetic monopoles*, Phys. Lett. B **727** (4-5) (2013) 548-553.

[39] D. Bazeia, E. Belendryasova, V.A. Gani, *Scattering of kinks in a non-polynomial model*, J. Phys.: Conf. Ser. **934** (2017) 012032.

[40] D. Bazeia, M.A. Liao, M.A. Marques, *Geometrically constrained kinklike configurations*, Eur. Phys. J. Plus **135** (2020) 383.

[41] N. Benchtaber, D. Sánchez, L. Serra, *Scattering of topological kink-antikink states in bilayer graphene structures*, Phys. Rev. B **104** (2021) 155303.

[42] C. Becker, et al., *Oscillations and interactions of dark and dark–bright solitons in Bose–Einstein condensates*, Nature Phys. **4** (2008) 496.

[43] L. Bernasconi, *Chaotic soliton dynamics in photoexcited trans-polyacetylene*, The Journal of Physical Chemistry Letters, **6** (5) (2015) 908–912.

[44] A.R. Bishop, J.A. Krumhansl and S.E. Trullinger, *Solitons in condensed matter: A paradigm*, Physica D **1** (1980) 1.

[45] E. Bour, *Theorie de la deformation des surfaces*, Journal de l'École impériale polytechnique, **22** (39) (1931) 1–148.

[46] E.B. Bogomolny, *Stability of Classical Solutions*, Sov. J. Nucl. Phys. **24** (1976) 449.

[47] G. Chen, T. Ma, A.T. N'Diaye, H. Kwon, C.Won, Y.Wu, A.K. Schmid, *Tailoring the chirality of magnetic domain walls by interface engineering*, Nat. Commun. **4** (39) (2013) 2671.

[48] S. Cheng, S. Dong, *Manipulation of Magnetic Domain Walls by Ferroelectric Switching: Dynamic Magnetoelectricity at the Nanoscale*, Phy. Rev. Lett. **126** (2021) 117603.

[49] A. Chumak, V. Vasyuchka, A. Serga, et al. *Magnon spintronics*, Nature Phys. **11** (2015) 453–461.

[50] A.E.R. Chumbes, M.B. Hott, *Reconstruction of deformed defects in field theory from deformed zero modes and applications*, Phys. Rev. D **81** (2010) 045008.

[51] S. Coleman, *There are no Goldstone bosons in two dimensions*, *Com. Math. Phys.* **31** (1973) 259-264.

[52] A. Cortijo, M.A.H. Vozmediano, *Effects of topological defects and local curvature on the electronic properties of planar graphene*, Nucl. Phys. B **763**, Issue 3 (2007) 293-308.

[53] W. T. Cruz, M. O. Tahim, C.A.S. Almeida, *Results in Kalb-Ramond field localization and resonances on deformed branes*, EPL **88** (2009) 41001.

[54] A.S. Davydov, *Solitons in molecular systems*, D. Reidel, Dordrech, 1985.

[55] A. de Souza Dutra, *Continuously deformable topological structure*, Physica D **238** (2009) 798.

[56] G.H. Derrick, *Comments on nonlinear wave equations as models for elementary particles*, J. Math. Phys. **5** (1964) 1252-1254.

[57] P.A.M. Dirac, *Quantized Singularities in the Electromagnetic Field*, Proc. R. Sot. A **133** (1931) 60-72.

[58] M.P. do Carmo, *Riemannian geometry*, Birkhäuser, 1992.

[59] R.K. Dodd, R.K. Bullough, *Bäcklund transformations for the sine–Gordon equations*, Proc. R.Soc.Lond. A **351** (1976) 499-523.

[60] N. Dorey, *The BPS spectra of two-dimensional gauge theories with twisted mass terms*, JHEP **11** (1998) 005.

[61] P.G. Drazin, R.S Johnson, *Solitons: an introduction*, Cambridge Univ. Press, Cambridge, 1996.

[62] M. El-Batanouny, S. Burdick, K.M. Martini, P. Stancioff, *Double-sine-gordon solitons: A model for misfit dislocations on the au (111) reconstructed surface*, Phys. Rev. Lett. **58** (1987) 2762.

[63] A.H. Eschenfelder, *Magnetic Bubble Technology*, Springer-Verlag, Berlin, 1981.

[64] M. Eto, Y. Isozumi, M. Nitta, K. Oshasi, N. Sakai, *Solitons in the Higgs phase -the moduli matrix approach*, Jour. Phys. A **39** (2006) R315-R392.

[65] E. Fermi, J. Pasta, S. Ulam, *Studies in Nonlinear Problems. I*, contained in *Nonlinear Wave Motion*, Lectures in Applied Math., **15** (1974) 142-155, Amer. Math. Soc., Providence.

[66] C.S. Gardner, J.M. Greene, M.D. Kruskal, R.M. Miura, *Method for solving the Korteweg-de Vries equation*, Phys. Rev. Lett. **19** (1967) 1095-1097.

[67] J. P. Gauntlett, R. Portugues, D. Tong, P. K. Townsend, *D-brane solitons in supersymmetric sigma models*, Phys. Rev. D **63** (2001) 085002.

[68] M. Gell-Mann, M. Lévy, *The axial vector current in beta decay*, Nuovo Cim. (10) **16** (1960) 705-726.

[69] M. Giaquinta, S. Hildebrandt, *Calculus of variations I*, Springer Science Business Media, 2004.

[70] J. Goldstone, *Field Theories with Superconductor Solutions*, Nuovo Cim. **19** (1961) 154.

[71] M.A. Gonzalez Leon, *Kinks, Sistemas Integrables y Geodésicas: Solitones en el Modelo Sigma $O(3)$ Lineal*, Tesis doctoral USAL, 2001.

[72] P. Guillamat, C. Blanch-Mercader, G. Pernollet, et al., *Integer topological defects organize stresses driving tissue morphogenesis*, Nat. Mater. **21** (2022) 588–597.

[73] C. Halcrow, E. Babaev, *Stable kink-kink and metastable kink-antikink solutions*, arXiv:2211.02413 [hep-th] (2023).

[74] F.D.M. Haldane, *Nonlinear field theory of large-spin Heisenbert antiferromagnets: semiclassically quantized solitons of the one-dimensional easy-axis Neel state*, Phys. Rev. Lett. **50** n. 16 (1983) 1153.

[75] A.J. Heeger, S. Kivelson, J.R. Schrieffer, W.-P. Su, *Solitons in conducting polymers*, Rev. Mod. Phys. **60** (1988) 781.

[76] A. Hubert, R. Schafer, *Magnetic domains: the analysis of magnetic microstructures*, Springer (1998).

[77] A. Hirohata, K. Takanashi, *Future perspectives for spintronic devices* J. Phys. D: Appl. Phys. **47** (2014) 193001.

[78] A. Hirohata, K. Yamada, Y. Nakatani, I.L. Prejbeanu, B. Diény, P. Pirro, B. Hillebrands, *Review on spintronics: Principles and device applications*, J. of Magn. Magn. Mater. **509** (2020) 166711.

[79] Y. Isozumi, M. Nitta, K. Oshasi, N. Sakai, *All exact solutions of a 1/4 Bogomolnyi-Prasad-Sommerfield equation*, Phys. Rev. D **71** (2005) 065018.

[80] H. Ito, *Kink energy sum rule in a two-component scalar field model of 1+1 dimensions*, Phys. Lett. A **112** (1985) 119-123.

[81] H. Ito and H. Tasaki, *Stability theory for nonlinear Klein-Gordon Kinks and Morse's index theorem*, Phys. Lett. A **113** (1985) 179-182.

[82] A.S. Johnson, W. Winlow, *The soliton and the action potential-Primary elements underlying sentience*, Front. Physiol. **9** (2018) 779.

[83] F. Jona, G. Shirane, *Ferroelectric Crystals*, New York, Dover, 1993.

[84] J. Jost, *Riemannian Geometry and Geometric Analysis*, Springer Science Business Media, 2017.

[85] P.O. Jubert, R. Allenspach, A. Bishof, *Magnetic domain walls in constrained geometries*, Phy. Rev. B **69** (2004) 220410(R).

[86] M. Kardar. *Statistical physics of fields*. Cambridge University Press, 2007.

[87] P.G. Kevrekidis, J. Cuevas-Maraver (Editors), *A Dynamical Perspective on the ϕ^4 Model*, Springer (2019).

[88] T.W.B. Kibble, *Topology of cosmic domains and strings*, J. Phys. A: Math. Theor. **9** (1976) 1387.

[89] T. Kimura, N. Hashimoto, S. Yamada, et al. *Room-temperature generation of giant pure spin currents using epitaxial Co2FeSi spin injectors*, NPG Asia Mater **4** (2012) e9.

[90] J. Khoury, B.A. Ovrut, P.J. Steinhardt, N. Turok, *Ekpyrotic universe: Colliding branes and the origin of the hot big bang*, Phys. Rev. D, **64** (2001) 123522.

[91] E.W. Kolb, M.S. Turner, *The Early Universe*, Addison-Wesley, Redwood/CA, 1990.

[92] K. Koumpouras, A. Bergman, O. Eriksson, D. Yudin, *A spin dynamics approach to solitonics*, Scientific Reports 6: 25685.

[93] D.J. Korteweg, G. de Vries, *On the change of form of long waves advancing in a rectangular canal, and on a new type of long stationary waves*, Phil. Mag. **39** (1895) 422.

[94] L. D. Landau, *On the theory of phase transitions I*, JETP **7** (1937) 1.

[95] L. D. Landau, *On the theory of phase transitions II*, JETP **7** (1937) 627.

[96] E. Lesne, Y.Fu, S. Oyarzun, et al., *Highly efficient and tunable spin-to-charge conversion through Rashba coupling at oxide interfaces*, Nat. Mater. **15** (2016) 1261–1266.

[97] T. Machon, G.P. Alexander, R.E. Goldstein, A.I. Pesci, *Instabilities and Solitons in Minimal Strips*, Phy. Rev. Lett. **117** (2016) 017801.

[98] E. Magyari, H. Thomas, *Solitary waves in a 1D anharmonic lattice with two-component order parameter*, Phys. Lett. A **100** (1) (1984) 11-14.

[99] N. Manton, P. Sutcliffe, *Topological Solitons*, Cambridge University Press, 2004.

[100] F. Martin-Vergara, F. Rus, F.R. Villatoro, *Fractal structure of the soliton scattering for the graphene superlattice equation*, Chaos, Solitons and Fractals, **151** (2021) 111281.

[101] J. Mateos Guilarte, *Stationary phase approximation and quantum soliton families*, Annals of Physics **188** no. 2 (1988) 307-346.

[102] J. Milnor, *Morse Theory*. Princeton Univ. Press, Princeton, 1973.

[103] L.F. Mollenauer, J.P. Gordon, *Solitons in optical fibers - Fundamentals and applications*. Academic Press, Burlington, 2006.

[104] C. Montonen, *On solitons with an Abelian charge in scalar field theories: (I) Classical theory and Bohr-Sommerfeld quantization*, Nucl. Phys. B **112** (1976) 349-357.

[105] P.M. Morse, H. Feshbach, *Methods of theoretical physics*, **1** (1953) 1651-1658.

[106] D.C. Moreira, F.A. Brito, D. Bazeia, *Localized scalar structures around static black holes*, Nucl. Phys. B **987** (2023) 116090.

[107] M. Naganuma, M. Nitta, N. Sakai, *BPS walls and junctions in SUSY nonlinear sigma models*, Phys.Rev. D **65** (2002) 045016.

[108] Y. Nambu, *A Superconductor Model of Elementary Particles and its Consequences*, Talk given at a conference at Purdue (1960), reprinted in T. Eguchi, K. Nishijima (eds), *Broken Symmetries, Selected Papers by Y. Nambu*, (World Scientific, Singapore, 1995).

[109] S.P. Novikov, S.V. Manakov, L.P. Pitaevskii, V.E. Zakharov, *Theory of solitons. The inverse scattering method*, Plenum Press, New York-London, 1984.

[110] R. Palais, *The symmetries of solitons*, Bull. Amer. Math. Soc. **34** (1997) 339-403.

[111] H.B. Pandey, *Cartesian product of two manifolds*, Indian J. pure appl. Math. **12** (1981) 55-60.

[112] A. Perelomov, *Integrable Systems of Classical Mechanics and Lie Algebras*, Birkhäuser, Boston, MA, 1990.

[113] M.E. Peskin, D.V. Schroeder, *An Introduction to Quantum Field Theory*, CRC Press, 2018.

[114] C.J. Pethick, H. Smith, *Bose–Einstein Condensation in Dilute Gases*, Cambridge University Press, 2008.

[115] S.D. Pollard, J.A. Garlow, K.-W. Kim, S. Cheng, K. Cai, Y. Zhu , H. Yang, *Bloch chirality induced by an interlayer Dzyaloshinskii-Moriya interaction in ferromagnetic multilayers*, Phy. Rev. Lett. **125** (2020) 227203.

[116] R. Rajaraman, E.J. Weinberg, *Internal symmetry and the semiclassical method in quantum field theory*, Phys. Rev. D **11** (1975) 2950.

[117] R. Rajaraman, *Solitons and Instantons*, North-Holland, Amsterdam, 1982.

[118] V.A. Rubakov, M.E. Shaposhnikov, *Do we live inside a domain wall?*, Phys. Lett. B **125** (2-3) (1983) 136–138.

[119] J. Scott Russell, *Report on Waves*, 14th Meeting of the British Association for the Advancement of Science, York, 1844, pp. 311-390 and 11 plates.

[120] M. Saffman, T.G. Walker, K. Mølmer, *Quantum information with rydberg atoms*, Reviews of Modern Physics **82** (2010) 2313.

[121] S. Sarker, S.E. Trullinger, A.R. Bishop, *Solitary-wave solution for a complex one-dimensional field*, Phys. Lett. A **59** (1976) 255-258.

[122] T. Schneider, *Nonlinear optics in Telecommunications*, Springer, Heidelberg, 2004.

[123] A.A. Serga et al, *YIG magnonics*, J. Phys. D: Appl. Phys. **43** (2010) 264002.

[124] M. Shifman, A. Yung,*Supersymmetric solitons*, Rev. Mod. Phys. **79** (2007) 1139.

[125] Y. Shnir, *Topological and Non-Topological Solitons in Scalar Field Theories*, Cambridge Monographs on Mathematical Physics (2018).

[126] B.A. Strukov, A.P. Levanyuk, *Ferroelectric Phenomena in Crystals: Physical Foundations*, Springer-Verlag, Berlin, 1998.

[127] W.P. Su, J.R. Schrieffer, A.J. Heeger, *Solitons in polyacetylene*, Phys. Rev. Lett., **42** (1979) 1698.

[128] C.L. Terng, K. Uhlenbeck, *Geometry of solitons*, Notices Amer. Math. Soc. **47** (1) (2000) 17-25.

[129] Y. Togawa, T. Koyama, K. Takayanagi, S. Mori, Y. Kousaka, J. Akimitsu, S. Nishihara, K. Innoue, A.S. Ovchinnikov, J. Kishine, *Chiral magnetic soliton lattice on a chiral helimagnet*, Phys. Rev. Lett. **1008** (2012) 107202.

[130] A.V. Ustinov, *Solitons in Josephson junctions*, Physica D **123** (1998) 315–329.

[131] T. Vachaspati, *Kinks and Domain walls: An Introduction to classical and quantum solitons*, Cambridge University Press, Cambrigde, UK, 2006.

[132] A. Vanhaverbeke, A. Bischof and R. Allenspach, *Control of Domain Wall Polarity by Current Pulses*, Phy. Rev. Lett. **101** (2008) 107202(R).

[133] A. Vilenkin, *Cosmic strings and domain walls*, Physics Reports **121** Issue 5 (1985) 263-315.

[134] A. Vilenkin, E.P.S. Shellard, *Cosmic strings and other topological defects*, Cambridge University Press, Cambridge, UK, 2000.

[135] E.J. Weinberg, *Classical solutions in Quantum Field Theory: Solitons and Instantons in High Energy Physics*, Cambridge University Press, 2012.

[136] L. Wilets, *Nontopological Solitons*, World Scientific, 1989.

[137] L.V. Yakushevich, *Nonlinear Physics of DNA*, Wiley-VCH, Weinheim, 2004.

[138] R.D. Yamaletdinov, V.A. Slipko, Y.V. Pershin, *Kinks and antikinks of buckled graphene: A testing ground for the ϕ^4 field model*, Phys. Rev. B **96** (2017) 094306.

[139] N.J. Zabusky, M.D. Kruskal, *Interaction of "solitons" in a collisionless plasma and the recurrence of initial states*, Phys. Rev. Lett. **15** (1965) 240.

[140] J. Zinn-Justin, *Quantum Field Theory and Critical Phenomena*, Oxford University Press, Oxford, 2002.